EXPERIMENTAL AND ANALYTICAL STUDY OF STEAM TURBINE TWO-PHASE OPERATION IN NUCLEAR REACTOR COOLING SYSTEMS

A Dissertation

by

ASHRAF ALI MAJED ALFANDI

Submitted to the Graduate and Professional School of
Texas A&M University
in partial fulfillment of the requirements for the degree of

DOCTOR OF PHILOSOPHY

Chair of Committee,	Karen Vierow Kirkland
Committee Members,	Yassin Hassan
	Mark Kimber
	Adolfo Delgado-Marquez
Head of Department,	Michael Nastasi

December 2021

Major Subject: Nuclear Engineering

ABSTRACT

Prior to Fukushima accident, the Reactor Core Isolation Cooling (RCIC) system operational limits were based on manufacturers data, in which the system's Terry turbine and pump were assumed to be ideal. The Beyond Design Basis Event (BDBE) operating conditions were evaluated according to conservative Probabilistic Risk Assessment (PRA) applications.

In response to the current lack of knowledge and poor understanding of RCIC system performance under BDBE conditions, the current study investigates the Terry turbine performance at BDBEs using steam-water mixtures. These tests serve to expand the available database for model development, validation and verification, and dimensional analysis, in a cost-effective manner without the potential of severely damaging a nuclear grade full-scale Terry Turbine.

Additionally, single-phase air tests were also performed during the current testing efforts to benchmark against previous data bases of air and air-water data of a small-scale and full-scale Terry turbines. These tests will inform proposed full-scale experimental design and testing. The tests described herein were conducted at conditions as close as possible to those which were recorded during operation of plant RCIC systems and therefore provide essential data for scaling from small laboratory sizes up to full-scale RCIC system size. Toward that end, a complete set of nondimensionalized characterization of the small-scale turbine has been performed at different steam inlet pressures, back pressures, and steam qualities.

Over 20 US BWRs employ a RCIC system. If the RCIC System can be shown efficient over a wider range of conditions, the plants would like to have more cost savings and additional safety margin.

DEDICATION

To my heart-beloved country, The Hashemite Kingdom of Jordan.

To my Mom and Dad. To my brothers, Amjad, Mohammad, Abdullah, and Ahmad. To my sisters Raghad and Farah.

To the love of my life, Lubna, for her love, patience, and never-ending support. To my little princess Lana and my champs Hashim, and Laith.

ACKNOWLEDGEMENTS

"My success comes only through Allah. In Him I trust and to Him I turn" (The Qur'an, 11:88)

First and foremost, I would like to praise and thank God, the Almighty, who has granted me countless blessing, guidance, and support to accomplish this work.

I would like thank Dr. Kirkland for her for her patience, motivation, and immense knowledge. A special thanks to Dr. Matthew Solom from Sandia National Laboratory for his technical guidance in-person and online.

I would like to thank my wonderful lab mates, the efforts of Dallin Keesling, Tugce Kesat, Thomas Freyman, Colten Buendel, Christopher Bayne, Kenne Fossum, and Phillip Olivarez are truly appreciated. I also want to extend my thanks to a number of people who were helpful in contributing to the success of this work including Doug Osborn, Abhay Patil, Josh Vendervort, Marie Kasprzyk, Ahamad Bashaireh, Ala'a Altaweel, Mike Kerstetter, and Revak-Keene staff for their most generously provided expertise, facility tours and assistance with the turbine maintenance and operation.

From the bottom of my heart, I'd like to thank my Mom, Dad, Brothers and Sisters. Their cheering spirit along this journey was crucial to get this done. My kiddos, Lana, Hashim, and Laith, thank you for giving me one more reason to be a better dad.

To my true love, the lady I respect, adore and love, Lubna. I couldn't find enough words to thank you for all what you've done and still doing to me and to our family during this journey. It's our success and you're its backbone.

CONTRIBUTORS AND FUNDING SOURCES

Contributors

This work was supervised by a dissertation committee consisting of Professor Karen Vierow Kirkland, Professor Yassin Hassan, and Professor Mark Kimber of the Department of Nuclear Engineering and Professor Adolfo Delgado of the Department of Mechanical Engineering.

The Terry turbine used in this research was donated by Revak-Keene Turbomachinery Services. Dr. Matthew Solom aided substantially in the design and construction of the experimental facility. The LabVIEW code main structure was programmed by a fellow graduate student, Dallin Keesling.

All other work conducted for the thesis was completed by the student independently.

Funding Sources

This work was made possible in part by the three contracts on the RCIC project. Institute of Applied Energy (Japan), Research Agreement No. M1702670. Battelle Energy Alliance, LLC, (BEA), contract no. 183672, Operating Under U. S. Government Contract No. DE-AC07-05ID14517. And Pooled Equipment Inventory Company by Southern Nuclear Services, LLC (US nuclear industry partner) Purchase Order No. 201953. Its contents are solely the responsibility of the authors and do not necessarily represent the official views of the Department of Energy.

NOMENCLATURE

EDG	Emergency Diesel Generators
SFP	Spent Fuel Pool
RCIC	Reactor Core Isolation Cooling
BWR	Boiling Water Reactor
1F2	Fukushima Daiichi Unit 2
1F3	Fukushima Daiichi Unit 3
RPV	Reactor Pressure Vessel
MSL	Main Steam Line
CST	Condensate Storage Tank
SP	Suppression Pool
TDS	Total Dissolved Solids
DAQ	Data Acquisition System
URV	Upper Range Value
NI	National Instruments
I/O	Input/Output
TB	Terminal Block
IAPWS	International Association for the Properties of Water and Steam
EPRI	Electric Power Research Institute
PID	Proportional, Integral, Derivative
FOPDT	First Order Plus Dead Time

NHTS	Laboratory of Nuclear Heat Transfer Systems
PVC	PolyVinyl Chloride
HX	Heat Exchanger
CTS	Cooling Tower System
P&ID	Piping and Instrumentation Diagram
BEP	Best Efficiency Point
Ma	Mach number
NRC	Nuclear Regulatory Commission

TABLE OF CONTENTS

Page

ABSTRACT II

DEDICATION IV

ACKNOWLEDGEMENTS V

CONTRIBUTORS AN FUNDING SOURCES VI

NOMENCLATURE VII

TABLE OF CONTENTS IX

LIST OF FIGURES XII

LIST OF TABLES XVIII

1. INTRODUCTION 1

1.1. Fukushima Accident 1
1.2. Reactor Core Isolation Cooling (RCIC) system 1
1.3. Terry Turbine 4

2. DISSERTATION OVERVIEW 10

2.1. Problem Statement 10
2.2. Objectives 10
2.3. Motivation 11
2.4. Significance of Research 12
2.5. Technical Approach 12

3. EXPERIMENTAL FACILITY 14

3.1. Overview 14
3.2. Steam Generator (SG) 18
3.2.1. Electric Heaters 22
3.2.2. Moisture Separator 23
3.3. Main Control Valve 24
3.4. ZS-1 Terry Turbine 25
3.5. Suppression Pool (SP) 28

3.6. RCIC pump analog 30
3.7. Dynamometer 31
3.8. Load Cell 34
3.9. Tachometer 35
3.10. Torquemeter 36
3.11. Azbil/Yamataki Flowmeters 38
3.12. Data Acquisition (DAQ) System 40

4. FACILITY UPGRADES PERFROMED FOR THESE EXPERIMENTS 45

4.1. Turbine Disassembly 45
4.2. Shaft Sealant 46
4.3. Turbine Re-Assembly 48
4.4. Steam Nozzle Valve 50
4.5. Safety Coupling 51
4.6. Shaft Alignment 56
4.7. Control Valves 64
4.8. Cooling System 67
4.8.1. Cooling Tower 68
4.8.2. Heat Exchanger (HX) 73
4.9. Water treatment Station 75

5. TEST PROCEDURES 77

5.1. Pre-test Mode 77
5.2. Warmup Mode 78
5.3. Data collection Mode 79
5.4. Cooldown Mode 81
5.5. Shutdown Mode 82

6. RESULTS AND DISCUSSION 84

6.1. ZS-1 Terry Turbine Characterization Tests 85
6.1.1. Testing parameters 85
6.1.2. Recorded Parameters 85
6.1.3. Testing Outputs 85
6.1.4. Equations 86
6.1.5. Effect of Steam Inlet Pressure 87
6.1.6. Turbine Oil Temperature Effect 89
6.1.7. Effect of Steam Quality 94
6.1.8. Effect of Turbine Back Pressure 100
6.2. Turbopump characterization tests 107
6.2.1. Testing Parameters 107
6.2.2. Recorded Parameters 108
6.2.3. Testing Outputs 108

6.2.4. Effect of Inlet Steam Pressure 108
6.2.5. Effect of Steam Quality 112

7. SCALING ANALYSIS 114

7.1. Equations 115
7.2. NHTS vs. TurboLab ZS-1 Experimental Data Benchmarking 117
7.3. Power Plant Data (Dry Steam) vs. GS2 Experimental Data (Dry Air) 120
7.4. ZS Experimental Data vs GS Actual Data 121
7.5. NHTS Experimental Data vs. Power Plant Data 124
7.5.1. Steam Inlet Pressure 124
7.5.2. Steam Quality effect 125
7.5.3. Back Pressure Effect 128

8. ERROR ANALYSIS 136

8.1. Data Qualification 136
8.2. Automated Steady State detection 136
8.3. Uncertainty Analysis: Measured Parameters 139
8.4. Error Propagation: Derived Parameters 143

9. FUTURE WORK 145

10. CONCLUSION 146

REFERENCES 149

APPENDIX A 154

APPENDIX B 160

APPENDIX C 177

APPENDIX D 192

APPENDIX E 207

APPENDIX F 216

APPENDIX G 218

LIST OF FIGURES

Page

Figure 1.1 BWR Mark I Containment [5] 3

Figure 1.2 Schematic diagram of the RCIC System in a BWR with the Mark I containment [6] 4

Figure 1.3 (Right) Terry turbine cross-sectional view. (Left) The steam flow path through the steam nozzle[5] 6

Figure 1.4 Compound velocity feature in the impulse turbines [7] 7

Figure 1.5 Reactive turbines velocity and pressure profile inside the blades [8] 8

Figure 3.1 Facility Flow diagram for the Turbine Characterization Tests 16

Figure 3.2 P&ID of the Experimental Facility 17

Figure 3.3 Steam Generator with visual water level indicator 20

Figure 3.4 P&ID of the Steam Generator and city-water treatment station 21

Figure 3.5 Heater control panel 22

Figure 3.6 The u-tube shaped immersion heaters for the Steam Generator 23

Figure 3.7 Separator downstream of the steam generator outlet 24

Figure 3.8 Main Control Valve (V-1) 25

Figure 3.9 ZS-1 Terry Turbine [11] 26

Figure 3.10 Turbine wheel and reversing steam [12] 27

Figure 3.11 Suppression Pool front side (left) and wide view (right) 28

Figure 3.12 P&ID of the Suppression Pool and Terry turbine 29

Figure 3.13 Five-stage centrifugal RCIC pump 30

Figure 3.14 XS-19 Stuska absorption water break dynamometer [11] 31

Figure 3.15 General design schematic of absorption water brake dynamometer [14] 32

Figure 3.16 Stuska XS-19 Break Horsepower (BHP) curve [14] 33

Figure 3.17 Load Cell [11] 34

Figure 3.18 (Left) Tachometer laser sensor. (Right) Tachometer reading displayer 35

Figure 3.19 HBM Torque meter model no. T21WN/20NM coupled on the same shafts of the turbine and the pump. 36

Figure 3.20 The transducer connection cable pin assignment in the housing connector. [16] 37

Figure 3.21 Electrical terminal block for torquemeter transducer cable connection to DAQ 38

Figure 3.22 Magnetic Flowmeter detector at the water injection line. The detector has a model number of (MGG18D-015P21LS5AAA-XX-Y) and a product number of (R-9AH1E-41-021A). 39

Figure 3.23 Magnetic Flowmeter convertor at the water injection line. The convertor of a product number (MGG14C-MH4H-1B1N-YAH) and serial number (R-F3396-A1-011) 40

Figure 3.24 NI PXIe-1075 chassis with modules installed 41

Figure 3.25 LabVIEW control panel for the Turbine standalone setup 42

Figure 3.26 LabVIEW control panel for the Turbopump setup 43

Figure 3.27 LabVIEW control panel for generating the thermodynamic properties and flow conditions based on the fluid pressure and temperature. 44

Figure 4.1 The ZS-1 Terry turbine shaft sealant. (left) One piece of three semi-circular pieces that forms the complete set of carbon gland. (Right) The four carbon glands installed around the shaft setting in their housing 47

Figure 4.2 Sealant quality check. The dial gauge reads less than 5 mils, which is the clearance between the shaft outer surface and the carbon inner surface. 47

Figure 4.3 Shaft sealant housing before and after cleaning. 49

Figure 4.4 Permatex #2 sealant applied on the bottom part of the oil well cover -pump side. 49

Figure 4.5 Application of Temp Tight II on the bottom part of the casing. 50

Figure 4.6 Steam Nozzle Valve. (left) Complete structure of the valve. (Right) Valve stem and sealant 51

Figure 4.7 The turbopump safety coupling setup. The dial indicators were mounted as a part of the reverse dial indicator method for shaft vertical alignment. 52

Figure 4.8 Lovejoy L110 rubber spider coupling mounted between the turbine and the dyno. 53

Figure 4.9 Dynamometer-Turbine (Standalone) setup with main components. 54

Figure 4.10 Metal Bellows coupling allowable misalignment. The red and blue boxes rectangles the corresponding coupling specs [21]. 55

Figure 4.11 Love Joy L110 - Jaw coupling allowable misalignment. The red box rectangles the corresponding coupling in this research [22] 56

Figure 4.12. Bar sag measurement setup. 58

Figure 4.13. Horizontal misalignment setup. 62

Figure 4.14 PI Controller tunning guide ([23], Page 80, Figure 8.9) 66

Figure 4.15 Set point and process variable 67

Figure 4.16 NHTS Heat Rejection System 70

Figure 4.17 NHTS Cooling Tower 71

Figure 4.18 Detailed technical drawing along with dimensional parameters [24]. 73

Figure 4.19 Technical details of the Plate-type Heat Exchanger used for the Heat Rejection System system in the NHTS lab 74

Figure 4.20 Heat Rejection System Water Treatment Station 76

Figure 6.1 The effect of the steam inlet the pressure of 30, 45, and 60 psi on turbine power output during single phase operation at atmospheric back pressure ... 88

Figure 6.2 ZS-1 Terry turbine's Isentropic Efficiency (η) vs Rotational Speed (ω) at dry steam inlet pressures of 30, 45, and 60 psia, and atmospheric back pressure. 89

Figure 6.3 The effect of the dry steam inlet the pressure and turbine oil temperature on power output at atmospheric back pressure. 90

Figure 6.4 The effect of Terry turbine oil temperature on the power output at different rotational speed. 91

Figure 6.5 The relationship between viscosity and temperature during 6-hour test for fresh and degraded oil at 121°C. [29]....92

Figure 6.6 ZS-1 shaft internal losses torque with turbine oil temperature. Figure 5.15 at [29] 92

Figure 6.7 ZS-1 Terry Turbine Power Output vs. Rotational Speed at different steam inlet pressures of 30, 45, and 60 psia. 94

Figure 6.8 ZS-1 terry turbine power output (kW) during two-phase flow operation at 30 psia inlet steam pressure and atmospheric back pressure....95

Figure 6.9 Measured Torque of the ZS-1 Terry Turbine while operated at variant steam qualities at 30 psia inlet pressure, atm back pressure....96

Figure 6.10 ZS-1 terry turbine efficiency during two-phase flow operation at 30 psia inlet steam pressure and atmospheric back pressure....96

Figure 6.11 Terry turbine's power output vs Rotational Speed (ω) at steam qualities of 0.05 – 1.00, steam inlet pressure and back pressure of 45 psia, and 14.6(atm), respectively....97

Figure 6.12 Terry turbine power output vs Rotational Speed (ω) at steam qualities of 0.05 – 1.00, steam inlet pressure and back pressure of 60 psia, and 14.6(atm), respectively....98

Figure 6.13 ZS-1 Terry turbine's Isentropic Efficiency (η) vs Rotational Speed (ω) at steam qualities of 0.05 – 1.00, steam inlet pressure and back pressure of 45 psia, and 14.6(atm), respectively....99

Figure 6.14 ZS-1 Terry turbine's Isentropic Efficiency (η) vs Rotational Speed (ω) at steam qualities of 0.5 – 1.00, steam inlet and back pressure of 60 psia, and 14.6(atm), respectively....100

Figure 6.15 ZS-1 Terry turbine's power output vs Rotational Speed (ω) at pressure ratios of 0.32, 0.39, and 0.44 and DRY steam inlet pressure of 45psia....101

Figure 6.16 ZS-1 Terry turbine's Isentropic Efficiency (η) vs Rotational Speed (ω) at pressure ratios of 0.32, 0.39, and 0.44 and DRY steam inlet pressure of 45psia. 102

Figure 6.17 ZS-1 Terry turbine power output vs Rotational Speed (ω) at pressure ratios of 0.49, 0.59, and 0.67 and DRY steam inlet pressure of 30psia. 103

Figure 6.18 ZS-1 Terry turbine power output vs Rotational Speed (ω) at pressure ratios of 0.24, and 0.29 and DRY steam inlet pressure of 60psia 104

Figure 6.19 Back pressure effect on the dry steam vs. wet steam operated ZS1 turbine at an inlet pressure of 30 psia and pressure ratios of 0.49, 0.59, and 0.67.....105

Figure 6.20 Back pressure effect on the dry steam vs. wet steam operated ZS1 turbine at an inlet pressure of 45 psia and pressure ratios of 0.32, .39, and 0.44.....106

Figure 6.21 Back pressure effect on the dry steam vs. wet steam operated ZS1 turbine at an inlet pressure of 60 psia and pressure ratios of 0.24 and 0.29.....107

Figure 6.22. The effect of the turbine inlet pressures on the rotational speeds at different pump outlet flowrates.....109

Figure 6.23. RCIC Pump power input (kW) vs. flowrate (GPM) under different inlet pressure of 35 and 40 psia 110

Figure 6.24. RCIC Pump performance curve; pressure drop (psia) vs. outlet flowrate (GPM) at 40 psia steam inlet, atmospheric back pressure. Of average rotational speed of 3620 rpm.....111

Figure 6.25 Turbopump power output (kW) at steam inlet pressures of 35 and 40 psia. 112

Figure 6.26 Steam Quality effect at 30 psia steam pressure inlet. The operational limit triangle shows the degradation effect on the turbopump flowrate performance.....113

Figure 7.1 Comparison between air operated ZS-1 turbine at the same pressure between NHTS lab (Alfandi) vs Turbo lab (Patil).....118

Figure 7.2 The turbine performance in terms of shaft torque (τ) vs rotational speed (ω) 119

Figure 7.3 Turbolab GS-2 air test results benchmarking against actual power plant data at variant dry steam/dry air pressure values 121

Figure 7.4 Terry turbine's power output coefficient vs flow coefficient of Nuclear Power Plants (steam) and TAMU (Dry Air) different pressures w/ multiplier.....122

Figure 7.5. Terry turbine's power output coefficient vs flow coefficient of Nuclear Power Plants (steam) and TAMU (Dry Air) different pressures.....123

Figure 7.6 Terry turbine power output coefficient vs flow coefficient of nuclear power plants (steam) and NHTS (DRY Steam) different inlet pressures w/ multiplier 125

Figure 7.7 ZS-1 Terry Turbine flow coef. vs power coef. for variant steam qualities at inlet pressure of 45 psia. (NHTS Data) 126

Figure 7.8 ZS-1 Terry Turbine flow coef. vs power coef. for variant steam qualities at inlet pressure of 30 psia. (NHTS Data) 127

Figure 7.9 ZS-1 Terry Turbine flow coef. vs power coef. for variant steam qualities at inlet pressure of 60 psia. (NHTS Data) 128

Figure 7.10 ZS-1 Terry Turbine flow coef. vs power coef. at inlet pressure of 30 psia but pressure ratios of 0.49, 0.59, and 0.67.....129

Figure 7.11 ZS-1 Terry Turbine flow coef. vs power coef. at inlet pressure of 45 psia, but pressure ratios of 0.32, 0.39, and 0.44 130

Figure 7.12 ZS-1 Terry Turbine flow coef. vs power coef. at inlet pressure of 60 psia, but pressure ratios of 0.24, and 0.29 131

Figure 7.13 ZS-1 Terry Turbine flow coef. vs power coef. at inlet pressure of 30 psia but steam qualities of 1.0 and 0.25, and pressure ratios of 0.49, 0.59, and 0.67 (NHTS Data) 133

Figure 7.14 ZS-1 Terry Turbine flow coef. vs power coef. at inlet pressure of 45 psia but steam qualities of 1.0 and 0.25, and pressure ratios of 0.34, 0.39, and 0.44 (NHTS Data) 134

Figure 7.15 ZS-1 Terry Turbine flow coef. vs power coef. at inlet pressure of 60 psia but steam qualities of 1.0 and 0.25, and pressure ratios of 0.24, and 0.29 (NHTS Data) 135

Figure 8.1 Illustration of time series data samples (circular markers) and the sliding window t-values (cross markers) where the t-values in the current analysis represent the turbine rotational speed. [33] 137

Figure 8.2 ZS-1 Turbine standalone performance at the same turbine rotational speed. 139

Figure 8.3 ZS-1 Turbopump turbine speeds at the same pump outlet flowrate. 140

LIST OF TABLES

Page

Table 4.1. Alignment Sheet 63

Table 4.2 Cooling tower technical specification [24] 72

Table 8.1 Data qualification criteria 136

Table 8.2 The uncertainty values in a number of measured values in the turbine standalone mode 142

Table 8.3 The uncertainty values in a number of measured values in the turbine Turbopump mode 143

Table 8.4 Derived measurement uncertainty 144

Table C.1 List of valve functions, locations, and operational status 177

Table D.1 Steam Testing Matrix, Dry Steam 192

Table D.2 Steam Testing Matrix, Wet Steam, x = 0.9 195

Table D.3 Steam Testing Matrix, Wet Steam, x = 0.65 198

Table D.4 Steam Testing Matrix, Wet Steam, x = 0.25 201

Table D.5 Steam Testing Matrix, Wet Steam, x = 0.05 204

Table F.1 ZS-1 Air tests (NHTS data) 216

Table F.2 ZS-1 Air Tests (Turbolab) [32] 217

Table G.1 GS-2 Terry Turbine air tests results from the Turbolab [25] 218

Table G.2 Power Plant RCIC system performance at different operating pressure 220

1. INTRODUCTION

1.1. Fukushima Accident

In 2011, an exceptionally powerful earthquake of magnitude 8.9 hit the east coast of Japan. More than 18,400 people were missing or dead and cities were destroyed or devastated [1]. Nuclear power plants in those areas were no exception, as the Fukushima Daiichi Nuclear Power Plant was severely affected. The earthquake spawned tsunami waves (up to 15 meters high) which greatly exceeded the sea wall height and submerged the lower parts of the reactor buildings. The Emergency Diesel Generators (EDG) failed and all the offsite power was lost as well. The plant, as a result, was left in an "on-site and off-site station blackout". Consequently, the emergency cooling systems failed in Units 1, 2 and 3. Unit 4 had been previously defueled, meaning that all that unit's fuel was in the Spent Fuel Pools (SFP) and not subject to similar loss of cooling events. Units 5 and 6 were in cold shutdown and were reconfigured after the tsunamis to enable sufficient core cooling, thereby avoiding core damage.

Despite the extremely dearth conditions, investigations found that one cooling system in Units 2 and 3 had performed remarkably well, far beyond its design operating conditions: The Reactor Core Isolation Cooling (RCIC) System [2].

1.2. Reactor Core Isolation Cooling (RCIC) system

The RCIC System is one of the systems important to safety that is deployed in 20 Boiling Water Reactors (BWRs) in the U.S. Figure 1.2 shows a schematic diagram of the RCIC System in a BWR with the containment type Mark I; Fukushima Daiichi Unit 2

and Unit 3, referred to as 1F2 and 1F3, employed this design. The system, which is intended for reactor isolation events, is designed to provide cooling water to the Reactor Pressure Vessel (RPV) by utilizing the steam generated by decay heat in the reactor and flowing through the Main Steam Line (MSL) to run a Terry turbine-driven pump [3]. The pump suction is the Condensate Storage Tank (CST), shown in Figure 1.2, and later from the Suppression Pool (SP), that is the doughnut shaped tank shown in Figure 1.1. Both tanks perform as a water source for the RCIC System. The Terry turbine design is resilient even with two-phase ingestion [4], which is believed to have occurred due to RPV water spillover during the Fukushima accidents.

Investigations reported that damage to Unit 2 was less serious than to Units 1 and 3 due to the extended operation of the RCIC System [2]. The RCIC System is set to trip at a specified RPV water level to prevent water spillover into the Main Steam Line. However, due to the loss of electrical power, high RPV water level did not cause a RCIC System trip and the turbine is believed to have operated under two-phase flow conditions for much of the first 68 hours of the accident [2]. The potential for operation under two-phase conditions and without functioning RCIC turbine controls has generated interest in knowing the true operational limits/margins for RCIC Systems. Currently, there is no information available regarding the quality of the steam/water mixture at the RCIC turbine inlet or its effect on turbine performance during the Fukushima accidents.

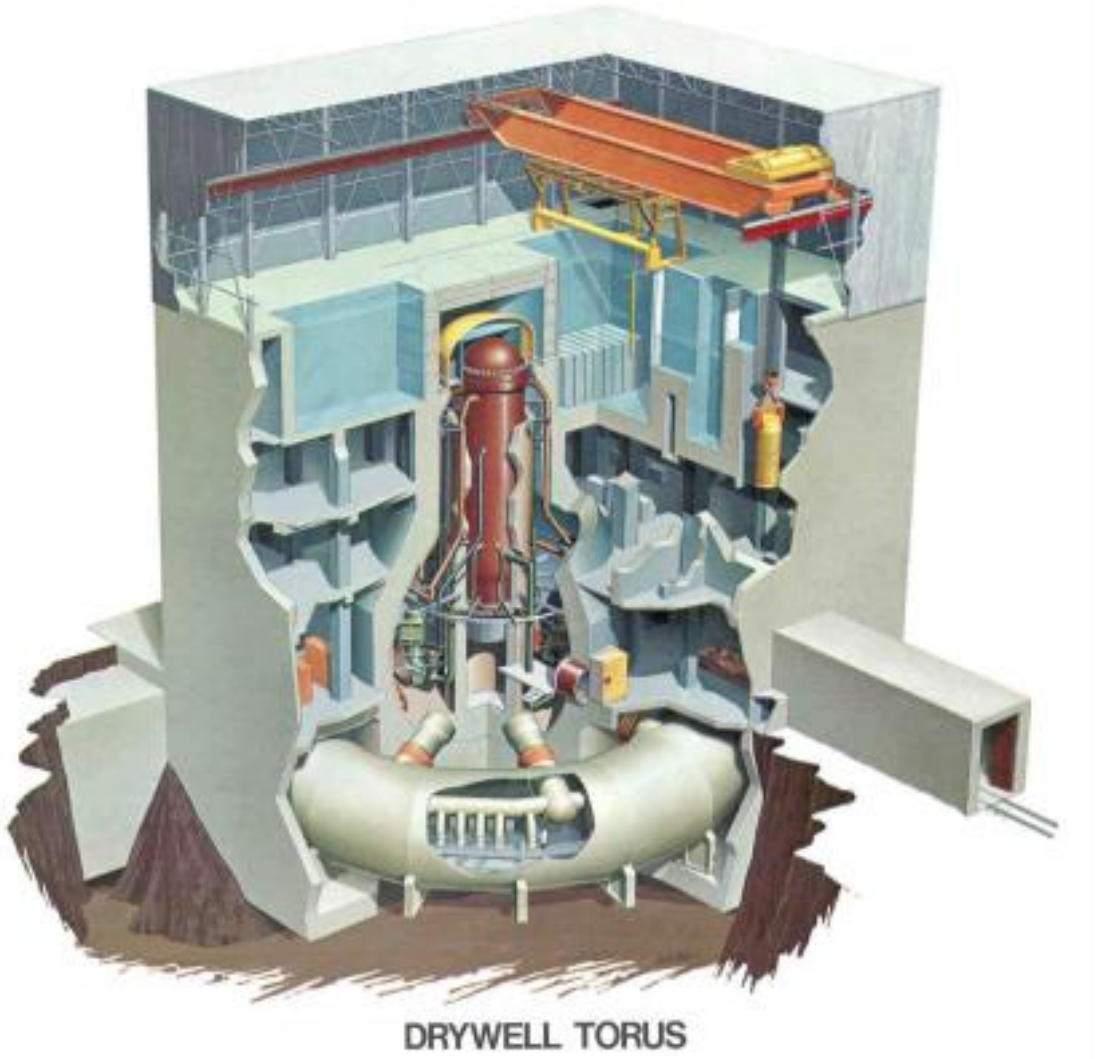

Figure 1.1 BWR Mark I Containment [5]

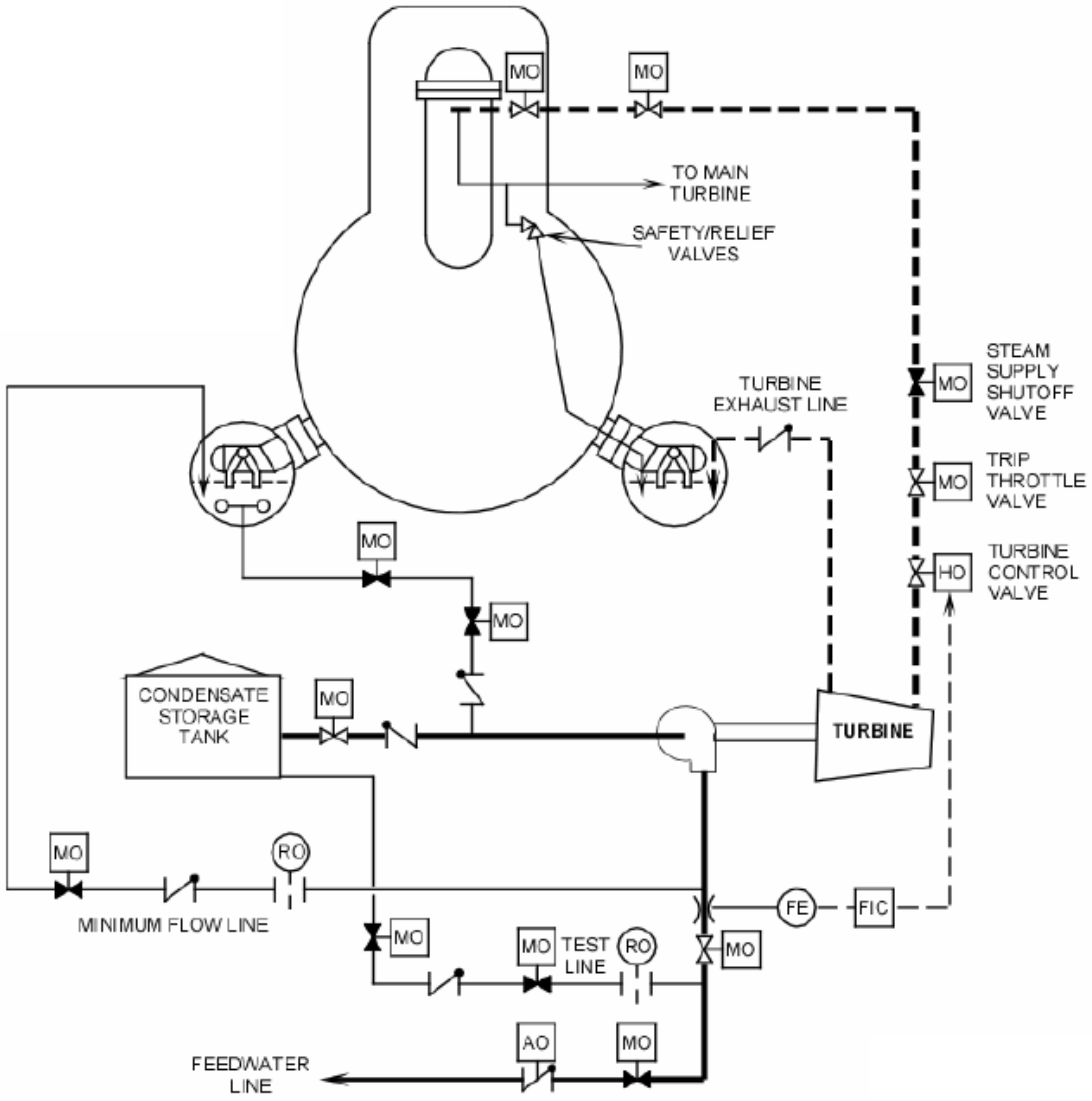

Figure 1.2 Schematic diagram of the RCIC System in a BWR with the Mark I containment [6]

1.3. Terry Turbine

The Terry Turbine is a single-stage, compound-velocity, impulse turbine that was introduced to the market by the Terry Steam Turbine Company. It was designed for waste steam applications due to the following merits [4],

1- Low or atmospheric operating pressure within the turbine casing;

2- Flexible, resilient operation under off-normal operating conditions (i.e., water slug injection); and
3- Low maintenance needs.

The steam is admitted to the turbine through nozzles installed on the steam ring. Those nozzles redirect the steam from being coaxial to the turbine wheel to being tangential to the wheel "buckets", machined semi-circular volumes that are shaped into the body of the wheel. This flow path maximizes the steam impulse. The steam then completely expands before impinging upon the buckets. The steam expansion process converts the steam thermal energy to kinetic energy that produces the impulse on the turbine wheel. The nozzle is 3-5 buckets away from the wheel edge so that a "reversing chamber" can receive the steam and redirect it back to the wheel buckets, forming the compound velocity configuration. The reversing chambers are attached to the inside wall of the turbine's casing, as shown in Figure 1.3, and have hemispherical, secant-shaped holes to allow for steam final exhaust. Such a process maximizes the energy extraction from the incoming steam as seen in Figure 1.4.

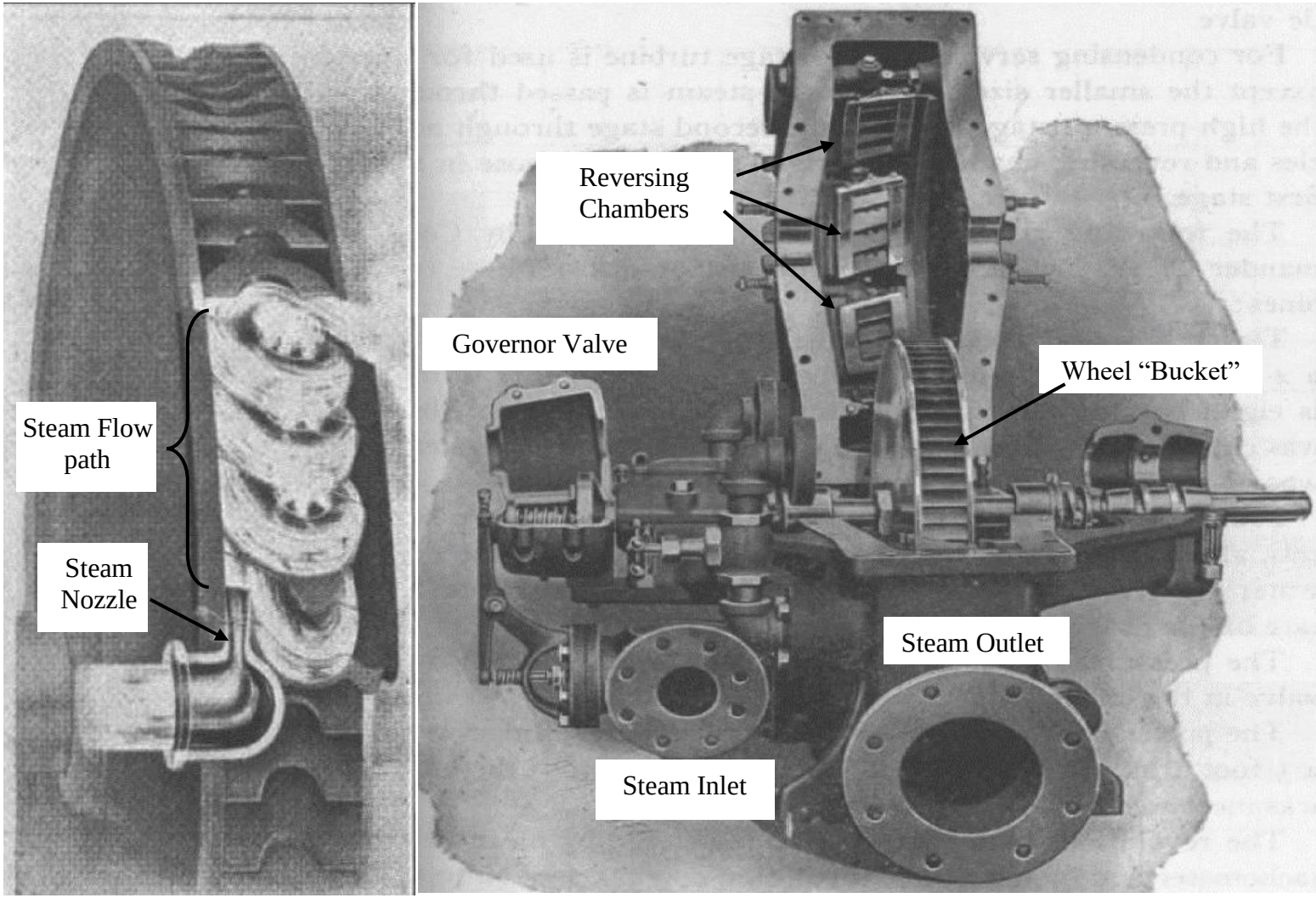

Figure 1.3 (Right) Terry turbine cross-sectional view. (Left) The steam flow path through the steam nozzle[5]

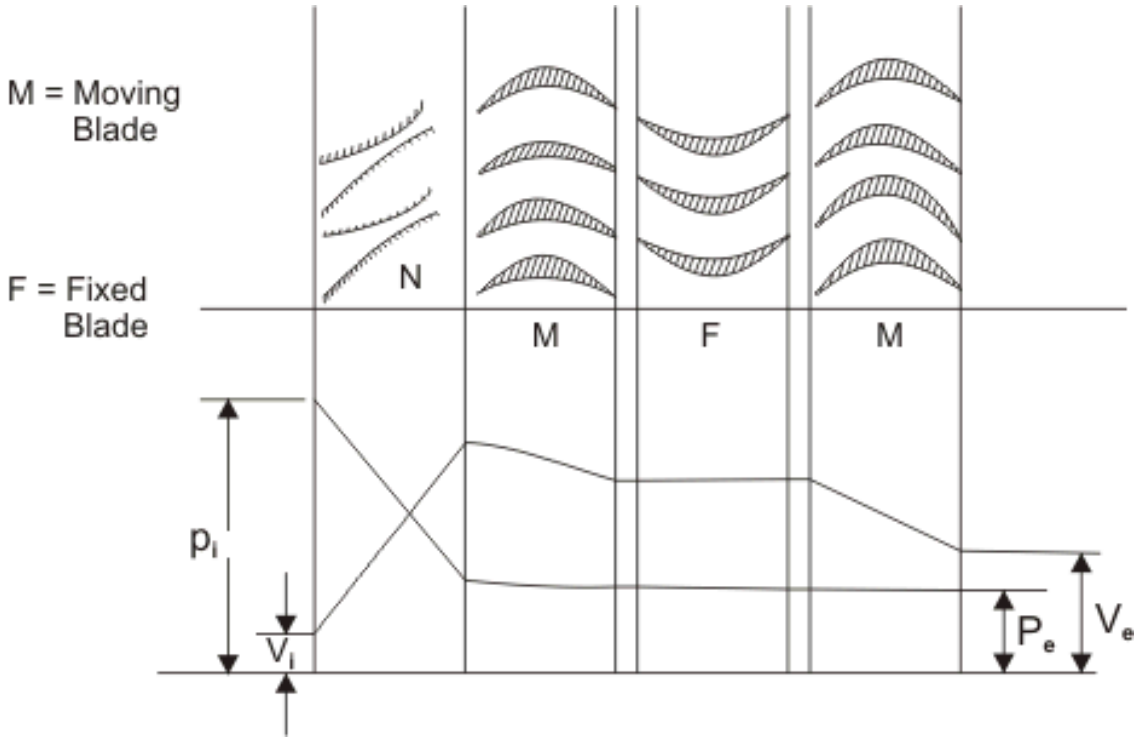

Figure 1.4 Compound velocity feature in the impulse turbines [7]

Unlike Terry turbines, reactive turbines undergo steam expansion within moving blades that acts like steam nozzles. Figure 1.5 shows the steam static pressure and absolute velocity profile within the turbine. In general, reactive turbines have slightly higher efficiency compared to impulse turbines at the same thermal energy drop. However, Terry turbines requires less manufacturing cost, which makes them competitive.

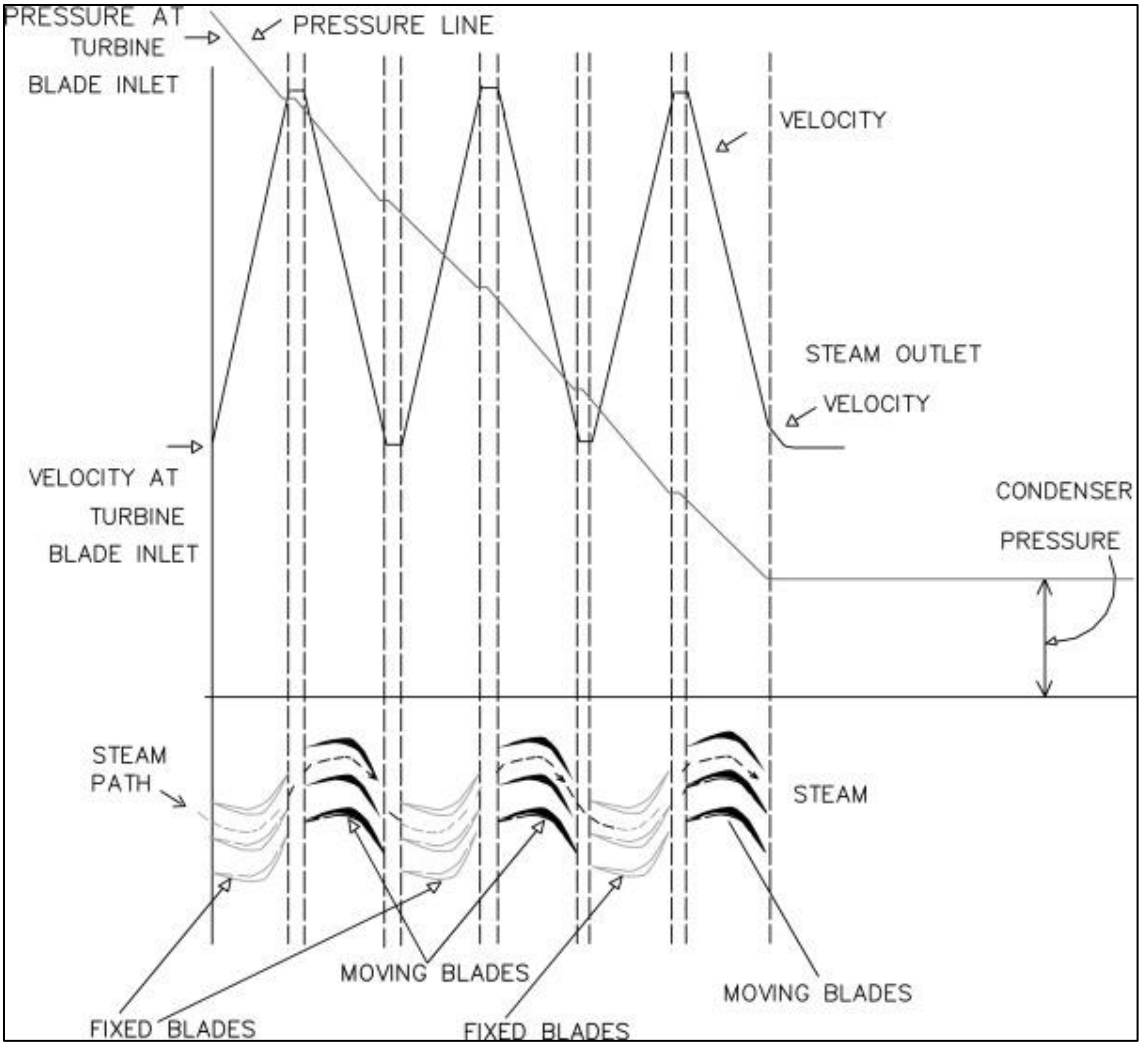

Figure 1.5 Reactive turbines velocity and pressure profile inside the blades [8]

Over 20 U.S Boiling Water Reactors use the model “G-series” Terry Turbines for their RCIC system. The letter G stands for the wheel size of 24inch wheel diameter. While the letter Z stands for the smaller version of these turbines at a size of 18-inches wheel diameter. The letter “S” in some models, stands for the casing material of steel. The model name includes number 1 or 2. Number 1 stands for steam nozzles in the

bottom of the casing only, whereas the number 2 stands for steam nozzles in the bottom and top of the casing.

The team expansion is assumed to be isentropic, which implies adiabaticity environment [9]. Thus, the turbine has been insulated to minimize any heat losses and protect the lab personnel from being exposed to high temperature surfaces, like the turbine casing.

2. DISSERTATION OVERVIEW

2.1. Problem Statement

Prior to the Fukushima accident, RCIC system operational limits were based on manufacturers data, in which the efficiencies for the turbine and pump were estimated assuming ideal behavior of the turbomachinery. Moreover, the system capabilities under Beyond Design Basis Event (BDBE) conditions were evaluated according to conservative Probabilistic Risk Assessments (PRA). In response to the current lack of knowledge and poor understanding of RCIC system performance, the current research investigates the Terry turbine performance under BDBE conditions using steam-water mixtures. Given that the system operation far exceeded design capabilities, a better understanding of RCIC operational limits will enable BWR plants to take better advantage of the system and can lead to enhanced safety of the current BWR fleet.

2.2. Objectives

The following are the main objectives of this research.

- Perform a set of characterization tests to examine the turbine performance as a single component at different inlet and back pressures and steam inlet qualities of 0.05-1.0.
- Investigate the turbine-driven pump potential at BDBE operating conditions based on turbopump tests at different inlet and steam qualities of 0.3, 0.7, and 1.0.

- Perform dimensionless analysis of the turbine performance to explore the scalability potential between the ZS and the GS series of Terry Turbines and between air/water and steam/water turbine inlet mixtures in Terry Turbines.

2.3. Motivation

Several motivations for this work exist. The development of a systems-level model to accurately model and simulate the principal operation of the RCIC system for DBDEs is critical to understand the available safety margins. The RCIC system is driven by a Terry impulse turbine, and there is a scarcity of data for BDBE performance of a Terry Turbopump for steam and steam-water conditions. Thus, these tests serve to expand the available database for model development, validation and verification, and dimensional analysis, in a cost-effective manner without the potential of severely damaging a nuclear grade GS-series Terry Turbopump. Moreover, the results will be used to investigate whether there is more safety margin in RCIC Systems than previously thought.

These ZS-1 tests will also inform proposed full-scale experimental design and testing. The tests described herein will be conducted at conditions as close as possible to those which were recorded during operation of plant RCIC systems and will therefore provide essential data for scaling from small laboratory sizes up to full-scale RCIC system size. Toward that end, a complete set of nondimensionalized characterization of the ZS Terry turbine has been performed at different steam inlet pressures, back pressures, and steam qualities.

2.4. Significance of Research

The current steam-water data set is considered a first-of-a-kind to explore the RCIC system potential for expanded operation under Beyond Design Basis Events. In particular, Terry Turbine two-phase flow performance is investigated experimentally at three turbine inlet and back pressures. Air tests were also performed to benchmark against a previous data base of air and air-water data by Patil et al. [10] and to establish scalability between air-water and steam-water mixtures.

2.5. Technical Approach

The Terry Turbine Characterization Tests has been conducted in two running modes, the turbine-dyno (stand-alone) and turbine-pump (i.e., Turbopump).

In the stand-alone mode, the turbine steady-state response tests are conducted with a dynamometer coupled to the Terry turbine on the turbine shaft. The torque vs. shaft rotational speed is recorded at a variety of turbine inlet pressures of 30-60 psia, backpressure at 14.6 (atm), 2 psig, and 5 psig, and steam qualities of 0.05-1.00. The steam is generated in a 135-gallon pressure vessel that is equipped with six electric heaters and a moisture separator to provide up to 115 psig dry steam. The steam outlet pressure is maintained using an automated control valve. The turbine inlet steam quality is adjusted by another automated control valve that regulates the water injection flowrate into the main steam line, based on the flow rate and thermodynamic properties of the steam (i.e., steam pressure, temperature, and enthalpy) at the turbine inlet. The IAPWS (International Association for the Properties of Water and Steam) Industrial Formulation 1997 for the Thermodynamic Properties of Water and Steam has been coded via C++

programming language before integrated to LabVIEW. A load cell has been attached to the dynamometer arm to measure hydraulic resistive force, which used to obtain the associated torque value. The dynamometer is also used to control the turbine rotational speed through controlling the dynamometer inlet and outlet water flow rates via control valve and hose clamps (manual adjustment) at the inlet and outlet lines, respectively.

In the turbopump running mode, the assembly steady-state response will be investigated by measuring the pump volumetric flow rate vs. head at a variety of turbine inlet pressures, backpressures and steam qualities. To do this, the turbine is coupled to a multistage centrifugal pump, as in the RCIC System. The pump has five stages. While the turbine inlet pressure and back pressure are controlled the same as in the turbine characterization tests, the turbine speed and shaft torque measurement will be different. A torque meter has been coupled on the same shaft with turbine and the RCIC pump. A flexi coupling is used for safety reasons. A control valve downstream of the pump outlet line is used to regulate the pump loading on the turbine shaft, which, theoretically, could affect the turbine speed.

Throughout these tests, a small-scale Terry ZS-1 turbine is used to create a basis for a scientific understanding of a full-scale GS-series Terry Turbopump in a cost-effective manner. The turbine has an 18-inch diameter wheel and a single converging-diverging steam inlet nozzle installed, with a throat diameter of 0.38 inches. In comparison, the GS-series has a 24-inch wheel, five or ten nozzles depending on the turbine, and a larger throat diameter around 0.584 inches.

3. EXPERIMENTAL FACILITY

3.1. Overview

Conduct of experiments required redesigning and constructing a new piping system at the Laboratory of Nuclear Heat Transfer System (NHTS).

The major components, as shown in Figure 3.1, are a steam generator, a steam turbine, centrifugal pumps, and a pressure vessel, which in total simulate the Suppression Chamber of a BWR Mark I containment. A heat rejection system was designed and deployed to enable long-term steam-water tests. The new Data Acquisition (DAQ) system features feedback control, a greater amount of instrumentation, and recording of additional quantities including turbine vibration.

Figure 3.2 shows the experimental facility that was built to perform two-phase flow testing. A steam flow is supplied from the 157-kW heating power steam generator. A 5-stages centrifugal pump (P-1) is used to inject the water into the Main Steam Line (for different steam qualities) through the Water Injection Line. The two-phase mixture (if any) flows into the turbine through the Turbine Steam Admission Valve (V-33) and exhausts to the Suppression Pool through the Turbine Exhaust Valve (V-38). A five-stage centrifugal pump (different than P-1) serves as the RCIC pump to return water back to the Main Steam Line/ Suppression Pool tank. The Feedwater pump (P-1) returns water back to the steam generator based on the steam flow rate in the Main Steam Line. Such analogy has been adapted to avoid water level decrease below the top of the steam generator electric heaters due to potential shortage in RCIC pump outlet flowrate. The

line thickness in the Figure 3.1 reflects the actual piping diameter. For example, if the line thickness in the Visio file is 1.5 pt., it means that pipe diameter is 1.5".

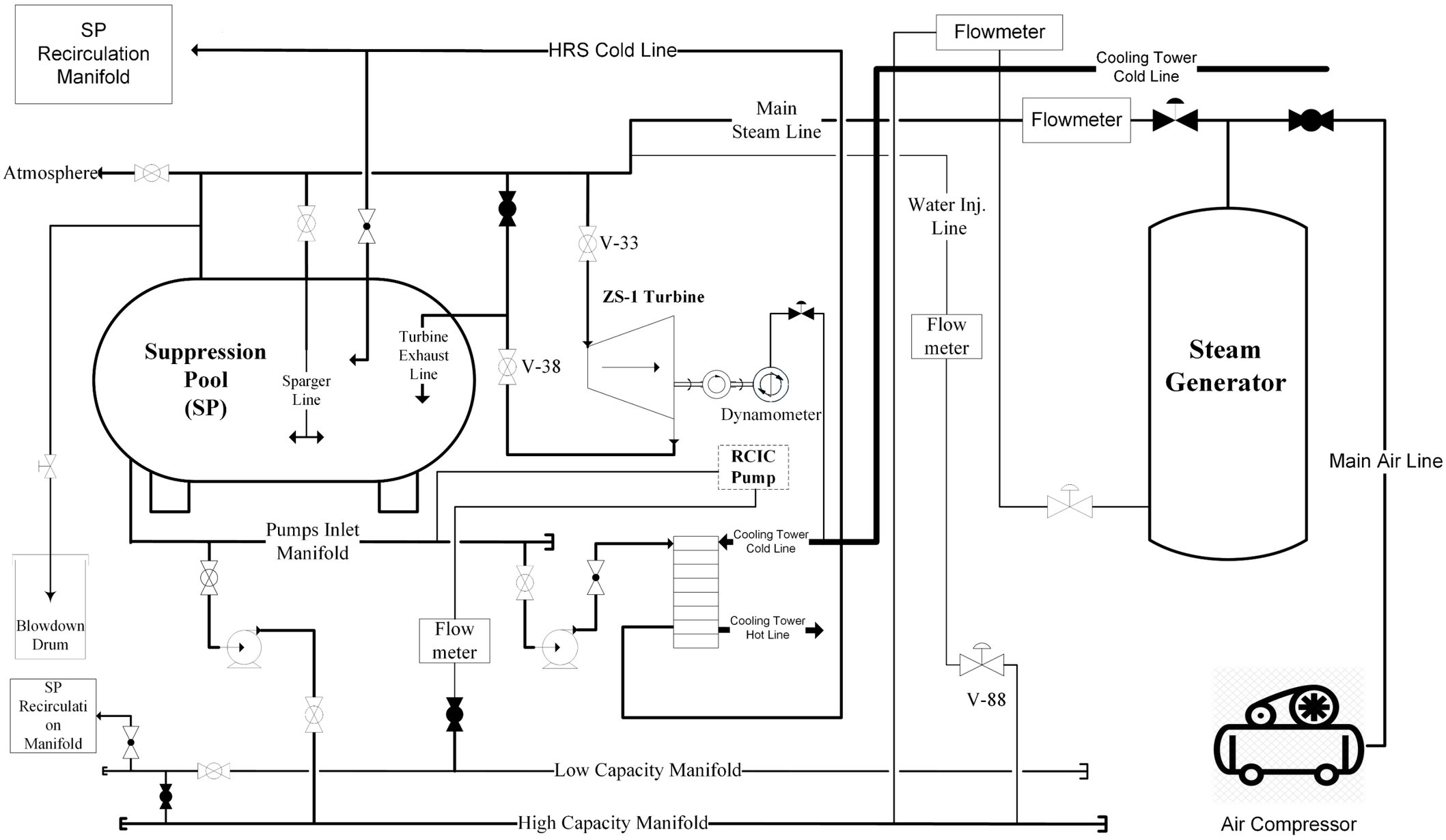

Figure 3.1 Facility Flow diagram for the Turbine Characterization Tests

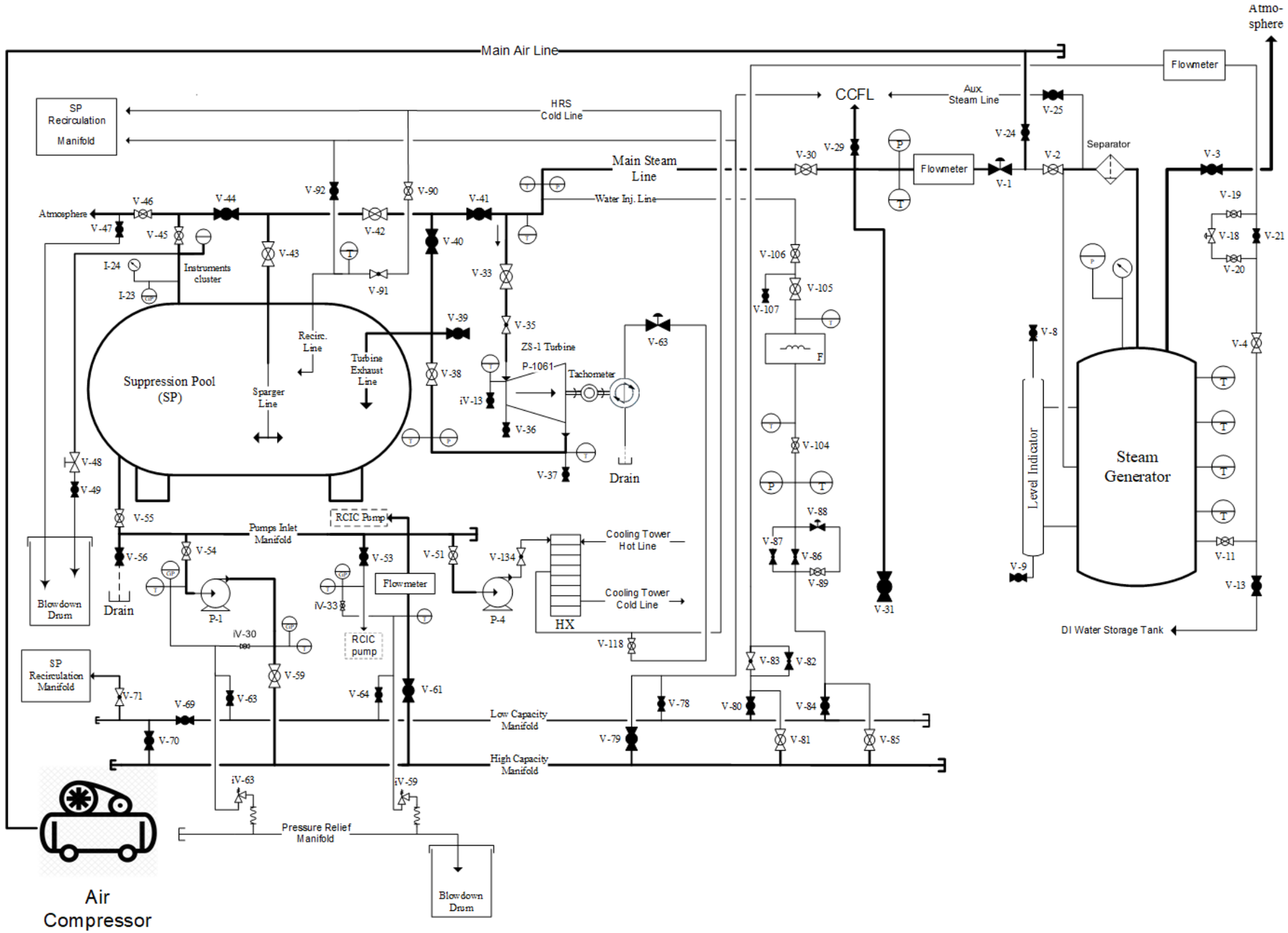

Figure 3.2 P&ID of the Experimental Facility

3.2. Steam Generator (SG)

Throughout the course of experiments, the steam is generated in a pressure vessel that is equipped with electric heaters and a moisture separator to provide up to 115 psig dry steam at the outlet. See Figure 3.3. The Steam Generator safety relief valves (iV-110 and iV-111 shown in Figure 3.4) are set to open at 115 psig which is a little lower than the corresponding 118 psig saturation pressure of the Steam Generator design temperature value of 350 ^{o}F. It should be noted that bringing the Steam Generator pressure (during operation) higher than the Feedwater line pressure will cause back flow in the Feedwater line.

The demi water (i.e., demineralized water) is heated to power level from 2 kW to 157 kW (full power) through six immersion electric heaters planted at different levels, thus allowing fine control of the outlet steam pressure and flow rate. It's recommended to keep the lowest heaters on while turning the top ones off to enhance temperature distribution throughout the tank through water natural circulation due to bouncy. It's also recommended to use Heater#4, 5 and 6 to regulate the Steam Generator power while using the Heater #1 and 2 (at least Circuit #1) for base heat load.

The steam outlet flow rate is adjusted using the control valve (V1) through the LabVIEW main display panel. Two check valves and an air filter have been connected to the Steam Generator sidewall to prevent vacuum formation in the Steam Generator vessel.

The water level, shown on the Steam Generator water level indicator, must always be above 50 cm (24 inches) to ensure the Steam Generator heaters won't be

uncovered during operation. However, the Feedwater flowrate from the suppression pool is regulated to compensate for the water level drop in the Steam Generator tank because of steam generation. The feedback logic in the feedwater control valve is based on the Main Steam Line flowrate, downstream the main control valve. The Suppression pool water level should be slightly over half-full prior to testing to ensure enough hydrostatic head for the Feedwater pump.

A water treatment station is used for demi water production. The station main components, as shown in Figure 3.4, are an activated carbon prefilter, cartridge pre- and post- filters and two mixed-bed resin tanks in series. The water treatment station is installed on a portable cart to allow for water treatment in the Suppression Pool tank.

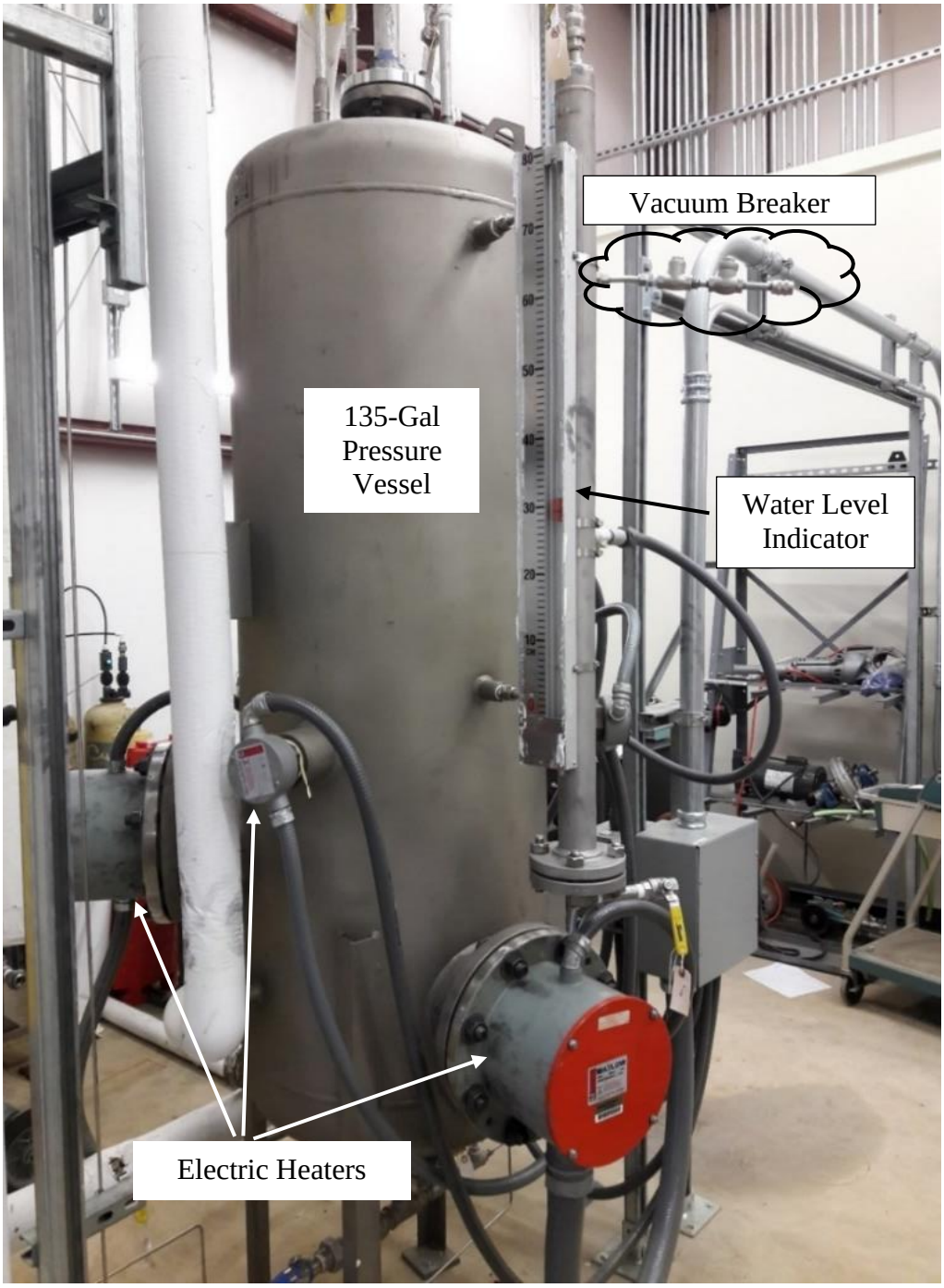

Figure 3.3 Steam Generator with visual water level indicator

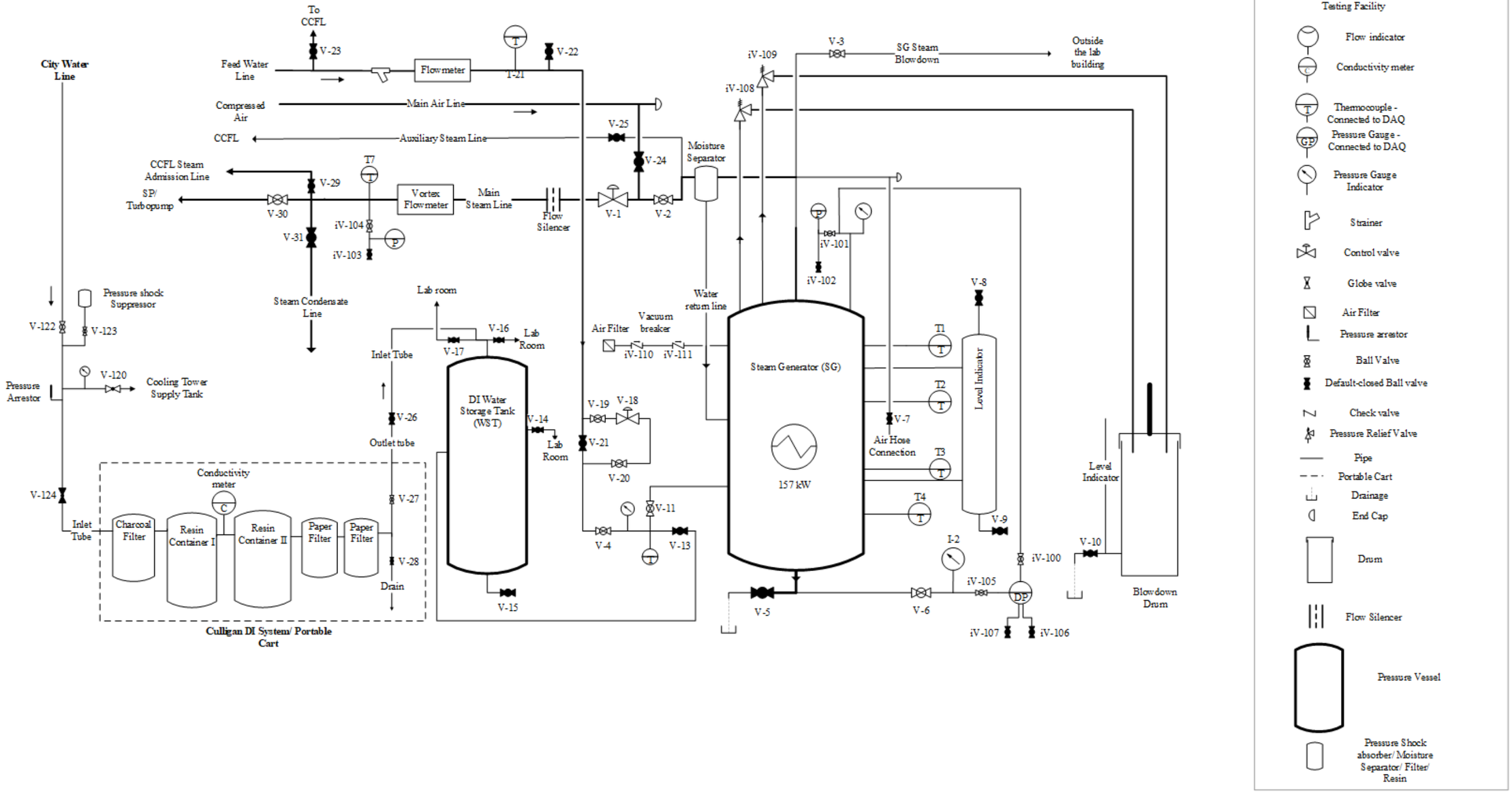

Figure 3.4 P&ID of the Steam Generator and city-water treatment station

3.2.1. Electric Heaters

The heaters different power capabilities (from 2 kW to 25 kW) allow for fine and coarse control of the steam outlet pressures and flowrates. Figure 3.5, below, shows the electric panel at the NHTS facility that includes the heaters switches. Figure 3.6 shows the u-tube shaped immersion heaters inserted through flange necks on the Steam Generator side walls. The Steam Generator heater flange bolts should be fastened periodically at 180 in-lbs. torque.

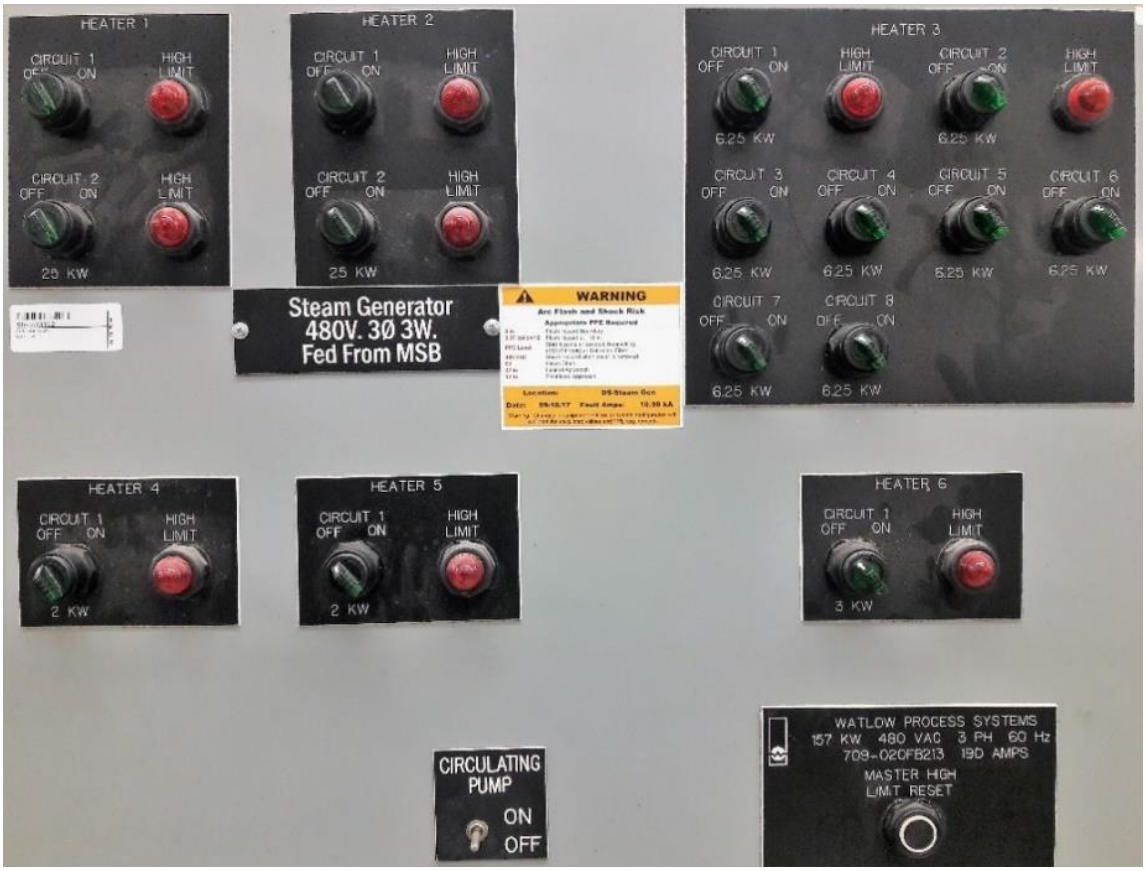

Figure 3.5 Heater control panel

Figure 3.6 The u-tube shaped immersion heaters for the Steam Generator

3.2.2. Moisture Separator

The moisture separator, shown in Figure 3.7, is mainly used for removing water droplets in the steam, the removed water is directed back to the Steam Generator through the water return line.

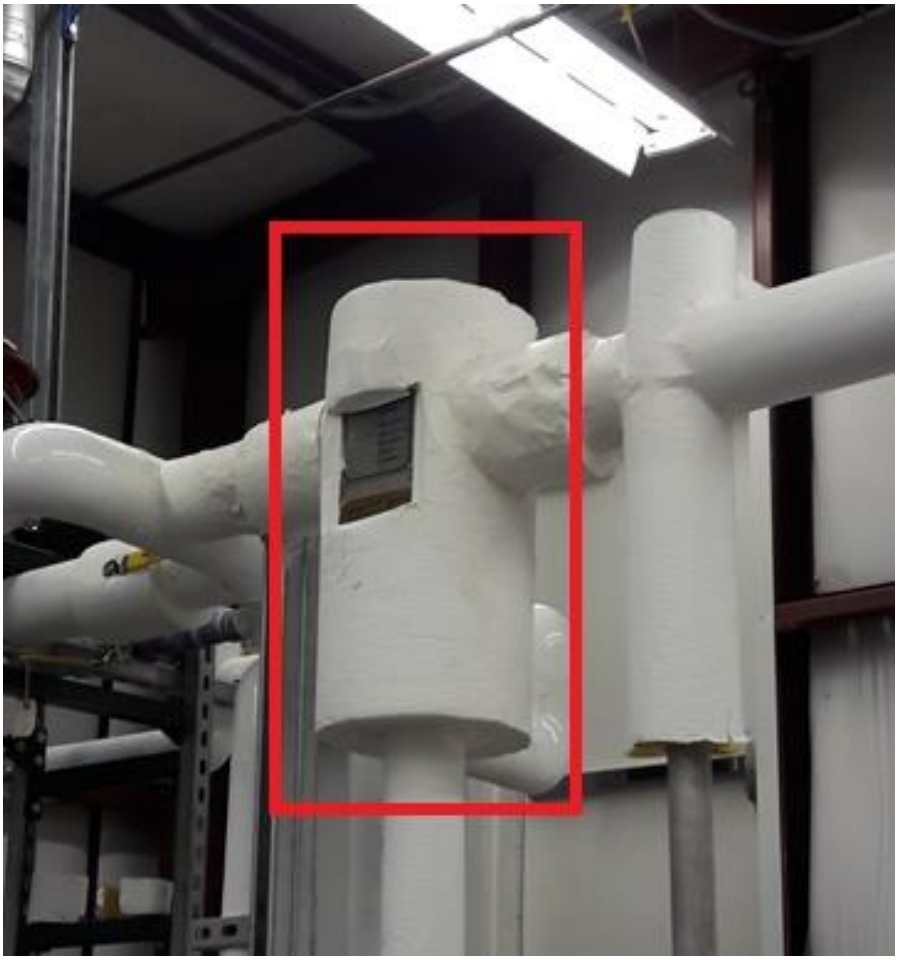

Figure 3.7 Separator downstream of the steam generator outlet

3.3. Main Control Valve

An automatic control valve is installed on the Main Steam Line downstream of the Steam Generator outlet to control the steam flow rate, as shown Figure 3.8

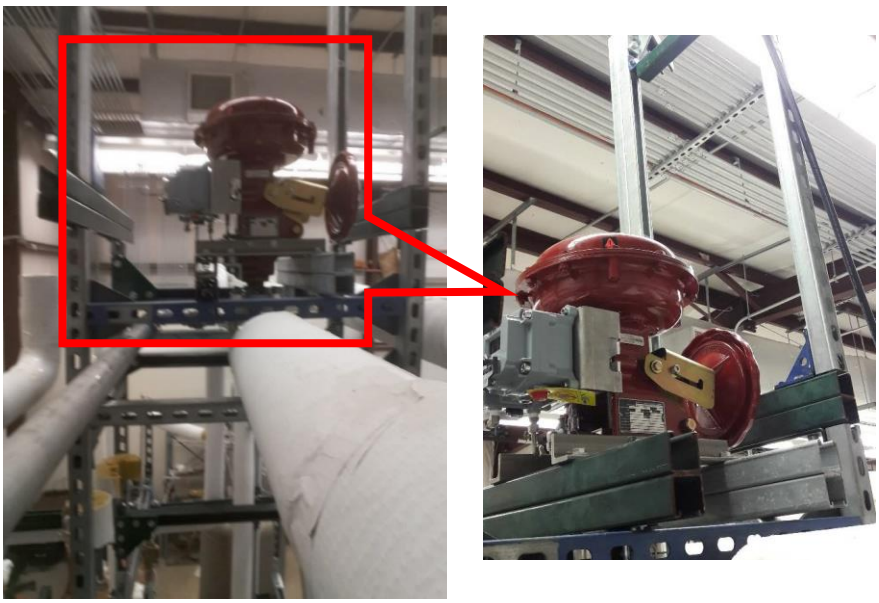

Figure 3.8 Main Control Valve (V-1)

3.4. ZS-1 Terry Turbine

Figure 3.9 shows the major component of the RCIC system: the ZS-1 Terry turbine. During the stand-alone testing mode, the turbine was coupled with a dynamometer to measure the turbine shaft power output under various boundary conditions. Similarly, a 5-stages centrifugal pump was coupled on the same turbine shaft, during the integral testing mode, to obtain the turbopump horsepower curve.

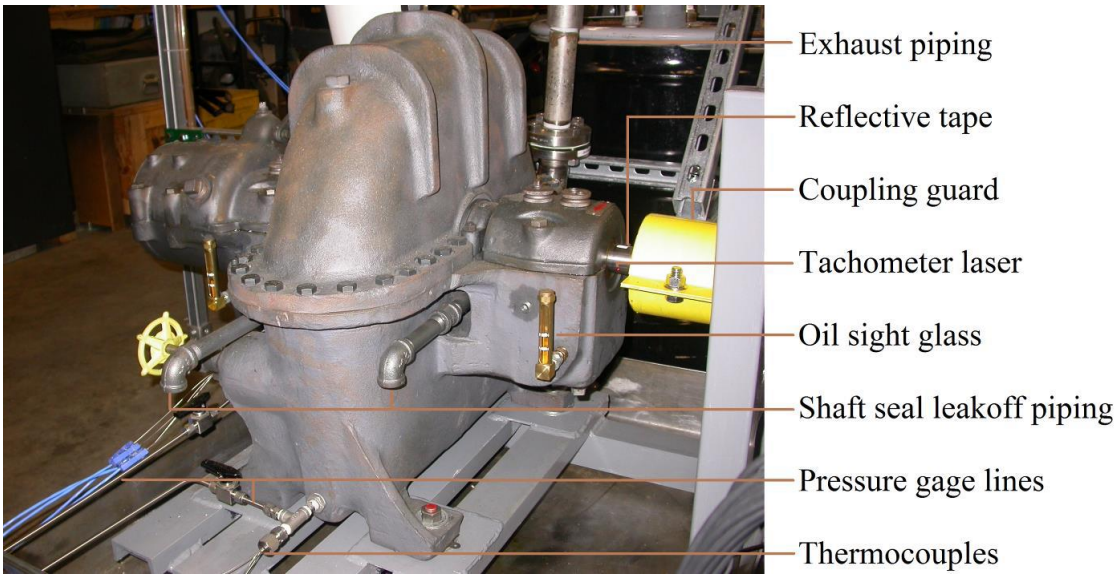

Figure 3.9 ZS-1 Terry Turbine [11]

The Terry turbine wheel has crescent-shaped bucket cuts as shown in Figure 3.10. When the high velocity steam flows into the turbine, the steam velocity decreases as it passes every bucket. The resulting increase in steam volume requires a progressively larger volume to accommodate the expanded steam. To avoid this, the crescent holes were added to release a portion of the expanded steam and thus reduce the volume in proportion to the lower velocity.

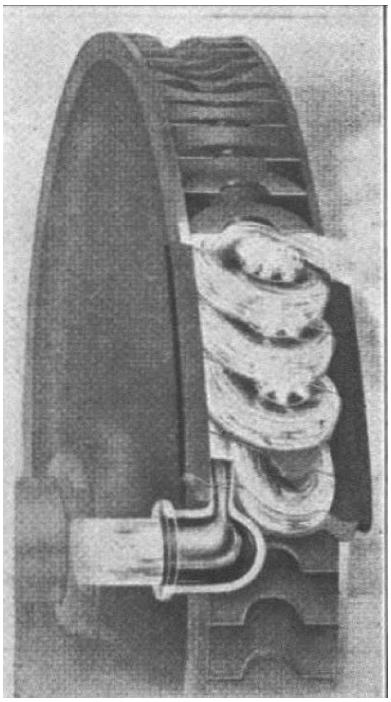

Figure 3.10 Turbine wheel and reversing steam [12]

The turbine wheel spins due to the impact force of the steam (or steam-water mixture) on the wheel buckets shown in Figure 3.10. In RCIC Terry turbines, reversing chambers are attached to the inside wall of the turbine's casing. Such process is to maximize the energy extraction from the steam by reversing the steam back to the wheel buckets before final exhaust through the hemisphere secant-shaped hole in the reversing chamber. Throughout these experiments, the turbine was not equipped with a governor valve trip mechanism. Instead, the main control valve (V1), acted as a governor valve. The trip mechanism that is usually based on the turbine speed setpoints is included in the current setup. The LabVIEW code is set to trip the main control valve (V1) in case the turbine reaches 4000 rpm. Moreover, a warning alarm is set to flash, then flash with beeps at 3800, and 3900 rpm, respectively.

A synthetic ISO Grade 68 turbine oil has been used for lubrication [13]. The oil level in the turbine oil wells was maintained between the two sharpie marks, shown in Figure 3.9, on the oil sight glass according to RevakKeene recommendation.

3.5. Suppression Pool (SP)

The suppression pool/chamber is shown in Figure 3.11. This a 1400-gallon stainless steel 304 pressure vessel, rated to 88 psig, 400 ^{O}F. The vessel is insulated to prevent heat loss through its walls and to provide safety to personnel from high operating temperatures during testing. The Suppression Pool tank air pressure can easily be adjusted using the Air Supply Line. With this line, the Suppression Pool tank air-pressure is adjusted to obtain the desired turbine's back pressure values. Figure 3.12 shows the detailed diagram of the Suppression Pool subsystems.

Figure 3.11 Suppression Pool front side (left) and wide view (right)

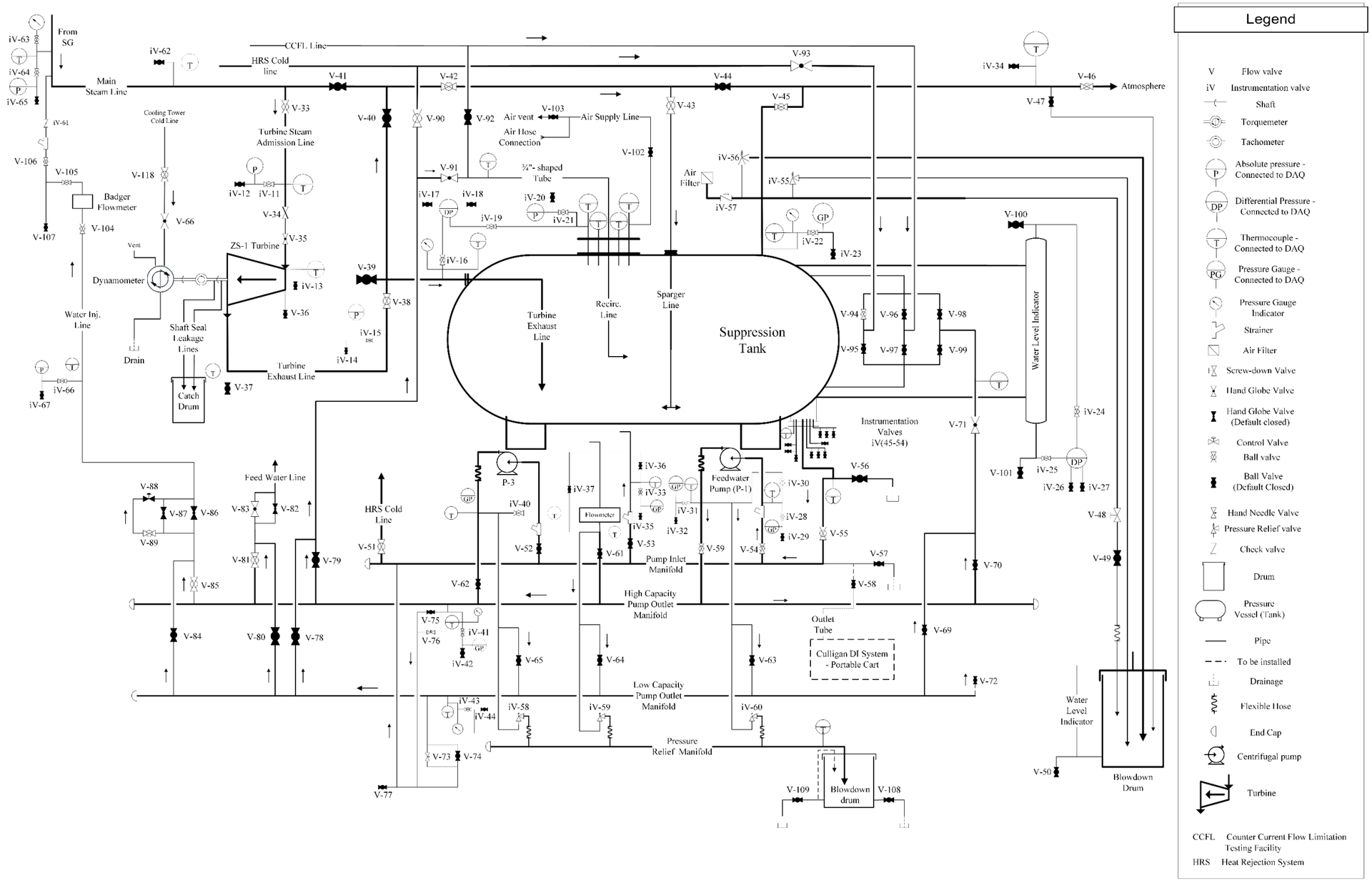

Figure 3.12 P&ID of the Suppression Pool and Terry turbine

3.6. RCIC pump analog

The vessel plays the role of the BWR suppression pool, from which a five-stage centrifugal pump is used to pump water back to the steam generator to complete the closed loop system. The pump shown in Figure 3.13 is connected to the Terry turbine on a common shaft to also serve as the RCIC system pump.

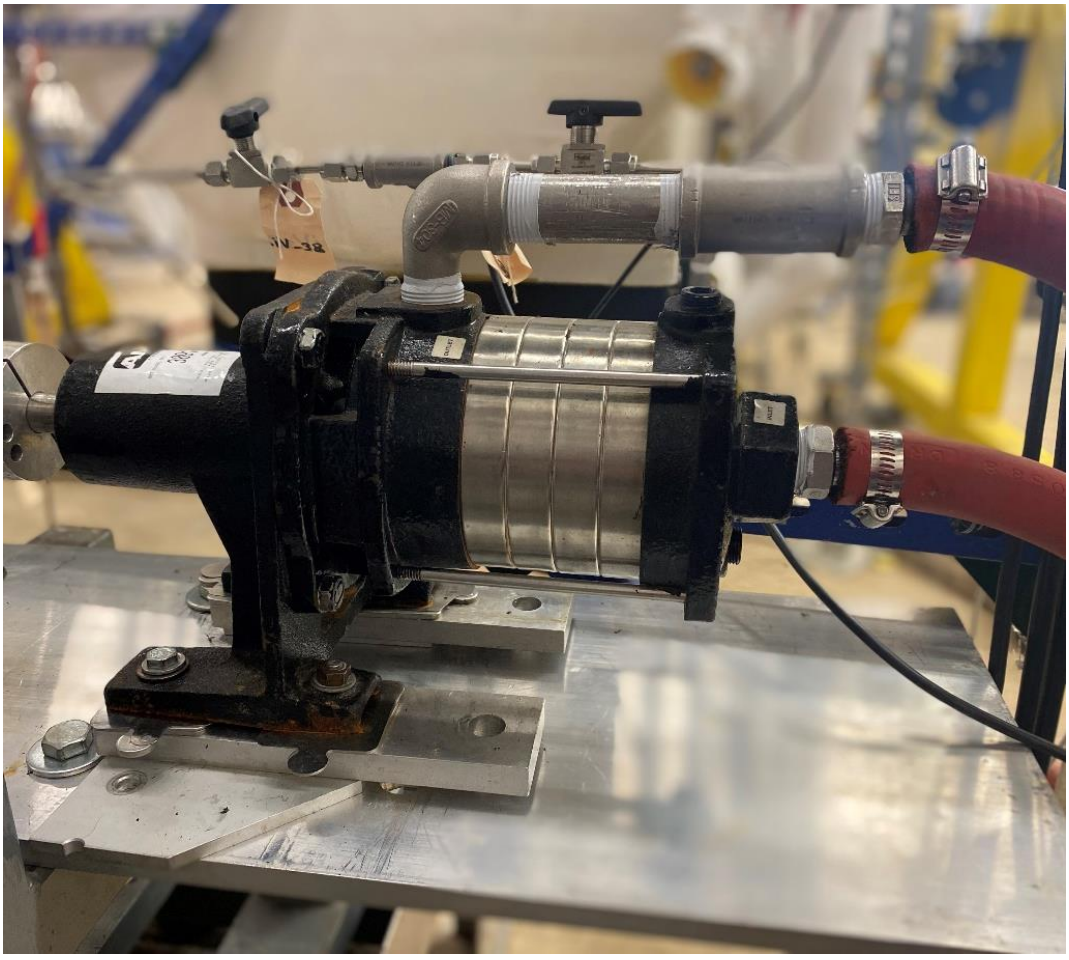

Figure 3.13 Five-stage centrifugal RCIC pump

3.7. Dynamometer

An absorption water brake dynamometer has been used throughout the characterization tests for turbine speed regulation and torque measurement. Figure 3.14 shows the XS-19 model that was used throughout these experiments. Dynamometers of this type use water flow to create controllable resistance on the turbine by adjusting the water flow through the dynamometer to match the desired load/speed. The stator load is proportional to the introduced water flowrate [14]. The stator is attached to a "Torque Arm", which transmits the resultant load to a load cell measurement of the resistive force (F). See Figure 3.15

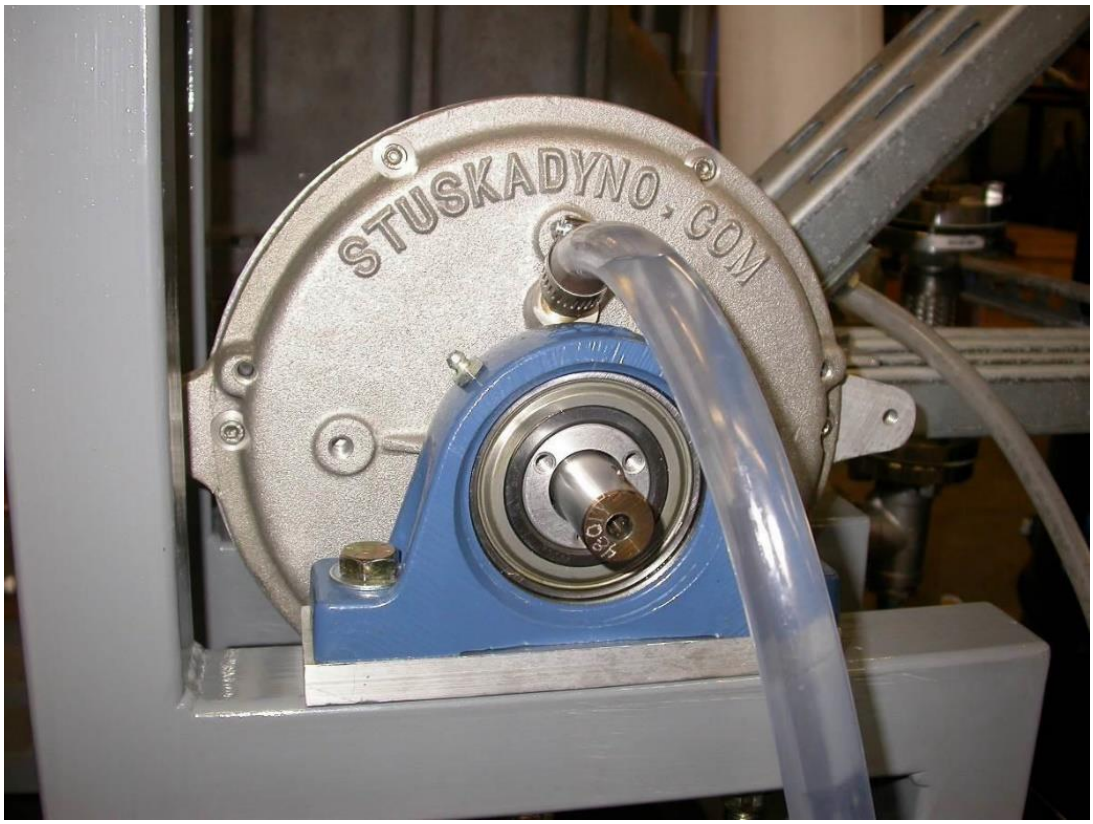

Figure 3.14 XS-19 Stuska absorption water break dynamometer [11]

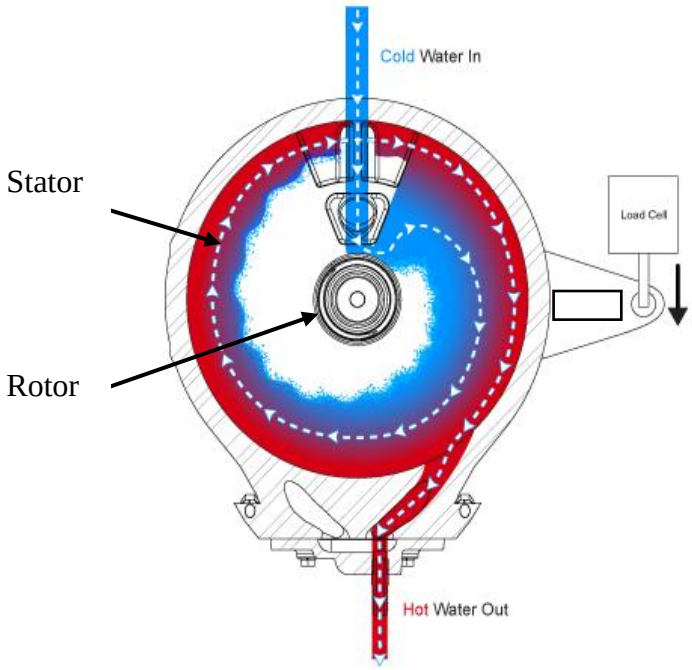

Figure 3.15 General design schematic of absorption water brake dynamometer [14]

With the torque arm length, the torque can be calculated using equation (3.1)

$$\textbf{Torque}\ (\textbf{ft.lbs}) = \mathbf{F} \times \mathbf{d} \qquad (3.1)$$

Where:

F: The force measured via Load Cell (lbs.)

d: The distance between the rotor center and the point of force application, 0.525 ft [14].

The Stuska XS-19 model was designed to handle up to 200 Break Horse Power (BHP) shaft power. However, the current test rig maximum shaft power output was about 3.5 hp at 3600 rpm, which is within the limits shown by the red triangle in Figure 3.16.

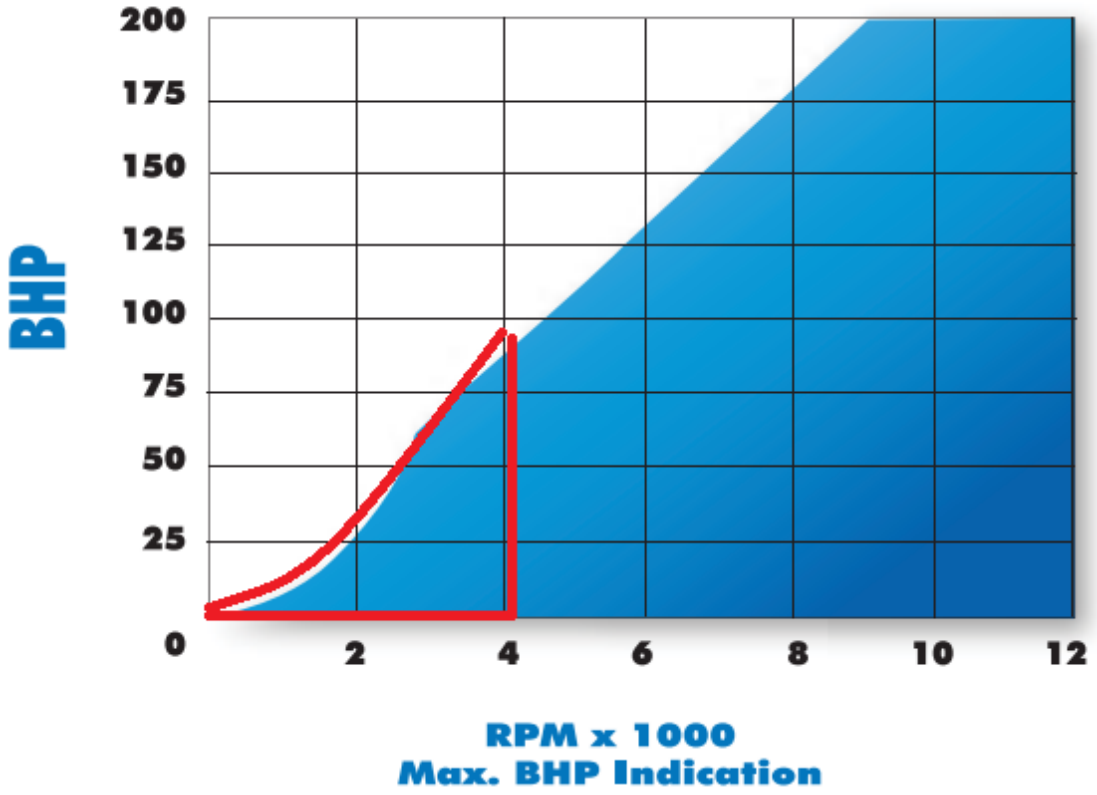

Figure 3.16 Stuska XS-19 Break Horsepower (BHP) curve [14]

The water inlet flow rate and pressure are vital in determining the water brake potential to load the turbine shaft. Water pressure should be consistent throughout operation to get a steady state loading. An important feature of the lab setup is to have the dynamometer inlet line located downstream of a water pump instead of downstream of a city water line, where pressure discrepancies were observed. On the other hand, since the size of the drain fitting affects the dynamometer unloading, the minimum size was installed to obtain the maximum loading.

3.8. Load Cell

A Stainless-Steel S-Beam load cell from Omega Engineering was used to measure the dynamometer resistive force. The model LC101-25 is a tension type, that is rated for 25 lbf maximum force measurement [15]. At higher pressure testing, the torque arm experienced higher force than 25lbf. Accordingly, a new load cell with a higher rated maximum force of 100 lbf was coupled with the dynamometer arm using the same setup, as shown in Figure 3.17.

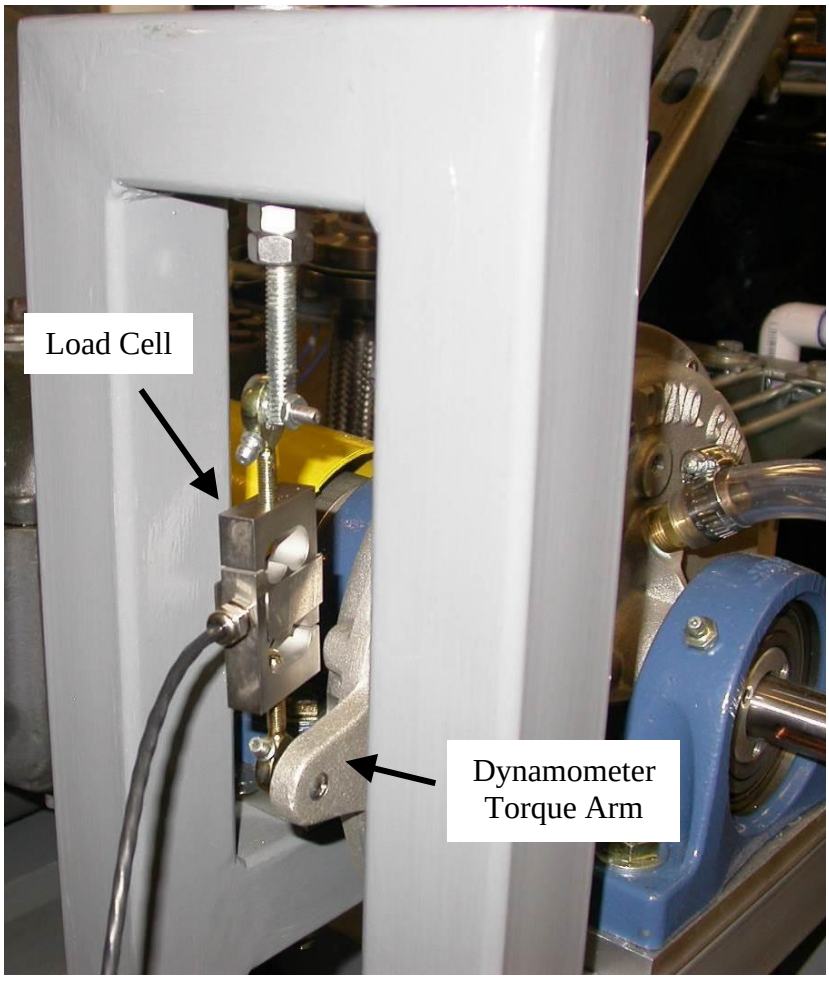

Figure 3.17 Load Cell [11]

3.9. Tachometer

The turbine rotational speed was measured and recorded using a two-component tachometer system as shown in Figure 3.18. A Monarch ROLS-W laser sensor was used to detect the frequency at which a white tape (taped on the shaft surface) crossed the laser red dot, shown on the left side of Figure 3.18. The 4-20mA signal was then transmitted to the Data Acquisition System (DAQ) through a Monarch ACT-3X signal transmitter that also served as a turbine speed display, shown on Figure 3.18.

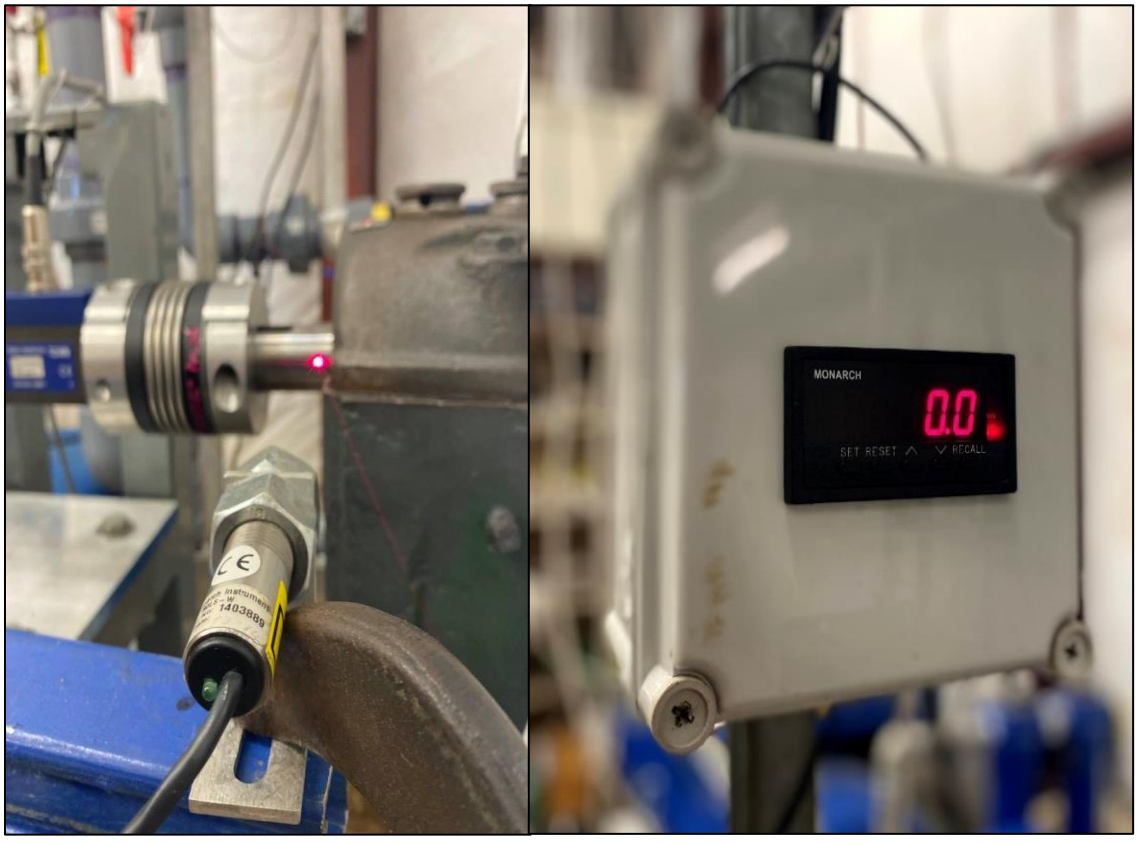

Figure 3.18 (Left) Tachometer laser sensor. (Right) Tachometer reading display

3.10. Torquemeter

For the turbopump experimental setup, the torque was directly measured by the HBM Torque Transducer (model no. T21WN/20NM). The torque meter was mounted in an upward direction as shown in Figure 3.19. The transducer signal cable pin assignment is shown in Figure 3.20. The transducer cables were connected to the DAQ via an electrical terminal block, as shown in Figure 3.21.

Figure 3.19 HBM Torque meter model no. T21WN/20NM coupled on the same shafts of the turbine and the pump.

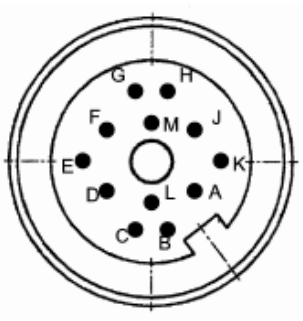

Pin	Pin assignment	Wire colour	Release calibration signal (without VK20A)
A	Torque measurement signal (frequency output; 5V)[1)2)]	BK	
B	Measurement signal speed/ angle of rotation 5 V	RD	
C	Measurement signal torque ±10 V	BN	
D	Measurement signal torque 0 V	WH	Bridge
E	Ground (supply+speed/ angle of rotation)	YE	Bridge
F	Supply voltage +10 V … 28.8 V	VT	Switch (NO)
G	Measurement signal speed/ angle of rotation 5 V, 90° phase shifted	GN	Switch (NO)
H	No function	PK	Switch (NO)
J	Measurement signal - ready for measurement	GY	Switch (NO)
K	Control signal trigger	GY/PK	Switch (NO)
L	Torque measurement signal (frequency output; 5V)[1)2)]	BU/RD	
M	Voltage reference for rotational speed/angle [3)]	BU	

Figure 3.20 The transducer connection cable pin assignment in the housing connector. [16]

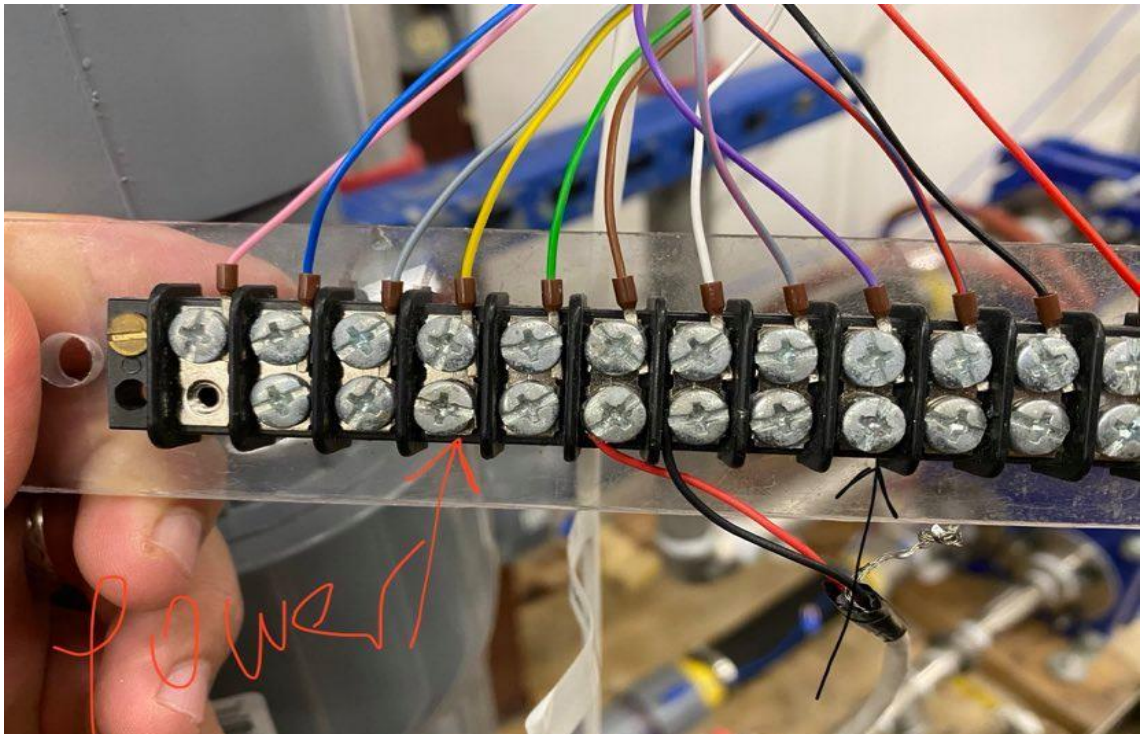

Figure 3.21 Electrical terminal block for torquemeter transducer cable connection to DAQ

3.11. Azbil/Yamataki Flowmeters

Three magnetic Azbil/Yamataki flowmeters were used to detect and record water flow rates throughout the experimental facility. A magmeter consists of two parts, the detector and the convertor shown in Figure 3.22 and Figure 3.23, respectively. The detector creates a signal related to the strength of the magnetic field generated when a conductive fluid passes through the detector. The convertor interprets the signal from the detector and converts it to a frequency signal in the range of 4-20 mA for transmission to the DAQ. The convertor also converts this signal to a volumetric flow rate which is displayed on the convertor screen. Azbil MagneW 3000 PLUS flowmeters were installed on the Water Injection Line and the Feedwater line with an Upper Range Value (URV)

of 15 GPM. However, the Yamataki Flowmeter (MGG18D-015P21LS5AAA-XX-Y/ MGG14C-CB4H-XBXX-YAH) that was installed on the RCIC pump outlet line has an URV of 20 GPM. The Foxboro Vortex Flowmeter was used to detect the steam/gas flowrate. The setup was performed by other fellow grad student, full details found on [17].

Figure 3.22 Magnetic Flowmeter detector at the water injection line. The detector has a model number of (MGG18D-015P21LS5AAA-XX-Y) and a product number of (R-9AH1E-41-021A).

Figure 3.23 Magnetic Flowmeter convertor at the water injection line. The convertor of a product number (MGG14C-MH4H-1B1N-YAH) and serial number (R-F3396-A1-011)

3.12. Data Acquisition (DAQ) System

Figure 3.24 shows the National Instruments (NI) PXIe Data Acquisition System (DAQ) that is used throughout these experiments. The system, in which NI PXIe-1075 chassis provides power, cooling, and a communication backplane for I/O modules, is used as a platform for gathering experimental data and monitoring and controlling operational parameters in instrumentation installed throughout the system. A total of 7 modules were installed as follows, 4 NI TB-4353 modules each with 32 channels for

thermocouples, 1 NI TB-4322 with 8 analog output channels for valve control, 1 NI TB-4302 with 32 filtered analog input channels configured for -10-10V signals, and 1 NI TB-4302C with 32 filtered analog input channels configured for 4-20mA signals.

Figure 3.24 NI PXIe-1075 chassis with modules installed

LabVIEW 2019 programming software was used for monitoring and controlling and recording testing parameters. The LabVIEW code main structure was programmed by a fellow graduate student, Dallin Keesling. It was then modified to add new structures and modify existing others to address the main features of the Standalone and the Turbopump experimental setups, as shown in Figure 3.25 and Figure 3.26, respectively.

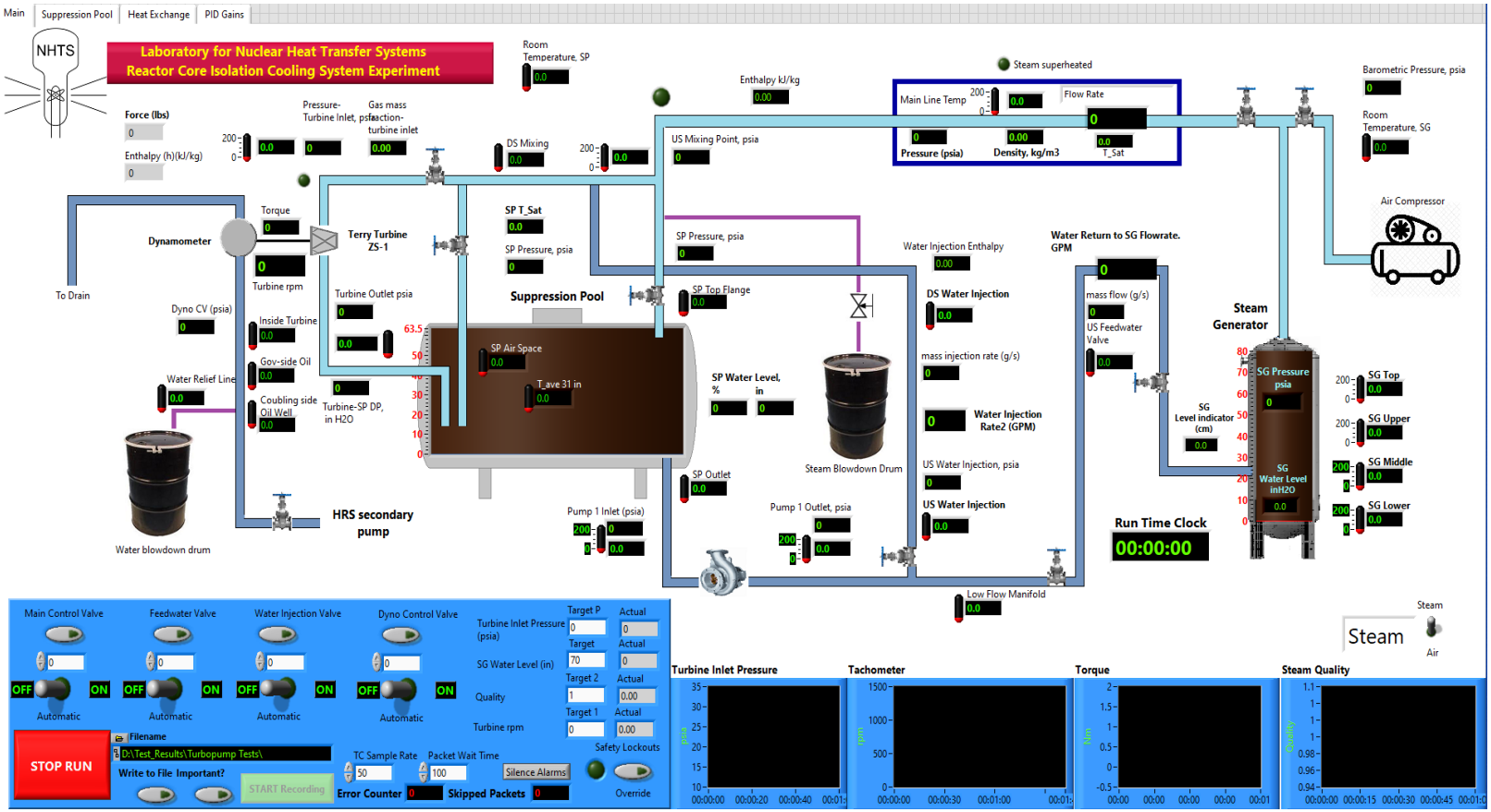

Figure 3.25 LabVIEW control panel for the Turbine standalone setup

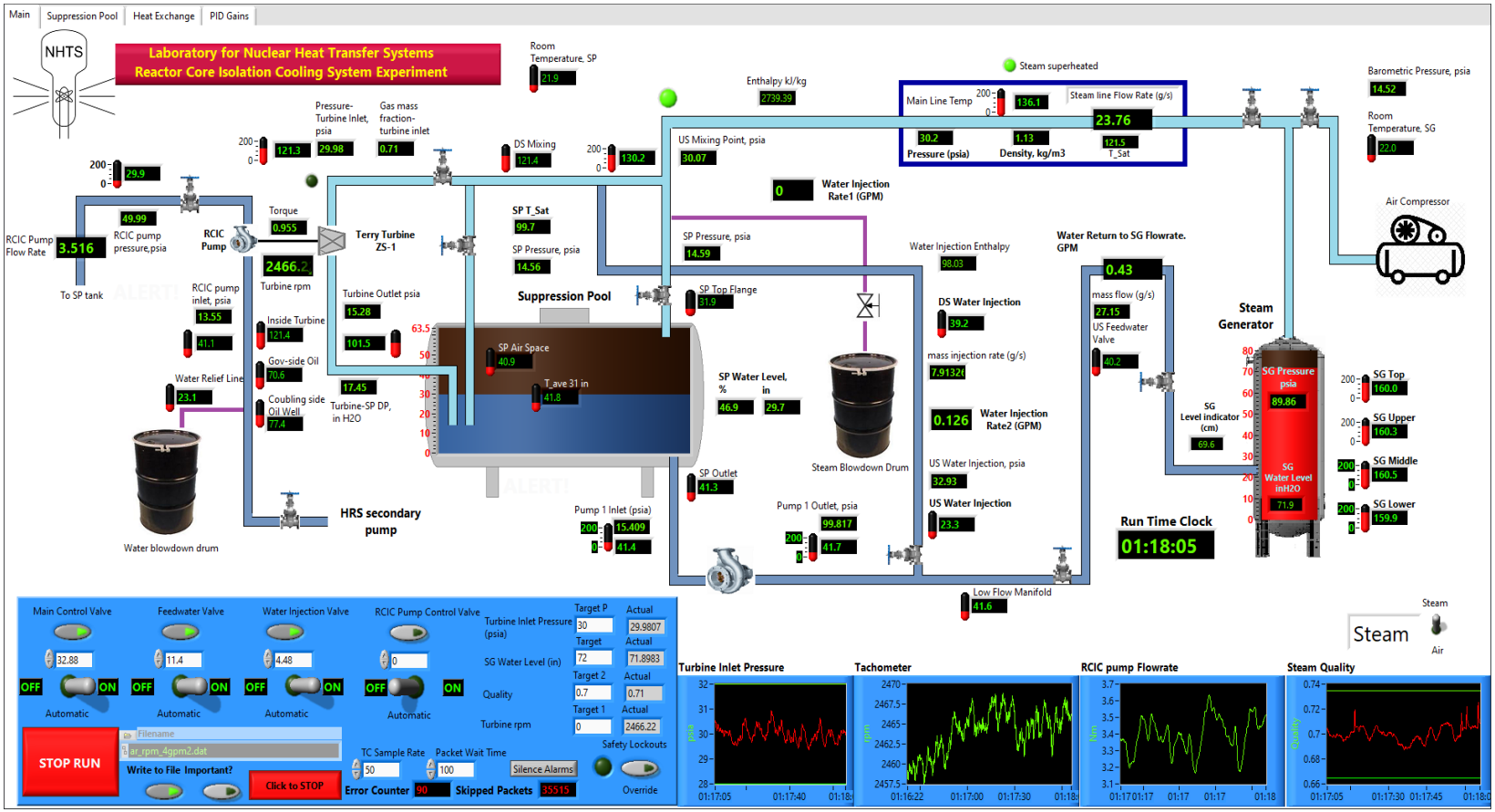

Figure 3.26 LabVIEW control panel for the Turbopump setup

A steam-water properties code was programmed using C programming language and been integrated with the experiment's LabVIEW code to implement empirical formulas and generate the desired values as per input parameters (i.e., pressure and temperature) collected from the system as shown in Figure 3.27. The water and steam properties empirical formulas were obtained from the Revised Release on the IAPWS Industrial Formulation 1997 for the Thermodynamic Properties of Water and Steam report [18]. The entire code can be found on APPENDIX A.

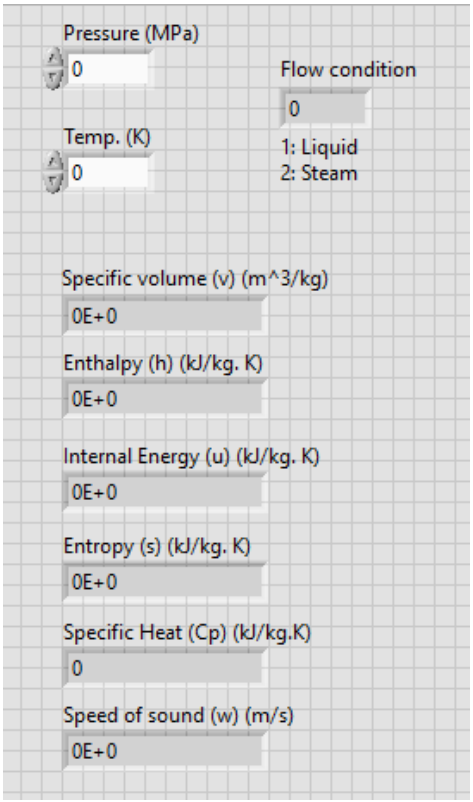

Figure 3.27 LabVIEW control panel for generating the thermodynamic properties and flow conditions based on the fluid pressure and temperature.

4. FACILITY UPGRADES PERFROMED FOR THESE EXPERIMENTS

4.1. Turbine Disassembly

Throughout this research project, the turbine has been through an overhaul cleanup before start testing, which included replacement of the reversing chamber due to rubbing with the wheel and replacement of the shaft sealant due to a steam leak from the turbine casing. To that end, the turbine has been disassembled and reassembled several times as per the following procedures:

1. Disconnect the load cell from both ends (i.e., the Dynamometer torque arm and the turbine skid).
2. Disconnect the hoses and hose fittings from the dynamometer.
3. Remove the turbine coupling cover.
4. Loosen the shaft-coupling Allen screws. Those screws to keep the coupling in-place on the shaft.
5. Unscrew the dyno bolts.
6. Take the alignment plates & shims away. Write down the number of shims and their values for re-alignment purposes.
7. Slid the dyno out of the turbine shaft.
8. Screw out the casing bolts and alignment pins. Pins should be tapped with a hammer from the bottom.
9. Screw out both bearing covers bolts; the coupling side and the governor side.
10. Cover oil sumps to prevent introduction of foreign material.

11. Screw out the governor valve covering plate bolts and remove the covering plate.
12. Remove the shaft sealant leakage drainage pipes.
13. A two-person job:
    a. Using the crane to lift up the upper case. Redeem the upper case by hitting the upper case with a rubber hammer gently.
    b. Lift the wheel away from the turbine casing by holding the shaft from its ends.
14. Let it rest on a smooth surface to avoid forming any scratches on the shaft surface.
15. Remove the shaft sealant housing.
16. Remove the turbine-side coupling.
17. Remove the upper section of the bearing.

4.2. Shaft Sealant

The current design uses carbon seals (or glands) sealants. The seal comes in three semi-circular pieces of carbon that clamp around the shaft via a spring, as shown in Figure 4.1. Replacement parts are ordered from RevakKeene Turbomachinery in La Porte, TX. Figure 4.2 shows that the new sealant has less than 5 mils clearance off the shaft surface as per the manual criteria [19]. The glands tolerance gap is supposed to close due to friction heat between the glands and the turbines shaft while spinning. The draining hoses are designed to drain any leaked steam/condensate steam after being trapped in any of the three-sealant champers.

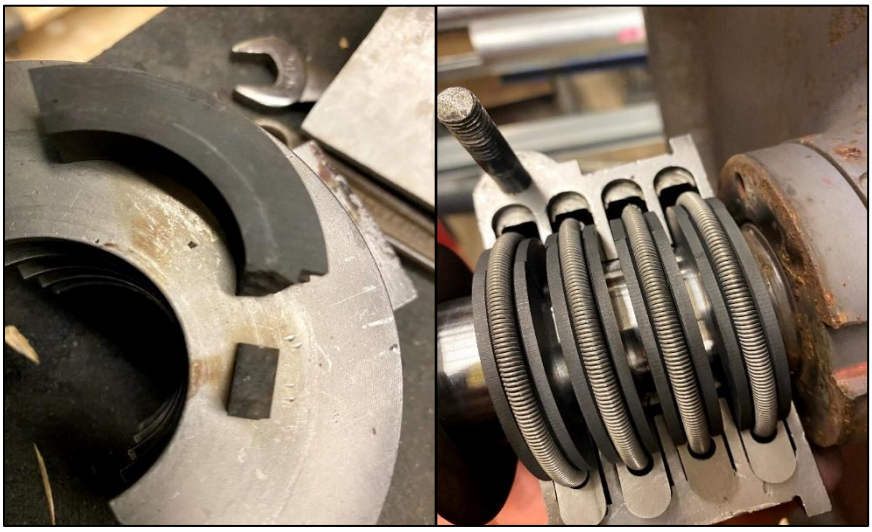

Figure 4.1 The ZS-1 Terry turbine shaft sealant. (left) One piece of three semi-circular pieces that forms the complete set of carbon gland. (Right) The four carbon glands installed around the shaft setting in their housing

Figure 4.2 Sealant quality check. The dial gauge reads less than 5 mils, which is the clearance between the shaft outer surface and the carbon inner surface.

4.3. Turbine Re-Assembly

To reassemble the turbine, follow the disassembly procedures in reverse, with the following hints in mind,

- Clean all the dirty surfaces from previous sealant materials. See Figure 4.3
- Make sure the wheel fits the case very well before final placement (i.e., before applying the sealant)
- Use Permatex #2 between the upper and lower parts of the oil well covers and the shaft sealant housing. See Figure 4.4
- Use Temp Tight II, as per the internally-kept EPRI manual, between the casing upper and lower cases to seal. See Figure 4.5
- Apply a thin coat of anti-seize to turbine bolts before reinstalling.
- Use a torque wrench at 30-35 lbf/ft to tight the turbine bolts on a diagonal basis.

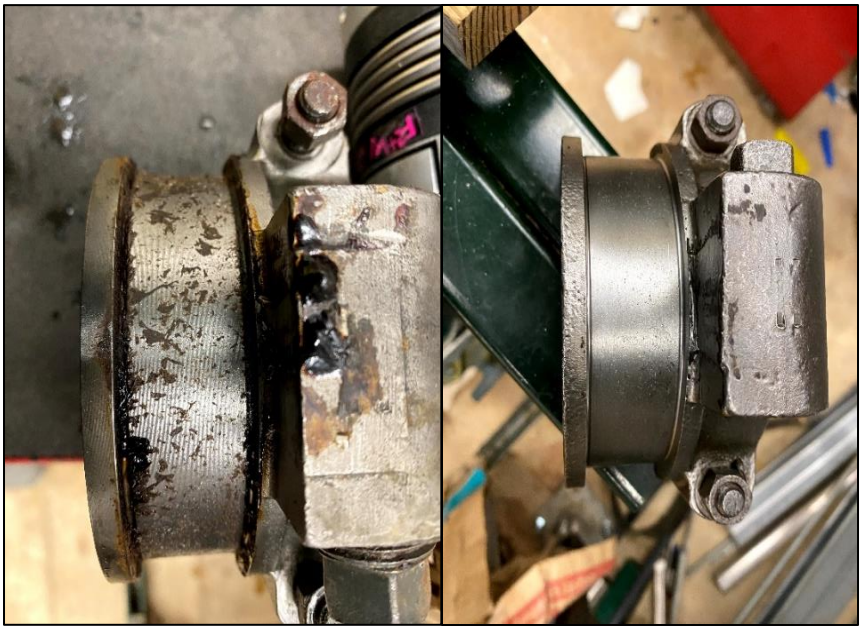

Figure 4.3 Shaft sealant housing before and after cleaning.

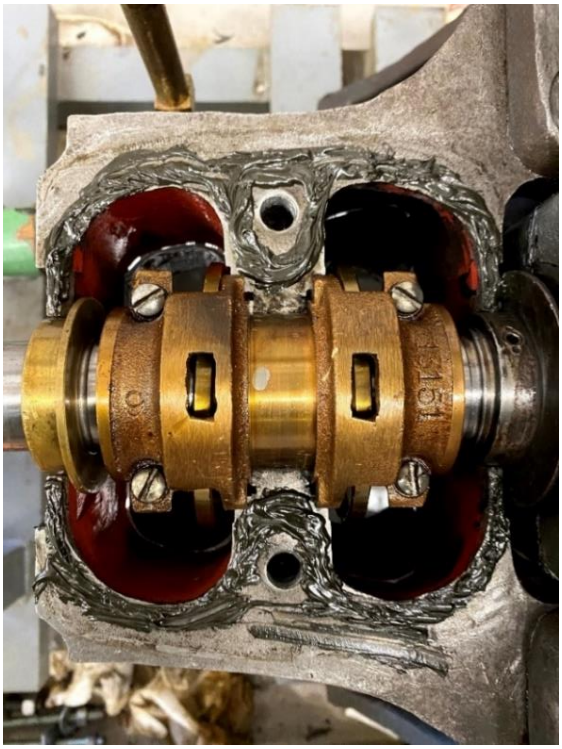

Figure 4.4 Permatex #2 sealant applied on the bottom part of the oil well cover - pump side.

Figure 4.5 Application of Temp Tight II on the bottom part of the casing.

4.4. Steam Nozzle Valve

The nozzle was found leaking during the shakedown testing. John-Crane #187-I sealant has been used as per the ZS-1 manual [19]. Replacement was done as per the following procedures,

1. Close the valve all the way shut.
2. Remove the valve handle by screwing out the ½" nut.
3. Pull out the old sealant from the ap between the valve steam and its housing, using a wooden screw.

4. Wrap 12” inches long of the new packing material around the valve steam as shown in Figure 4.6. [20]
5. Replace the stem to its previous position and tight the bonnet strong enough to prevent any leaks. Currently the bonne is tightened very strongly to the point where the valve is not turning. It is left wide open. The steam admission to the turbine is controlled via the main steam control valve (V1).
6. Replace the valve handle.

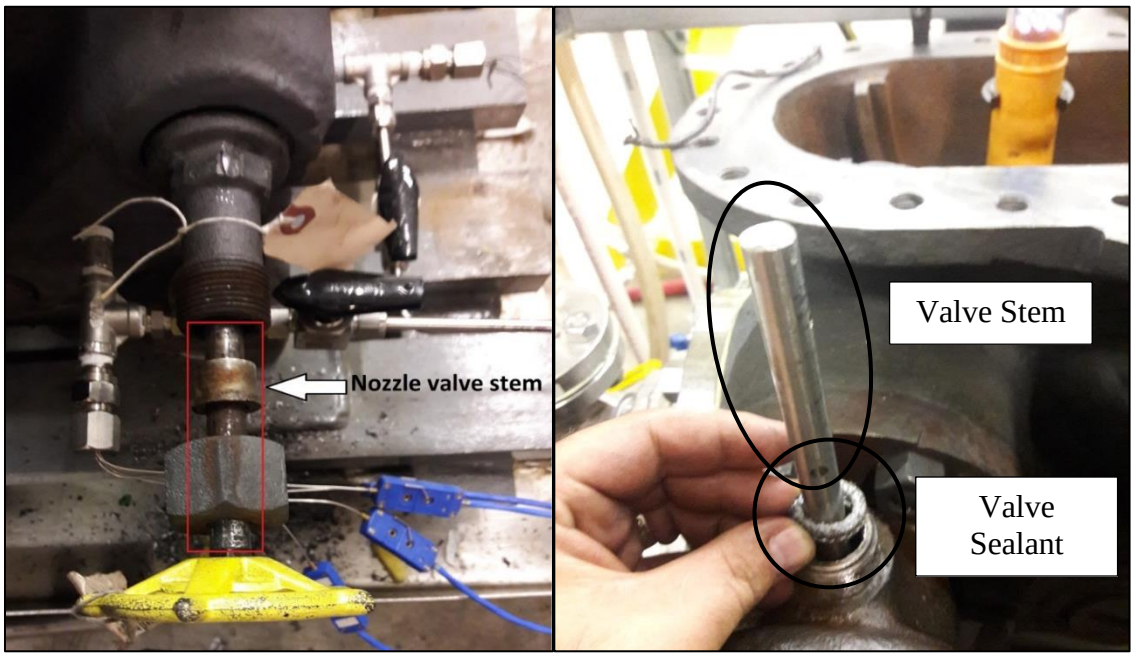

Figure 4.6 Steam Nozzle Valve. (left) Complete structure of the valve. (Right) Valve stem and sealant

4.5. Safety Coupling

The turbine and the pump were coupled using an R+W America torque limiter, model SK2. The torque limited purchased for earlier experiments with this turbine is a

model SK2, rated for a 20 N.m disengagement torque value. The torque limiter protects the torque meter that is mounted on the shaft of the turbine and the pump from shaft overloading. See Figure 4.7. A coupling was needed due to different diameters of the torque limiter and the shaft. The torque limiter supplier, R+W America, manufactured a coupling of model BKC. The coupling was machined to fit the turbine, the pump, and the torque meter shaft diameters of 1 3/8 inch, ¾ inch, and 16 mm respectively. The BKC type tend to accommodate higher lateral, axial, and angular shaft misalignment as shown in Figure 4.10.

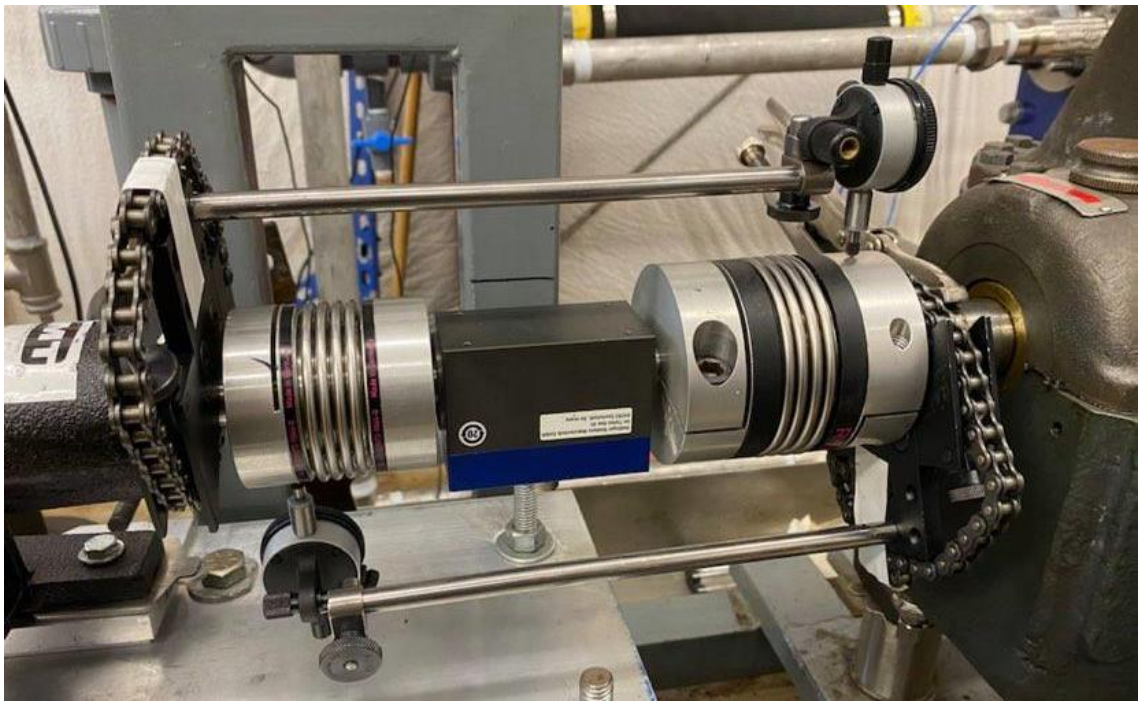

Figure 4.7 The turbopump safety coupling setup. The dial indicators were mounted as a part of the reverse dial indicator method for shaft vertical alignment.

Safety couplings were not used for the Turbine standalone setup because a torquemeter was not installed. Instead, Lovejoy L110 rubber spider couplings were used between the shafts of the dynamometer and the turbine as seen in Figure 4.8. However, a coupling guard shown in Figure 4.9 was installed over the shaft to protect the working personnel from any problematic consequences of the shaft overloading. Moreover, the turbine rotational speed is controlled by the steam inlet flowrate and pressure. The main steam control valve (V1) is LabVIEW-programmed to shut off the steam flow to the turbine at 4000 rpm, which prevents the turbine from experiencing over speed issues. Figure 4.11 shows the lateral, axial, and angular shaft allowable misalignments.

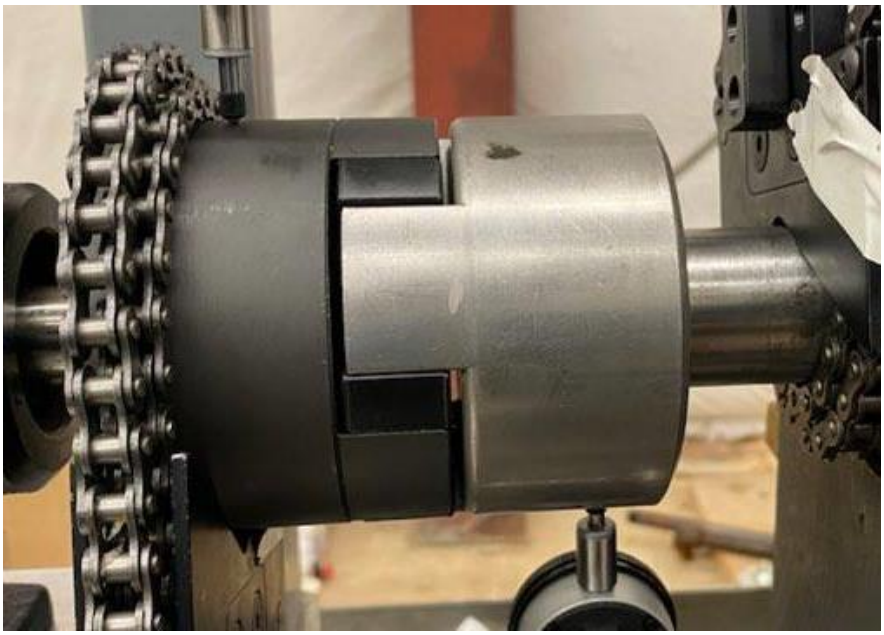

Figure 4.8 Lovejoy L110 rubber spider coupling mounted between the turbine and the dyno.

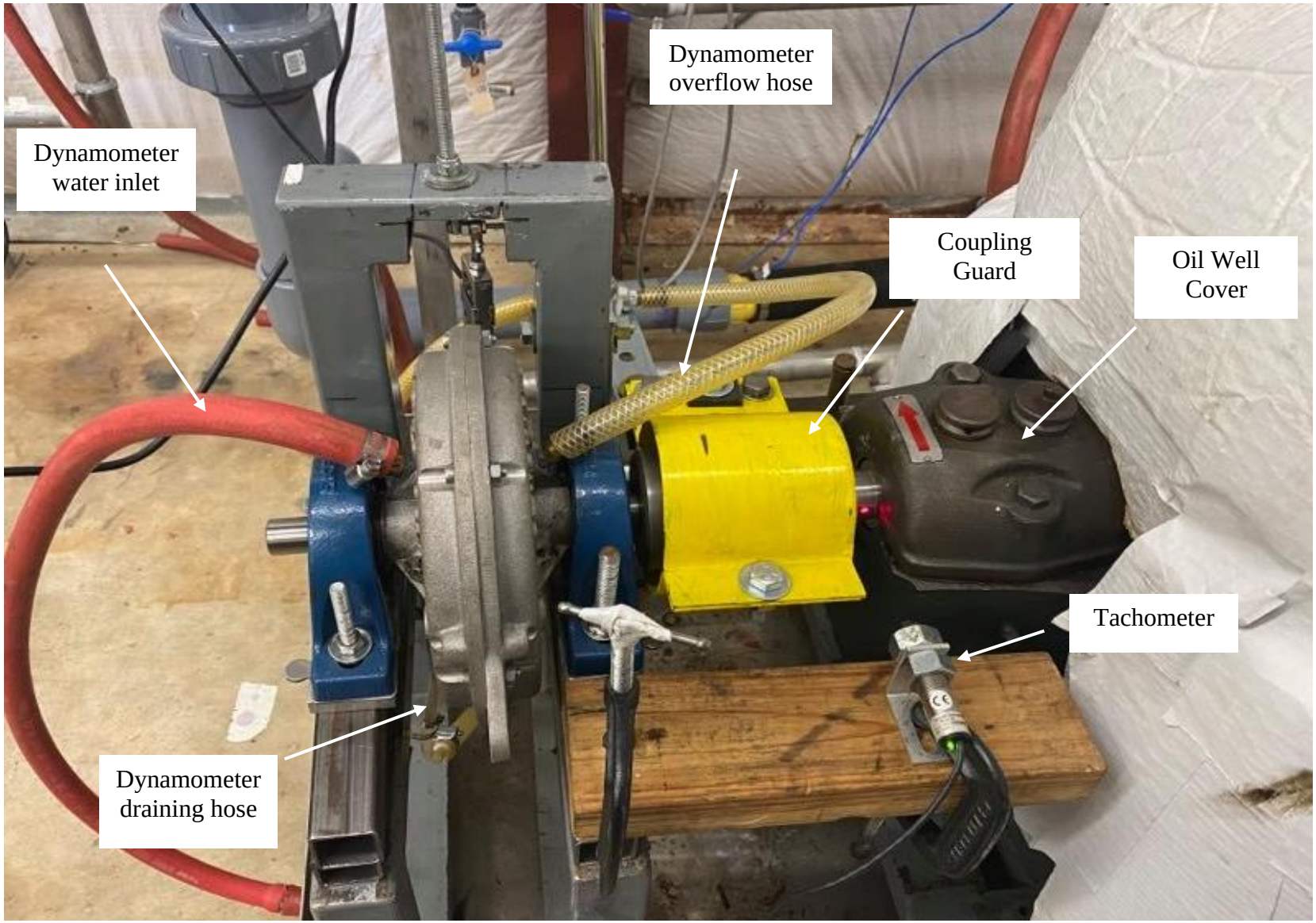

Figure 4.9 Dynamometer-Turbine (Standalone) setup with main components.

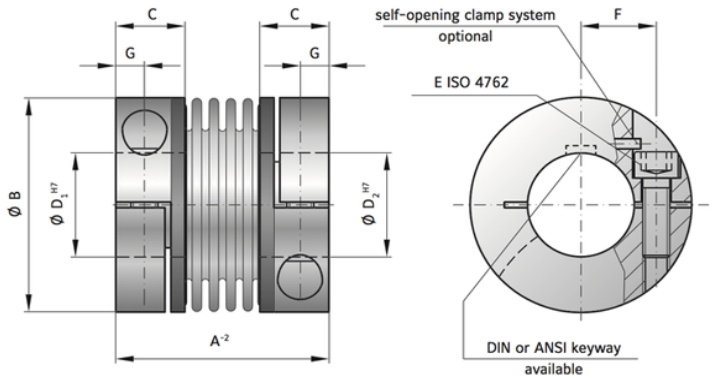

SPECIFICATIONS BKC

BKC Series		15	30	60	150	300	500
Rated torque (Nm)	T_{KN}	15	30	60	150	300	500
Overall length (mm)	A^{-2}	48	58	67	78	94	100
Fit length (mm)	C	16,5	21	23	27,5	34	34
Inside diameter possible from Ø to Ø H7 (mm)	D_1/D_2	8-28	12-32	14-35	19-42	24-60	32-75
Outside diameter (mm)	B	49	56	66	82	110	123
Moment of inertia (10^{-3} kgm^2)	$J_{ges.}$	0,05	0,1	0,26	0,65	6,3	9
Approximate weight (kg)		0,13	0,21	0,37	0,72	3,26	3,52
Torsional stiffness (10^3 Nm/rad)	C_T	23	31	72	141	157	290
Axial ± (mm))	max.	1	1	1,5	2	2	2,5
Lateral ± (mm)	max.	0,2	0,2	0,2	0,2	0,2	0,2
Angular ± (degree)	max.	1	1	1	1	1	1
Axial spring stiffness (N/mm)	C_a	30	50	67	77	112	72
Lateral spring stiffness (N/mm)	C_r	315	366	679	960	2940	2200
Fastening screw (ISO 4762)	E	M5	M6	M8	M10	M12	M12
Tightening torque of the fastening screw (Nm)	E	8	15	40	75	120	125
Distance between centerlines (mm)	F	17,5	20	23	27	39	45
Distance (mm)	G	6,5	7,5	9,5	11	13	13
Hub material		Aluminium	Aluminium	Aluminium	Aluminium	Steel	Steel
Speed max. with G = 2.5 balancing (min-1)		80000	70000	60000	50000	40000	30000
		15	30	60	150	300	500

Figure 4.10 Metal Bellows coupling allowable misalignment. The red and blue boxes rectangles the corresponding coupling specs [21].

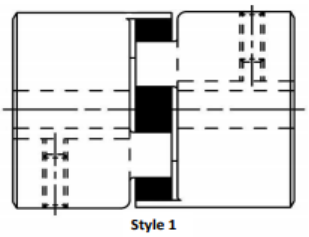

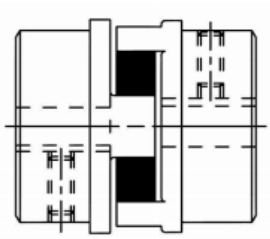

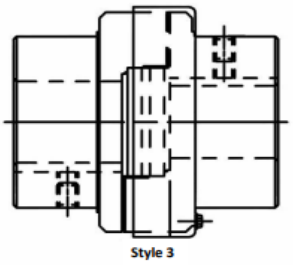

Table 4 - Jaw Couplings Allowable Misalignment

Size	Style	Gap 'G' (BSE) Width In	Allowable Misalignment at 3,600 RPM or Slower [1]								
			NBR or Urethane up to L225			Hytrel			Bronze [2]		
			Parallel	Angular		Parallel	Angular		Parallel	Angular	
			in	Degrees	Δ 'G' in	in	Degrees	Δ 'G' in	in	Degrees	Δ 'G' in
L 035	1	0.281	0.015	1°	0.010	--	--	--	--	--	--
L/AL 050	1	0.469	0.015	1°	0.018	0.015	1/2°	0.012	0.010	1/2°	0.012
L/AL 070	1	0.500	0.015	1°	0.022	0.015	1/2°	0.012	0.010	1/2°	0.012
L/AL 075	1	0.500	0.015	1°	0.030	0.015	1/2°	0.015	0.010	1/2°	0.015
L/AL 090	1	0.500	0.015	1°	0.035	0.015	1/2°	0.018	0.010	1/2°	0.018
L/AL 095	1	0.500	0.015	1°	0.035	0.015	1/2°	0.018	0.010	1/2°	0.018
L/AL 099	1	0.750	0.015	1°	0.040	0.015	1/2°	0.022	0.010	1/2°	0.022
L/AL 100	1	0.750	0.015	1°	0.040	0.015	1/2°	0.022	0.010	1/2°	0.022
L/AL 110	1	0.875	0.015	1°	0.055	0.015	1/2°	0.030	0.010	1/2°	0.030
L 150	1	1.000	0.015	1°	0.065	0.015	1/2°	0.033	0.010	1/2°	0.033
AL 150 [3]	1	1.000	0.015	1°	0.070	--	--	--	--	--	--
L 190	2	1.000	0.015	1°	0.075	0.015	1/2°	0.040	0.010	1/2°	0.040
L 225	2	1.000	0.015	1°	0.085	0.015	1/2°	0.044	0.010	1/2°	0.044
L 276	2	1.625	0.015	1°	0.100	--	--	--	--	1/2°	--
C 226	3	1.500	0.015	1°	0.090	0.015	1/2°	0.046	0.010	1/2°	0.046
C 276	3	1.625	0.015	1°	0.100	0.015	1/2°	0.054	--	--	--
C 280	3	1.625	0.015	1°	0.130	0.015	1/2°	0.065	--	--	--
C 285	3	1.625	0.015	1°	0.145	0.015	1/2°	0.075	--	--	--
C 295	3	1.875	0.015	1°	0.160	0.015	1/2°	0.080	0.010	1/2°	0.080
C 2955	3	1.875	0.015	1°	0.160	0.015	1/2°	0.080	0.010	1/2°	0.080
H 3067	3	2.125	0.015	1°	0.180	0.015	1/2°	0.090	0.010	1/2°	0.090
H 3567	3	2.375	0.015	1°	0.195	0.015	1/2°	0.100	0.010	1/2°	0.100
H 3667	3	2.625	0.015	1°	0.210	0.015	1/2°	0.105	0.010	1/2°	0.105
H 4067	3	2.875	0.015	1°	0.235	0.015	1/2°	0.120	0.010	1/2°	0.120
H 4567	3	3.125	0.015	1°	0.265	0.015	1/2°	0.135	0.010	1/2°	0.135

Notes
1. Maximum speed for all L-Line Hytrel L050 through L276 is 3,600 RPM. See catalog for larger sizes.
2. Maximum speed for all Bronze spiders or cushions is 250 RPM regardless of size
3. AL150 couplings are dimensionally larger in size than the standard L150. AL150 spiders have more legs than L150

Figure 4.11 Love Joy L110 - Jaw coupling allowable misalignment. The red box rectangles the corresponding coupling in this research [22]

4.6. Shaft Alignment

To avoid vibrational effect on the turbine performance, the turbine shaft has been aligned with the dynamometer or the pump shafts according to the reverse dial method as per the following procedures,

1. Bar sag measurement
    1) Mount the alignment dial gauges at the opposite ends of a straight pipe in which the left and the right gauge pointers are pointing vertically at 12 and 6 O'clock positions, respectively, as shown in Figure 4.12
    2) Reset the dial gauges at 0 mils.
    3) Rotate the pipe 180^{o}, the left gauge should become in the bottom and the right gauge on the top.
    4) Divide the readings on each gauge by two. The resultant values are the sagging value for each of the bars. These values will be used in further steps.
    5) The bar sag measurement has been done for two of the many bars that are available in the alignment kit box. The bar sag values are written on bar itself.
2. Rough alignment
    1) Use a ruler between the coupling front edges to check for major misalignment.
    2) Add shims beneath the moving component (i.e., a pump or a dyno) legs to adjust for vertical misalignment.
    3) Skew the moving component towards the 3 or 9 O'clock positions to adjust for horizontal misalignment.

Figure 4.12. Bar sag measurement setup.

3. Vertical misalignment measurement

    1) The dial gauge that is close to the fixed component (i.e., Turbine) will be designated as “F”. Whereas the dial gauge that is close to the movable component, whether it is a pump or a dynamometer, will be designated “M”.

    2) Mount the alignment gauges on both ends of the coupling, similar to the setup shown in Figure 4.7. The F dial indicator at the 12 O’clock position, and the M dial indicator at the 6 O’clock position (when looking at the F component).

3) Ensure the dial indicator needles are vertically pointing on the coupling surface.
4) Measure the coaxial distance between the two dial indicators (A), between the M and the moving component front leg (B), and between the moving component two legs (C).
5) Reset the dial gauges to zero.
6) Rotate the shaft counterclockwise (it's the turbine rotational direction) for 180^{o}.
7) Keep an eye on the indicator moving direction; positive or negative direction.
8) Record the values on the alignment sheet shown on page 63. Including the bar SAG value recorded in step 1.
9) Get the F_V, M_V values from the alignment sheet.

   Vertical misalignment correction

10) Apply the generated M_v and F_V values into equations (4.1) and (4.2):

$$y_1 = F_v + \frac{D_2 - D_1}{D_1}(M_V - F_V) \quad (4.1)$$

$$y_2 = F_v + \frac{D_3 - D_1}{D_1}(M_V - F_V) \quad (4.2)$$

Where,

y_1: The vertical misalignment for the front leg of the moving component,

y_2: The vertical misalignment for the back leg of the moving component,

D1: The coaxial distance between the two dial indicators (A),

D2: The coaxial distance between the F dial indicator and the moving component front leg (A+B),

D3: The coaxial distance between the F dial indicator and the moving component back leg (A+B+C)

11) The negative values, means that the moving component shaft is lower than the fixed component shaft, which requires adding more shims beneath the front and back legs by the values of y_1 and y_2.

12) The positive values of y_1 and y_2 means that the moving component shaft is higher than the fixed component shaft, which requires removing shims from the front and back legs by the values of y_1 and y_2.

4. Repeat the steps 3 and 4 until your measured F_V and M_V values are lower than the corresponding coupling maximum tolerance values shown in Figure 4.10 and Figure 4.11

5. Horizontal misalignment measurement

    1) Mount the alignment gauges on both ends of the coupling, similar to the setup shown in Figure 4.13. The M dial indicator (closer to the eyer) is at 3 O'clock position. The F dial indicator Further from the eyer) is at 9 O'clock position when looking at the F component.

    2) Ensure the dial indicator needles are vertically pointing on the coupling surface.

3) Measure the coaxial distance between the two dial indicators (A), between the M and the moving component front leg (B), and between the moving component two legs (C).
4) Reset the dial gauges to zero.
5) Rotate the shaft counterclockwise (it's the turbine rotational direction) for 180^{o}.
6) Keep an eye on the indicator moving direction; positive or negative direction.
7) Record the values on the alignment sheet shown on page 63. Including the bar SAG value recorded in step 1.
8) Get the F_h, M_h values from the alignment sheet.

6. Horizontal misalignment correction

1) Apply the generated M_h, and F_h values into equations (4.3) and (4.4):

$$x_1 = M_h + \frac{D_2 - D_1}{D_1}(M_h - F_h) \quad (4.3)$$

$$x_2 = M_h + \frac{D_3 - D_1}{D_1}(M_h - F_h) \quad (4.4)$$

Where,

X_1: The vertical misalignment for the front leg of the moving component,

X_2: The vertical misalignment for the back leg of the moving component,

2) The negative values of X_1 and X_2, means that the moving component requires moving toward 3 O'clock position by the values of X_1 and X_2.

3) The positive values of X_1 and X_2, means that the moving component requires moving toward 9 O'clock position by the values of X_1 and X_2. Repeat the steps 3 and 4 until your measured M_h, and F_h values are lower than the corresponding coupling maximum tolerance values shown in Figure 4.10 and Figure 4.11.

Figure 4.13. Horizontal misalignment setup.

Table 4.1. Alignment Sheet

Equipment No:				Date:
Operating RPM:		Coupling Type:		Coupling Face Gap:
Bar Sag	F:	M:		Thermal Growth:
Alignment Tolerance		/	M	F:
Tape Measurements		D1 (A):	D2 (A+B):	D3 (A+B+C):

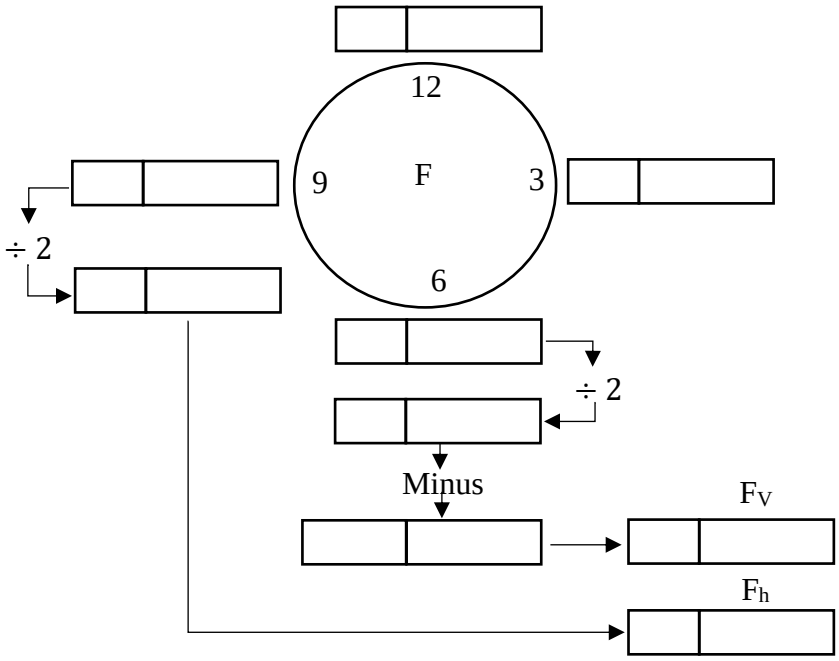

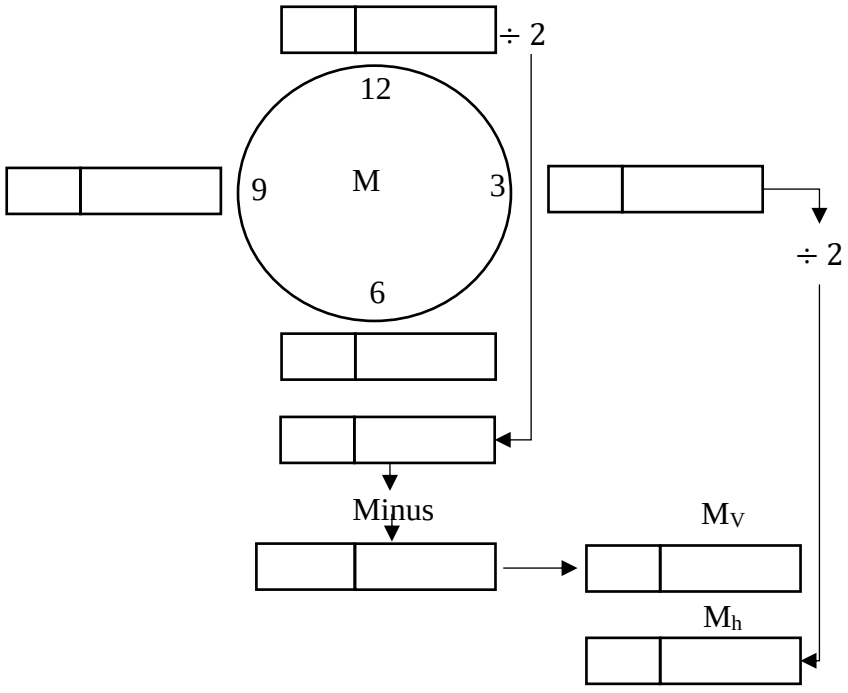

4.7. Control Valves

Throughout the experimental facility, control valves are used in several measurement points. Those points are forming the major boundary conditions for this research project. In particular, the steam pressure, the water injection flowrate that determines the steam quality, and the dyno control valve that controls the turbine rotational speed.

Control valves utilizes the feedback signal from a subsequent operating parameter to adjust the opening ratio on an ongoing manner. This dynamic process is governed by the following LabVIEW-PID controller model, shown in equation (4.5)

$$OP = OP_{bias} + \overbrace{K_c e(t)}^{\text{Proportional}} + \overbrace{\frac{K_c}{\tau_I}\int e(t)dt}^{\text{Integral}} - \overbrace{K_c \tau_D \frac{\partial PV}{\partial t}}^{\text{Derivative}} \quad (4.5)$$

Where:

OP: Controller Output

OP_{bias}: The current value of the process variable

PV: Process Variable (measured value)

S_P: Set point, the value of the target variable

e(t): Controller error = S_P – PV

K_C: Controller Gain

τ_I: Controller reset time

τ_D: Controller derivative action

The controller output is governed by mainly three controller gains: the proportional, the integral, and the derivative gains. Often referred to as PID controller. The terms in the equation right hand side are as follows. The first term represents the output shift, which is the controller output current value. The second term is referred to as the proportional term that has the prompt, most dominating role in controlling the controller output. The third term represents the Integral term that affects the controller response time. The Integral controller (τ_I) is in the denominator, which implies inverse proportionality between the controller output and the integral gain value. The fourth term represents the derivative term, which basically controls the slop of the controller output change to avoid overshoot. However, the derivative gain has not been used in tunning the current PID controllers, it was a PI controlling process. Figure 4.14 shows how the process variable behaves upon increasing/decreasing the tunning parameters values.

The First Order Plus Dead Time (FOPDT) model has been used to get the PID controllers/gains initial values for the LabVIEW code. The model is listed in equation (4.6)

$$\tau_p \frac{dy(t)}{dt} = -y(t) + K_p u(t - \theta_p) \qquad (4.6)$$

Where:

y(t): The process variable, check Figure 4.15

u(t): The controller output

K_p: The proportional gain $=\frac{\Delta y}{\Delta u}$,

τ_p: Process time constant = $y^{-1}(0.6329 \times \Delta y)$

θ_p: Process dead time,

Hence, the PID tunning parameters becomes,

$$K_c = \frac{1}{K_P}, \tau_I = \tau_p, \tau_D = \theta_p$$

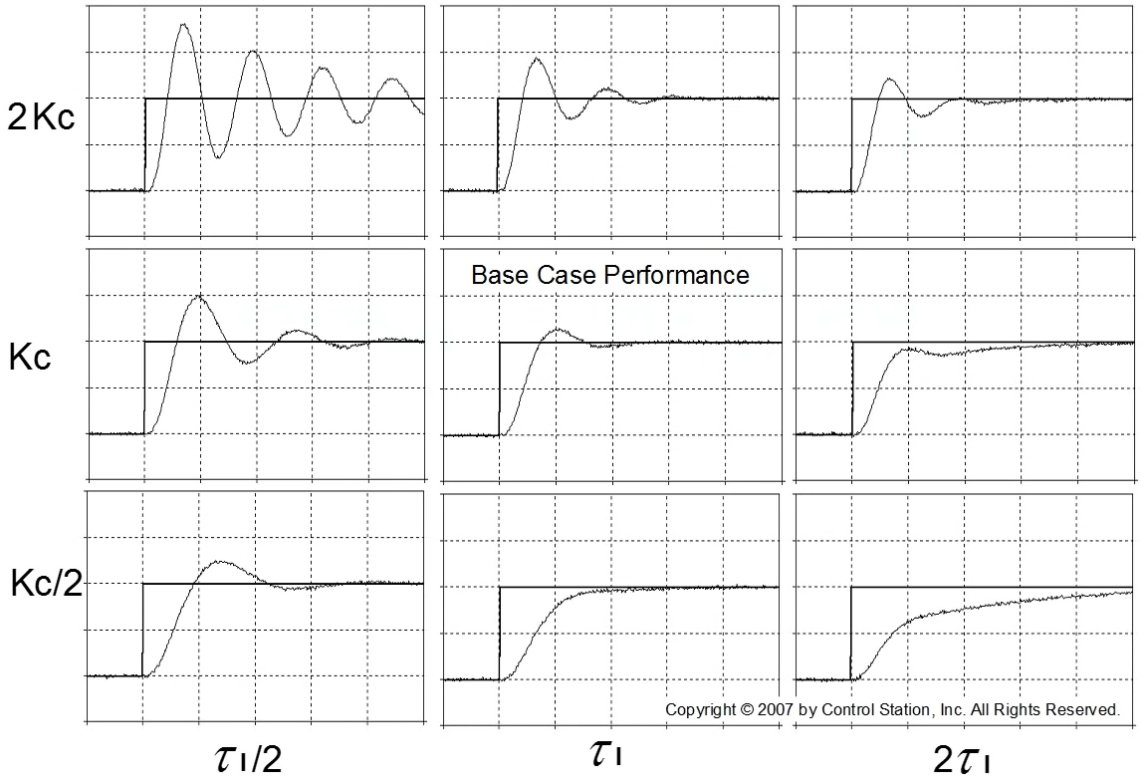

Figure 4.14 PI Controller tunning guide ([23], Page 80, Figure 8.9)

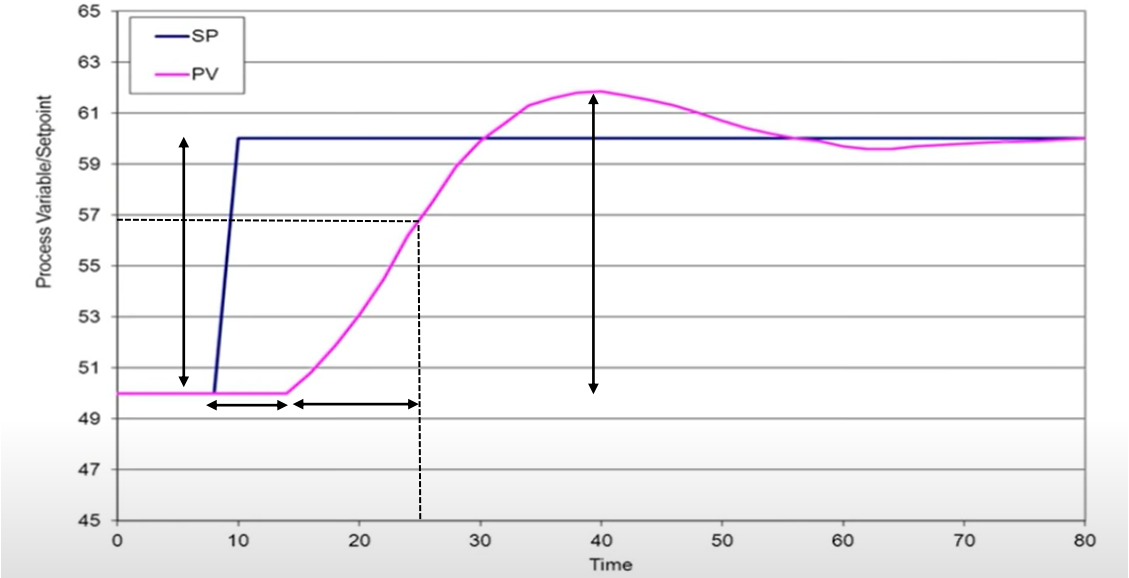

Figure 4.15 Set point and process variable

Due to the non-linearity process of turbine speed regulation and steam quality, the dyno control valve (V-66), as well as the water inject control valve (V-88) controllers required further tunning beyond FOPDT model approach. Further manual tunning was conducted as per the guide sown in Figure 4.14**.**

4.8. Cooling System

The Main Steam Line is penetrating the Suppression Pool through multiple pathways, in which the steam lines are submerged at variant levels and profiles. During the current set of experiments, the turbine exhaust line directs steam through a down comer straight pipe to 15 inches from the bottom of the tank under water surface. The Suppression Pool tank design temperature of 400^{o}F requires continuous cooling for longer duration steam tests, in which high temperature steam is continuously fed into the

tank. Otherwise, the test series would be delayed by an unacceptably long time to cool down the Suppression Pool before performing the subsequent test.

The cooling system was accordingly designed and constructed to remove up to 200 kW of steam flow through a stainless-steel plate-type heat exchanger that was manufactured to meet NHTS experimental operating conditions. The system is composed of primary and secondary sides. The secondary side runs city water through a cooling tower, a 5 horse power centrifugal pump, and a 500-gallon closed tank via 3-inch diameter PVC pipes of schedule 80. On the other hand, the primary side runs demi water through stainless pipes, a pump and the suppression pool.

The secondary-side Cold-Water Line was installed to flow by gravity from the cooling tower basin into a 500-gallon closed tank, and then pumped by the secondary-side pump through the Heat Exchanger (HX) back to the cooling tower via the secondary side Hot-Water Line. On the other hand, the Suppression Pool water, which is major source of heat that needs to be removed, is cooled by pumping the water through the primary side of the Heat Exchanger and back to the Suppression Pool by the primary side pump via stainless steel pipes. Figure 4.16 shows a simplified schematic of the cooling system along with design parameters.

4.8.1. Cooling Tower

The cooling tower was obtained from Cooling Tower System, Inc [24]. The CTS250 model, shown in Figure 4.17, has a total 65-ton cooling capability at 150 gpm flow rate. Technical specifications are shown in Table 4.2. The Heat Exchanger was manufactured so the water temperature in the Cooling Tower Hot Line (see Figure 4.16)

is lower than 120^{o}F to prevent any damage to the PVC pipes. A 10^{o}F temperature difference is expected to be removed through the cooling tower.

This cooling tower is open type (wet) in which the hot water is sprayed through nozzles into the tower's fill. The tower is equipped with a 38.5-inch diameter fan to draw the air at axial flow at 11500 cfm. Thus, the heat is transferred by convection over the falling water droplet surfaces. The collected cold water in the basin is drained by gravity to the 500-gallon tank, and then pumped to the system via the secondary side pump. Figure 4.18 below shows a detailed technical drawing along with dimensional parameters. At times of stagnation, in which cooling tower operation is not required, the 500-gallon tank is used to drain a total of estimated 300-gallon of water from the system that is normally circulating in the secondary side. This in turn prevents any corrosion and scale buildup in the system.

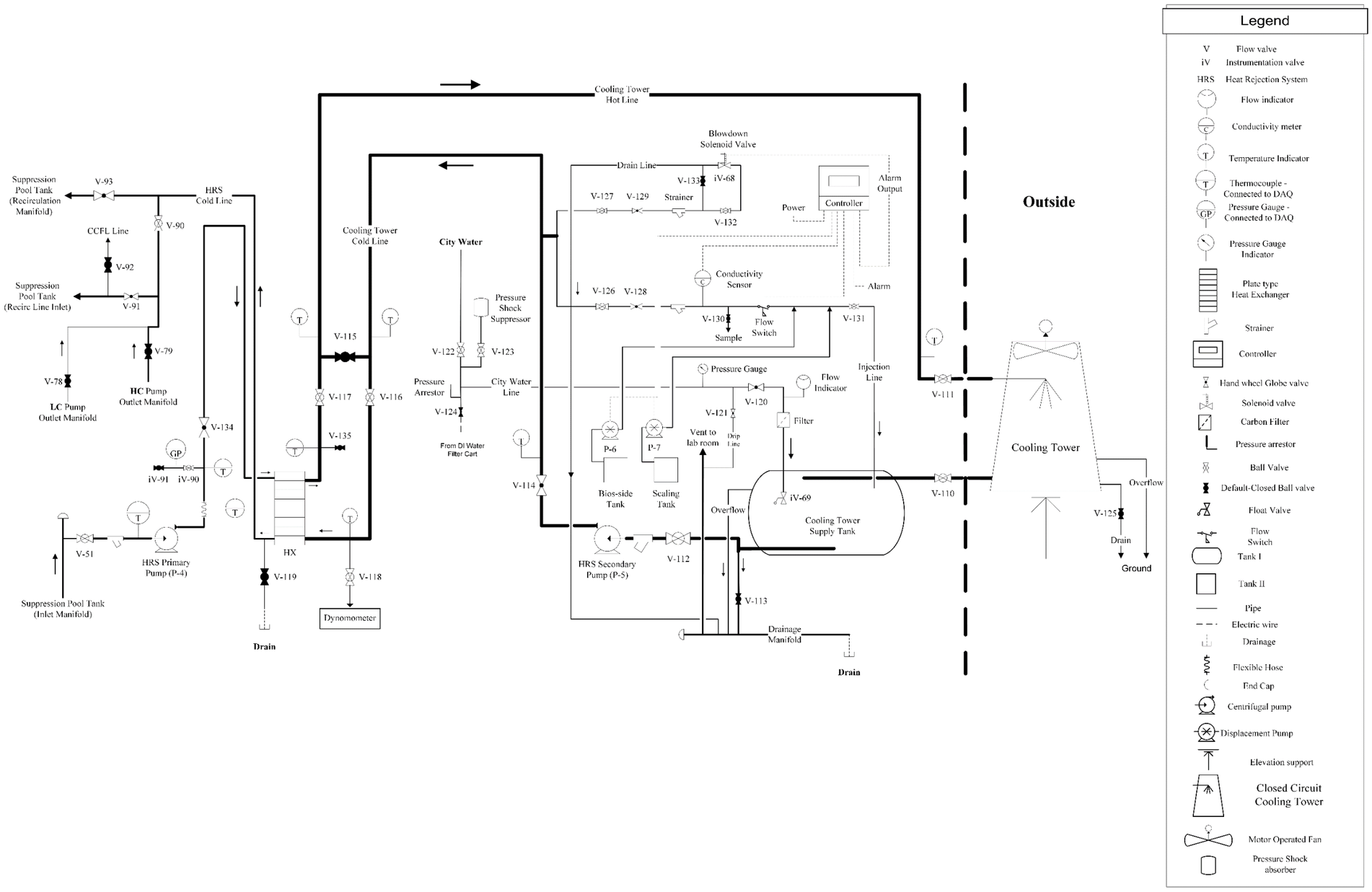

Figure 4.16 NHTS Heat Rejection System

Figure 4.17 NHTS Cooling Tower

Table 4.2 Cooling tower technical specification [24]

Design and Operating Conditions		**Water Distribution System Construction Materials**	
Tower Type:	Counter Flow Induced Draft	Stand Pipe:	PVC
Water Flow Rate (GPM):	148 GPM	Sprinkler Head:	AC
Entering Water Temperature	95°F	Sprinkler Pipes:	PVC
Leaving Water Temperature	85°F	**Mechanical Equipment**	
Wet Bulb Temperature:	75°F	Fan Unit:	One Unit per Tower
Total Fan BHP:	1.5 HP	Type:	Axial Flow
Total Pump Head:	6.6'	Manufacturer:	CTS
Drift Loss of Water Flow:	0.1%	Diameter:	38.25"
Evaporation Loss of Water Flow:	0.93%	Blade Material:	AC
Design Wind Load:	30.7 lbs/sq. ft.	Hub Material:	AC
Structural Details		Nominal Air Volume:	11,500 CFM
Overall Diameter:	78 3/4"	**Fan Motor**	
Overall Height:	74.5"	Number of motors:	One Unit per Tower
Dry Weight:	342 lbs.	Type:	Induction
Operating Weight:	1,657 lbs.	Manufacturer:	CTS
Basic Tower Construction Materials		Insulation:	F Class
Tower Support Frame Assembly	FRP	Rated HP:	1.5 HP
Casing:	FRP	Voltage and phase:	220/440V/3
Casing Supporters	Nylon	**Piping Connections**	
Cold Water Basin	FRP	Primary Water Inlet Diameter	3"
Filling:	PVC	Primary Water Outlet Diameter:	3"
Filling Supports:	HDGS	Auto fill inlet diameter:	3/4"
Fan Guard	HDGS	Quick fill inlet diameter:	-
Mechanical Equipment Supports:	HDGS	Overflow outlet diameter:	1"
Inlet Louvers:	PVC	Drain diameter:	1"
Bolts, Nuts & Washers:	STS	Water Flow (GPM):	148 GPM

Materials Key			
FRP	Fiberglass Reinforced Polyester	STS	Stainless Steel
HDGS	Hot Dipped Galvanized Steel	AC	Aluminum Alloy Cast

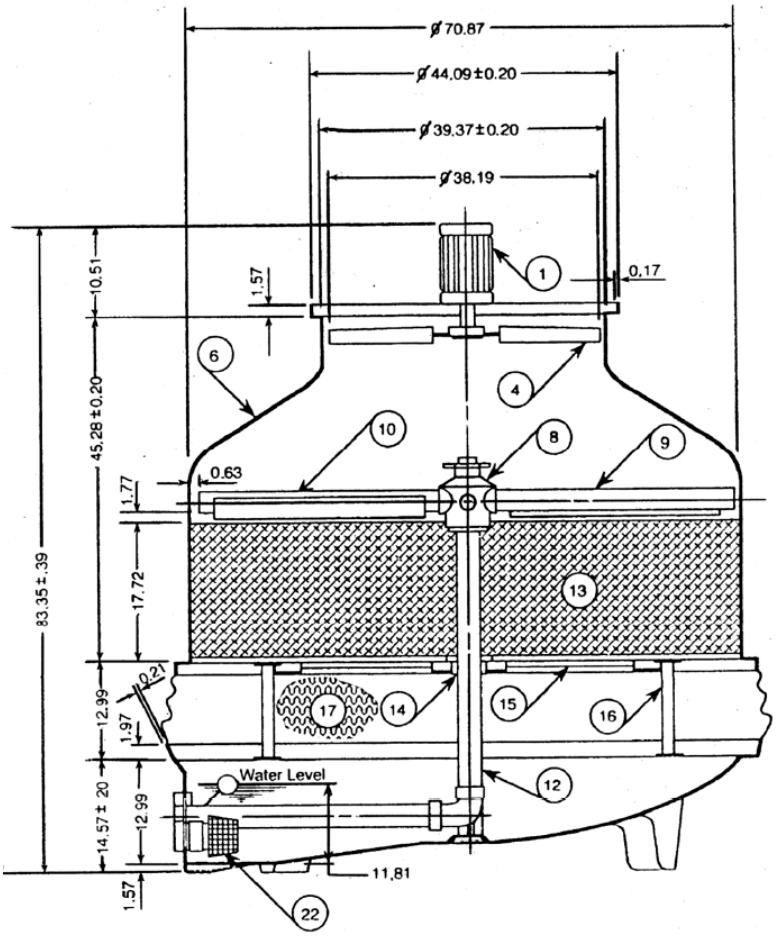

Figure 4.18 Detailed technical drawing along with dimensional parameters [24].

4.8.2. Heat Exchanger (HX)

A stainless-steel plate type heat exchanger was obtained from Alfa Laval. The model AQ3-MFG removes 200 kW, which is the 157 kw from the steam generator plus the heat added from pump operations. It was customized to meet the suppression pool vessel rated pressure and temperature of 150 psia, 400 ^{o}F, respectively. Figure 4.19 shows more technical details.

Technical specification

Gasketed Plate Heat Exchanger

Project ref:	Texas Specialty Products 46002	
Line ref:		ALICE 5.0.0.14
Model:	AQ3-MFG	AHRI LLHE PHE 1.2
No of units:	1	Date: 11/29/2018

		Hot side	Cold Side
Fluid:		Water	Water
Density:	lb/ft³	61.22	61.70
Specific heat capacity:	Btu/lb,°F	1.00	1.00
Thermal conductivity:	Btu/ft,h,°F	0.378	0.369
Viscosity inlet:	cP	0.3967	0.6145
Viscosity outlet:	cP	0.5076	0.5568
Volume flow rate:	GPM	46.8	138.7
Inlet temperature:	°F	160.0	110.0
Outlet temperature:	°F	130.0	120.0
Pressure drop:	psi	1.5	9.8
Heat exchanged:	kBtu/h	685.0	
L.M.T.D:	°F	28.9	
Heat transfer area:	ft²	22.0	
Relative directions of fluids:		Countercurrent	
Effective margin:	%	1.3	
Effective fouling resistance * 10000:	ft²,h,°F/Btu	0.120	
Connection positions and flow directions:		S1 -> S2	S4 <- S3
Connections: S1,S2,S3,S4		FLANGE ASME B16-5 150# NPS 3 Unlined	
Number of passes:		1	1
Design pressure (MAWP):	psi	150	150
Test pressure:	psi	195	195
Design temperature max:	°F	400.0	400.0
Design temperature min (MDMT):	°F	32.0	32.0
Channel Arrangements:		1*6MH	1*7ML
Pressure vessel code:		ASME	
Number of plates:		14	
Nominal A-dimension:	mm	62	
Extension capacity:		21 plates	
Plate material/thickness:		ALLOY 316/0.50 mm	
Gasket material and attachment:		EPDMP ClipGrip™	EPDMP ClipGrip™
Unit dimensions (length x width x height):	in	30.1 x 16.4 x 35.0	
Net weight, empty / operating:	lb	468 / 489	
Type of package:		PLYWOOD BOX LYING	
Packed length x width x height:	in	40.3 x 18.3 x 39.2	
Packed volume:	ft³	16.71	
Packed weight:	lb	562.8	

Figure 4.19 Technical details of the Plate-type Heat Exchanger used for the Heat Rejection System in the NHTS lab

4.9. Water treatment Station

While the primary side of the system has demineralized water as a cooling fluid, the secondary side carries city water that has a Total Dissolved Solids (TDS) level of ~ 3500 ppm. A new water treatment station, shown in Figure 4.20 was designed and installed to avoid scaling and corrosion buildup in the Heat Exchanger and circulating pipes. The subsystem is primarily composed of two displacement pumps, a conductivity sensor, a solenoid valve, scale and biocide inhibitors, and a controller that regulate the TDS levels of the water in the cooling tower lines, based on the water conductivity level. Chemical handling and initial runs are controlled by a nationally recognized water treatment company: Garret Callahan.

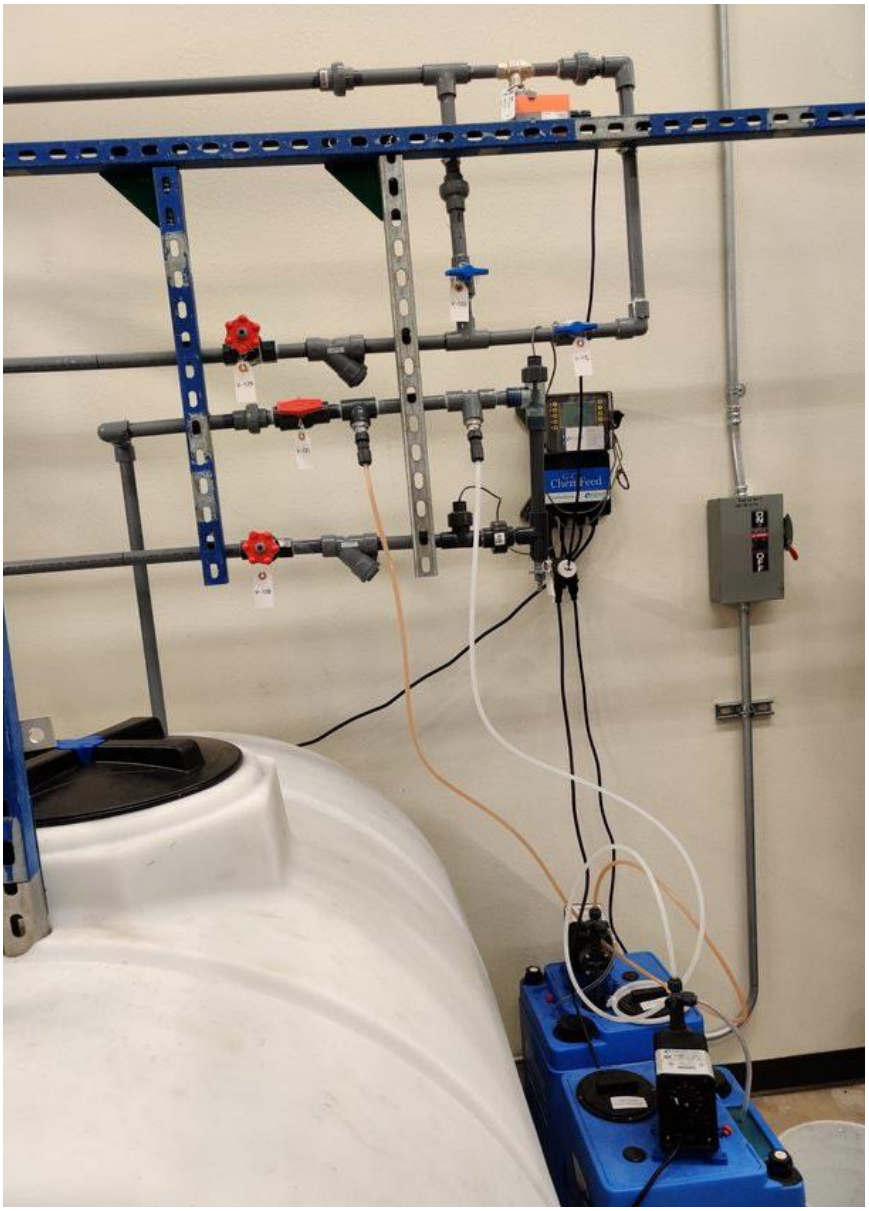

Figure 4.20 Heat Rejection System Water Treatment Station

5. TEST PROCEDURES

The following section included an executive summary of the testing procedures. APPENDIX B includes the full detailed testing procedures with facility P&IDs per each operating mode. Moreover, the appropriate valve status throughout the tests is tabulated in APPENDIX C. In total, there are 135 valves in use in the facility.

5.1. Pre-test Mode

1. Ensure Personnel safety
2. Ensure Experimental Equipment's security
    1. Close all of the steam generator vent valves.
    2. Check that none of the electrical instrument and connections is exposed to water/hot surfaces.
    3. Confirm that the Steam Generator electric heaters power panel is secure/locked.
3. Data Acquisition System Initiation
    1. Making sure all the instruments are well connected.
    2. Making sure instruments are powered on
    3. Powering on DAQ chassis and DC power supply.
    4. Opening the Turbopump_Test_RT.vi to initiate the chassis Real Time measurement recording.
4. Turn on the switch for the Quincy air compressor.
5. On the LabVIEW control panel,

1. Enter the minimum Steam Generator water level at 70 inches
2. Toggle on the Feedwater Valve switch to automatic.

6. Check open V-55, V-54, V-59, V-81, and V-83
7. Turn on the Feedwater Pump (P-1) switch
8. Check the water level of the Suppression Tank is half filled, and Steam Generator is more than 50 cm (on the level indicator.
9. Heat Rejection System operation
   - ❖ Follow the procedures in Section 5.1.4 “Cooling Mode”.
10. Check Turbine oil level, and
11. Check shut turbine draining valves

5.2. Warmup Mode

1. Check shut V-1, V-24, V-25, V-29, V-31, V-33, V-38, V-44, V-106, and V-115.
2. Keep V-2 (Steam Generator Outlet Valve) fully open during testing
3. Crack V-1 (Main Control Valve) 2% open on the LabVIEW control panel.
4. Check that V-30 is open (RCIC Facility Steam Admission Valve).
5. Energize the Steam Generator electric heaters to full power (157 kW) until the Steam Generator pressure reaches ~ 90 psia.
6. Check OPEN V-40, V-41, V-42, V-43, V-45, and V-46.
7. [IN CASE OF CHARACTERIZATION TESTS] On the LabVIEW control panel, crack open Dynamometer Control Valve to 15% to avoid dry-operation for the Dynamometer.

8. Once the Steam Generator pressure is at 95 psia, further crack open V-1 (Main Control Valve) to 25%.
9. Once the steam temperature at the Q-measurement point is 100^{o}C, CAREFULLY, crack open V-31 (Steam Condensate Drainage valve)
10. Maintain the Steam Generator pressure by adjusting the Steam Generator heater power (as needed).
11. Enter the first test's steam pressure value on the LabVIEW control panel.
12. Once the steam pressure in the Main Steam Line is around the desired value, turn the switch, on LabVIEW control panel, to automatic mode.
13. Once the MSL steam is superheated, Open/Close the following valves IN ORDER AND QUICKLY (as possible)
    1. OPEN V-33 (Turbine inlet), then
    2. CLOSE V-41, then
    3. OPEN V-38 (Turbine Outlet), then
    4. CLOSE V-40.
14. Maintain the Steam Generator pressure by adjusting the Steam Generator heater power as needed.
    - ❖ DO NOT USE HEATER#6.
15. Once the steam temperatures in the Main Steam Line and at the turbine inlet are steady, the warm up process can be called complete. It might take hours!

5.3. Data collection Mode

1. Enter the desired data file location and name.

2. Hit the “Record” button on the LabView display panel to start data recording.
3. Non-atmospheric back pressure setting:
    1. Open V-49
    2. Close v-46.
    3. Adjust the screw valve to match the desired back pressure value
4. Check the MSL steam pressure to be as required. If not Enter the new value.
5. Steam quality adjustment on the LabVIEW control panel:
    1. Check the value of the steam quality to be as desired. If not, enter the new one.
    2. Check the Water Injection Valve switch is on the automatic mode.
6. [CHARACTERIZATION TESTING] Turbine Speed adjustment on the LabVIEW control panel display.
    1. Enter the value of the desired turbine speed.
    2. Check the Dynamometer Valve switch is the automatic mode (it is supposed to be 15% open on manual mode before doing this step)
7. Monitor the values of the Steam Generator pressure, steam temperature, turbine speed, and quality. The system state is called steady when the inlet pressure value is within ± 0.5 psia, the back pressure value within ± 1.0 psia, the turbine rotational speed is within ±10 rpm, and the steam quality is within ±0.02 for a full two minute. These values are based on the operational experience during the shakedown tests.

8. Once the values of the turbine speed and steam quality are steady for one minute,
    1. Close shut V-33 & V-38
    2. Open V-41.
9. Monitor the turbine's cast down speed profile for one minute, then
    1. Open V-33 and Open V-38
    2. Close V-41.
10. Monitor the turbine spinning speed profile as it reaches back to the SAME steady state values. This might take longer than expected!
11. Hit "Stop data recording" button on the LabVIEW code.
12. Repeat steps 3.1 through 3.11 for the following turbine speeds (rpm): 3,500, 2500, 2,000, 1,500, and 1,000, as possible!
13. Repeat steps 3.1 through 3.11 for the following steam qualities 0.65, 0.25, and 0.05
14. Repeat steps 3.1 – 3.11 for the following pressures (psia): 45, 60.
15. Repeat steps 3.1 – 3.11 for the following back pressures (psia): 16.6 and 19.6.

5.4. Cooldown Mode

1. Primary Side
    1. Check open V-51, V-71, V-90, V-91, V-93, V-94, V-134
    2. Turn on the Heat Rejection System primary pump (P-4) switch
2. Secondary Side
    1. Cold water line

1. Check shut the CTS tank drainage valve, V-113.
2. Check open the Heat Rejection System secondary pump inlet valve, V-112.
3. Check open cooling tower inlet and outlet valves, V-110, and V-111.
4. Turn on the Heat Rejection System secondary pump, P-5.
5. Turn on the fan motor. The on/off switch is outside, by the cooling tower.

2. Water treatment station
    1. Check open the intake line valve, V-126, V-128, and V-131
    2. Check open the water drainage valves, V-127, V-129, and V-132.
    3. Check shut the bypass line valve, V-133.
    4. Check open the flow switch.
    5. Turn on the controller.

5.5. Shutdown Mode

1. Turn off all the Steam Generator heaters AND the overall power switch on the electric panel.
2. Once the turbine speed is zero,
    1. Close V-33, and V-38
    2. Open V-40, and V-41
    3. Toggle off (Close) the switch for the dynamometer valve (V-66).
3. On the LabVIEW control panel,

    1. Turn the V-1 switch to manual and enter 70% as the opening ratio.
    2. Toggle off (Close) the button for the water injection valve (V-88).
    3. Increase the opening ratio gradually at 80% and 100%
    4. Toggle off (Close) the switch for the feed water valve (V-18).
4. Once the Steam Generator pressure is atmospheric, close V-1; toggle off the button for the water injection valve.
5. Crack open V-8 to vent out any remaining pressurized steam.
6. Turn off the air compressor switch.
7. Open the Turbine drain valves, V-36 and V-37 to vent remaining condensed steam.
8. Turn off the feedwater pump (P-1) via the power switch.
9. Turn off the Heat Rejection System primary pump (P-4) via the power switch.
10. Turn off the Heat Rejection System secondary pump (P-5) via the power switch.
11. Turn off the Cooling tower fan by turning the power switch (located in the electric room) to OFF.
12. Turn off the controller.
13. Open V-31.
14. Make sure the Steam Generator pressure is atmospheric before leaving the lab.

6. RESULTS AND DISCUSSION

The current steam-water data sets are considered first-of-a-kind to explore the RCIC systems potential for expanded operation. In particular, a Terry Turbine performance is investigated experimentally over a wide range of turbine inlet pressures from 30-75 psia, back pressures from 14.6 – 20 psia, and steam qualities from 0.05 to 1.0 (dry steam) as per the testing matrix in APPENDIX D. Single-phase air tests were also performed to benchmark against a previous data base of air and air-water data of a ZS turbine by Patil et al. [10] and a GS turbine by Vandervort et al. [25]. Moreover, the current benchmarking was also used to establish scalability between Z and G model air-water data and the Z model steam-water data as discussed in chapter 7.

The first section in this chapter discusses the turbine performance characterization in terms of turbine power output under variant operating conditions.

The second section includes the RCIC turbopump analog performance in terms of the RCIC pump horsepower curves at low and medium inlet pressure and steam qualities of 1, 0.70, and 0.30.

Throughout this research MATLAB software has been used for data analysis. The entire MATLAB code can be found in APPENDIX E. Additionally, the XSteam MATLAB code [26] has been integrated with the data analysis MATLAB code to generate steam and water thermodynamic properties, specifically the steam and water specific volumes for the calculations of steam-water mixture density.

6.1. ZS-1 Terry Turbine Characterization Tests

The current section discusses the turbine performance evaluation in terms of isentropic efficiency, and power output at several operation scenarios, as follows,

6.1.1. Testing parameters

- Steam pressure (psia): 30, 45, 60, 75
- Air pressure (psia): 30
- Steam quality*:1, 0.95, 0.90, 0.85, 0.65, 0.45, 0.25, 0.05
- Turbine's rotational speed* range (rpm): 300 – 3700
- Turbine back pressure* (psia): 14.6 (~ 1 atm), 16.6, 19.6

  * Values varied by test.

6.1.2. Recorded Parameters

- Steam (or gas) temperature, pressure, and flow rate.
- Water injection temperature, pressure, and flow rate.
- Main Steam Line (steam or air) flow rate.
- Turbine rotational speed.
- Turbine shaft force.
- Steam Quality.

6.1.3. Testing Outputs

- Turbine power curves (i.e., shaft power output vs. speed).
- Turbine efficiency curves (i.e., efficiency vs. speed).
- Turbine power input.
- Turbine shaft torque.

6.1.4. Equations

The power input as well as the turbine power output and efficiency is calculated using equations (6.1) - (6.5) to characterize the turbine performance. The power output, in particular, reflects the rate of energy deposition on the turbine wheel by the incoming fluid and therefore is a good parameter with which to characterize turbine performance.

$$\eta_{isentropic} = \frac{P_{output}}{P_{Input}} = \frac{\dot{W}_{shaft}}{P_{steam} + P_{water}} \quad (6.1)$$

$$\dot{W}_{shaft} = \left(\frac{2\pi}{60}\right) \times (\tau \cdot \omega) \quad (6.2)$$

$$P_{steam} = \frac{k}{(1-k)} p_{inlet} Q_{steam} \left[(p_r)^{\frac{k-1}{k}} - 1\right] \quad (6.3)$$

$$P_{water} = Q_w \cdot \Delta p \quad (6.4)$$

$$p_r = \frac{p_{outlet}}{p_{inlet}} \quad (6.5)$$

Where:

P: Power (W)

$\dot{W}_{shaft}$: Turbine shaft output power (W)

τ: The measured shaft torque (N.m)

ω: Shaft Rotational Speed (rpm)

p: Absolute pressure (Pa)

p_r: Pressure ratio

Q: Volumetric Flow rate (m^3/s)

Δp: pressure drop across ZS-1 turbine/RCIC pump (Pa)

k: Specific heat ratio ($=c_p/c_v$) 1.32 for steam (or 1.4 for air) [27]

6.1.5. Effect of Steam Inlet Pressure

Figure 6.1 and Figure 6.2 show the effect of the steam inlet pressure on the turbine power output and efficiency at steam quality (x) of 1.0. It can be seen that the power output as well as the turbine efficiency are higher at higher pressure. Moreover, the turbine is generally more efficient at higher operational speeds. However, this behavior is more apparent at higher pressure than at lower pressures as seen in Figure 6.2. The efficiency peaks at a certain turbine speed, with the optimal speed occurring at higher values in the higher-pressure curves. For the lowest pressure curve, the turbine has almost the same efficiency at the lowest speed as at the highest speed. The turbine exhibits approximately twice higher efficiency at the highest speed compared to the lowest speed at steam inlet pressure of 60 psia, with the peak in the curve not reached for the range of turbine speeds tested.

It was found that the power input at 60 psia steam inlet pressure was three times higher than that for the 30 psia tests, which illustrates the efficiency profile shown in Figure 6.2. The power input at 60, 45, and 30 psia was 9.5, 6.0, and 2.7 kW, respectively. However, during same pressure experiments, the energy extraction (power output) is higher at higher rotational speeds due to the turbine wheel drag coefficient (C_d). It should be mentioned that the turbine wheel drag coefficient (C_d) is conversely proportional to the rotational speed squared [28], thus the C_d is minimum at higher speeds. The Best Efficiency Point (BEP) tends to be at higher rotational speeds at higher pressures, as shown in Figure 6.2**.** These findings are consistent with other work conducted by Patil et al [10]**.**

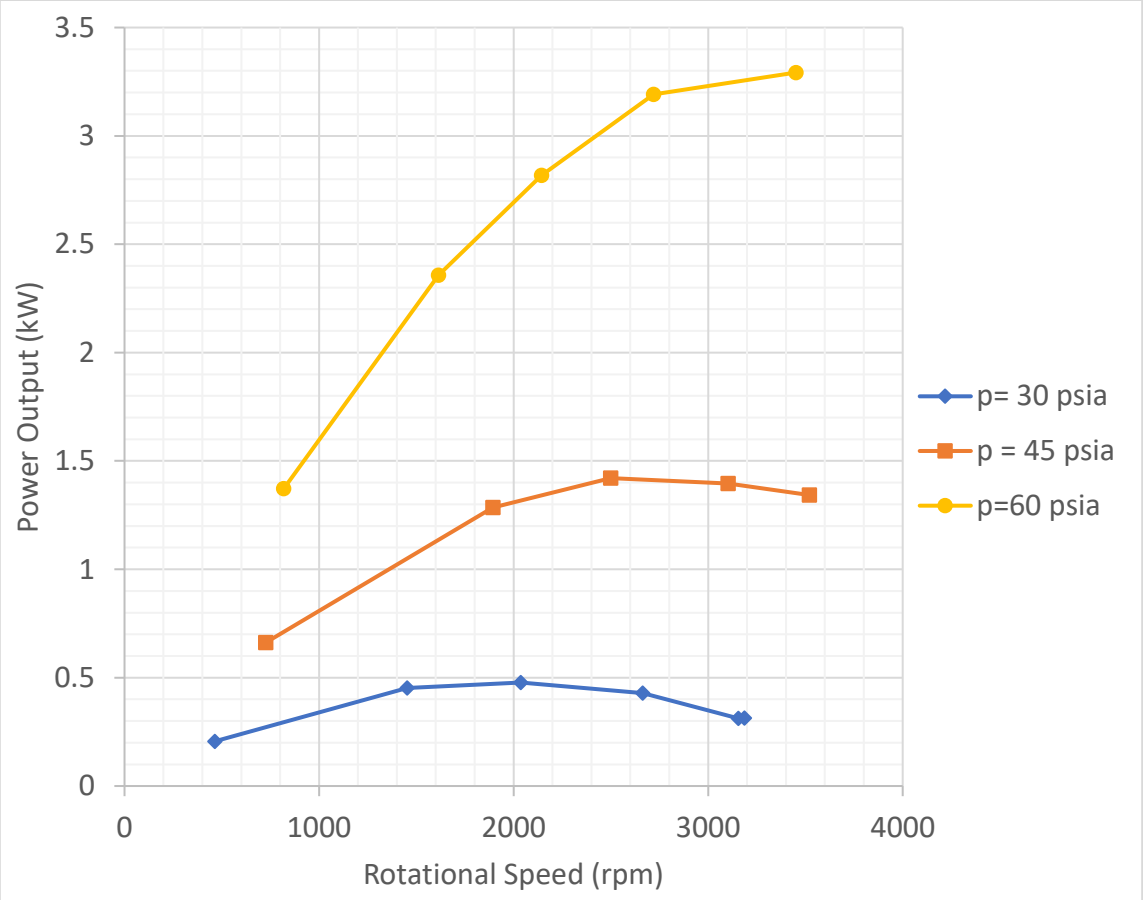

Figure 6.1 The effect of the steam inlet the pressure of 30, 45, and 60 psi on turbine power output during single phase operation at atmospheric back pressure

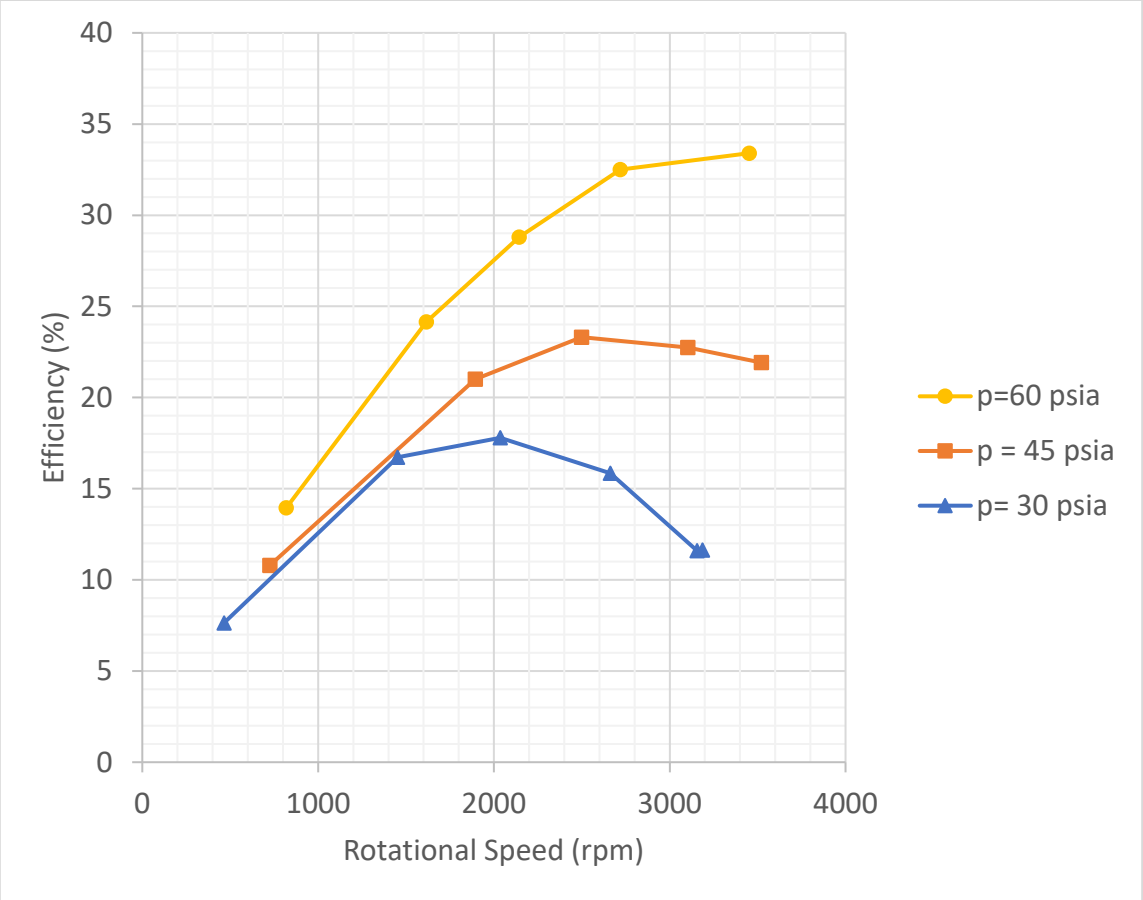

Figure 6.2 ZS-1 Terry turbine's Isentropic Efficiency (η) vs Rotational Speed (ω) at dry steam inlet pressures of 30, 45, and 60 psia, and atmospheric back pressure.

6.1.6. Turbine Oil Temperature Effect

Figure 6.3 shows the initial data set of the power output at 60 psia. The power output profile shows off-trend behavior around the data point where the speed is 1900 rpm. Both the power output and the turbine efficiency were noticeably lower than expected as seen in the 30 psia and 45 psia testing results on the same plots.

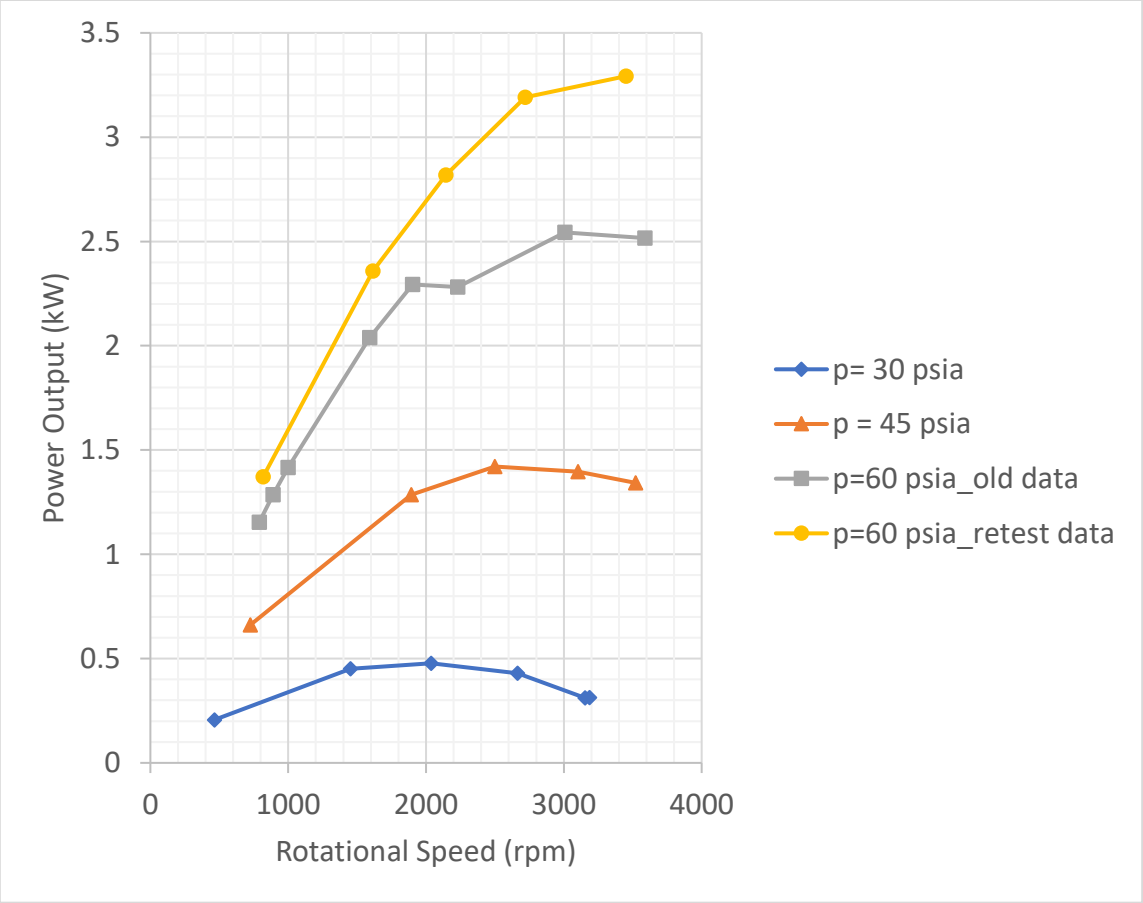

Figure 6.3 The effect of the dry steam inlet the pressure and turbine oil temperature on power output at atmospheric back pressure.

Upon reviewing the testing operating conditions on that test, it was found that the turbine oil temperature on that test (i.e., of 1900 rpm) was 77.6 ^{o}C compared to 74.6^{o}C at the test of 2230 rpm as shown in Figure 6.4. These data points were generated two weeks apart. The tests of speeds of ~ 2230 rpm and above were conducted on October 15, while the other ones (i.e., of lower speeds) were conducted on November 05.

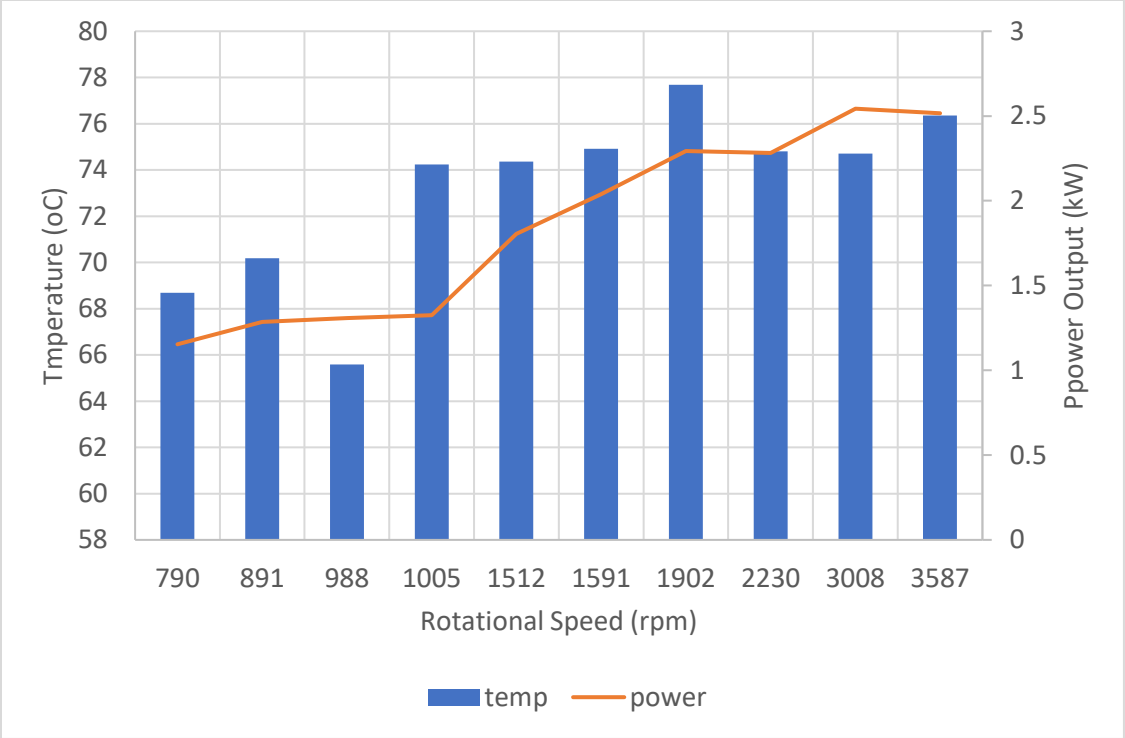

Figure 6.4 The effect of Terry turbine oil temperature on the power output at different rotational speed.

Previous work on terry turbine heated oil extended operations [29] showed that increasing the oil temperature will reduce the frictional load on the shaft due to lower viscosity at higher temperature. Figure 6.5 shows that at room temperature (~22^{o}C) the oil had a viscosity of about 85 cSt, and at 121^{o}C the oil had a viscosity of about 4 cSt; this equates to a 95% decrease. Figure 6.6 shows that the shaft internal losses torque is inversely proportionality to the turbine oil temperature at a fixed rotational speed of 3000 rpm for 6-hour continuous operation.

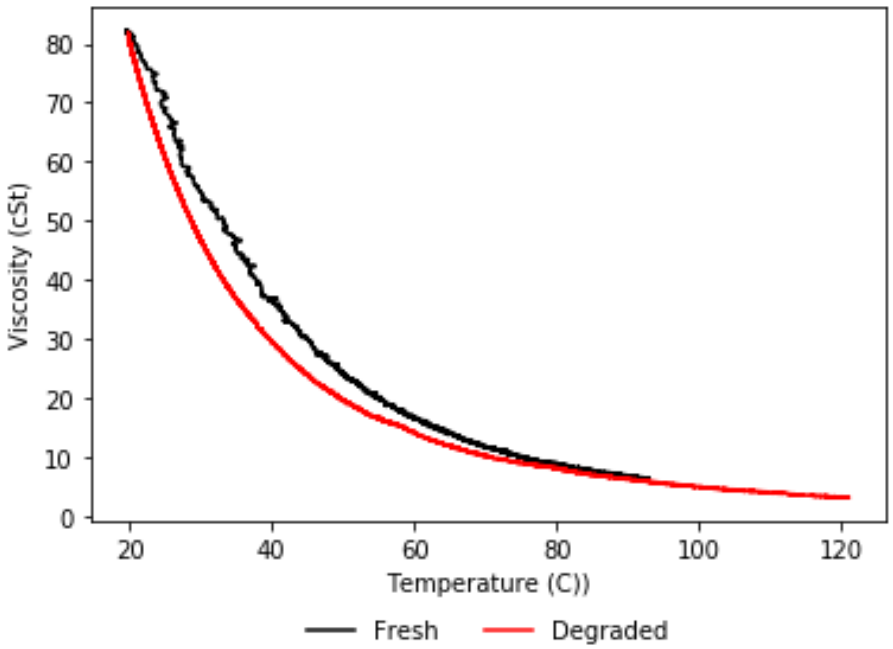

Figure 6.5 The relationship between viscosity and temperature during 6-hour test for fresh and degraded oil at 121ºC. [29]

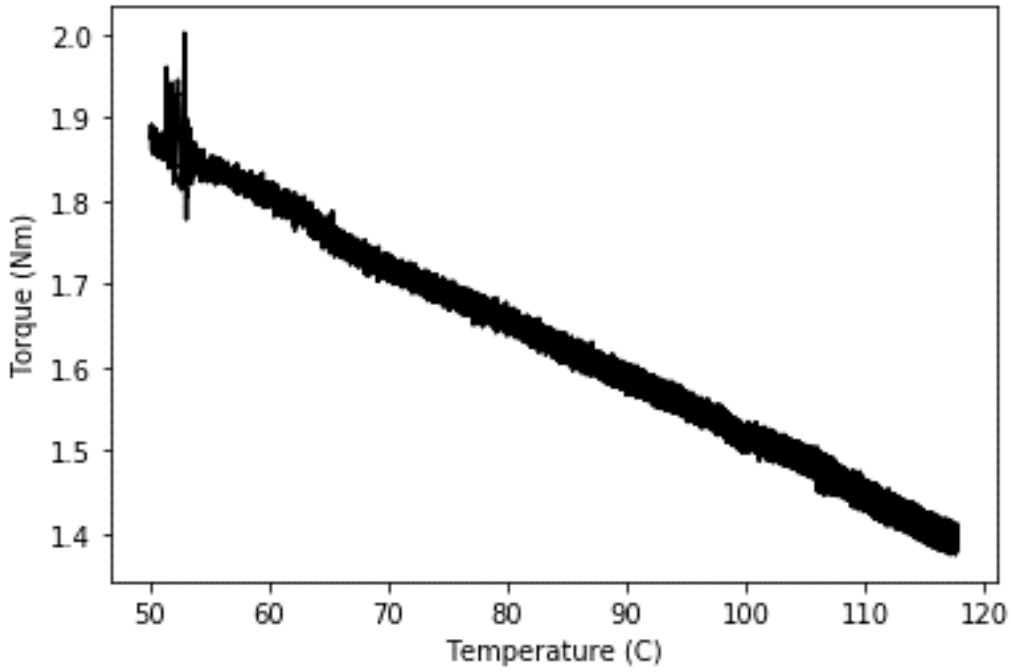

Figure 6.6 ZS-1 shaft internal losses torque with turbine oil temperature. Figure 5.15 at [29]

Further re-testing has been performed to confirm this conclusion. The turbine full-range power output was re-evaluated at a 60 psia steam inlet pressure, atmospheric back pressure, and steam quality of 1.0, to avoid any oil temperature/time variation effect on the turbine performance. The new data set shows consistency with the data sets at other pressures. However, with less energy dissipation due to friction, the new tests exhibited higher torque values than the previous tests performed with oil at a lower temperature. This can be seen in Figure 6.7, where he upper two curves (i.e., the rounded and squared data points) represents the turbine performance at the same inlet pressure of 60 psia, but different oil temperature during each test. It can be concluded that the distorted power output data point is related to the high oil temperature during that test.

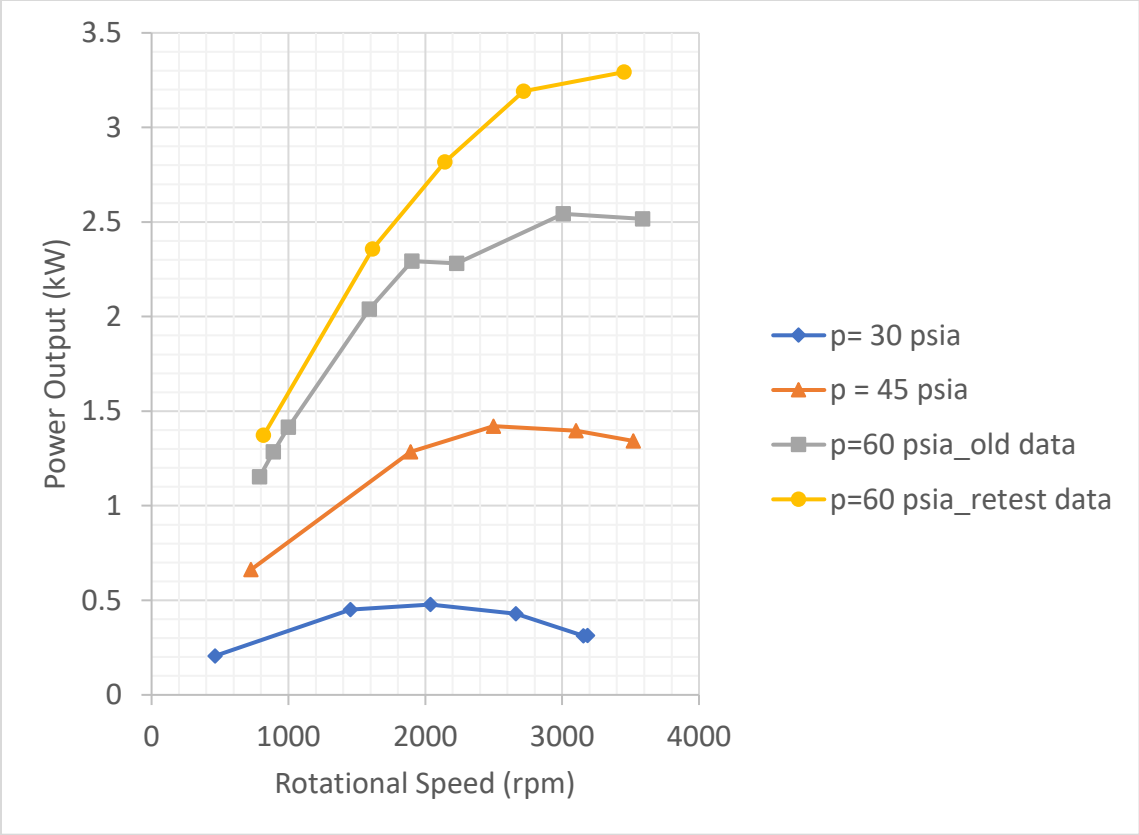

Figure 6.7 ZS-1 Terry Turbine Power Output vs. Rotational Speed at different steam inlet pressures of 30, 45, and 60 psia.

6.1.7. Effect of Steam Quality

This section highlights the two-phase flow effect on the turbine performance in terms of power output and efficiency. Figure 6.8 shows that at higher steam quality, the turbine power output is higher. The maximum power output is not related with the highest rotational speeds but the moderate ones instead, as observed for the dry steam data previously presented. This is mainly due to the small torque values at higher speeds, as shown in Figure 6.9. The same pattern was observed for the turbine efficiency in Figure 6.10.

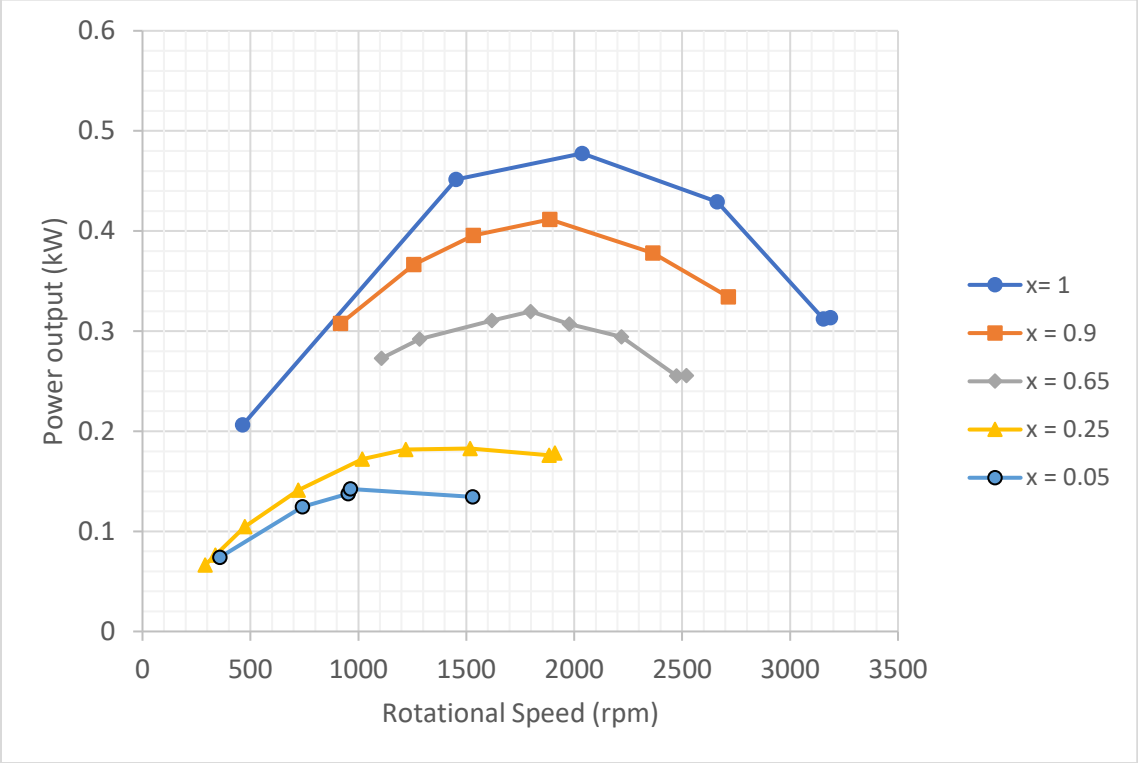

Figure 6.8 ZS-1 terry turbine power output (kW) during two-phase flow operation at 30 psia inlet steam pressure and atmospheric back pressure

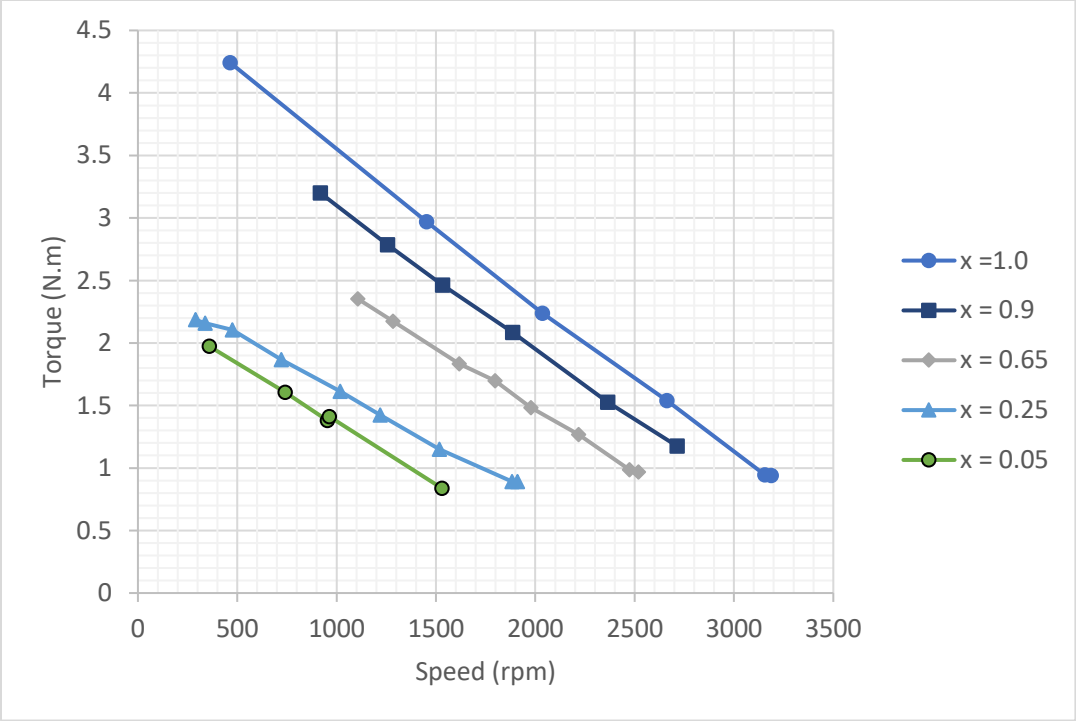

Figure 6.9 Measured Torque of the ZS-1 Terry Turbine while operated at variant steam qualities at 30 psia inlet pressure, atm back pressure

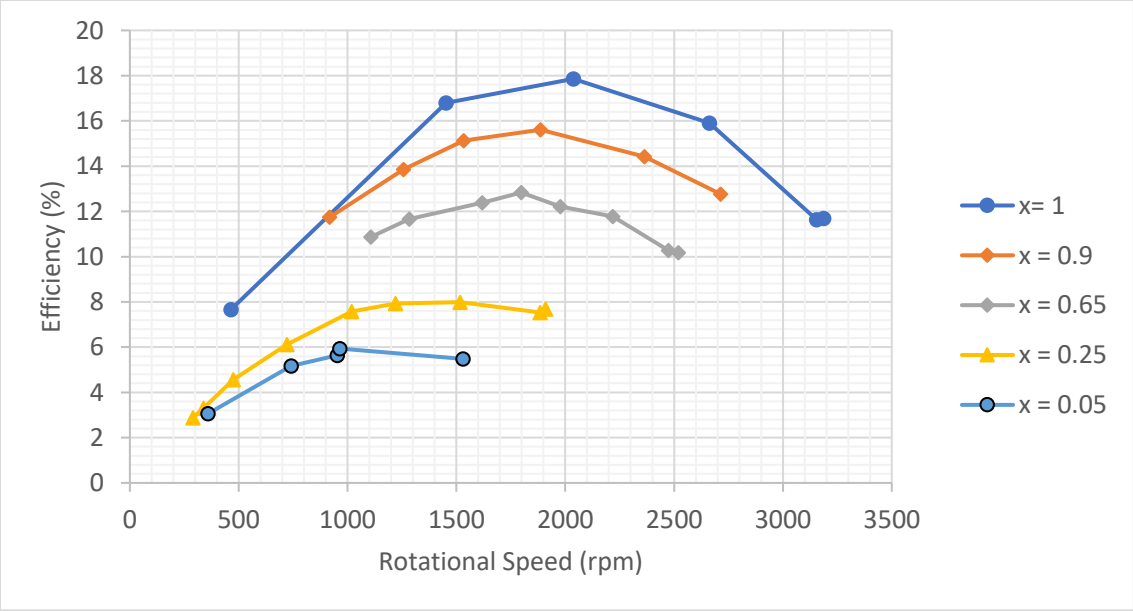

Figure 6.10 ZS-1 terry turbine efficiency during two-phase flow operation at 30 psia inlet steam pressure and atmospheric back pressure

Figure 6.13 and Figure 6.14 depict the steam quality effect on the turbine power output at steam inlet pressures of 45 and 60 psia and atmospheric back pressure. It can be noted that the decrease in steam quality limits the steam impact force, or the maximum jet velocity. However, the effect of steam quality is lower at higher pressures due to the higher power input. On the other hand, the efficiency curves in Figure 6.13 and Figure 6.14 tend to collapse closer together at lower speeds, while diverging at higher speeds. This is mainly because the turbine wheel drag coefficient effect is higher at lower speed, thus the steam quality effect is minimum. Whereas at higher speeds the drag coefficient is lowest, thus the steam quality effect is highest.

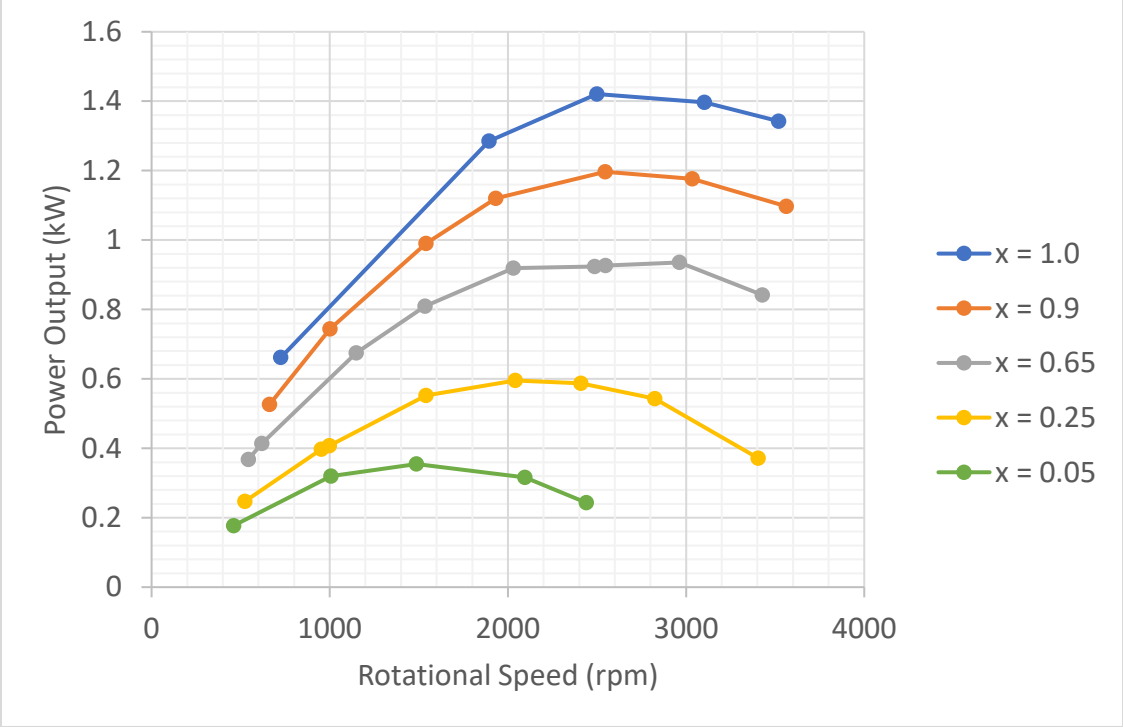

Figure 6.11 Terry turbine's power output vs Rotational Speed (ω) at steam qualities of 0.05 – 1.00, steam inlet pressure and back pressure of 45 psia, and 14.6(atm), respectively.

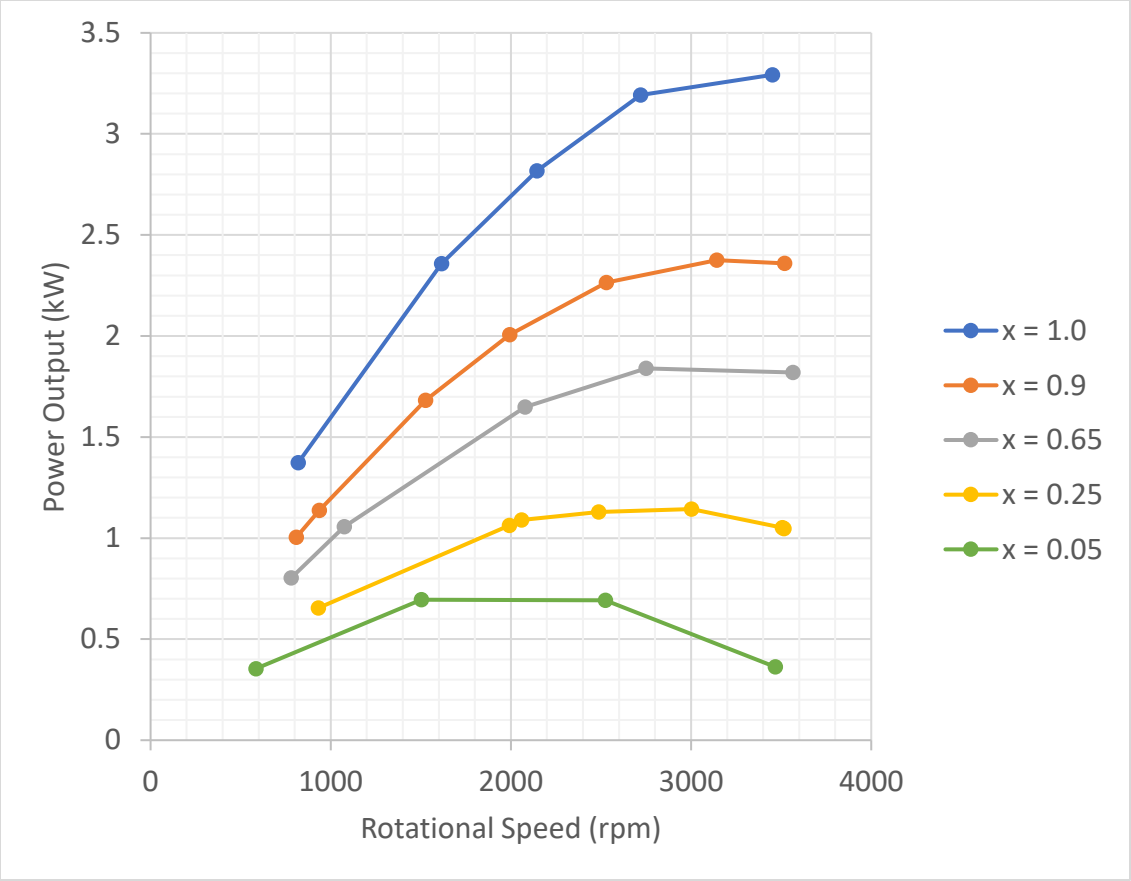

Figure 6.12 Terry turbine power output vs Rotational Speed (ω) at steam qualities of 0.05 – 1.00, steam inlet pressure and back pressure of 60 psia, and 14.6(atm), respectively

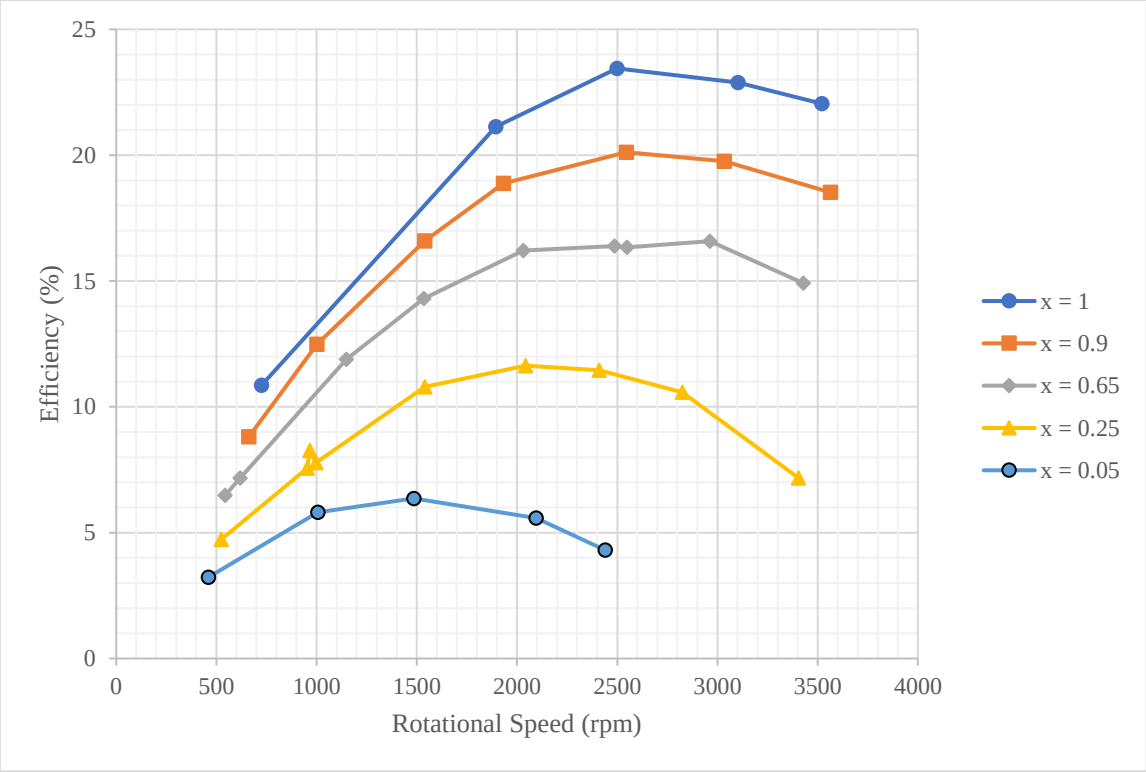

Figure 6.13 ZS-1 Terry turbine's Isentropic Efficiency (η) vs Rotational Speed (ω) at steam qualities of 0.05 – 1.00, steam inlet pressure and back pressure of 45 psia, and 14.6(atm), respectively.

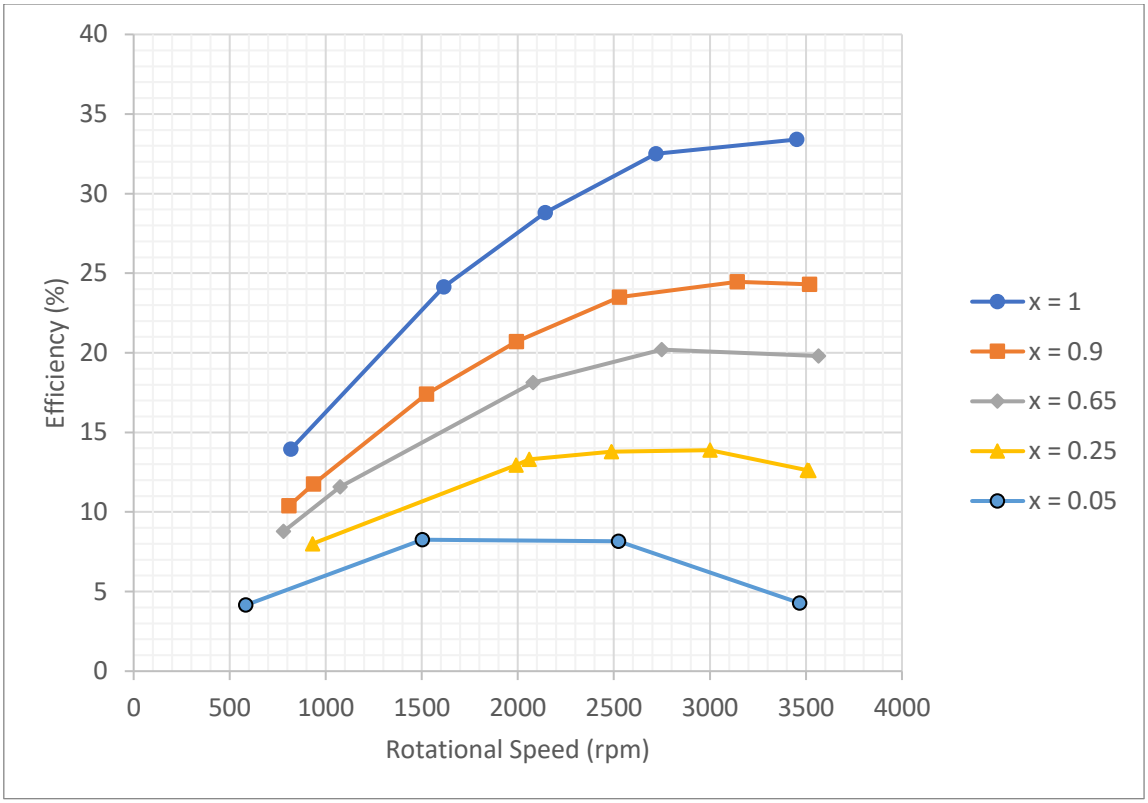

Figure 6.14 ZS-1 Terry turbine's Isentropic Efficiency (η) vs Rotational Speed (ω) at steam qualities of 0.5 – 1.00, steam inlet and back pressure of 60 psia, and 14.6(atm), respectively.

6.1.8. Effect of Turbine Back Pressure

6.1.8.1. Dry steam operation

Extended operation of RCIC system increases the wetwell water temperature and pressure at the exhaust side of the turbine, thus, the turbine back pressure is higher. Such scenarios stimulate the necessity to investigate the effect of back pressure on terry turbines performance.

Figure 6.16 shows turbine power output at x=1, 45 psia inlet pressures, but different back pressures (i.e., pressure ratios). The turbine exhaust steam pressure affects

the steam nozzle exit pressure. The steam pressure drop across the turbine is highest with atmospheric back pressure [30], which results in the highest jet velocity that impacts the turbine. Hence the momentum of the steam is highest with the highest turbine pressure drop. Increasing the back pressure, will decrease the pressure drop, and hence decrease the maximum jet velocity that generates most of the impact force on the turbine wheel.

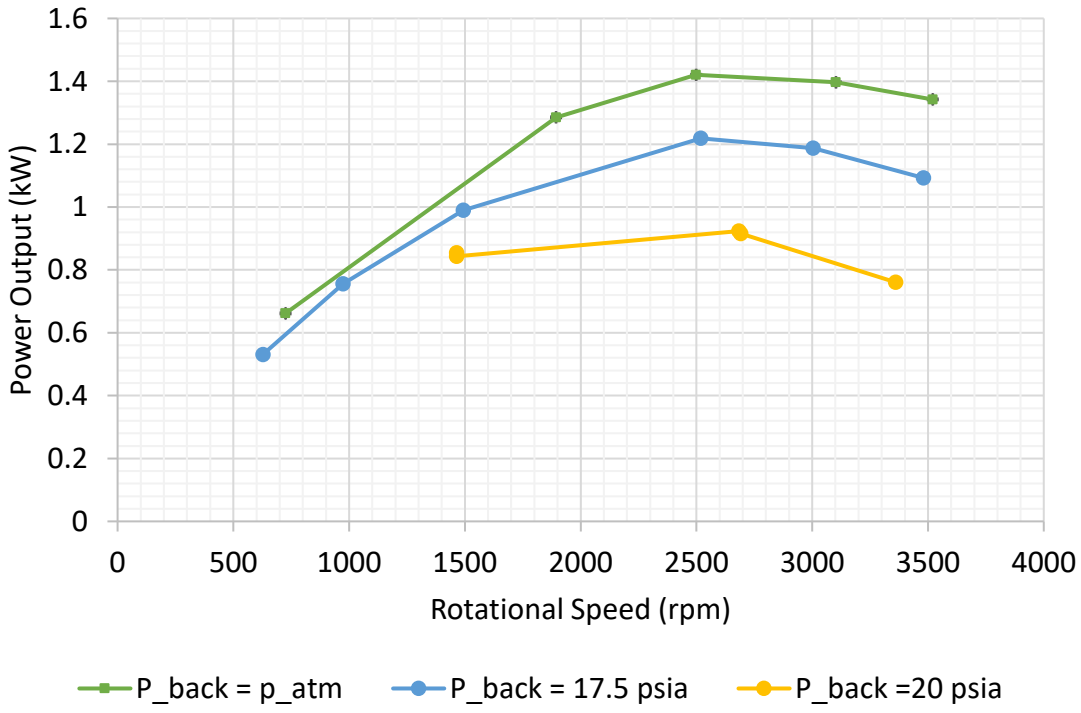

Figure 6.15 ZS-1 Terry turbine's power output vs Rotational Speed (ω) at pressure ratios of 0.32, 0.39, and 0.44 and DRY steam inlet pressure of 45psia

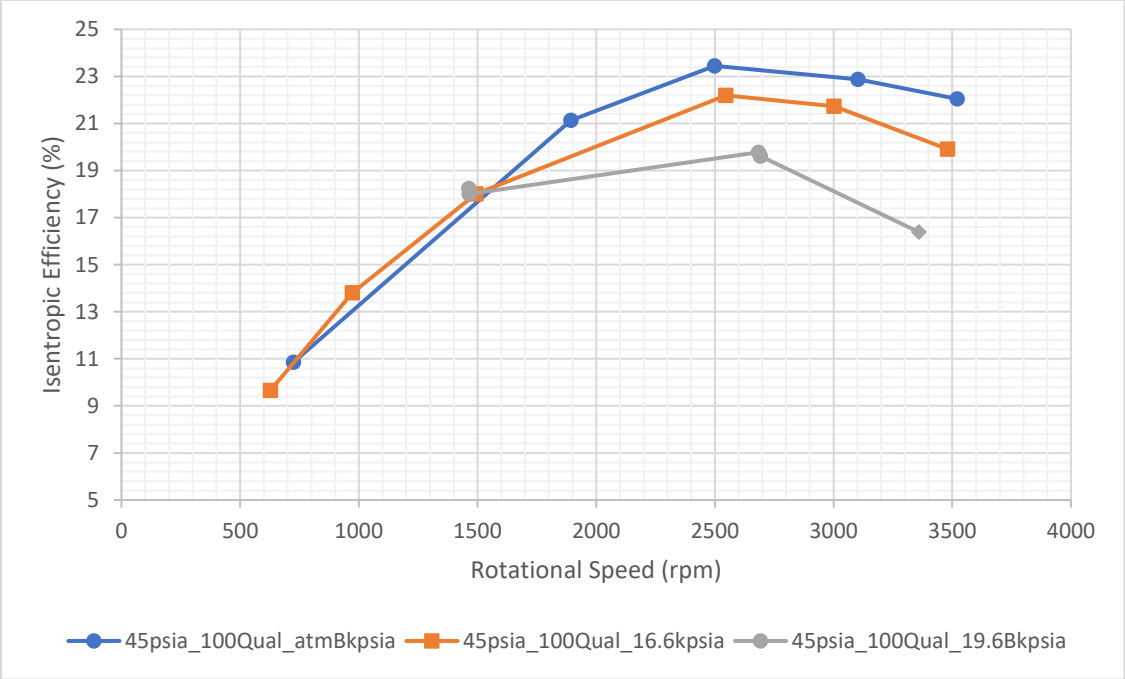

Figure 6.16 ZS-1 Terry turbine's Isentropic Efficiency (η) vs Rotational Speed (ω) at pressure ratios of 0.32, 0.39, and 0.44 and DRY steam inlet pressure of 45psia.

Figure 6.17 and Figure 6.18 show the back pressure effect for inlet pressures of 30, and 60 psia. The power output curves of the 30 psia tests, in Figure 6.17, are distinct each other at different back pressures. In contrast, the curves almost collapse onto each other at the higher pressure of 60 psia. From this observation comes the conclusion that the back pressure affects are lower at higher inlet pressure.

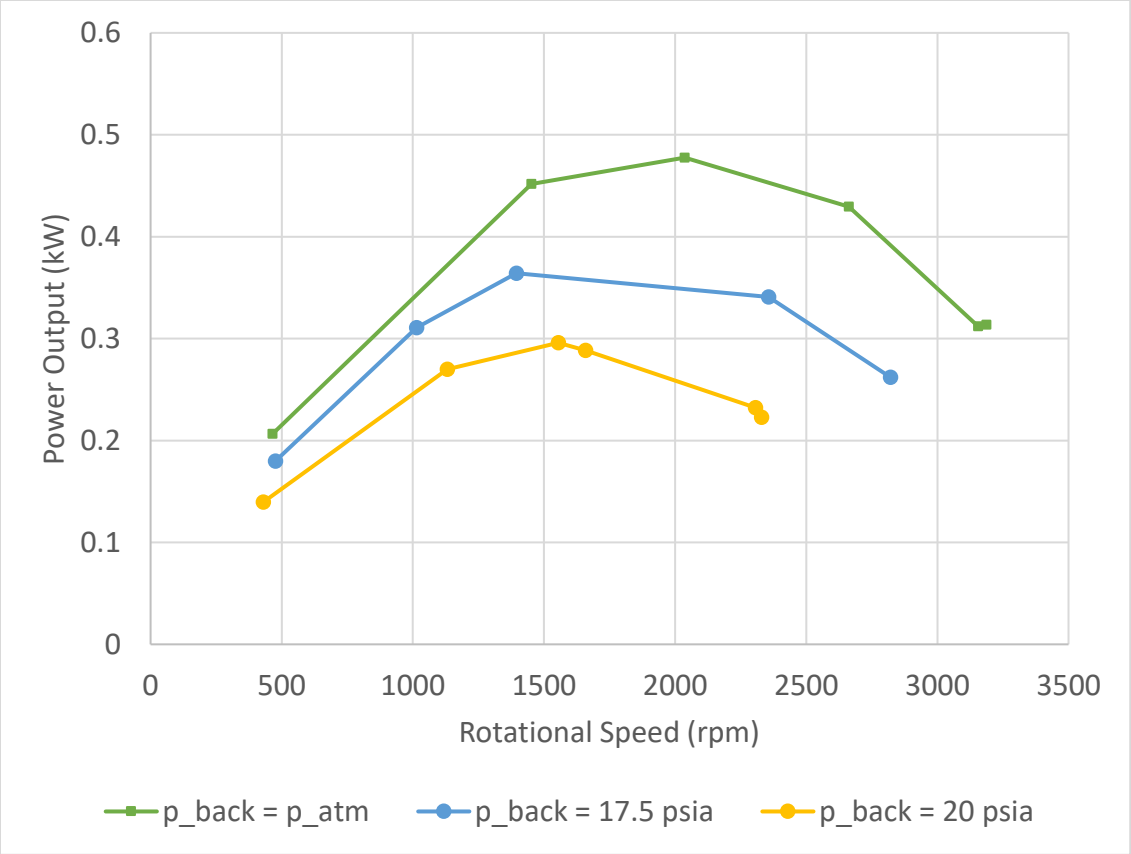

Figure 6.17 ZS-1 Terry turbine power output vs Rotational Speed (ω) at pressure ratios of 0.49, 0.59, and 0.67 and DRY steam inlet pressure of 30psia.

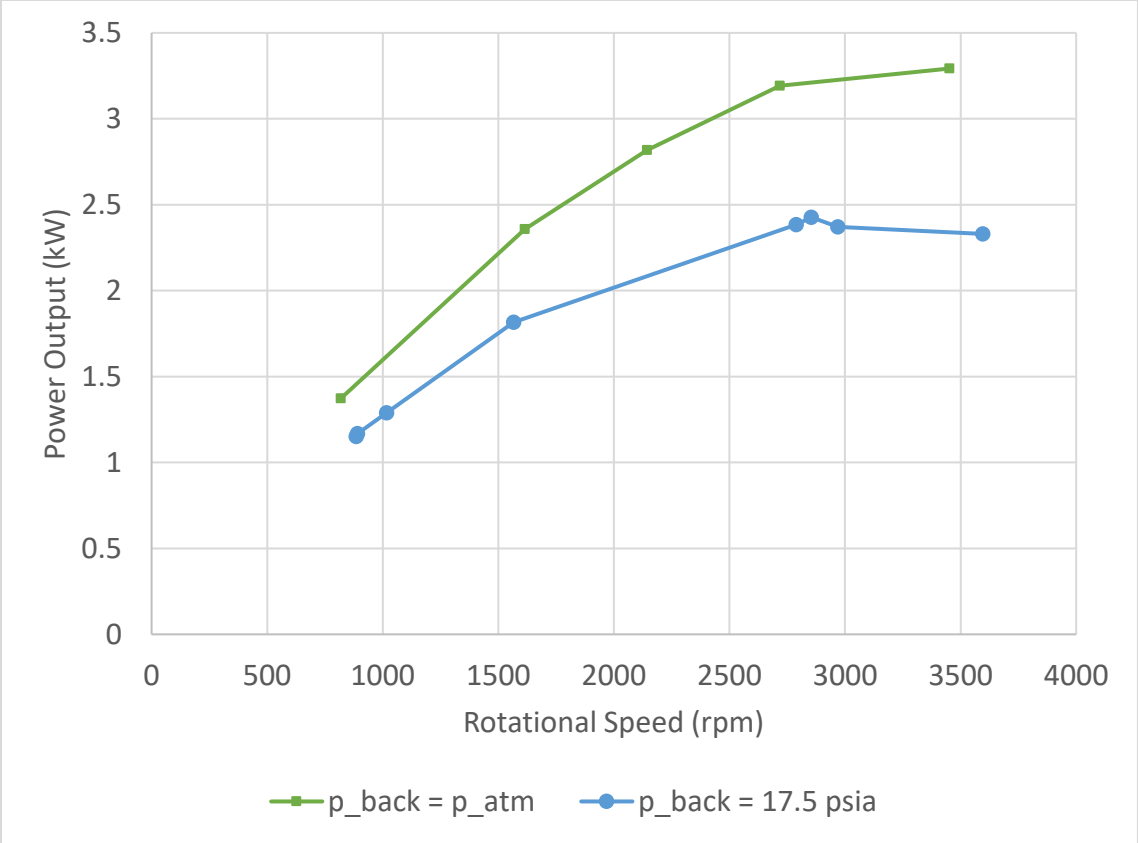

Figure 6.18 ZS-1 Terry turbine power output vs Rotational Speed (ω) at pressure ratios of 0.24, and 0.29 and DRY steam inlet pressure of 60psia

6.1.8.2. Wet steam operation

This section illustrates the turbine performance at different back pressures when operated with different steam qualities. Figure 6.19 shows the back pressure effect on the dry steam vs. wet steam tests with an inlet pressure of 30 psia. The back pressure effect is more apparent for dry steam operation than for wet steam operation. The presence of water minimizes the back pressure effect on the turbine performance as the steam expansion is less efficient with water presence. The same torque curves can be seen at higher pressures of 45 psia, and 60 psia in Figure 6.20 and Figure 6.21, respectively.

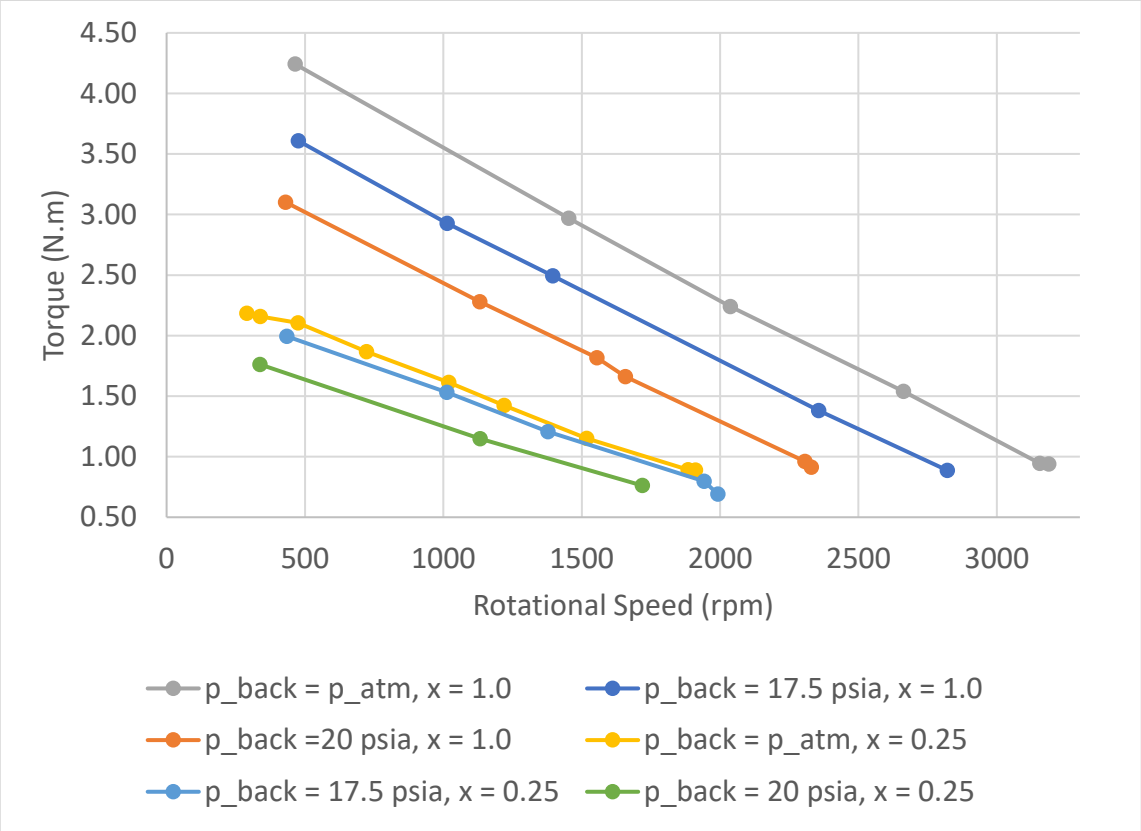

Figure 6.19 Back pressure effect on the dry steam vs. wet steam operated ZS1 turbine at an inlet pressure of 30 psia and pressure ratios of 0.49, 0.59, and 0.67

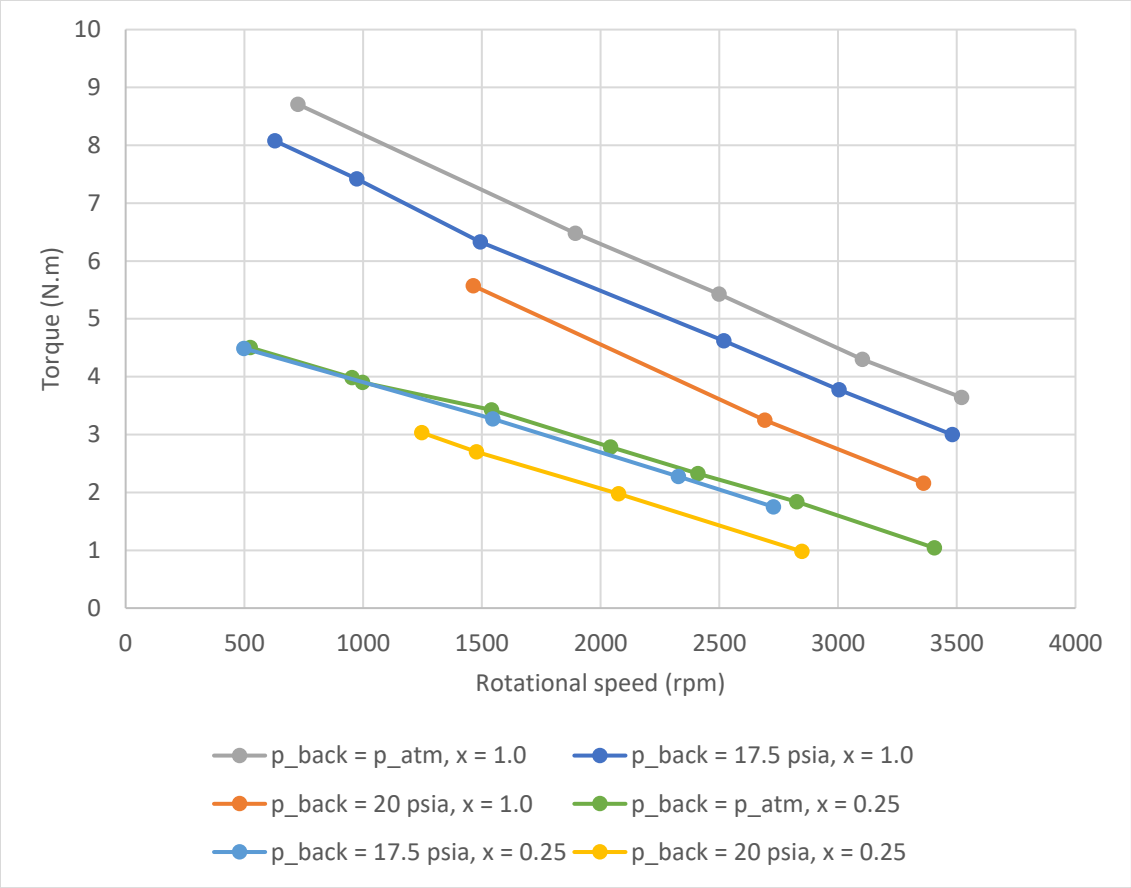

Figure 6.20 Back pressure effect on the dry steam vs. wet steam operated ZS1 turbine at an inlet pressure of 45 psia and pressure ratios of 0.32, .39, and 0.44

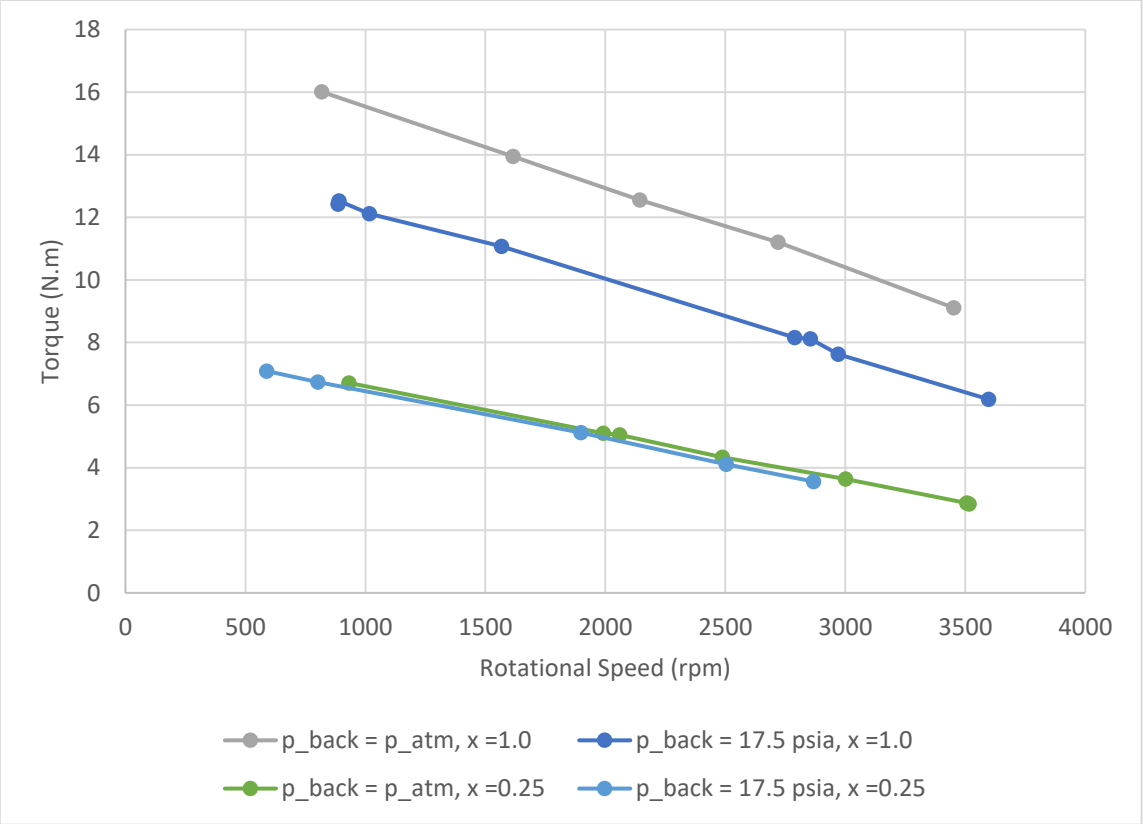

Figure 6.21 Back pressure effect on the dry steam vs. wet steam operated ZS1 turbine at an inlet pressure of 60 psia and pressure ratios of 0.24 and 0.29.

6.2. Turbopump characterization tests

This section includes the results of the turbopump tests, in which the RCIC turbopump analog performance is investigated in terms of the power output and the efficiency at low and medium inlet pressure and steam qualities of 1.00, 0.70, and 0.30.

6.2.1. Testing Parameters

- Steam pressure (psia): 25, 30, 40
- Steam quality*: 1.00, 0.90, 0.70, 0.30, 0.05
- Turbopump rotational speed* range (rpm): 300 – 3800

- Turbopump back pressure* (psia): 14.6 (~ atm), 16.6, 19.6

* Values varied by test.

6.2.2. Recorded Parameters

- Steam (or gas) temperature, pressure, and flow rate
- Water injection temperature, pressure, and flow rate
- Turbine Inlet and Back (Outlet) Pressures.
- RCIC pump pressure drop.
- RCIC pump outlet flowrate.
- Turbopump rotational speed.
- Turbopump Torque.

6.2.3. Testing Outputs

- Turbopump horsepower curves (i.e., shaft power output vs. speed).
- Turbopump efficiency curves (i.e., efficiency vs. speed).
- Turbopump power input curves (i.e., RCIC pump speed vs. flow rate)

6.2.4. Effect of Inlet Steam Pressure

The effect of changing the pump flow rate on rotational speed approach is used to evaluate the turbopump (or the RCIC pump) at different operational scenarios. Figure 6.22 shows the effect of the turbopump (i.e., the turbine) inlet pressures on the pump performance in terms of rotational speeds at different pump outlet flowrates. The pump performance is higher at higher turbine inlet pressures. The RCIC pump maximum loading on the turbine shaft is not associated with its minimum flowrate. Instead, the maximum pump loading occurs at the maximum power input, which is at moderate

operating flowrates, as shown in Figure 6.23**.** Moreover, the RCIC pump performance curve shows that the pressure drop is higher at low flowrate, but lower at higher flowrates. See Figure 6.23. Since power input is the multiplication of these two values, points at neither end of the curves would result in any maximum power input, but moderate values will.

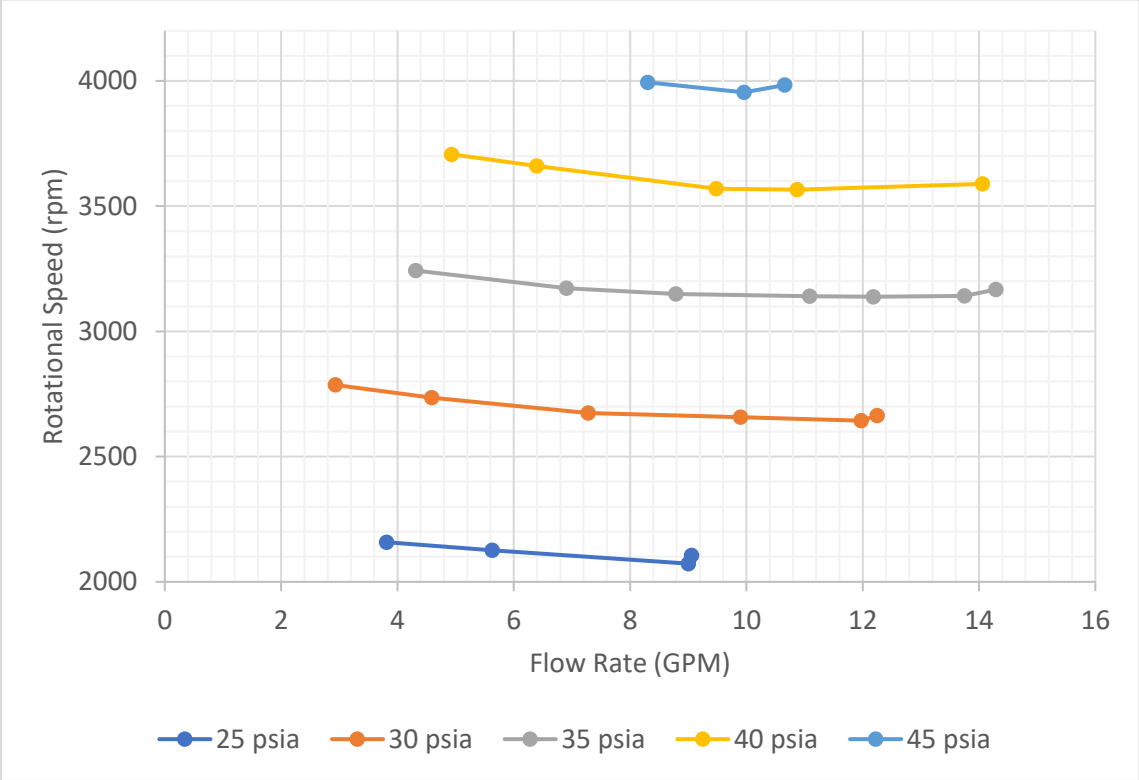

Figure 6.22. The effect of the turbine inlet pressures on the rotational speeds at different pump outlet flowrates

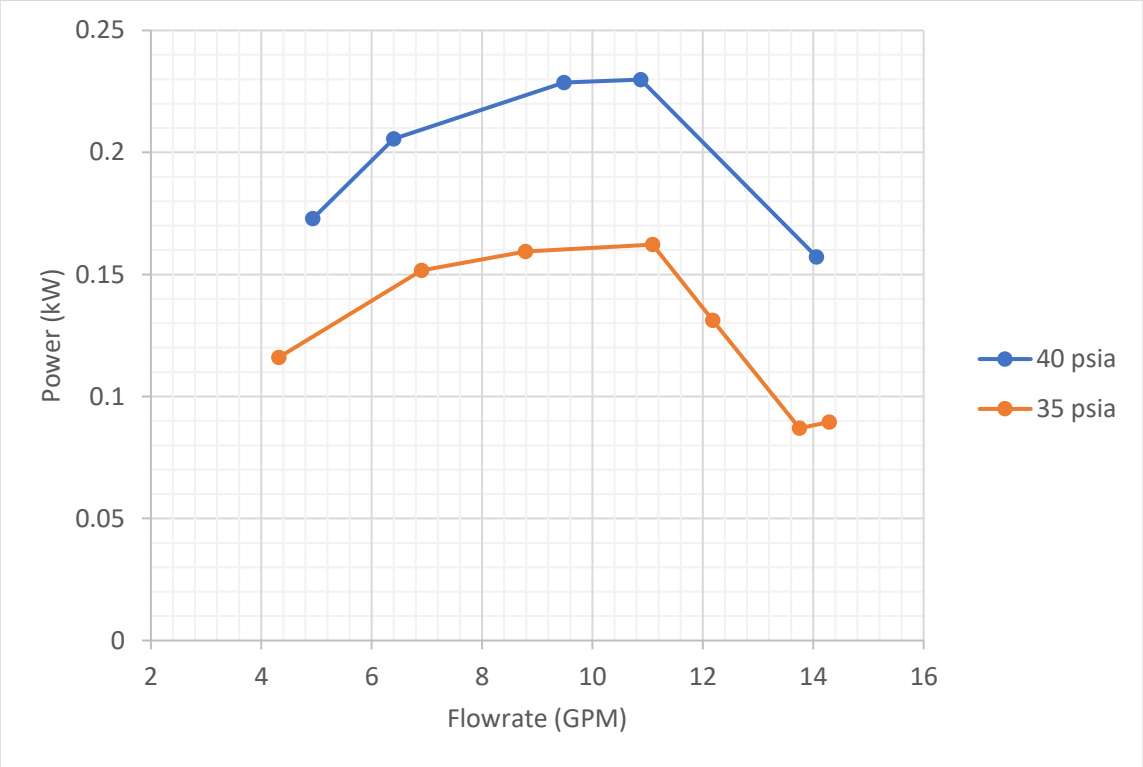

Figure 6.23. RCIC Pump power input (kW) vs. flowrate (GPM) under different inlet pressure of 35 and 40 psia

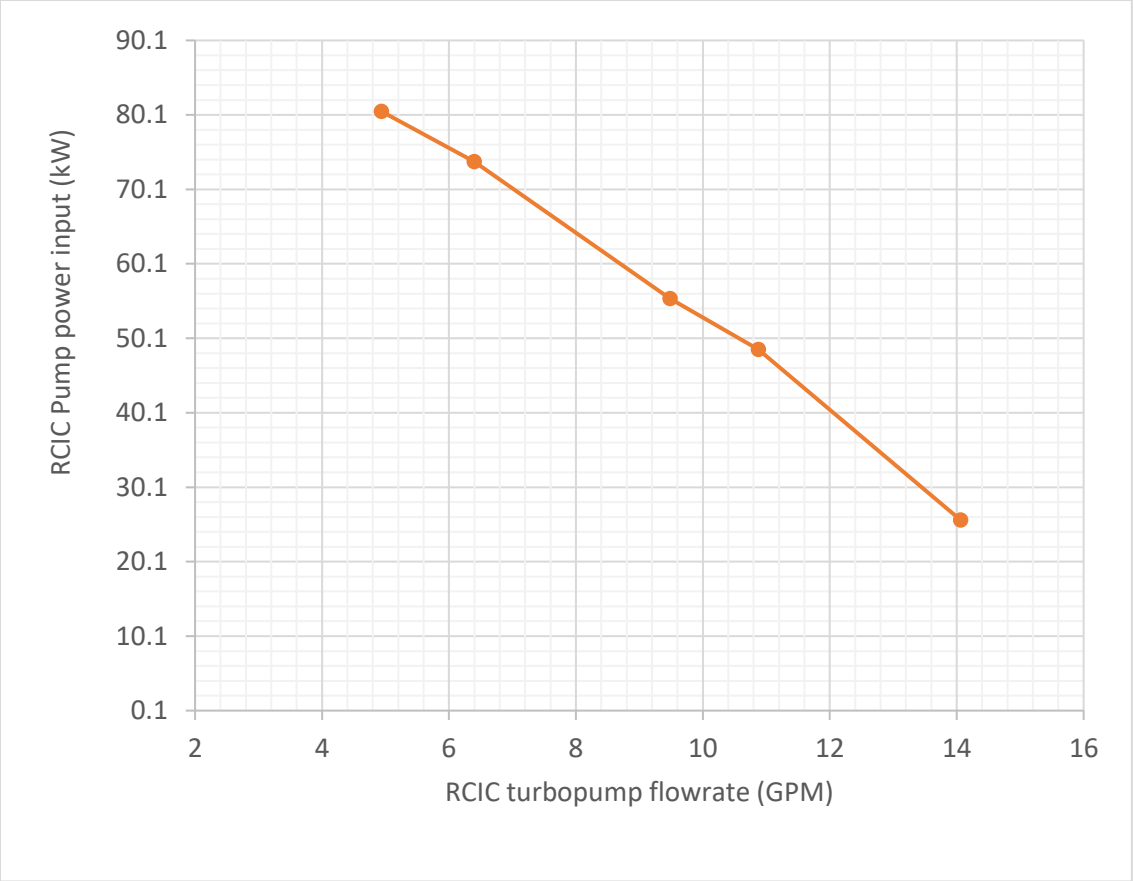

Figure 6.24. RCIC Pump performance curve; pressure drop (psia) vs. outlet flowrate (GPM) at 40 psia steam inlet, atmospheric back pressure. Of average rotational speed of 3620 rpm.

On the other hand, the turbopump Best Efficiency Point (BEP) skews to the left at higher pressure, which means that the turbopump become more efficient at moderate operation than at the higher end, as seen in Figure 6.25. The BEP trends can be seen in Figure 6.22, where the minimum rotational speed was spotted at higher flowrates vs lower inlet pressures.

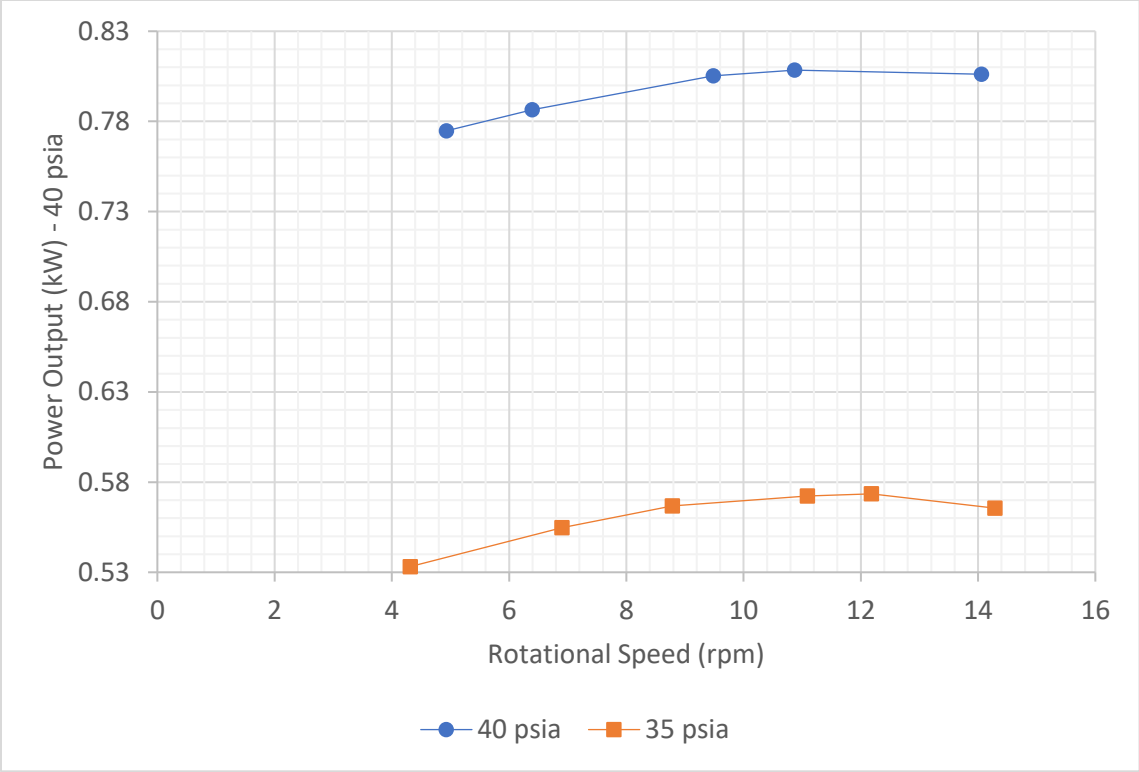

Figure 6.25 Turbopump power output (kW) at steam inlet pressures of 35 and 40 psia.

6.2.5. Effect of Steam Quality

Figure 6.26 shows the turbopump performance under two phase flow operation. It can be seen that the average rotational speed as well as the maximum outlet flowrate are dramatically decreasing with steam quality. On the other hand, the current results reaffirm previous findings two-phase operation potentials for RCIC terry turbines [10].

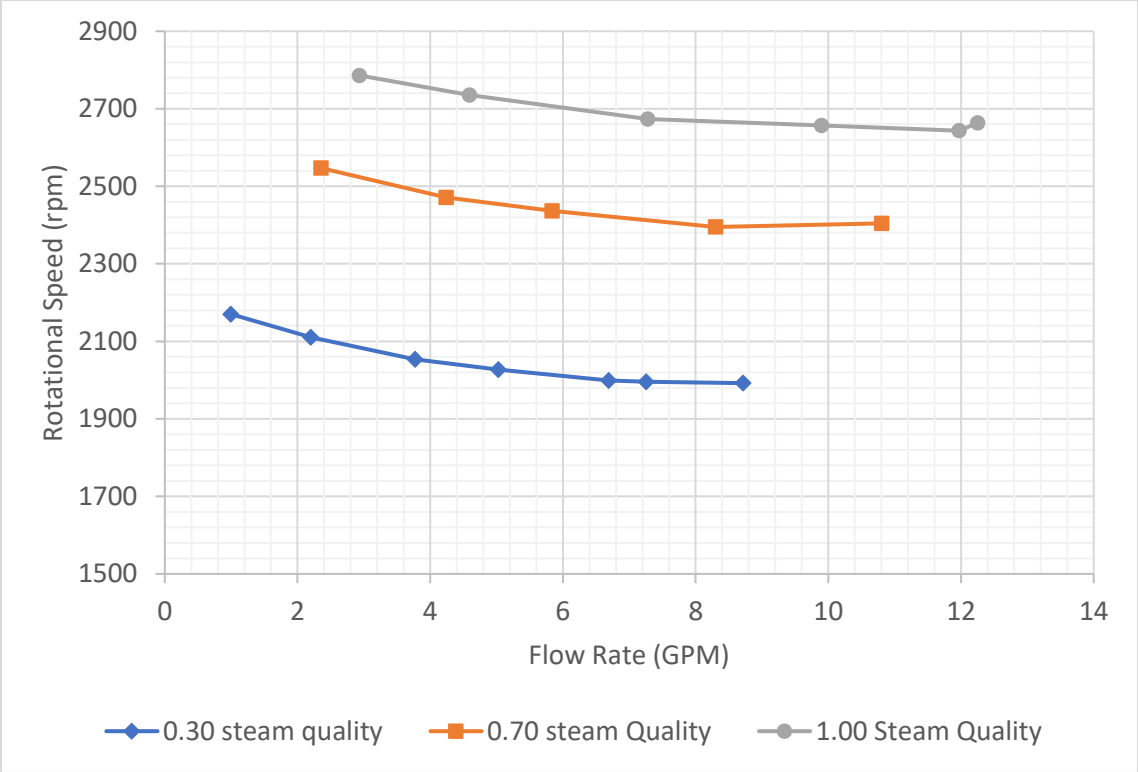

Figure 6.26 Steam Quality effect at 30 psia steam pressure inlet. The operational limit triangle shows the degradation effect on the turbopump flowrate performance.

7. SCALING ANALYSIS

Buckingham Pi Theorem [31] is used to establish the relationship between dimensional co-dependent variables. In which an independent physical quantity, represented by a dimensionless parameter, is a function of other depending variables. This approach was utilized in understanding the variation in the flow velocity, represented by the Flow Coefficient (Φ), as a function of the operational conditions and fluid properties, represented by the Power Output Coefficient (Π_{out}). In particular, the effects of density (ρ), rotational speed (ω), torque (τ), wheel size (D_z), and flow rate (Q), on the turbine power output were investigated.

The single-phase Flow Coefficient (Φ) and Power Output Coefficient (Π_{out}), proposed by [32], have been used throughout this discussion to carry a dimensionless analysis of Z and G Terry turbine performance at different operational conditions. As introduced earlier, the ZS is the smaller Terry turbine with the 18-inch diameter wheel and the GS is the full-scale (reactor size) turbine with the 24-inch diameter wheel. Moreover, the single-phase Affinity Laws (i.e., Π_{out} and Φ) have been modified to include two phase flow performance at different operational and flow conditions as shown in equations (7.1) - (7.6). The use of such approach, reduces the turbine performance curves into a distinct dimensionless performance curve which legitimize the benchmarking efforts.

Toward that end, the NHTS lab ZS-1 air test results (i.e., torque curves) have been benchmarked against TurboLab ZS-1 air test results [10] and GS-2 model air test

results [25] to validate the current scaling analysis efforts. Moreover, steam and air experimental data (i.e., Power Output Coefficient vs Flow Coefficient) has been benchmarked against real G-model Terry Turbine data from currently operating BWR power plants. To account for the size difference between Z and G models, the experimental values of the ZS-1 flow coefficients have been multiplied by a steam inlet nozzle diameter scaling factor.

7.1. Equations

The non-dimensional parameters used for this performance evaluation are as follows,

$$\Phi_{mix} = \frac{Q_{mix}}{\omega {D_z}^3} \tag{7.1}$$

$$Q_{mix} = Q_{water} + Q_{gas} \tag{7.2}$$

$$\Pi_{mix,out} = \frac{\omega . \tau}{\rho_{mix} \omega^3 D_z^5} \tag{7.3}$$

$$\rho_{mix} = \alpha \rho_g + (1 - \alpha)\rho_l \tag{7.4}$$

$$\alpha = \frac{x}{x + S(1 - x)(\frac{\rho_g}{\rho_g})} \tag{7.5}$$

$$S = \frac{V_g}{V_L} \tag{7.6}$$

$$Ma = \frac{V_e}{c} \tag{7.7}$$

$$V_e = \sqrt{2c_p(T_o - T)} \quad (7.8)$$

$$T_e = T_o \left(\frac{p_e}{p_o}\right)^{\frac{k-1}{k}} \quad (7.9)$$

$$c = \sqrt{kRT_e} \quad (7.10)$$

Where:

Q: Volumetric flow rate (cfm) of steam (or gas) and water.

ω: Shaft Rotational speed (rpm)

τ: Shaft Torque (N.m)

ρ: Density (kg/m^3)

ν_f: Liquid phase specific volume (m^3/kg)

ν_g: Steam (or gas) phase specific volume (m^3/kg)

α: Volumetric Fraction (of steam or gas)

x: Steam Quality (or Air Mass Fraction)

D_z: Diameter of the ZS-1 the turbine wheel, 18 in. for Z models and 24 in. for G model.

S: Slip Ratio. Assumed homogenous model, S = 1.

V: Velocity

Ma: Mach number

c : speed of sound at the medium .

R: Steam Gas Constant, 462 J/Kg.K

k: Specific heat ratio ($=c_p/c_v$) 1.32 for steam (or 1.4 for air) [27]

c_p: specific heat at constant pressure.

T_O: Stagnation Temperature at the Nozzle Inlet

p_o: Stagnation Pressure at the Nozzle Inlet

g: gas, steam or air.

L: Liquid, water.

e: steam nozzle exit

mix: gas-water mixture

7.2. NHTS vs. TurboLab ZS-1 Experimental Data Benchmarking

The NHTS lab ZS-1 air test results have been benchmarked against TurboLab ZS-1 air test results to validate the current scaling analysis efforts, see Figure 7.1. The two curves to the right in Figure 7.1 show that the TurboLab-generated 30 psia tests torque values were higher than those of the NHTS. Since the air testing temperatures during the TurboLab tests were higher than that at the NHTS (~ 20^OC), the power output coefficient was expected to be higher. Basically, larger temperature changes indicate greater expansion across the nozzle, hence larger power output [10]. Test results are included in APPENDIX F.

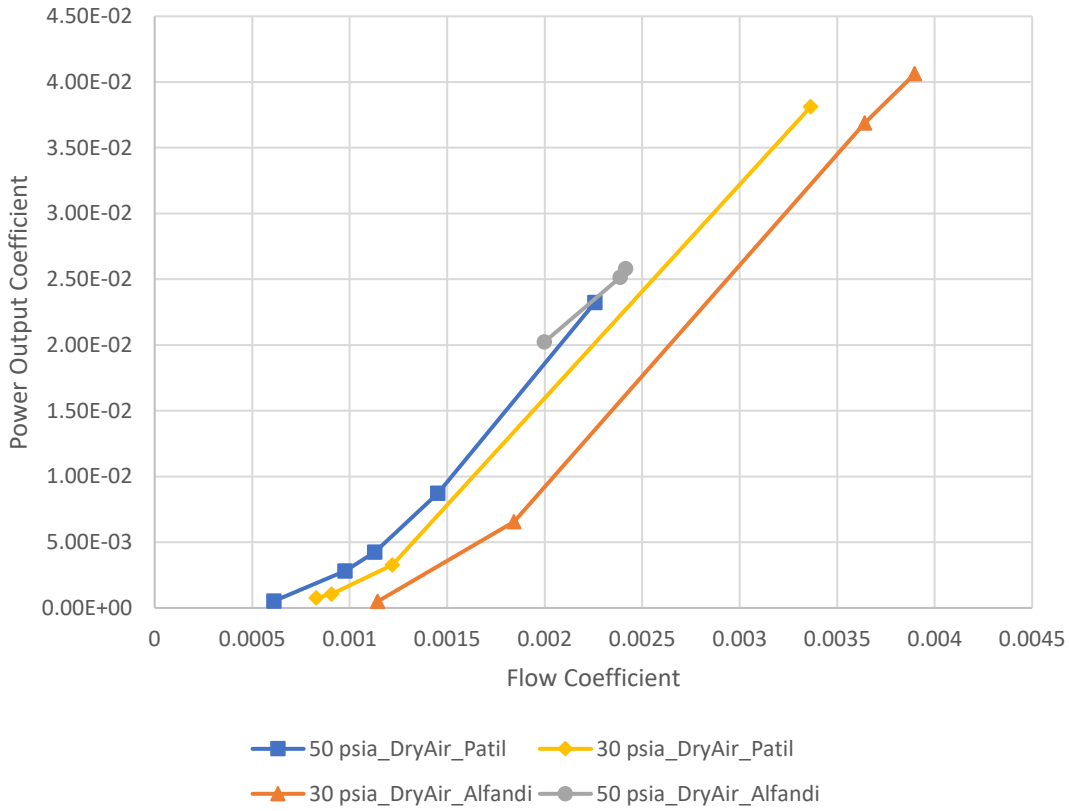

Figure 7.1 Comparison between air operated ZS-1 turbine at the same pressure between NHTS lab (Alfandi) vs Turbo lab (Patil)

Figure 7.2 depicts the turbine's performance in terms of shaft torque (τ) vs rotational speed (ω) at different turbine inlet pressures for Air and Steam. The intent here is to investigate the fluid scaling. The direct conclusion is that the turbine shaft torque for both steam and air tests was higher at higher pressure, which is mainly due to higher power input at higher inlet pressures.

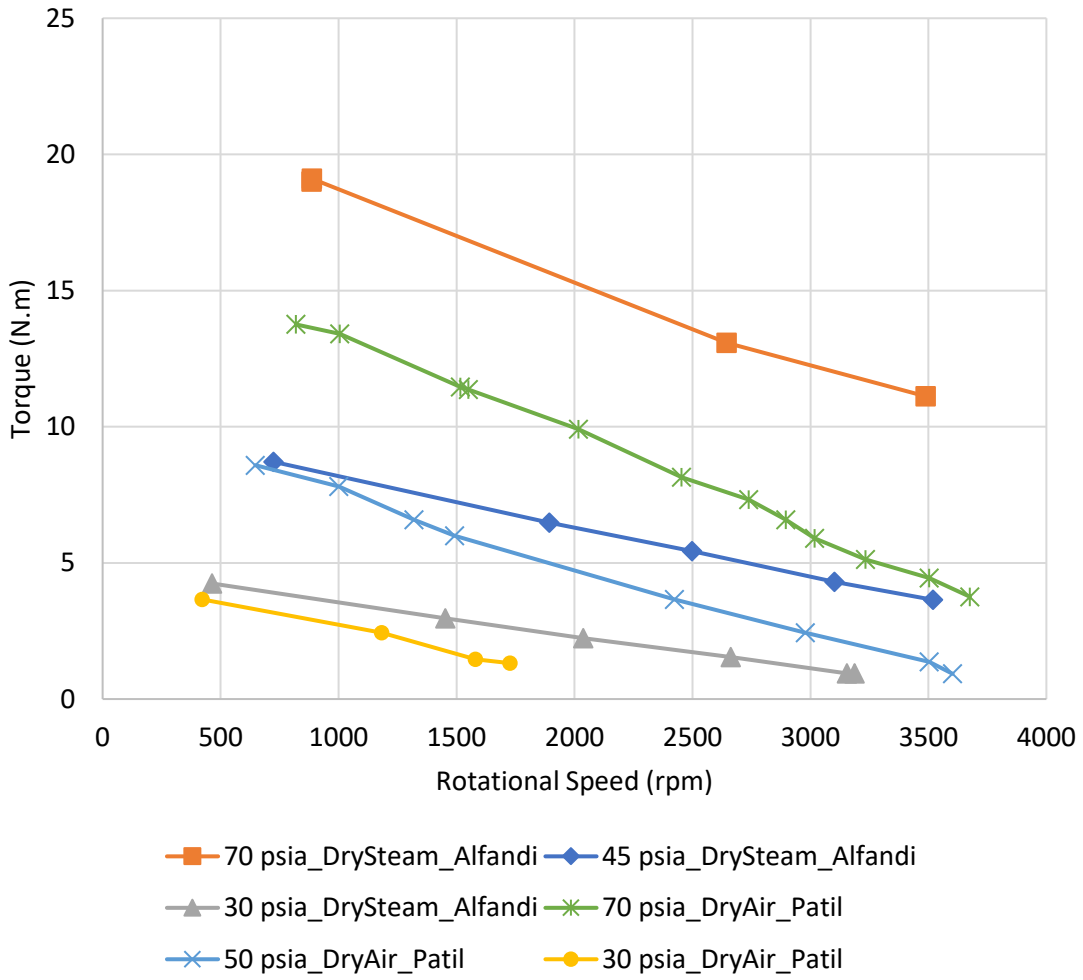

Figure 7.2 The turbine performance in terms of shaft torque (τ) vs rotational speed (ω)

The turbine shaft torque was found higher for steam operation than air for higher turbine speed due to steam higher enthalpies. However, this trend found less apparent at lower rotational speeds due to higher friction applied by the dynamometer loading and bearings on the turbine at lower speed vs higher speed (i.e., wheel drag coefficient effect). Eventually, the steam high internal energy effect is more apparent at higher speed (or at lesser drag coefficient effect), but less apparent at lower speed (or a higher

drag coefficient effect). It should be mentioned that the drag coefficient effect is decreasing with higher inlet pressure. This can be seen clearly in Figure 7.2, where the gap between the air torque curve and the steam torque curves is decreasing with inlet pressure increase.

7.3. Power Plant Data (Dry Steam) vs. GS2 Experimental Data (Dry Air)

Figure 7.3 shows the Turbolab GS-2 air test results benchmarked against actual power plant data that validate the current scaling analysis efforts. It was found that the $\Pi-\Phi$ curves are consistent with earlier findings that the turbine power output is higher at higher pressures. This explains the curves shifting to the left as the pressure increases. Tests results and matrix are included in APPENDIX G.

However, the curve of the 30 psia inlet pressure seems off scaling though. The airflow Mach number has been calculated using equations (7.7) - (7.10). It was found that the flow velocity is almost sonic and thus the expansion process is underestimated. Moreover, the turbine performance tends to be identical at higher pressures, where the flow at the nozzle exit plane is supersonic. On the other hand, the power output decreases at higher rotational speeds, where the power output is also at a minimum as shown earlier.

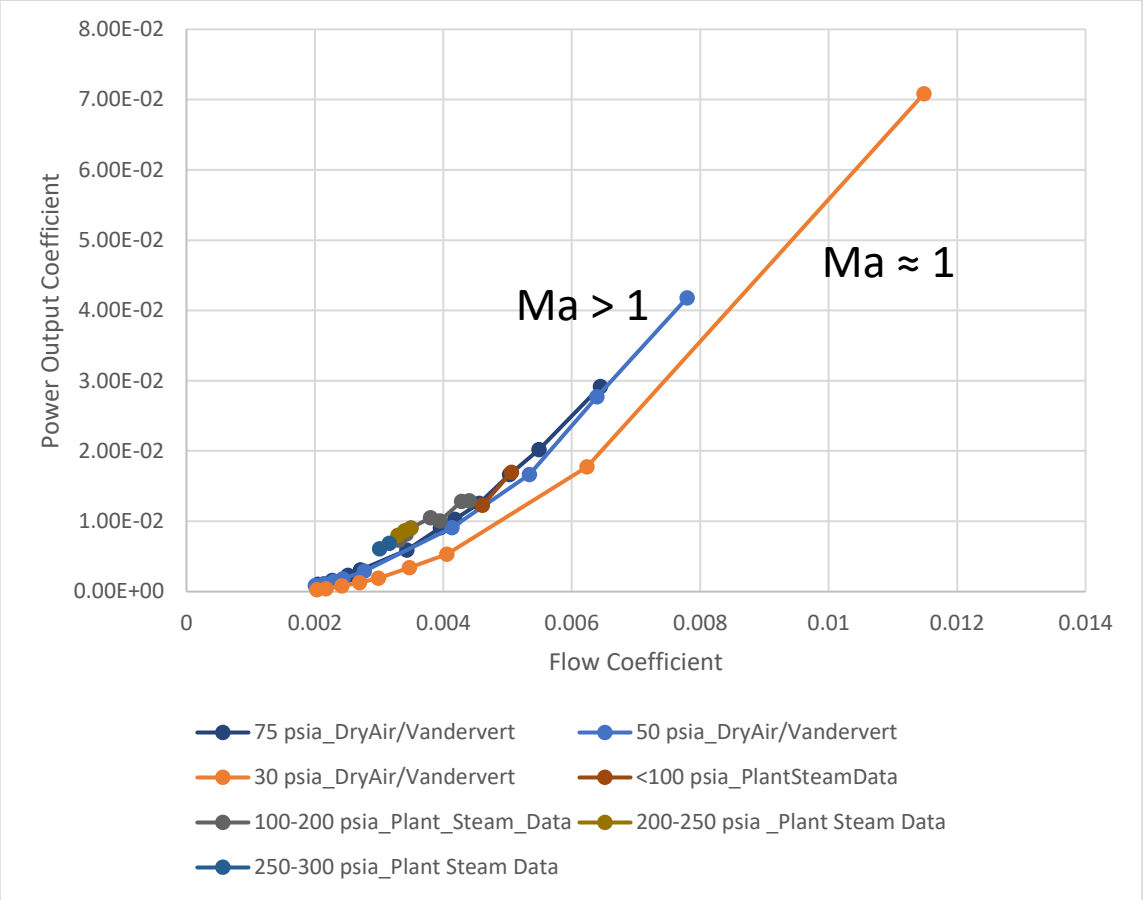

Figure 7.3 Turbolab GS-2 air test results benchmarking against actual power plant data at variant dry steam/dry air pressure values

7.4. ZS Experimental Data vs GS Actual Data

Figure 7.5 shows the Terry turbine power output coefficient vs flow coefficient for nuclear power plants (steam) and Experimental data (dry air) at different pressures. The Power Coefficient is seen to be directly proportional to the Flow Coefficient, for both fluids, due to the momentum increase of the flow at higher flowrates that is associated with higher power input. However, the effect of the size difference between the Plant GS-2 turbine and the ZS-1 Turbine is reflected in Figure 7.4.

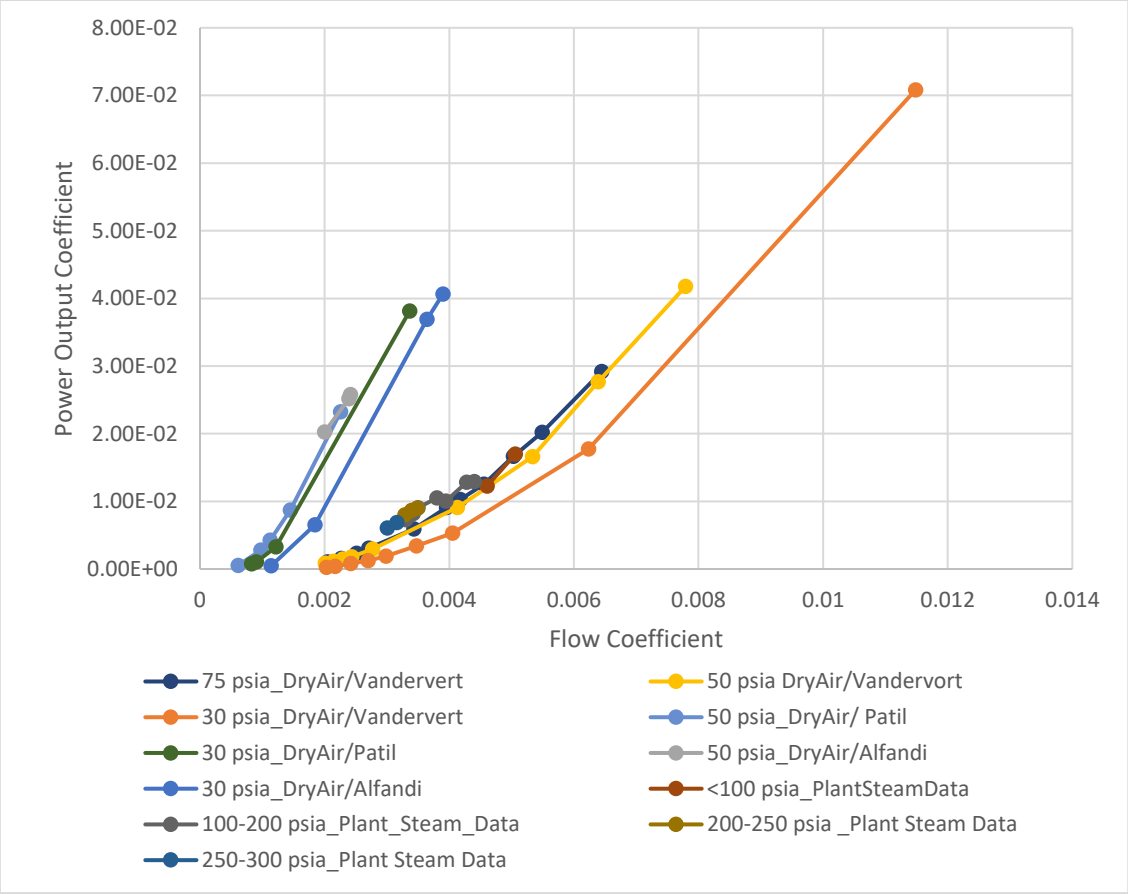

Figure 7.4 Terry turbine's power output coefficient vs flow coefficient of Nuclear Power Plants (steam) and TAMU (Dry Air) different pressures w/ multiplier

To account for nozzle size difference, the experimental values of the ZS-1 flow coefficients values from the TurboLab have been multiplied by a steam inlet nozzle diameter scaling factor, as follows. See Figure 7.5**.**

$$\text{Scaling Multiplier} = \left(\frac{D_G}{D_Z}\right)^2 = \left(\frac{0.548}{0.380}\right)^2 = 2.362$$

Where:

D_G: The G model Terry Turbine nozzle diameter (inches).

D_Z: The Z model Terry Turbine nozzle diameter(inches).

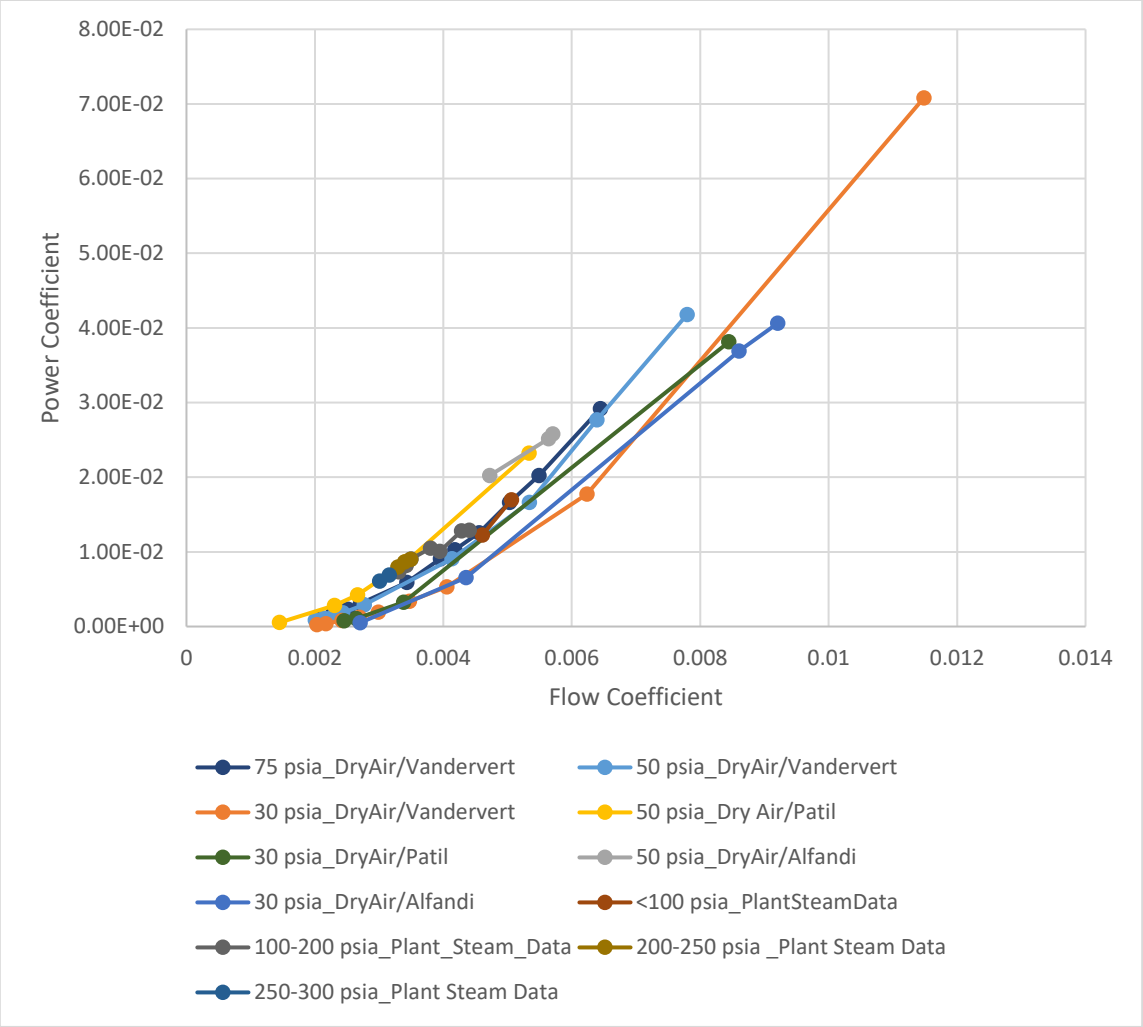

Figure 7.5. Terry turbine's power output coefficient vs flow coefficient of Nuclear Power Plants (steam) and TAMU (Dry Air) different pressures

At this point, the NHTS ZS-1 data is clearly scalable to the actual plant GS-2 data. The next sections investigate a dimensionless characterization of the turbine performance at different inlet pressures and back pressures, as well as different steam qualities.

7.5. NHTS Experimental Data vs. Power Plant Data

7.5.1. Steam Inlet Pressure

This section investigates the effect of different inlet steam pressures on the scaled analysis of a ZS-1 Terry turbine. Figure 7.6 depicts the nondimensional characterized response of the turbine when operated at different steam inlet pressures of 25, 30, 45, 60, and 75 psia. It was found that the $\Pi-\Phi$ curves are consistent with earlier findings in Section 6.1.5, in which the turbine power output is higher at higher pressures. This in turn explains the curves shift to the left as the pressure increases.

It was observed that the turbine performance at higher pressure is less affected by the internal losses within the turbine. Therefore, the $\Pi-\Phi$ curves tend to overlap as the pressure increases where the steam experiences supersonic flow at the nozzle exit. However, at steam pressure of 25 psia, the flow is subsonic at the nozzle exit, which explains the off-trend behavior as seen in the last curve in Figure 7.6. Equations (7.7) - (7.10) have been used to calculate the Mach number (Ma) at the turbine exit, assuming the inlet velocity is very small compared to the exit velocity.

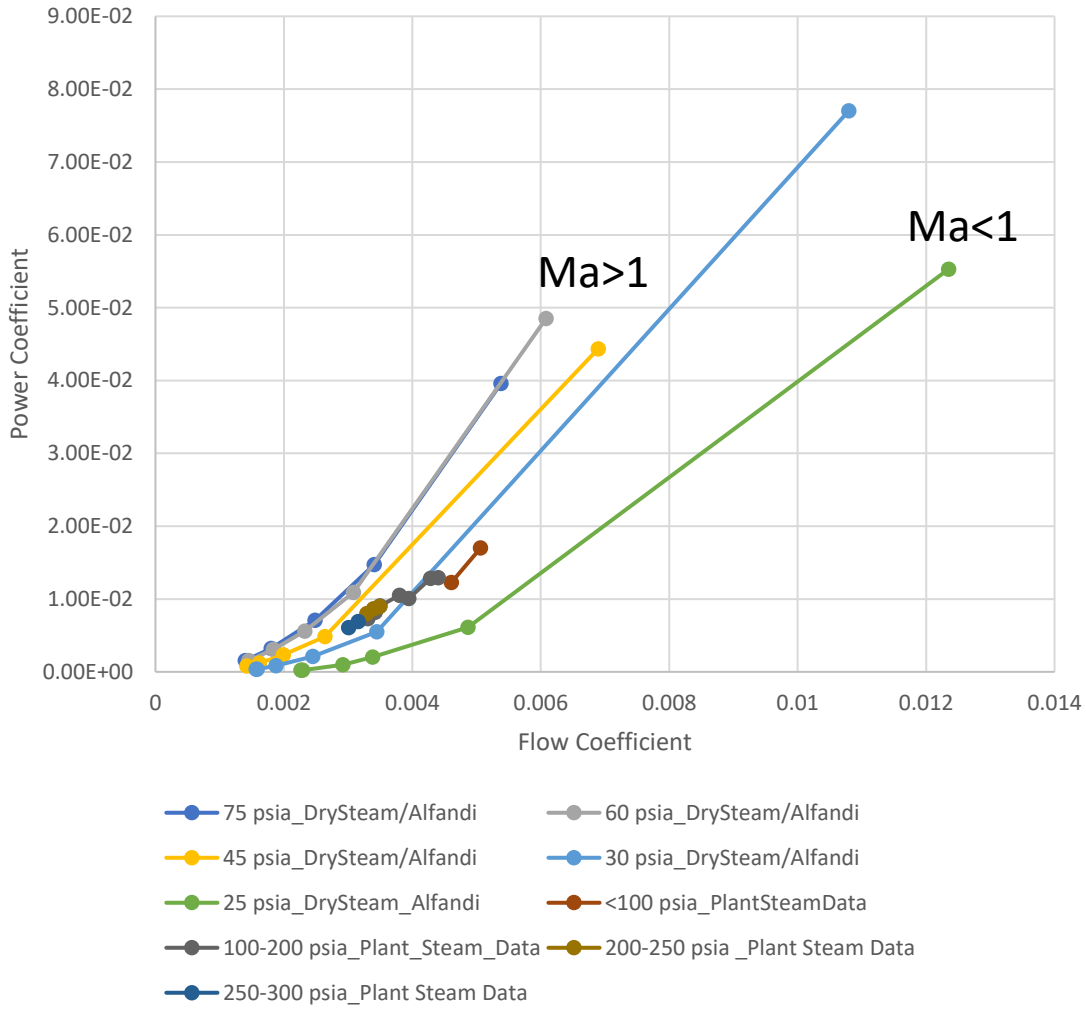

Figure 7.6 Terry turbine power output coefficient vs flow coefficient of nuclear power plants (steam) and NHTS (DRY Steam) different inlet pressures w/ multiplier

7.5.2. Steam Quality effect

Figure 7.7 shows the ZS-1 Terry turbine flow coef. vs power coef. for various steam qualities at 45 psia steam inlet pressure. It can be seen that the turbine power output coefficient is lower at lower steam qualities for the same flow coefficient. This is due to the momentum decrease of the steam as there is more water present in the

incoming flow. The same effect can be seen at different inlet pressures of 30 and 60 psia in Figure 7.8 and Figure 7.9, respectively.

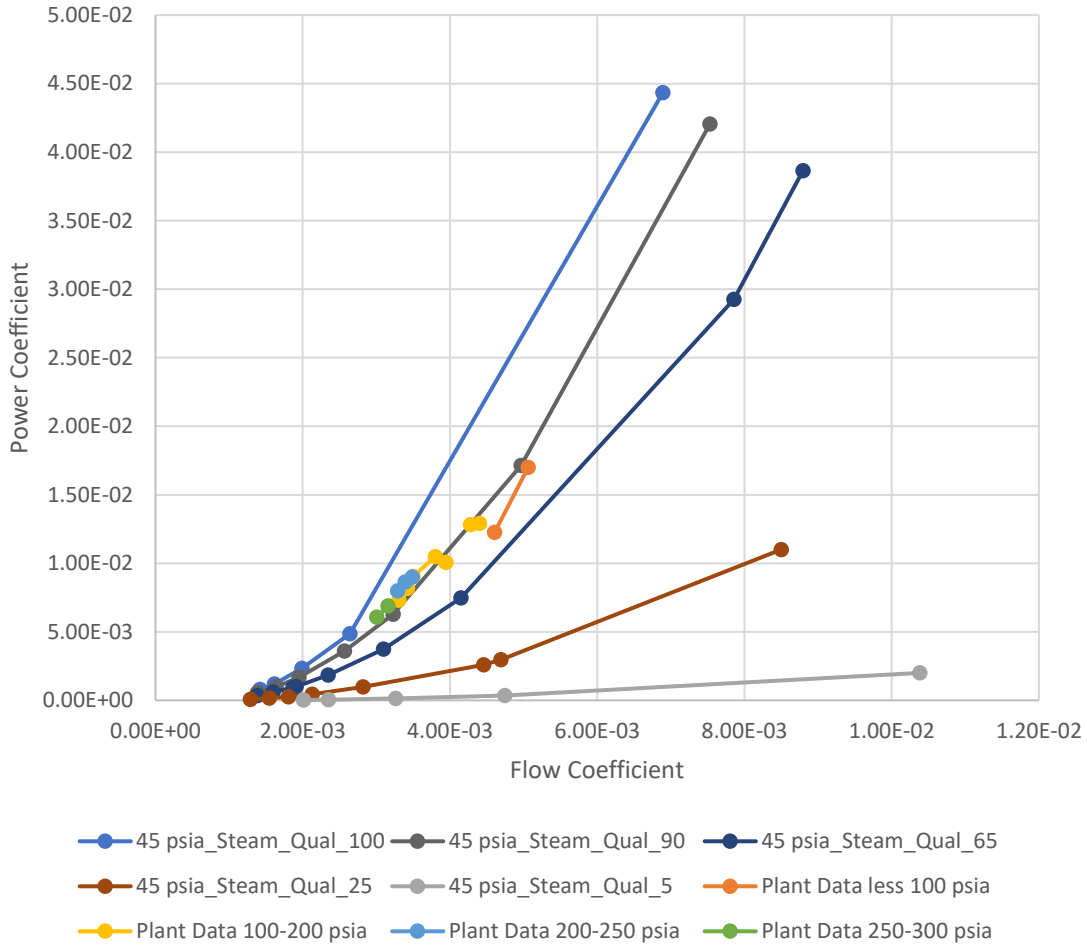

Figure 7.7 ZS-1 Terry Turbine flow coef. vs power coef. for variant steam qualities at inlet pressure of 45 psia. (NHTS Data)

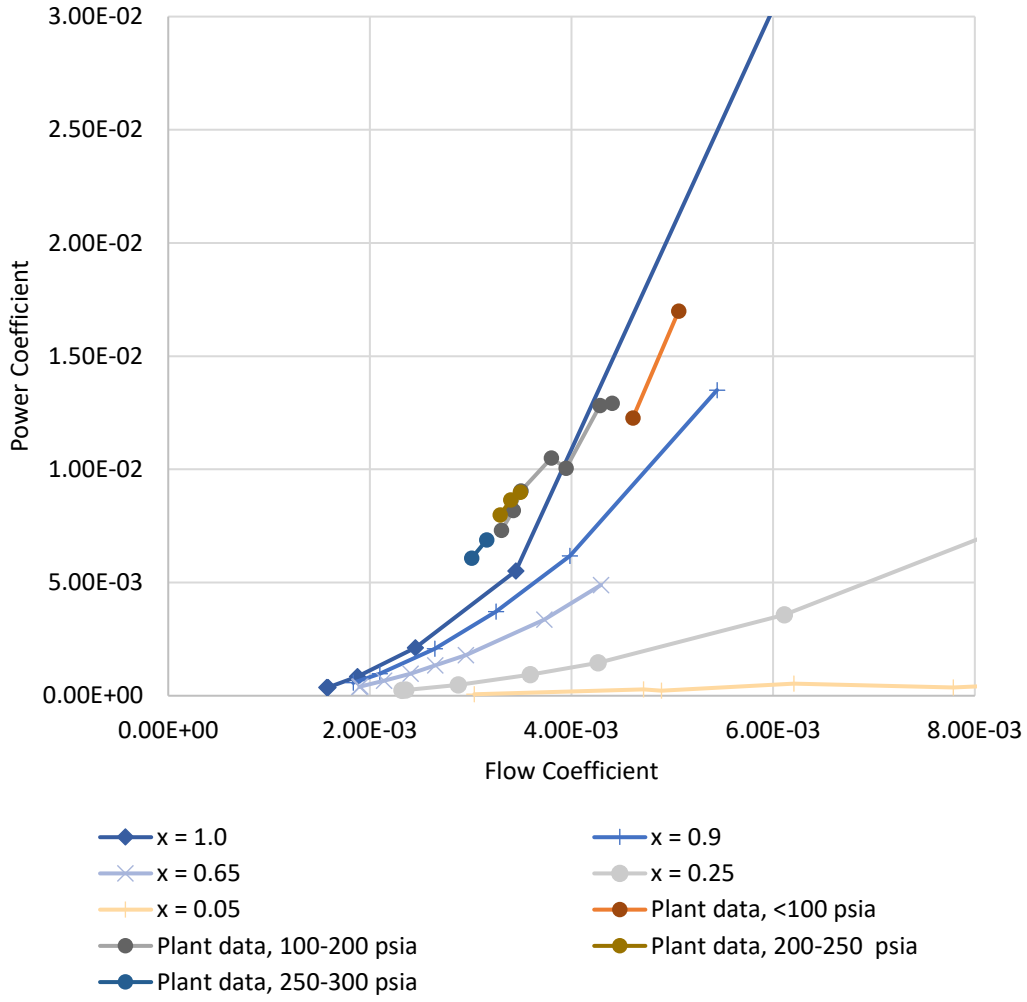

Figure 7.8 ZS-1 Terry Turbine flow coef. vs power coef. for variant steam qualities at inlet pressure of 30 psia. (NHTS Data)

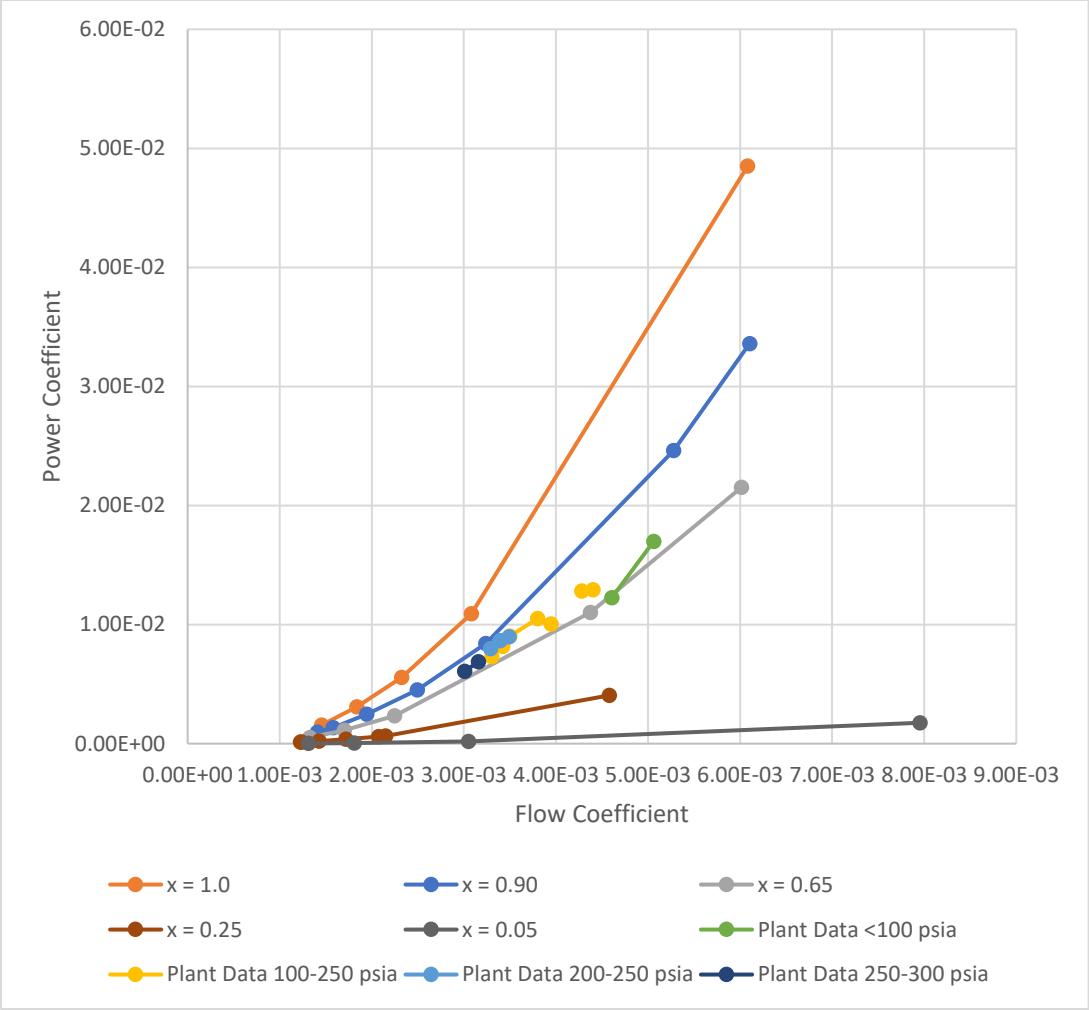

Figure 7.9 ZS-1 Terry Turbine flow coef. vs power coef. for variant steam qualities at inlet pressure of 60 psia. (NHTS Data)

7.5.3. Back Pressure Effect

7.5.3.1. Dry Steam

The turbine performance at different back pressures seems consistent with the physics of the steam expansion in the nozzle. In general, steam expansion is larger at higher pressure drop across the turbine. In the case of increasing back pressure, the pressure drop across the turbine becomes smaller, and thus the steam expansion is less.

Figure 7.10 shows that as the pressure drop across the turbine decrease, the power output of the turbine decreases. The curves tendency to shift to the right as the back pressure increase, supporting the above-mentioned hypothesis. The same turbine profiling was noticed at different inlet pressures of 45 psia and 60 psia as shown in Figure 7.11 and Figure 7.12. It was also noted that the back pressure effect diminished at higher rotational speeds, where the power output coefficient is minimum.

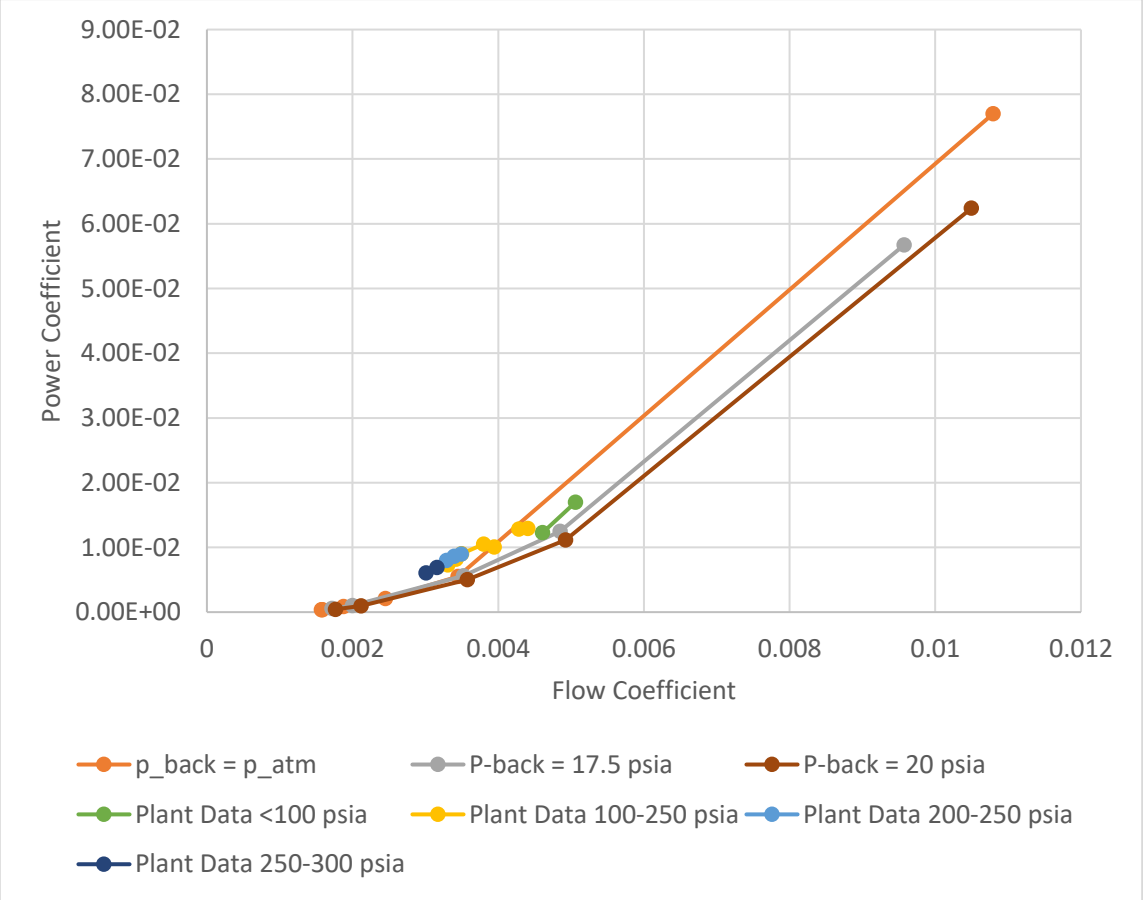

Figure 7.10 ZS-1 Terry Turbine flow coef. vs power coef. at inlet pressure of 30 psia but pressure ratios of 0.49, 0.59, and 0.67

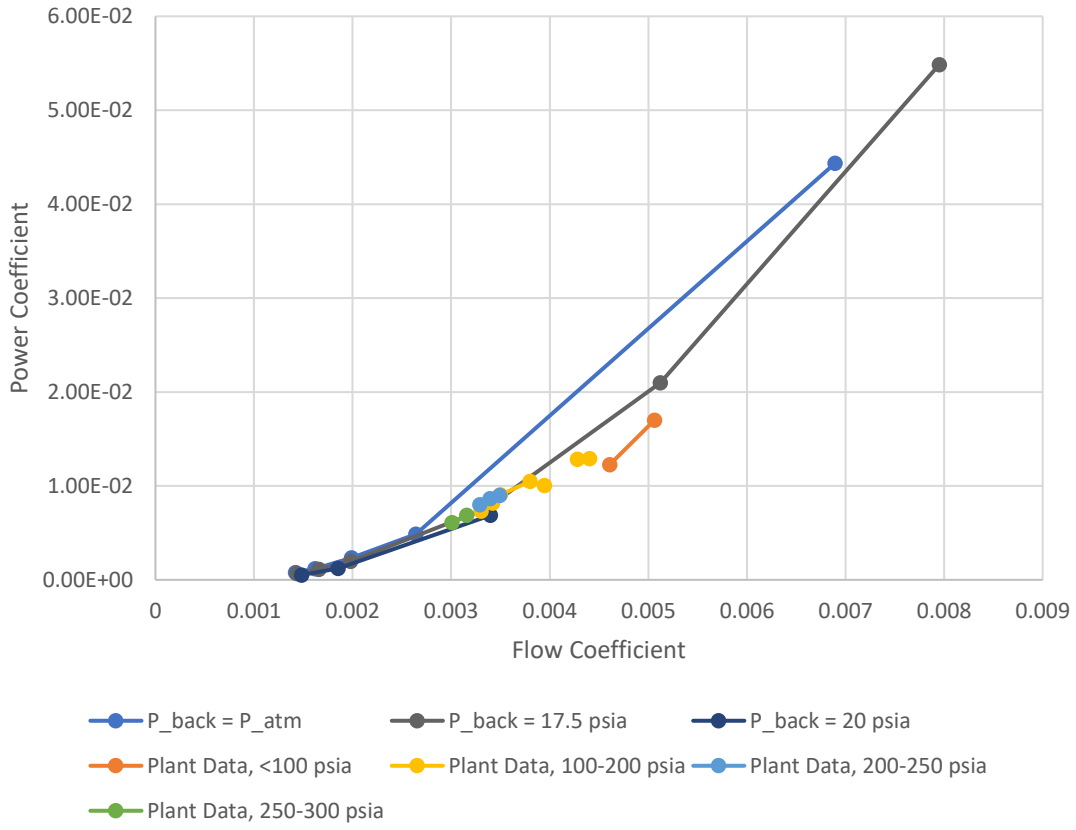

Figure 7.11 ZS-1 Terry Turbine flow coef. vs power coef. at inlet pressure of 45 psia, but pressure ratios of 0.32, 0.39, and 0.44

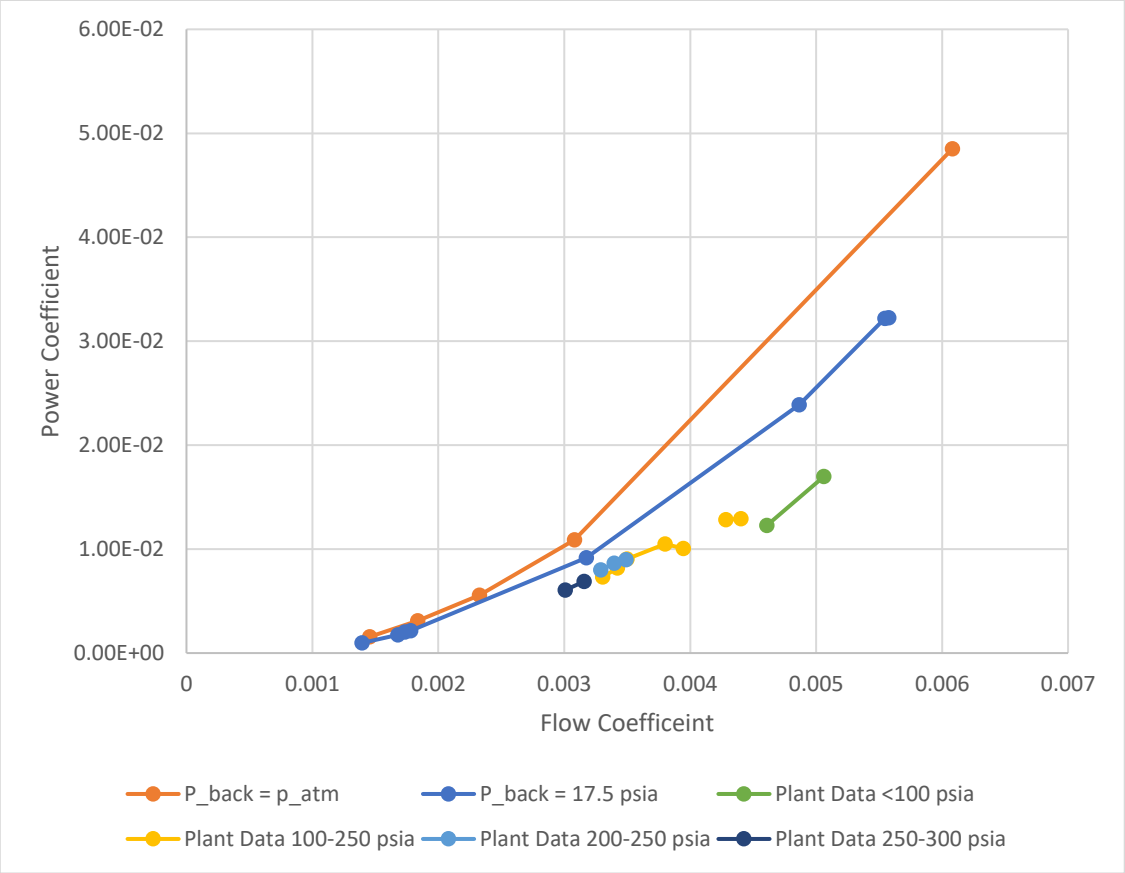

Figure 7.12 ZS-1 Terry Turbine flow coef. vs power coef. at inlet pressure of 60 psia, but pressure ratios of 0.24, and 0.29

7.5.3.2. Wet Steam

The current section investigates the back pressure effect on wet steam operation of the Terry turbine, and its correlation to the actual power plant data. Toward that end, the turbine performance has been investigated at different inlet steam qualities while at a higher than atmospheric back pressure. Figure 7.13 depicts the difference in the turbine response between wet steam (x = 0.25) and dry steam (x=1) operation, each at a different back pressure of 14.7 psia, 17.5 psia, and 20 psia, while fixing the inlet pressure at 30 psia. The same experiment has been investigated with different inlet pressures of 45 psia, and 60 psia to see the effect of higher pressures, see Figure 7.14 and Figure 7.15. It was concluded that, regardless the value of the inlet pressure, the back pressure effect is always lower at lower steam qualities. The occurring momentum loss, due to the water droplets in the nozzle, dominates the effect of the back pressure.

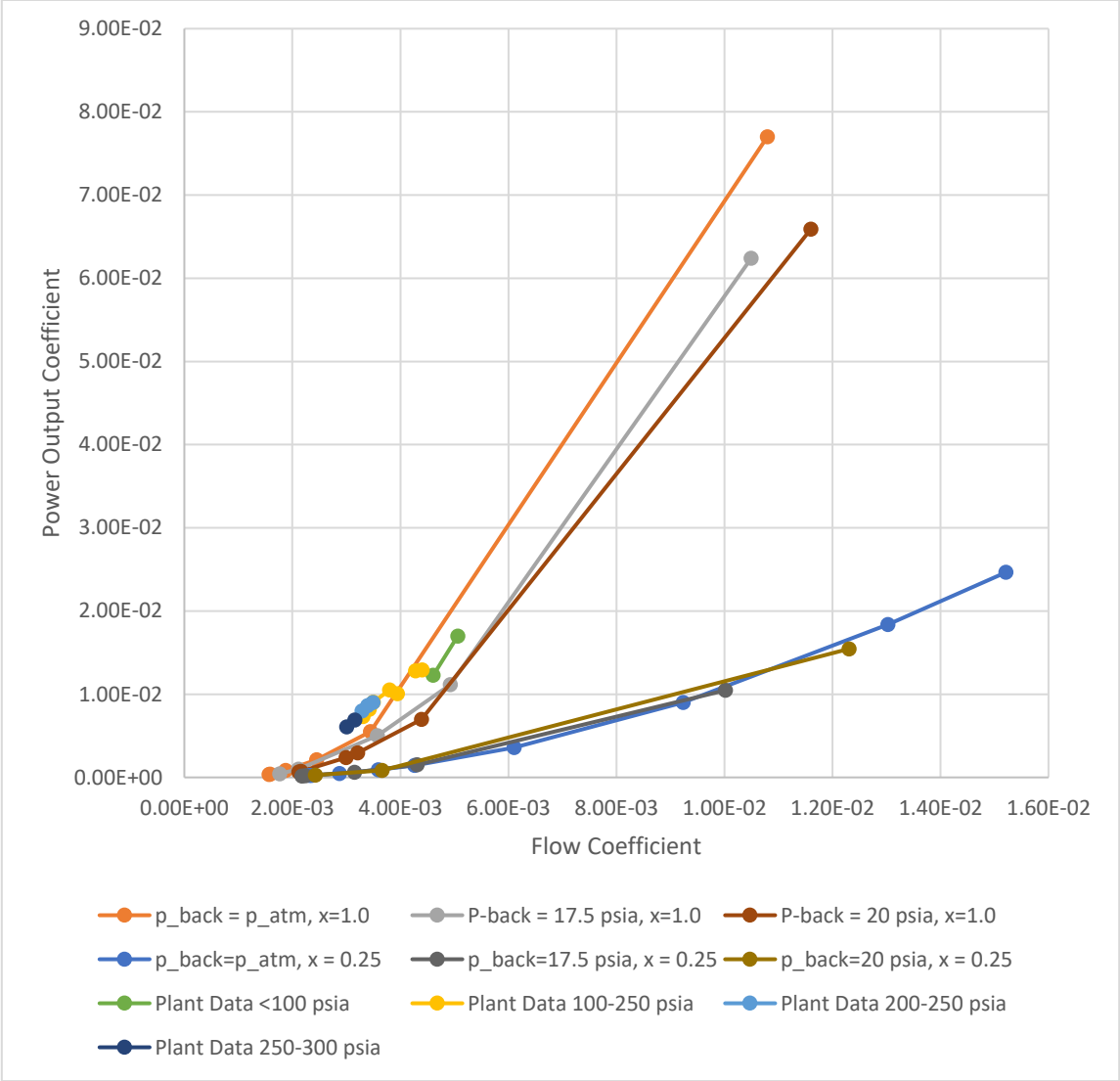

Figure 7.13 ZS-1 Terry Turbine flow coef. vs power coef. at inlet pressure of 30 psia but steam qualities of 1.0 and 0.25, and pressure ratios of 0.49, 0.59, and 0.67 (NHTS Data)

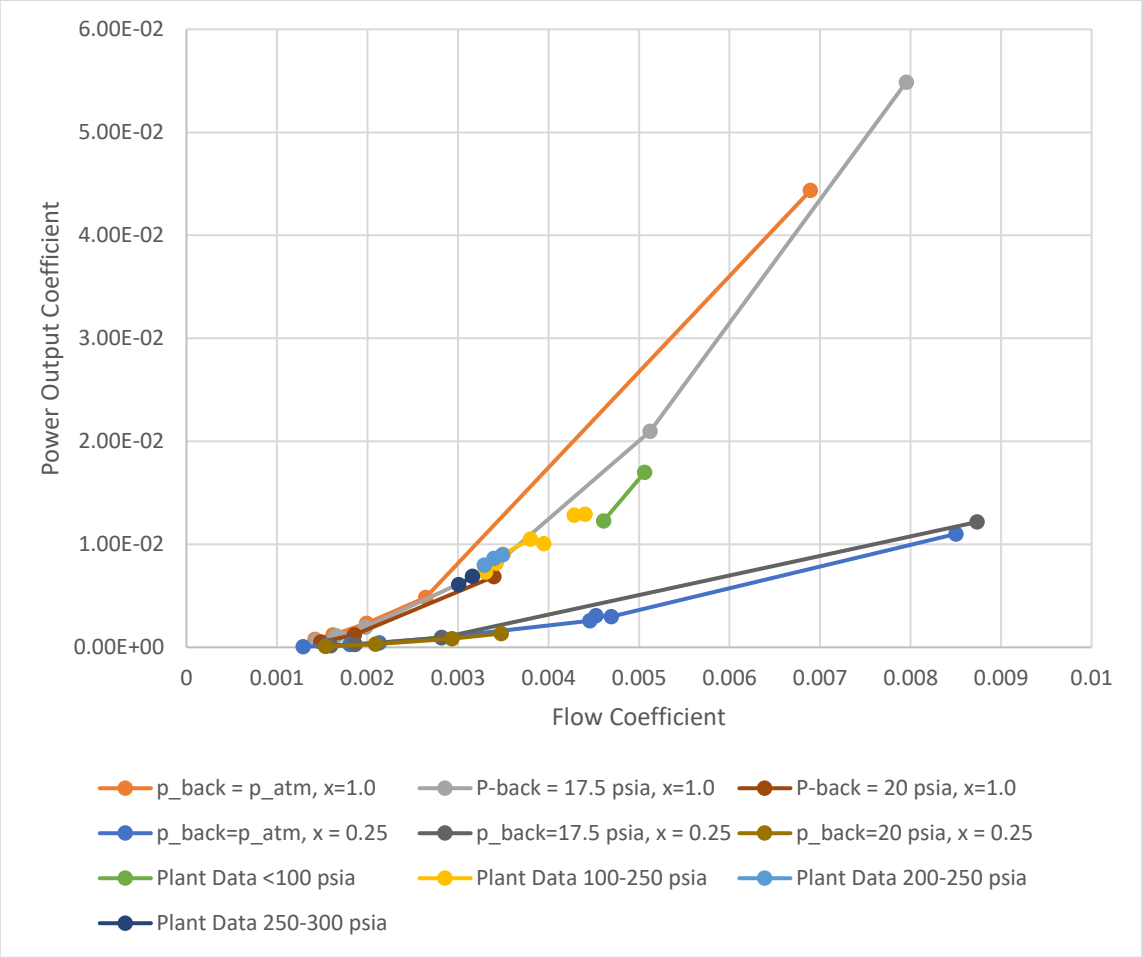

Figure 7.14 ZS-1 Terry Turbine flow coef. vs power coef. at inlet pressure of 45 psia but steam qualities of 1.0 and 0.25, and pressure ratios of 0.34, 0.39, and 0.44 (NHTS Data)

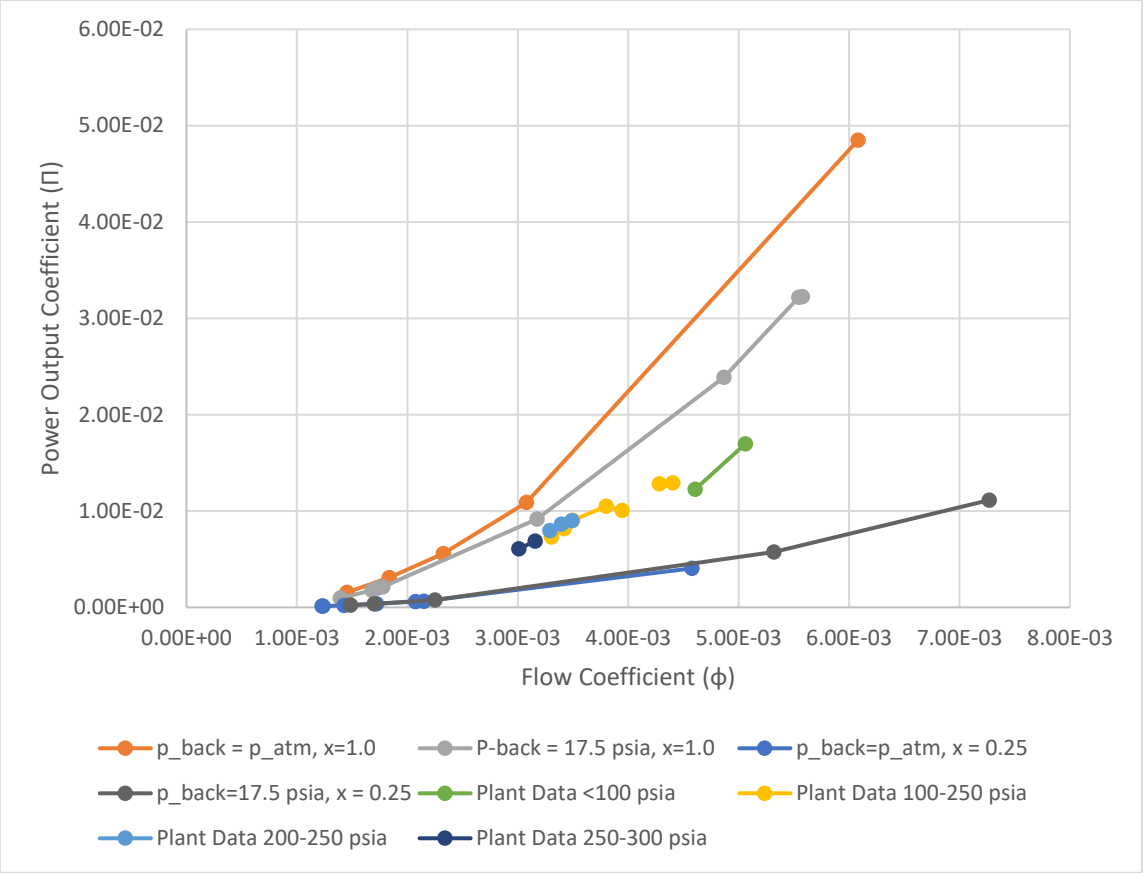

Figure 7.15 ZS-1 Terry Turbine flow coef. vs power coef. at inlet pressure of 60 psia but steam qualities of 1.0 and 0.25, and pressure ratios of 0.24, and 0.29 (NHTS Data)

8. ERROR ANALYSIS

8.1. Data Qualification

Throughout this experimental work, the turbine steady state performance during tests was evaluated by observing the turbine shaft torque and rotational speed and the flow pressure and steam quality. The turbine operational conditions and flow properties were required to be maintained within a given band for a full two minutes to constitute a qualified data point. Table 8.1 summarize these qualification criteria.

Table 8.1 Data qualification criteria

Measured Parameter	Tolerance band
Rotational Speed (RPM) **(Turbine Characterization Test)**	± 10
RCIC Pump Flowrate **(Turbopump Characterization Test)**	± 0.2
Inlet Pressure (psia)	± 1
Back Pressure (psia)	± 1.0
Steam Quality	± 0.02

8.2. Automated Steady State detection

The new improvement includes a computationally efficient method for identification of steady state using a statistical test, called the F-Type test. A sliding test

window approach, shown in Figure 8.1 was adopted. A *test window* is a set of data composed of n samples of the process variable x of the total test data points, N.

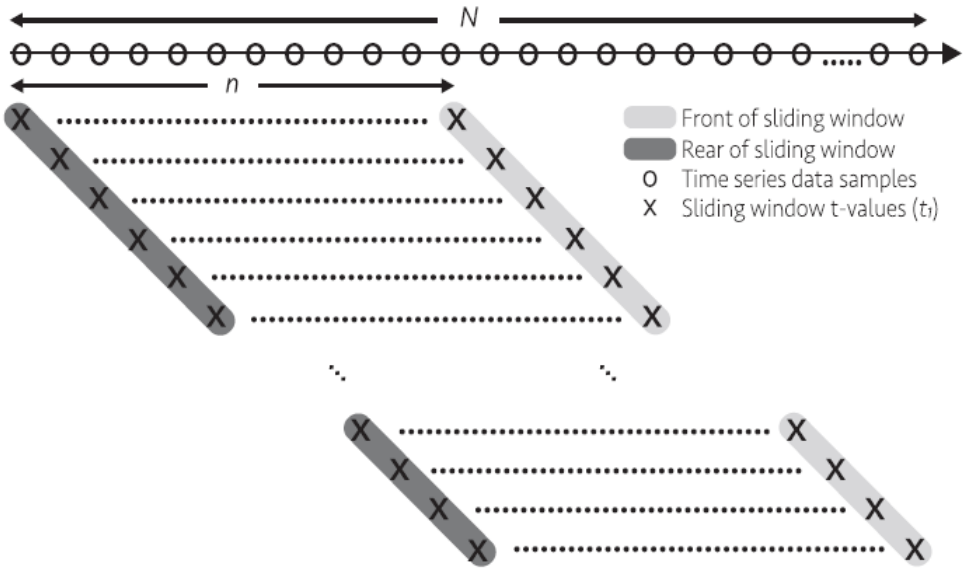

Figure 8.1 Illustration of time series data samples (circular markers) and the sliding window t-values (cross markers) where the t-values in the current analysis represent the turbine rotational speed. [33]

The underlying idea is to calculate the variance value (σ) of each data point in the test window using two different estimators as in equations (8.1) - (8.4). The ratio (*R*) between these two estimators is valid, or close to unity, only if the data within the test window is stationary and uncorrelated. The process is non-stationary if there is detectable accumulation error in the signal.

The value of the ratio, *R*, is calculated for each data point in the test window, then the average value of the ratio, *R*, is stored in the *i*th time step that represents the index of the first data item in the test window. The steadiest window is the one that has

the most stationary data, in which its *R* value is the closest to 1.0. Full details are included in the MATLAB code in APPENDIX E. Through the entire analysis, the turbine rotational speed (ω) is the main controlling process variable and the number of samples in the test window, n, is 450.

$$R = \frac{{\sigma_1}^2}{{\sigma_3}^2} \tag{8.1}$$

$${\sigma_1}^2 = \frac{1}{n-1}\sum_{i=1}^{n}(x_i - \bar{x})^2 \tag{8.2}$$

$$\bar{x} = \frac{1}{n}\sum_{i=1}^{n} x_i \tag{8.3}$$

$${\sigma_3}^2 = \frac{1}{2(n-1)}\sum_{i=1}^{n}(x_i - x_{i-1})^2 \tag{8.4}$$

Several reasons led to disqualification of test data, including dynamometer operation, a PID controller, and lack of operational experience. Initially, there was a problem with maintaining the water pressure to the dynamometer, which, basically, affects the dynamometer ability to create a controlling resistive force. Moreover, the LabVIEW PID controller improper value caused the control valves to take longer times to stabilize and thus longer testing times. The lack of operational experience in the initial stage of operation reflected on the tests data points, and resulted in disqualification from the analysis of this work. Changing the dynamometer water source, and enhancing the PID LabVIEW controllers, as mentioned in section 4.7, had a significant impact on the time at which the turbine reaches the steady state, Later tests were able to be conducted in minutes rather than hours.

8.3. Uncertainty Analysis: Measured Parameters

Repeatability tests [34] have been conducted to estimate the uncertainty in measured values. Two tests were repeated 10 times and 6 times in different testing modes, the standalone and the turbopump testing setups, respectively.

Figure 8.2 below shows the turbine performance during the standalone turbine test where the turbine was operated at 30 psia steam inlet pressure, atmospheric back pressure, and a steam quality of 1.0 (i.e., dry steam). The test was conducted 10 times at 2000 RPM. The turbine rotational speed and torque (i.e., Force) have been chosen to be the independent parameters in this analysis.

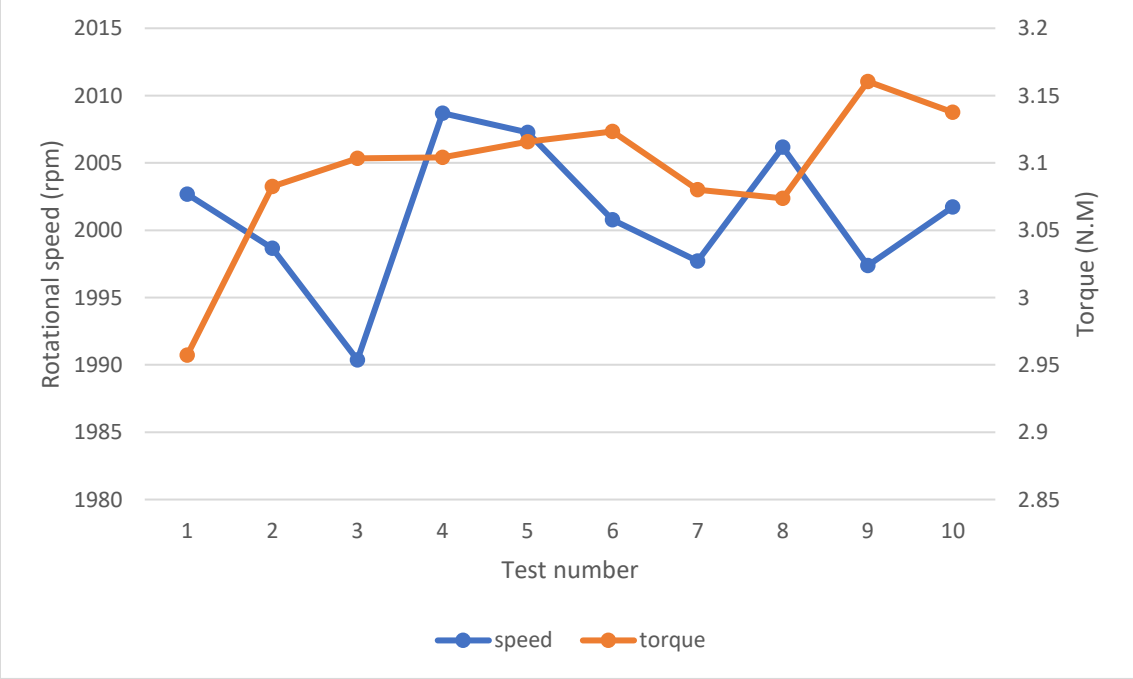

Figure 8.2 ZS-1 Turbine standalone performance at the same turbine rotational speed.

On the other hand, the turbopump performance has been investigated at 30 psia steam inlet pressure and atmospheric back pressure, but a steam quality of 0.7 (i.e., wet steam). The test was conducted 6 times at 3.33 GPM flowrate. The turbine rotational speed and pump outlet flowrate were chosen as independent parameters of this analysis as shown in Figure 8.3.

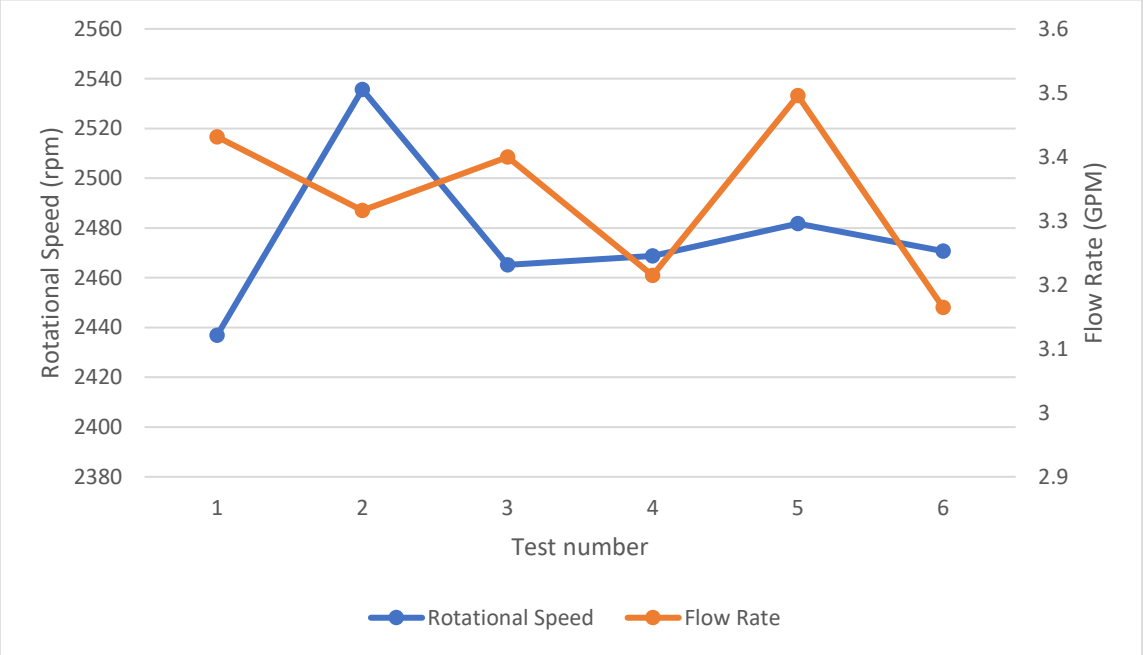

Figure 8.3 ZS-1 Turbopump turbine speeds at the same pump outlet flowrate.

These repeatability tests enable the calculation of the standard deviation in the mean values of the steam pressures, density and flow rate, the turbine rotational speed and torque, and the turbopump flowrates. The standard deviation of the mean values of a series of independent observation is defined as the standard uncertainty, $\boldsymbol{\sigma_i}$, and is calculated as per equations(8.5) and (8.6) [34].

$$\boldsymbol{\sigma_i} = \sqrt{\frac{\sum_{i=1}^{i=N}(\boldsymbol{x_i} - \overline{\boldsymbol{x}})^2}{\boldsymbol{N(N-1)}}} \tag{8.5}$$

$$\overline{\boldsymbol{x}} = \frac{\sum_{i=1}^{N} \boldsymbol{x_i}}{\boldsymbol{N}} \tag{8.6}$$

Where

N: The number of repeated tests.

x_i: A quantity of choice in a test, (i.e., pressure, rotational speed, etc.).

$\bar{x}$: The mean value.

However, the Expanded Uncertainty, $\boldsymbol{\sigma_U}$, is used for reporting the uncertainty as in equation (8.7)

$$\sigma_U = k_p * \sigma_i \tag{8.7}$$

In which the coverage factor, $\boldsymbol{k_p}$, is equal to a t-factor obtained from the t-distribution at degrees of freedom, $\boldsymbol{\nu_i}$, of 9 in order to meet the dictated requirement of providing a value of $\boldsymbol{\sigma_U}$ that defines an interval having a level of confidence close to 95%. The $\boldsymbol{k_p}$ of 2.26 was obtained from Table B.1 in [34].

It was found that the uncertainty error bars are so small that they are not discernable on the scale of the plot. Therefore, uncertainty values are tabulated in Table 8.2, Table 8.3, and Table 8.4 that summarize the uncertainty values in a number of measured values in both testing modes.

Table 8.2 The uncertainty values in a number of measured values in the turbine standalone mode

Quantity	Uncertainty values (±)
Steam Line Pressure (psia)	0.02
Steam Temperature (^{o}C)	0.2
Steam Density (kg/m^{3})	0.001
Steam Mass Flow Rate (g/s)	0.04
Turbine Inlet Pressure (psia)	0.02
Turbine Outlet Pressure (psia)	0.01
Turbine Rotational Speed (RPM)	4
Turbine Torque (N.m)	0.04

Table 8.3 The uncertainty values in a number of measured values in the turbine Turbopump mode

Quantity	Uncertainty values (±)
Steam Line Pressure (psia)	0.61
Steam Temperature (°C)	0.5
Steam Density (kg/m^3)	0.032
Steam Mass Flow Rate (g/s)	0.475
Water Mass Flow Rate (g/s)	0.175
Steam Quality	0.001
RCIC Pump Flowrate (GPM)	0.1
Turbine Inlet Pressure (psia)	0.02
Turbine Outlet Pressure (psia)	0.02
Turbine Rotational Speed (RPM)	30
Turbine Torque (N.m)	0.02

8.4. Error Propagation: Derived Parameters

For the derived measured parameters, the law of error propagation was used as per equation (8.8)

$$\sigma_u = \sqrt{\left(\frac{du}{dx}\right)^2 (\sigma_x)^2 + \left(\frac{du}{dy}\right)^2 (\sigma_y)^2 + \cdots} \qquad (8.8)$$

Where u= u (x, y,...) represents the derived quantity [35]

Table 8.4 Derived measurement uncertainty

Quantity	Uncertainty values (±)
Steam Mass Flow Rate (CFM)	0.15
Flow Coefficient	9.8E-06
Power Coefficient	3.9E-05
Turbine Power Input (kW)	7.0E-05
Turbine Power Output (kW)	0.01
Turbine Isentropic Efficiency	0.003

9. FUTURE WORK

The conduct of integral tests to investigation self-regulation under steam operation are of high interest. These tests are intended as a proof-of-concept to demonstrate the self-regulating mode thought to have occurred during the Fukushima Daiichi Unit 2 accident. In the integral operating mode for the investigation self-regulation tests, the turbine inlet pressure is held at a prescribed value and the flow rate and quality into the turbine are not controlled. Feedback is achieved via water injection into the steam line from the Suppression Pool through the RCIC pump. The two-phase ingestion from the steam line will reduce the turbine speed and the power to the RCIC pump, which is coupled, to the turbine via the turbine-pump shaft. The RCIC pump, which takes suction from the Suppression Pool, will inject water into the steam line at a correspondingly reduced rate.

10. CONCLUSION

Throughout this research, a ZS-1 Terry turbine has been tested against regular patterned boundary conditions. The turbine performance was experimentally investigated at high, medium, and low pressures of 25, 30, 45, 60, and 75 psia to cover the Terry turbine response at subsonic, sonic, and supersonic steam expansion. At each inlet pressure, the turbine was under two-phase flow operation of steam qualities from 0.05 to 1.00 in conjunction with atmospheric and non-atmospheric back pressures of 17.5 and 20 psia. The turbine performance was evaluated based on the torque and power output curves.

It was found that the turbine power output is higher at higher inlet pressures across all steam qualities. However, the power output was found to be maximum at the turbine moderate operating conditions (i.e., torque and rotational speed). The back pressure suppresses the turbine performance since the pressure drop across the turbine steam nozzle becomes smaller with back pressure increase. The drag coefficient was found to dominate the other operational effects at lower speeds, where the drag force is at its maximum.

During the turbopump tests, the RCIC turbopump analog performance was investigated in terms of the power output and the efficiency at low and medium inlet pressures of 30, 35, 40, and 45 psia and steam qualities of 1.00, 0.70, and 0.30. It was found that pump maximum operation occurs at the maximum power input where the pump flowrate and pressure drop are at moderate values. Moreover, the average

rotational speed as well as the RCIC pump maximum outlet flowrate dramatically decrease with steam quality.

The Power Output Coefficient ($\Pi_{mix,out}$) and Flow Coefficient (Φ_{mix}) has been used to develop a dimensionless scaling analysis of the Z (18-inch diameter wheel) and G (24-inch diameter wheel) Terry turbine performances. Toward that end, the NHTS lab ZS-1 air test results (i.e., torque curves) have been successfully benchmarked against TurboLab ZS-1 and GS-2 model air test results to validate the current scaling analysis efforts. Moreover, steam and air experimental data (i.e., Power Output Coefficient vs Flow Coefficient) have been benchmarked against real GS-model Terry Turbine data from currently operating BWR power plants. To account for the size difference between Z and G models, the experimental values of the ZS-1 flow coefficients have been multiplied by a steam inlet nozzle scaling factor.

The nondimensionalized (and scaled) ZS and GS experimental data at Texas A&M have shown a great scalability with the GS power plant data. As a result, a complete nondimensionalized characterization of the ZS Terry turbine has been performed at different steam inlet pressures, back pressures, and steam qualities. The scaling analysis shows a complete match of the turbine response between the dimensionalized and nondimensionalized factors.

Returning back to the objectives for this research, the effort reported herein successfully met the objectives. Specifically,

- A set of characterization tests has been conducted to examine the Terry turbine performance at different inlet and back pressures and steam inlet qualities.
- These tests serve to expand the available database for model development, validation and verification, and dimensional analysis. These are the first data for steam and steam-water injections into a Terry turbine under wide ranges of quality and inlet and back pressures.
- A nondimensionalized characterization of the ZS Terry turbine has been performed at different steam inlet pressures, back pressures, and steam qualities.
- Finally, the data were shown to enable scaling from small laboratory sizes up to full-scale RCIC system size and from air-water to steam-water fluid pairs. The verification provided herein that both size scaling (ZS-series to GS-series) and fluid scaling (air to water) can be achieved is a major milestone in development and validation of full-scale models in existing industry and Nuclear Regulatory Commission (NRC) codes.

REFERENCES

[1] NATIONAL POLICE AGENCY OF JAPAN and EMERGENCY DISASTER COUNTERMEASURES HEADQUARTERS, "Police Countermeasures and Damage Situation associated with 2011Tohoku district - off the Pacific Ocean Earthquake," 2021.

[2] NATIONAL RESEARCH COUNCIL , "Lessons Learned from the Fukushima Nuclear Accident for Improving Safety of U.S. Nuclear Plants," The National Academies Press, Washington, DC, 2014.

[3] M. Zhegang, K. Kellie, S. John and T. Wierman, "System Study: Reactor Core Isolation Cooling 1998 - 2018," Idaho National Laboratory, 2019.

[4] K. Ross, J. Cardoni, C. Wilson, C. Morrow, D. Osborn and R. Gauntt, "Modeling of the Reactor Core Isolation Cooling Response to Beyond Design Basis Operations – Phase 1," Sandia National Lab, 2015.

[5] D. Osborn and M. Solom, "Terry Turbopump Expanded Operating Band Full-Scale Component and Basic Science Detailed Test Plan – Final," Sandia National Laboratories, Albuquerque, NM, 2016.

[6] G. Electric, "Boiling Water Reactor GE BWR/4 Technology Advanced Manual," [Online]. Available: https://www.nrc.gov/docs/ML0230/ML023010606.pdf.

[7] NPTEL, "Figure 23.1, Lecture 23, Courses: Fluid Machinery," 21 06 2021. [Online]. Available: https://nptel.ac.in/content/storage2/courses/112104117/chapter_6/6_8.html.

[8] S. Basu and A. K. Denath, Power Plant Instrumentation and Control Handbook (Second Edition), Vols. Section 3.1.5 Impulse-Reactin Turbine, 2019, p. Figure 2.19.

[9] "Impulse Turbines," 15 06 2021. [Online]. Available: https://en.wikipedia.org/wiki/Steam_turbine#Impulse_turbines.

[10] A. Patil, W. Yintao, M. Solom, A. Alfandi, S. Shyam, K. V. Kirkland and G. Morrison, "Two-phase operation of a Terry steam turbine using air and water mixtures as working fluids," *Applied Thermal Engineering*, p. Volume 165, 2020.

[11] N. J. G. LUTHMAN, "EVALUATION OF IMPULSE TURBINE PERFORMANCE UNDER WET STEAM CONDITIONS," TEXAS A&M UNIVERSITY, COLLEGE STATION, 2017.

[12] K. Ross, N. Cardoni, C. . Wilson and D. Morrow, "Modeling of the Reactor Core Isolation Cooling Response to Beyond Design Basis Operations-Interim Report," Sandia National Laboratories (SNL-NM), 2015.

[13] "ISO Grade 68 turbine oil," McMaster Carr, [Online]. Available: https://www.mcmaster.com/8763T52/. [Accessed 12 10 2021].

[14] "Xs-19 Dynamometer water break," 16 06 2021. [Online]. Available: http://www.stuskadyno.com/wp-content/uploads/2015/11/waterbrake.pdf.

[15] "Omega S_Beam Load Cell data sheet," [Online]. Available: http://www.farnell.com/datasheets/2340179.pdf. [Accessed 2021].

[16] "Torque transducer - T20WN," [Online]. Available: http://static.celiss.com/products/oldc/files20166617183979440530 0.pdf.

[17] D. Keesling, "EXPERIMENTAL INVESTIGATION OF THERMAL STRATIFICATION IN BOILING WATER REACTOR SUPPRESSION POOLS DURING REACTOR CORE ISOLATION COOLING SYSTEM OPERATION AND REACTOR SAFETY IMPLICATIONS," Texas A&M University, College Station, Texas, 2021.

[18] I. A. f. t. P. o. W. a. Steam, "Revised Release on the IAPWS Industrial Formulation 1997 for the Thermodynamic Properties of Water and Steam," International Association for the Properties of Water and Steam, 2012.

[19] T. T. S. T. Co., "Terry Instruction manual Type Z-1 and ZS-1," The Terry Steam Turbine Co. , Hartford, Connecticut.

[20] EPRI, "Terry Turbine Maintenance Guide, RCIC Application: Replaces TR-105874 and TR-016909-R1," EPRI, Palo Alto, CA, 2012.

[21] RW-America, [Online]. Available: https://www.rw-america.com/products/precision-couplings/metal-bellows-couplings/bkc/?type=98. [Accessed August 2021].

[22] "Jaw Coupling LLine Install Guide," Love Joy, [Online]. Available: https://www.lovejoy-inc.com/wp-content/uploads/2017/11/JawCouplingLLineInstallGuide2012.pdf. [Accessed August 2021].

[23] D. J. Cooper, "Practical Process Control," 2005. [Online]. Available: https://apmonitor.com/che436/uploads/Main/PPC_Textbook.pdf.

[24] "CTS Cooling Tower Systems," 2019. [Online]. Available: https://cdn.shopify.com/s/files/1/1501/2204/files/Model_T-250_Tower_Specifications_0edc8fa5-c619-49f3-8cf3-0773560bedb1.pdf.

[25] J. Vandervort, G. Lukasik, B. Ayyildiz, M. Solom, A. Delgado, K. V. Kirkland and A. Patil, "Performance evaluation of a Terry GS-2 steam impulse turbine with air-water mixtures," *Applied Thermal Engineering,* vol. 191, no. June 2021, p. 116636, 2021.

[26] M. Holmgren, "www.x-eng.com," [Online]. Available: https://www.mathworks.com/matlabcentral/mlc-downloads/downloads/submissions/9817/versions/1/download/zip. [Accessed 2020].

[27] Y. A. Çengel and M. A. Boles, THERMODYNAMICS: AN ENGINEERING APPROACH, EIGHTH EDITION, New York, NY: McGraw-Hill Education, 2015.

[28] "NASA," [Online]. Available: https://www.grc.nasa.gov/www/k-12/airplane/dragco.html. [Accessed June 2021].

[29] G. Green, "Effect of degraded oil on terry turbine bearing performance at high temperature," Texas A&M University, 2020.

[30] H. Zhang and C. Blakley, "Development of RELAP5-3D Modeling of Reactor Core Isolation Cooling (RCIC) System," Idaho National Laboratory, 2020.

[31] E. Buckingham, "On physically similar systems; illustrations of the use of dimensional," *Phys. Rev.* , vol. 4, no. 4, pp. 345-376, 1914.

[32] A. Patil, S. . Shyam, Y. Wang, M. Solom, K. V. Kirkland and G. Morrison, "Characterization of steam impulse turbine for two-phase flow," *International Journal of Heat and Fluid Flow,* vol. 79, p. 108439, 2019.

[33] Ø. Ø. Dalheim and S. Steen, "A computationally efficient method for identification of steady state in time series data from ship monitoring," *Journal of Ocean Engineering and Science*, vol. 5, pp. 333-345, 2020.

[34] B. N. Taylor and C. E. Kuyatt, "Guidelines for Evaluating and Expressing the Uncertainty of NIST Measurement Results," U.S. Government Printing Office, Washington, DC, 1994.

[35] G. F. Knoll, Radiation Detection and Measurement, Ann Arbor, Michigan: John wiley & Sons, Inc, 2010.

APPENDIX A

LABVIEW CODE FOR THERMODYNAMIC PROPERTIES OF WATER AND STEAM

The following code has been programmed via C programming language. It aims to generate the water thermodynamic properties. To make this code running, a "LabView MathScript RT Module" has to be installed on the DAQ computer. It allows to insert complicated mathematics processes within the LabVIEW. It could be downloaded from the web.

```
#include <stdio.h>
#include <math.h>

// This function to sum up the arrays passed with any size
double sum(double input[], int sz)
{
    double res = 0;
    for (int i=0; i< sz; i++)
        res += input[i];
    return res;
}

int main()
{
    //double T = 500;          // K
    //double P = 3e6;       // MPa
    double T_star = 1;
    double P_star = 1e6;

    // The Saturation-Pressure equation
    double  n [10]= {0.11670521452767e4, -0.72421316703206e6, -
0.17073846940092e2, 0.12020824702470e5,
    -0.32325550322333e7, 0.14915108613530e2, -
0.48232657361591e4, 0.40511340542057e6,
    -0.23855557567849, 0.65017534844798e3};
    //printf("n[0]:%f\n", n[0]);
```

```
    double gamma = T/T_star;            // T is the given temp.
    double theta = gamma + n[8] / (gamma - n[9]);

    double A = pow(theta,2) + n[0]*theta + n[1];

    double B = n[2]*pow(theta,2) + n[3]*theta + n[4];
    double C = n[5]*pow(theta,2) + n[6]*theta + n[7];
    double alpha = pow(2*C / (-B + sqrt(pow(B,2) - 4*A*C)),4);
// Ps/P_star
    double beta = pow(alpha,0.25);   // Ps/P_star = Saturation
pressure
    double Ps = alpha;
        //printf("Ps:%f\n",Ps);

    // The Saturation-Temp
    double beta1 = pow((P/P_star),(0.25));
    double E = pow(beta1,2) + n[2]*beta1 + n[5];
    double F = n[0]*pow(beta1,2) + n[3]*beta1 + n[6];
    double G = n[1]*pow(beta1,2) + n[4]*beta1 + n[7];
    double D = 2*G / (-F-sqrt(pow(F,2) - 4*E*G));
    double Ts = 0.5 * (n[9] + D - sqrt(pow(n[9]+D,2) -
4*(n[8]+n[9]*D)));

    //printf("Ts:%f\n",Ts);

    if (T < Ts)
    {
        //int group_number = 1;
        //printf("Group %i\n",group_number);
        //printf("Liquid \n");
int c = 1;
double R = 0.461526e3;    // J/kg.K
        double P_star = 16.53e6;  // Pa = kg/m.s^2
        double T_star = 1386;     // Kelvin
        double P_ratio = P/P_star;
        double T_ratio = T_star/T;
        double I[34] = {0, 0, 0, 0, 0, 0, 0, 0, 1, 1, 1, 1, 1,
1, 2, 2, 2, 2, 2, 3, 3 ,3, 4, 4, 4, 5, 8, 8, 21, 23, 29, 30, 31,
32};
        double J[34] = {-2, -1, 0, 1, 2, 3, 4, 5, -9, -7, -1, 0,
1, 3, -3, 0, 1, 3, 17, -4, 0, 6, -5, -2, 10, -8, -11, -6, -29, -
31, -38, -39, -40, -41};
```

```
        double n[34] = {0.14632971213167, -0.84548187169114, -
3.7563603672040, 3.3855169168385,
            -0.95791963387872, 0.15772038513228, -
0.016616417199501, 0.81214629983568e-3,
            0.28319080123804e-3, -0.60706301565874e-3, -
0.018990068218419, -0.032529748770505,
            -0.021841717175414, -5.283835796993e-5, -
0.00047184321073267, -0.00030001780793026,
            4.7661393906987E-5, -4.4141845330846E-6, -
0.72694996297594E-15, -3.1679644845054E-5,
            -2.8270797985312E-6, -8.5205128120103E-10, -
2.2425281908E-6, -6.5171222895601E-7,
            -1.4341729937924E-13, -4.0516996860117E-7, -
1.2734301741641E-9, -1.7424871230634E-10,
                        -6.8762131295531E-19, 1.4478307828521E-
20, 2.6335781662795E-23, -1.1947622640071E-23,
            1.8228094581404E-24, -9.3537087292458E-26};
        double g [34];double g_pi [34];double g_t [34];double
g_tt [34];double g_pit [34];double g_pipi [34];

           for (int i=0; i<34; i++)
        {
            g[i] = n[i] * pow((7.1 - P_ratio),I[i]) *
pow((T_ratio - 1.222),J[i]);
            g_pi[i] = -n[i]*I[i]* pow((7.1 - P_ratio),(I[i]-1))
* pow((T_ratio-1.222),J[i]);
            g_t[i] = n[i] * pow((7.1 - P_ratio),I[i]) *
J[i]*pow((T_ratio - 1.222),(J[i]-1));
            g_tt[i]= n[i] * pow((7.1-P_ratio),I[i]) *
J[i]*(J[i]-1) * pow((T_ratio-1.222),(J[i]-2));
            g_pit[i]=-n[i]*I[i]*pow((7.1-P_ratio),(I[i]-1)) *
J[i] * pow((T_ratio-1.222),(J[i]-1));
            g_pipi[i]=n[i]*I[i] * (I[i]-1) * pow((7.1-
P_ratio),(I[i]-2)) * pow((T_ratio-1.222),J[i]);
        }
        double g_sum = sum (g,34);
        double g_pi_sum = sum (g_pi,34);
        double g_t_sum = sum(g_t,34);
        double g_tt_sum = sum(g_tt,34);
        double g_pipi_sum = sum(g_pipi,34);
        double g_pit_sum = sum(g_pit,34);

        double v = (R*T/P)* P_ratio * g_pi_sum;
```

```
        //printf("Specific Volume (m^3/kg) = %f\n",v);
           double h = (R*T*0.001) * (T_ratio * g_t_sum);
        //printf("Specific Enthalpy (kJ/kg.K) = %f\n",h);
           double u = (R*T*0.001)*(T_ratio * g_t_sum - P_ratio *
g_pi_sum);
           //printf("Specific Internal Energy (kg/kJ) = %f\n",u);
        double s = (R * 0.001) * ((T_ratio * g_t_sum) - g_sum);
        // printf("Specific Entropy (kJ/kg.K) = %f\n",s);
                double Cp= (R*0.001) * -1 * pow(T_ratio,2)
*g_tt_sum;
                //printf("Const. Pres. Specific heat (kJ/kg.K) =
%f\n",Cp);
        double w = sqrt (R*T * pow(g_pi_sum,2) /(pow((g_pi_sum -
T_ratio*g_pit_sum),2) / (pow(T_ratio,2)* g_tt_sum) -
g_pipi_sum));
        //printf("Speed of Sound (m/s) = %f\n",w);
                double Cv= (R*0.001) * (-pow(T_ratio,2)*g_tt_sum
+ pow((g_pi_sum - T_ratio*g_pit_sum),2) / g_pipi_sum);
           //printf("Const. Pres. Specific heat (kJ/kg.K) =
%f\n",Cv);
    }
        // Region 2
        if (T > Ts)
    {
       // int group_number = 2;
        //printf("Group%i\n",group_number);
//printf("Steam \n");
int c= 2;
double R = 0.461526e3;   // J/kg.K
        double P_star = 1e6;     // Pa = kg/m.s^2
        double T_star = 540;     //  Kelvin
        double P_ratio = P/P_star;
        double T_ratio = T_star/T;
        double J_o[9] = {0,1,-5,-4,-3,-2,-1,2,3};
        double n_o[9] = {-
0.96927686500217e1,0.10086655968018e2,-0.56087911283020e-2,
            0.71452738081455e-1,-
0.40710498223928,0.14240819171444e1,-0.43839511319450e1,-
0.28408632460772, 0.21268463753307e-1};
        double I_r[43]=
{1,1,1,1,1,2,2,2,2,2,3,3,3,3,3,4,4,4,5,6,6,6,7,7,78,8,9,10,10,10
,16,16,18,20,20,20,21,22,23,24,24,24};
```

```
        double J_r[43] =
{0,1,2,3,6,1,2,4,7,36,0,1,3,6,35,1,2,3,7,3,16,35,0,11,25,8,36,13
,4,10,14,29,50,57,20,35,48,21,53,39,26,40,58};
        double n_r[43] = {-0.17731742473213e-2,-
0.17834862292358E-1,-0.45996013696365e-1,-0.57581259083432e-1,-
0.50325278727930e-1,
                -0.33032641670203e-4,-0.18948987516315e-3,-
0.39392777243355e-2,-0.43797295650573e-1,-0.26674547914087e-4,
                0.20481737692309e-7,0.43870667284435e-6,-
0.32277677238570e-4,-0.15033924542148e-2 ,-0.40668253562649e-1,
            -0.78847309559367e-9,0.12790717852285e-
7,0.48225372718507e-6,0.22922076337661e-5,
            -0.16714766451061e-10,-0.21171472321355e-2,-
0.23895741934104e2,-0.59059564324270e-17,
            -0.12621808899101e-5,-0.38946842435739e-
1,0.11256211360459e-10,-0.82311340897998e1,
            0.19809712802088e-7 ,0.10406965210174e-18,-
0.10234747095929e-12,-0.10018179379511e-8,
            -0.80882908646985e-10,0.10693031879409,-
0.33662250574171,0.89185845355421e-24,
            0.30629316876232e-12,-0.42002467698208e-5,-
0.59056029685639e-25,0.37826947613457e-5,
            -0.12768608934681e-14,0.73087610595061e-
28,0.55414715350778e-16,-0.94369707241210e-6};
        double a_1[9];
        double a_2[9];
        double a_3[9];


        for (int i = 0; i<9; i++)
        {
            a_1[i] = n_o[i] * pow(T_ratio,J_o[i]);
            a_2[i] = n_o[i] * J_o[i] * pow(T_ratio,(J_o[i]-1));
            a_3[i] = n_o[i] * J_o[i] * (J_o[i]-1) *
pow(T_ratio,(J_o[i]-2));
        }
        double g_o = log(P_ratio) + sum (a_1,9);
        double g_o_pi =    1/P_ratio;
        double g_o_pipi = -1/pow(P_ratio,2);
        double g_o_t =  sum (a_2,9);
        double g_o_tt = sum (a_3,9);
        double go_pit = 0;
```

```
           double g_r[43];double g_r_pi[43];double
g_r_pipi[43];double g_r_t[43];double g_r_tt[43];double
g_r_pit[43];
        for(int i = 0;i<43;i++)
        {
            g_r[i] = n_r[i] * pow(P_ratio,I_r[i]) * pow((T_ratio
- 0.5),J_r[i]);
            g_r_pi[i] = n_r[i] * I_r[i] * pow(P_ratio,(I_r[i]-
1)) * pow((T_ratio - 0.5),J_r[i]);
            g_r_pipi[i] = n_r[i] * I_r[i] * (I_r[i]-1) *
pow(P_ratio,(I_r[i]-2)) * pow((T_ratio - 0.5),J_r[i]);
            g_r_t[i] = n_r[i] * pow(P_ratio,I_r[i]) * J_r[i] *
pow((T_ratio - 0.5),(J_r[i]-1));
            g_r_tt[i] = n_r[i] * pow(P_ratio,I_r[i]) * J_r[i] *
(J_r[i]-1) * pow((T_ratio - 0.5),(J_r[i]-2));
            g_r_pit[i] = n_r[i] * pow(P_ratio,(I_r[i]-1)) *
I_r[i] * J_r[i] * pow((T_ratio - 0.5),(J_r[i]-1));
        }
        double nom = 1+ 2*P_ratio*sum(g_r_pi,43) +
pow(P_ratio,2) * pow(sum(g_r_pi,43),2);
        double den1 = 1 - pow(P_ratio,2) * sum(g_r_pipi,43);
        double nom_den2 = pow((1 + P_ratio*sum(g_r_pi,43) -
T_ratio*P_ratio*sum(g_r_pit,43)),2);
        double den_den2 = pow(T_ratio,2) * (g_o_tt +
sum(g_r_tt,43));
        double den = den1 + nom_den2/den_den2;
        double v = (R*T/P) * P_ratio * (g_o_pi +
sum(g_r_pi,43)); //printf("Specifc Volume (m^3/kg)  =  %f\n",v);
        double h = (0.001*R*T) * T_ratio * (g_o_t +
sum(g_r_t,43)); //printf("Enthalpy (kJ/kg)  =  %f\n",h);
        double u = (0.001*R*T) * (T_ratio * (g_o_t +
sum(g_r_t,43)) - P_ratio*(g_o_pi + sum(g_r_pi,43)));
           //printf("Internal Energy (kJ/kg)  =  %f\n",u);
        double s = (0.01*R) * (T_ratio*(g_o_t + sum(g_r_t,43)) -
g_o - sum(g_r,43));
        //printf("Entropy (kJ/kg.K)  =  %f\n",s);
           double c_p = (0.01*R) * - pow(T_ratio,2) * (g_o_tt +
sum(g_r_tt,43));
           //printf("Specific Heat (kJ/kg.K)  =  %f\n",c_p);
        double w = sqrt(R*T* nom/den);
           //printf("Speed of Sound (m/s)  =  %f\n",w);
    }
}
```

APPENDIX B

FULL DETAILED TESTING PROCEDURE

Lead Operator: Date

2nd Operator/Observer:

1) Pre-test Procedures (Refer to Figure B.5)
    1) Ensure Personnel safety ☐
    2) Data Acquisition System Initiation
        1) Power on DAQ chassis and DC power supply. ☐
        2) Open the test LabVIEW project named " Turbine Project". Full Directory is "D:\Labview VIs\Turbine tests\Turbine Project.lvproj" ☐
        3) On the Turbine Project LabVIEW window, shown in Figure B.1, open the LabVIEW Real Time measurement file "Turbine_Test_RT1.2.vi" and the LabVIEW Front Panel file. Both files are highlighted on Figure 1. ☐
        4) Hit the "run" icon in the Tool bar in both LabVIEW files; Front Panel and Real Time measurement. ☐
        5) Ensure all the parameters values, on the Front Panel window, are real and as expected. ☐
        6) Ensure all the following instruments are powered on: ☐
            1) The Tachometer, located near the turbine shaft. ☐
            2) The Badger Flowmeter on the water injection line. ☐
            3) The Azbil Magnetic Flowmeter on the RCIC pump outlet line. ☐
            4) The Azbil Magnetic Flowmeter located near the control valve V-18 on the Feedwater line. ☐
    3) Ensure Experimental Equipment's security
        1) Close all of the following steam vent valves. ☐
            1) V-8 (Steam Generator water level indicator upper venting valve) ☐
            2) V-31 (Steam Condensate Line near RCIC DAQ station) ☐
            3) V-24 (Main Air Line near V-1) ☐

4) V-67 (Main Air Line vent)

2) Check that none of the electrical instrument and connections is exposed to water/hot surfaces.

3) Confirm that the Steam Generator electric heaters power panel is secure/locked.

4) Check open the following valves

1) V-2 (Steam Generator Outlet Valve)

2) V-30 (RCIC Facility Steam Admission Valve).

3) V-55 (Suppression Pool Tank lowest point outlet)

4) V-54 (Pump-1 inlet line)

5) V-59 (Pump-1 HC outlet manifold)

6) V-76 (on the Pump recirc. Line)

7) V-81 (near the High-Capacity Pump Outlet Manifold), and

8) V-83 (near the High-Capacity Pump Outlet Manifold)

5) Turn on the Feedwater Pump (P-1) switch

6) (Optional) The feedwater pump (P-1) could be operated in a recirculation mode to recirculate the water within the Suppression Pool tank. To do so, open the following valves:

1) V-70,

2) V-98, and

3) V-99

7) Turn on the switch for the Quincy air compressor. The Pressure at V-67 should be indicating higher than 60 psia.

8) On the LabVIEW Front Panel,

1) Enter the minimum Steam Generator water level at 70 inches. (That's about 63 cm on the magnetic visual level indicator)

2) Toggle on the Feedwater Valve switch to automatic.

9) Water Level verification for Steam Generator and SP

1) Ensure the Steam Generator water level, shown on the Steam Generator water level indicator, is above 50 cm (24 inches)

2) Confirm that the Suppression Pool water level, on the magnetic visual level indicator, is slightly over half-full prior to testing

10) Heat Rejection System operation

Follow the procedures in Section 4 “Cooling Mode”.

11) Turbopump assembly readiness

1) Check the ZS-1 turbine oil level in the oil wells is above the minimum level AND below its max level.

2) Check close the following turbine’s valves:

1) V-36

2) V-37, and

3) iV-13

3) Visually check the turbine – pump alignment.

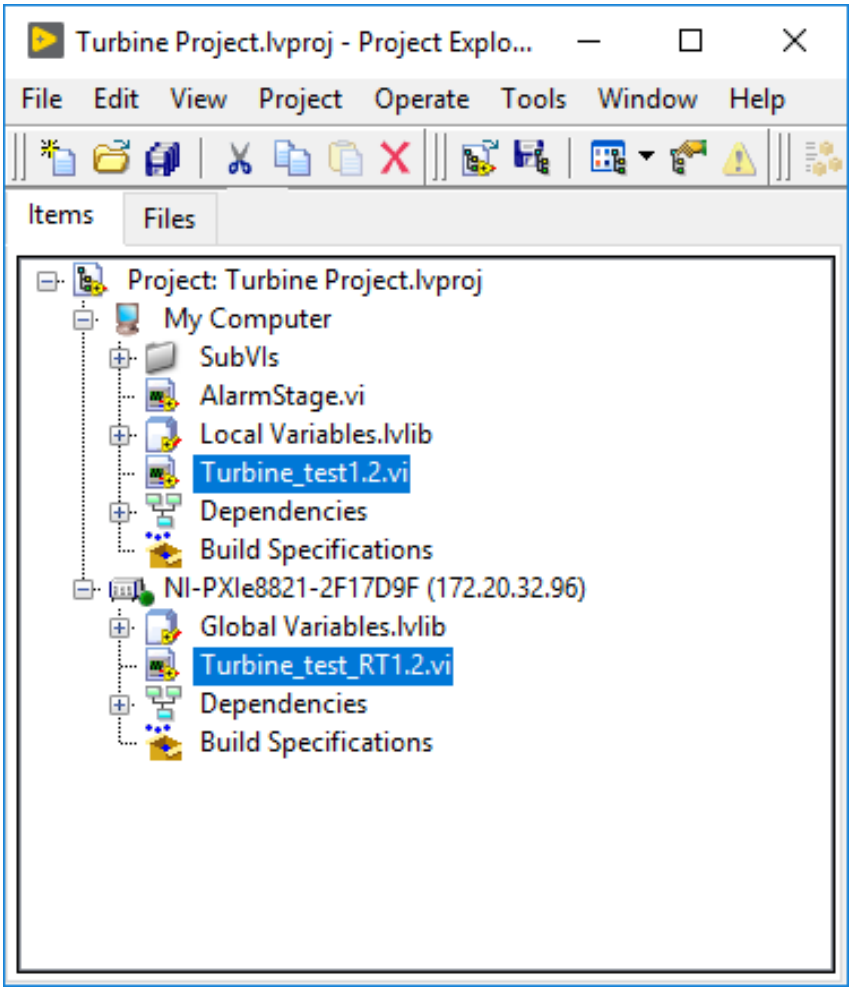

Figure B.1 The LabVIEW window of the Turbine Project

ENSURE THE VALVES'STATUS (I.E OPEN/CLOSE) ARE AS PER THE P&ID SHOWN IN FIGURE 2 BEFORE PROCEEDING TO THE NEXT OPERATIONAL MODE

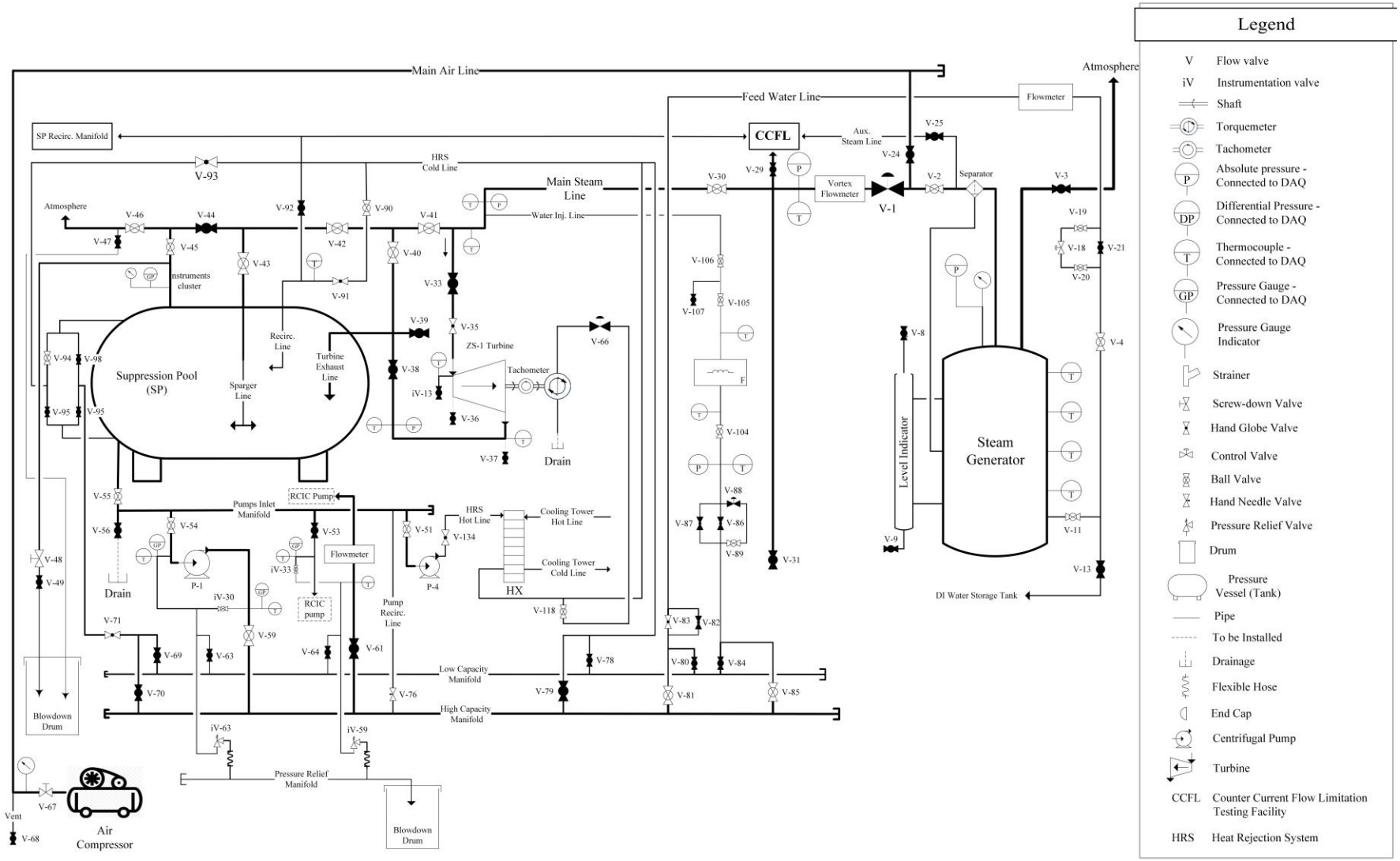

Figure B.2. Pre-Testing Condition Lab Schematic

2) Warmup Mode (Refer to Figure B.2)

1) Check shut the following valves:

1) V-1 (Main Steam Line) via DAQ
2) V-25 (Auxiliary Steam Line)
3) V-29 (CCFL Steam Admission Line)
4) V-31 (Steam Condensate Line),
5) V-33 (Turbine Steam Admission Line)
6) V-38 (Turbine Exhaust Line)
7) V-44 (Main Steam Line near the Suppression Pool tank front end)

2) Check OPEN the following valves (on the MSL- near the Suppression Pool tank):

1) V-40
2) V-41
3) V-42
4) V-43
5) V-45
6) V-46

3) DAQ Recording

1) Enter the desired data file location and name, including the date, test operating pressure, and "warmup". Example, on 12/15/2020, the steam test to be performed is at 30 psia. The file name format should be "201215_30psia_warmup.dat"
2) Hit the "START recording" button on the LabView Front Panel

4) Crack V-1 (Main Control Valve) 2% open on the LabVIEW Front Panel.

5) Energize the Steam Generator electric heaters to full power (157 kW) until the Steam Generator pressure reaches ~ 95 psia.

Steam Generator pressure should NOT be over 115 psig

Avoid bringing the Steam Generator pressure higher than the Feedwater line pressure. Doing so will trigger back-flow from the Steam Generator to the SP.

5) Once the Steam Generator pressure is at 95 psia,

1) On the LabVIEW Front Panel, crack open Dyno Control Valve to 15% to avoid dry-operation for the Dyno
2) Crack open V-1 (Main Control Valve) to 25%

6) Once the steam temperature at the Q-measurement point is 100°C, CAREFULLY, crack open V-31 (Steam Condensate Drainage valve) to purge any accumulated air and drain any condensed steam in to a bucket and then close it once all the water is out. ☐

7) Enter the first test's steam pressure value on the LabVIEW control panel. ☐

8) Steam Pressure:
Once the steam pressure in the Main Steam Line is around the testing value (say 30 psia), on LabVIEW Front Panel.

   1) Enter the value of the desired turbine speed ☐

   2) Toggle the Main Control Valve switch to automatic mode. ☐

9) Once the MSL steam is superheated, On the LabVIEW Front Panel,

   1) Toggle the Dyno Control Valve Power Switch to ON. The button lightens up. ☐

   2) Enter 15% on the dyno penning ratio to avoid dry-operation ☐

10) Open/Close the following valves IN ORDER AND QUICKLY (as possible)

   1) OPEN V-33 (Turbine inlet), then ☐

   2) CLOSE V-41, then ☐

   3) OPEN V-38 (Turbine Outlet), then ☐

   4) CLOSE V-40. ☐

11) Turbine Speed:
Once the turbine hits its maximum speed at the said pressure and dyno opening ratio,

   1) Enter the value of the test 1st desired turbine speed ☐

   2) Toggle the Dyno Valve switch to Automatic mode. ☐

12) Once the steam temperatures in the Main Steam Line and at the turbine inlet are steady, the warm up process can be called complete. It might take hours!

13) Hit "Click to STOP" button on the LabVIEW code ☐

Cut off the heaters as needed. It's recommended to keep the lowest heaters on while turning the top ones off to enhance temperature distribution throughout the tank through water natural circulation due to bouncy. It's also recommended to use Heater#4, 5 and 6 to regulate the Steam Generator power while using the Heater #1 and 2 (at least Circuit #1) for base heat load.

ENSURE THE VALVES'STATUS (I.E OPEN/CLOSE) ARE AS PER THE P&ID SHOWN IN FIGURE 3 BEFORE PROCEEDING TO THE NEXT OPERATIONAL MODE

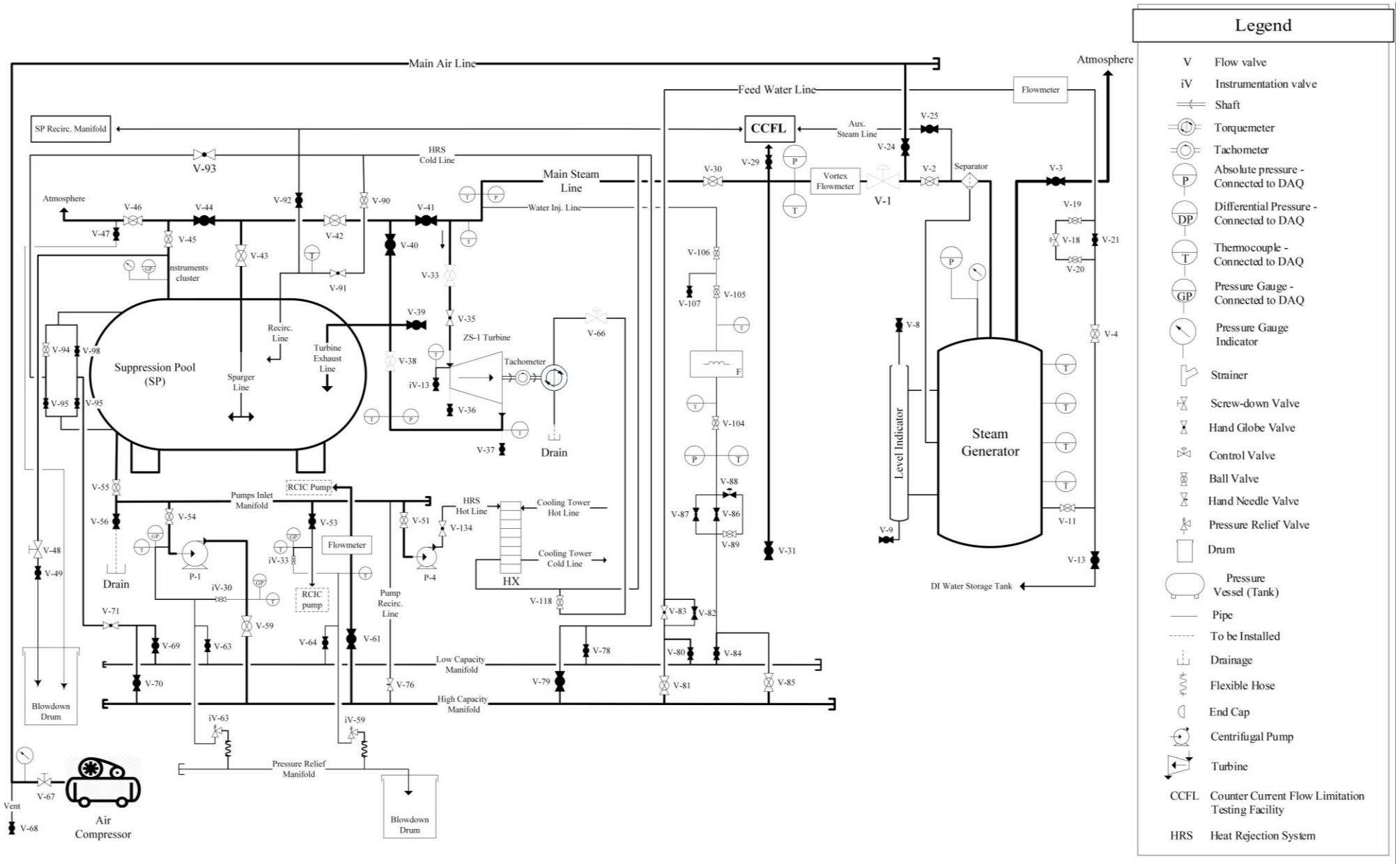

Figure B.3. Warm-up/Data collection Mode

3) Data collection Mode (Refer to Figure B.3)

1) DAQ Recording

1) Enter the desired data file location and name, including the date, test operating pressure, steam quality, and desired turbine speed. Example, on 12/15/2020, the steam test to be performed is at 30 psia, 45 steam quality and aiming for 3000 rpm turbine speed. The file name format should be "201215_30psia_45Qual_3000rpm.dat" ☐

2) Hit the "START recording" button on the LabView Front Panel ☐

2) Back pressure

1) (Skip if the current settings are atmospheric already) Atmospheric back pressure setting: ☐

1) Open V-46 ☐

2) Ensure V-49 is closed ☐

2) (Skip for atmospheric back pressure tests) non-atmospheric back pressure setting: ☐

1) Open V-49 ☐

2) Ensure V-46 & V-47 are closed. ☐

3) Adjust the screw valve to match the desired back pressure value

3) Steam Pressure: Check the MSL steam pressure to be as required. If not Enter the new value. ☐

4) Steam Quality

1) Check the value of the steam quality to be as desired. If not, enter the new one. ☐

2) Check the Water Injection Valve switch is on the automatic mode. ☐

5) Turbine Speed

1) Enter the value of the desired turbine speed. ☐

2) Ensure the Dyno Valve switch is the automatic mode. ☐

6) Monitor the values of the Steam Generator pressure, steam temperature, turbine speed, and quality. The system state is called steady when the inlet pressure value is within ± 0.5 psia, the back pressure value within ± 1 psia, the turbine rotational speed is within ±10 rpm, and the steam quality is within ±0.02. ☐

7) Once the values of the turbine speed and steam quality are steady for one minute,

1) Close shut V-33 ☐

2) Close V-38, and ☐

3) Open V-41. ☐

8) Monitor the turbine's cast down speed profile for one minute, then

   1) Open V-33,
   2) Open V-38, and
   3) Close V-41.

9) Monitor the turbine's spinning speed profile as it reaches back to the SAME steady state values. This might take longer than expected!

10) Hit "click to STOP" button on the LabVIEW code.

11) Repeat steps 3.1 through 3.10 for the following turbine speeds (rpm): 3000, 2000, 1000, 400 as possible!

12) Repeat steps 3.1 through 3.12 for the following steam qualities (%): 65, 25 and 5

13) Repeat steps 3.1 – 3.13 for the following pressures (psia): 30, 45, 60.

14) Repeat steps 3.1 – 3.14 for the following back pressures (psia): atm, 18, and 20

4) Cooling Mode (Refer to Figure B.4)

1) Primary Side

1) Check open the following valves

1) V-51 (on the Pump Inlet Manifold),

2) V-71 (Red globe valve near the Suppression Pool recirculation manifold)

3) V-90,

4) V-91 (Red globe valve near the ¾ U-shaped tube)

5) V-93 (on the Heat Rejection System Cold Line),

6) V-94 (on the Suppression Pool Recirculation Manifold), and

7) V-134 (on the Heat Rejection System Hot Line)

2) Turn on the Heat Rejection System primary pump (P-4) switch to run the water through the HX primary side

2) Secondary Side

1) Cooling Tower Cold Line

1) Make sure the water level in the Cooling Tower Supply Tank (CTST) is higher than the pump suction line, before initial operation.

2) Check close the CTST tank drainage valve, V-113.

3) Check open the Heat Rejection System secondary pump inlet valve, V-112.

4) Check open cooling tower outlet valves, V-110,

5) Check PARTIALLY open cooling tower inlet valve, V-111,

6) Turn on the Heat Rejection System secondary pump, P-5.

✋ MAKE SURE WATER TMPERATURE IN THE COLD LINE IS ALWAYS BELOW 130^{O}F.

2) Cooling Tower operation

1) Turn on the fan motor (The on/off switch is located behind the electric room door).

2) Check shut the cooling tower drain valve, V-125. (Outside the lab).

3) Check for no overflow from the cooling tower basin.

3) Water treatment station

1) Check open the intake line valve, V-126, V-128, and V-131

2) Check open the water drainage valves, V-127, V-129, and V-132.

3) Check shut the bypass line valve, V-133. ☐

4) Check open the flow switch. ☐

5) Turn on the controller. ☐

ENSURE THE VALVES'STATUS (I.E OPEN/CLOSE) ARE AS PER THE P&ID SHOWN IN FIGURE 4 BEFORE PROCEEDING TO THE NEXT OPERATIONAL MODE

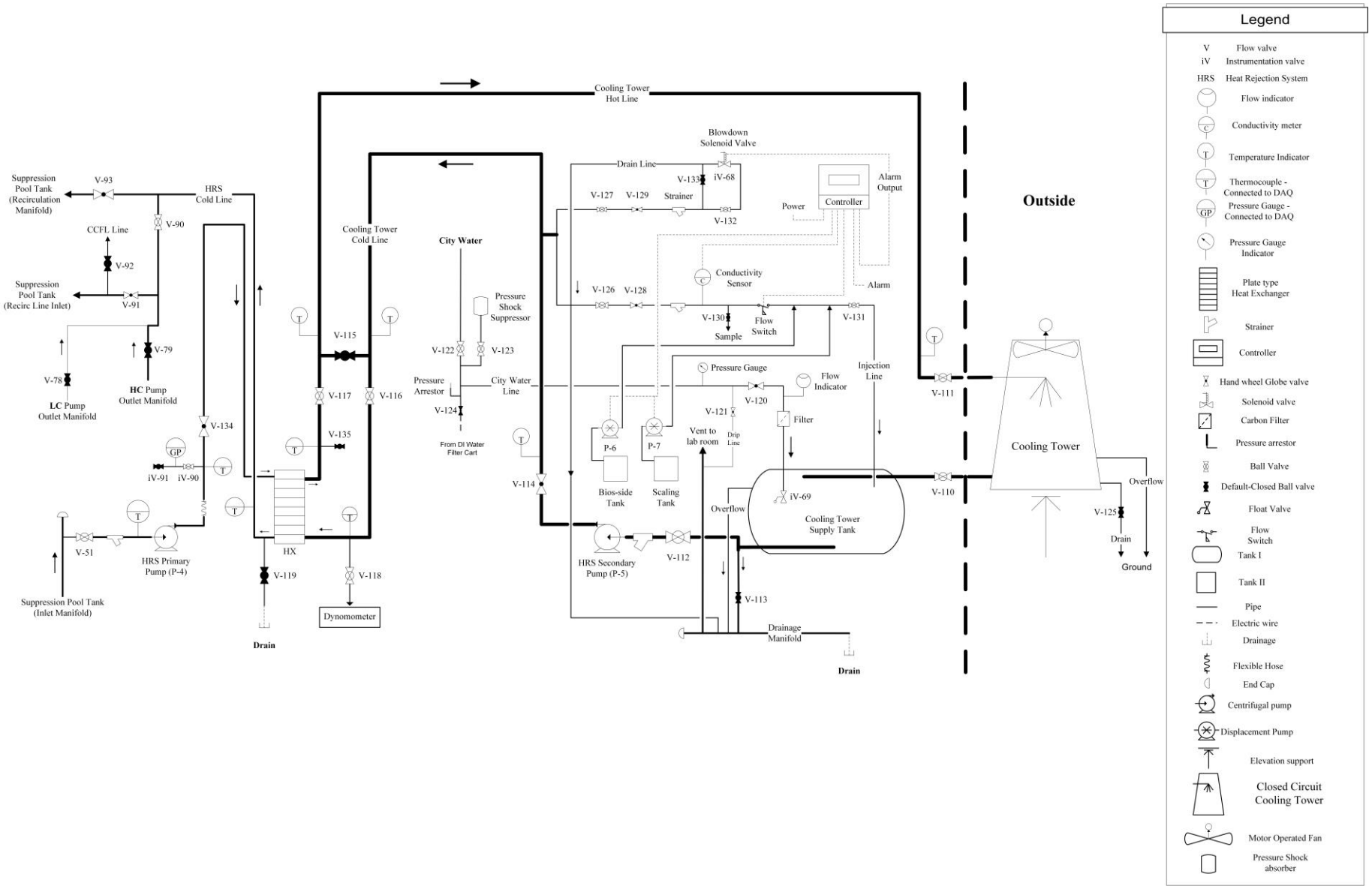

Figure B.4. Heat Rejection System operational schematic

5) Shutdown Mode (Refer to Figure B.3)

1) Turn off all the Steam Generator heaters AND the overall power switch on the electric panel. ☐

2) Once the turbine speed is zero,

   1) Close V-33 ☐
   2) Close V-38 ☐
   3) Open V-40, and ☐
   4) Open V-41 ☐

3) On the LabVIEW control panel,

   1) Turn the V-1 switch to manual and enter 50% as the opening ratio. ☐
   2) Toggle off (Close) the button for the water injection valve (V-88). ☐
   3) Once the MSL steam pressure is less than 20 psia, increase the opening ratio to 60% ☐
   4) Once the MSL steam pressure is less than 20 psia, increase the opening ratio to 80% ☐
   5) Once the MSL steam pressure is less than 20 psia, increase the opening ratio to 100% ☐
   6) Toggle off (Close) the switch for the dyno valve (V-66). ☐
   7) Toggle off (Close) the switch for the feed water valve (V-18). ☐
   8) Once the Steam Generator pressure is ~ atmospheric pressure, Toggle off (Close) the switch for the main control valve (V-1). ☐

4) Carefully, crack open V-8 to vent out any remaining pressurized steam. ☐

5) Turn off the air compressor switch. ☐

6) Open V-68 ☐

7) Open V-36 ☐

8) Open V-37 ☐

9) Turn off the feedwater pump (P-1) via the power switch. ☐

10) Turn off the Heat Rejection System primary pump (P-4) via the power switch. ☐

11) Turn off the Heat Rejection System secondary pump (P-5) via the power switch. ☐

12) Turn off the Cooling tower fan by turning the power switch (located in the electric room) to OFF. ☐

13) Turn off the controller. ☐

14) Open V-31. ☐

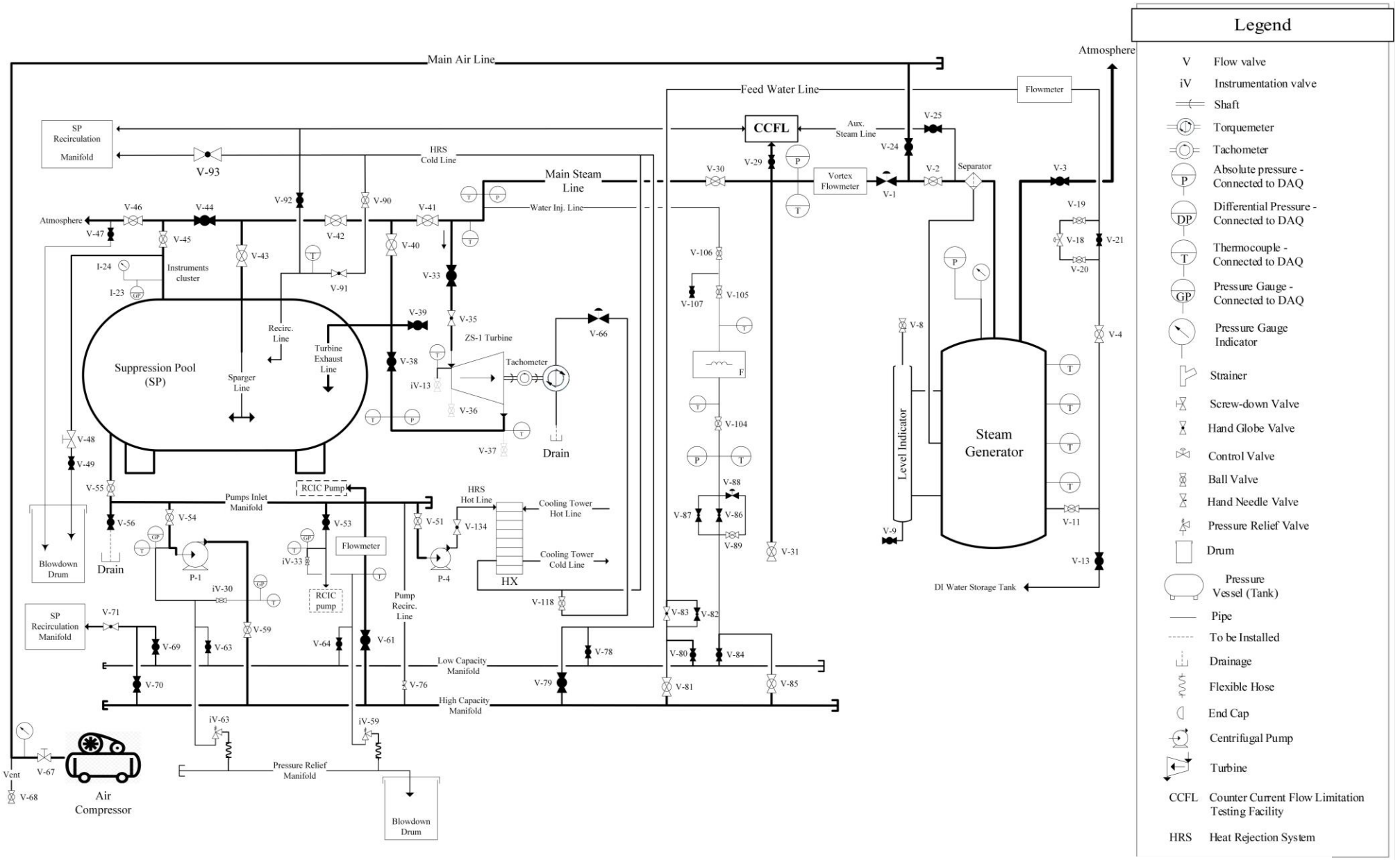

Figure B.5. Shutdown Condition Lab Schematic

ENSURE THE VALVES STATUS (I.E OPEN/CLOSE) ARE AS PER THE P&ID SHOWN IN FIGURE 5 BEFORE LEAVIG THE LAB

APPENDIX C

VALVE STATUS

Table C.1 summarizes the facility valve functions, locations, and operational status during the data collection operational mode for both set of tests.

Table C.1 List of valve functions, locations, and operational status

Valve #	Location		Function	Status (Open/Closed)	
	System	Location		Characterization Test	Self-Regulation Test
V-1	Steam Generator (SG)	SG Main Steam Line (MSL)	Adjust the outlet steam pressure	Open	Open
V-2	SG	SG MSL	Isolating the SG from the MSL	Open	Open
V-3	SG	SG Blowdown Line	Dumping the steam outside the lab building	Closed	Closed
V-4	SG	SG Feedwater Line	Feeding the SG with DI from the SP	Open	Open
V-5	SG	SG Drainage line	SG Drain	Closed	Closed
V-6	SG	SG-Bottom	Isolate the SG from the DP instrument (I—1) for maintenance purposes	Open	Open
V-7	SG	SG Auxiliary Air Line	Supply SG with air through portable compressor.	Closed	Closed

Valve #	Location		Function	Status (Open/Closed)	
	System	Location		Characterization Test	Self-Regulation Test
V-8	SG	SG Water Level indicator (Top)	Venting the SG	Closed	Closed
V-9	SG	SG Water Level indicator	Draining the Level indicator lines/SG	Closed	Closed
V-10	SG	SG Blowdown drum	Draining	Closed	Closed
V-11	SG	Feedwater Line	Admitting Water to the SG From feedwater line (SP) or the DI Water Storage Tank.	Open	Open
V-12	Allocated!				
V-13	DI Water Storage Tank (DI WST)	Feedwater Line	Feeding the SG with DI water from the DI Water Storage Tank	Closed	Closed
V-14	DI WST	Side	Currently unused	Closed	Closed
V-15	DI WST	Bottom	Draining the DI Water Storage Tank	Closed	Closed
V-16	DI WST	Top	Currently unused	Closed	Closed
V-17	DI WST	Top	Currently unused	Closed	Closed

Valve #	Location		Function	Status (Open/Closed)	
	System	Location		Characterization Test	Self-Regulation Test
V-18	SG	Feedwater Line	Automatic adjustment of the Feedwater flowrate from the SP to the SG based on the feedback signal of the steam flowrate in the main steam line (near V-30)	Open	Open
V-19	SG	Feedwater Line	Isolating V-18 from the Feedwater Line for maintenance purposes or Bypass	Open	Open
V-20	SG	Feedwater Line	Isolating V-18 from the Feedwater Line for maintenance purposes	Open	Open
V-21	SG	Feedwater Line	Bypassing the Feedwater control valve (V-18)	Closed	Closed
V-22	SG	Feedwater Line	Venting (?)	Closed	Closed
V-23	SG	Feedwater Line	Feeding water to the CCFL facility	Closed	Closed
V-24	SG	Main Air Line	Air Supply to SG and MSL.	Closed	Closed
V-25	SG	Auxiliary Steam Line	Steam supply to CCFL	Closed	Closed
V-26	DI WST	Inlet Tube	Isolating the DI Water Storage Tank from Culligan Water DI system Cart	Closed	Closed
V-27	Culligan DI Water System Cart	Outlet Tube	Isolating Culligan Water DI System Cart from the DI Water Storage Tank	Closed	Closed

Valve #	Location		Function	Status (Open/Closed)	
	System	Location		Character-ization Test	Self-Regulation Test
V-28	Culligan DI Water System Cart	Drain Line	Drainage	Closed	Closed
V-29	Main Steam Line		Supply Steam To CCFL	Closed	Closed
V-30	Main Steam Line		Supply Steam to RCIC Facility	Open	Open
V-31	Main Steam Line	Steam Condensate Line	Draining condensed seam	Closed	Closed
V-32	Allocated				
V-33	Turbopump	Turbine Steam Admission Line	Isolate the Turbine from the Main Steam Line	Open	Open
V-34	Turbopump	Turbine	Ideally, trips at speed higher than 3,600 rpm	Open	Open
V-35	Turbopump	Turbine Nozzle	Adjust the Steam Admitted to the Turbine	Open	Open
V-36	Turbopump	Turbine Drain line	Drainage	Closed	Closed
V-37	Turbopump	Exhaust line	Drainage	Closed	Closed

Valve #	Location		Function	Status (Open/Closed)	
	System	Location		Characterization Test	Self-Regulation Test
V-38	Turbopump	Exhaust line	Turbine Steam Outlet	Open	Open
V-39	Turbopump	Exhaust line	Steam Exhaust to other than SP tank	Closed	Closed
V-40	Turbopump	Exhaust line	Steam Admission to the Suppression Pool	Closed	Closed
V-41	Suppression Pool (SP)	Main Steam Line	Bypass the Turbine	Closed	Closed
V-42	SP	Main steam Line	Block steam from going into Sparger or atmosphere	Open	Open
V-43	SP	2nd Sparger Steam Inlet Line	Isolate the SP 2nd Sparger from Main Steam Line	Open	Open
V-44	SP	Main Steam Line	Isolate the Main Steam from Atmosphere	Closed	Closed
V-45	SP	Main Steam Line	Isolate the SP from Main Steam Line/Atmosphere	Open	Open
V-46	SP	Main Steam Line	Open to Atmosphere	Open	Open
V-47	SP Main Steam Line	Blowdown Line	Blowing down steam	Closed	Closed

Valve #	Location		Function	Status (Open/Closed)	
	System	Location		Character-ization Test	Self-Regulation Test
V-48	SP	Blowdown Line	Adjusting the SP back pressure	Open	Open
V-49	SP Main Steam Line	Blowdown Line	Closing the SP blowdown valve	Closed	Closed
V-50	SP	Blowdown drum	Drainage	Closed	Closed
V-51	SP	HRS Cold Line	Hot water to the Heat Exchanger	Open	Open
V-52	SP Inlet Manifold	Pump-1 Inlet Line	Admitting/Isolating Pump (P-3)	Closed	Closed
V-53	SP Inlet Manifold	Pump-2 Inlet Line	Admitting/Isolating RCIC Pump (P-2)	Closed	Open
V-54	SP Inlet Manifold	Pump-3 Inlet Line	Admitting/Isolating the Feed Water Pump (P-1)	Open	Open
V-55	SP	Inlet Manifold	Admitting SP water to the Inlet Manifold	Open	Open
V-56	SP	Tank Lower Outlet	Drainage	Closed	Closed
V-57	SP	Inlet Manifold	Drainage	Closed	Closed
V-58	SP	Inlet Manifold	Water Admission to Culligan DI Water System Filter Cart from SP tank	Closed	Closed

Valve #	Location		Function	Status (Open/Closed)	
	System	Location		Characterization Test	Self-Regulation Test
V-59	SP High Capacity (HC) Outlet Manifold	Feed Water Pump Outlet Line	Admitting/Isolating the Feed Water Pump (P-1) from the HC Outlet Manifold	Open	Open
V-60	Turbopump	RCIC Pump outlet Hose Line	Adjusting RCIC Pump outlet flowrate	N/A	Open
V-61	SP HC Outlet Manifold	RCIC Pump Outlet Line	Admitting/Isolating RCIC Pump (P-2) from the HC Outlet Manifold	Closed	Closed
V-62	SP HC Outlet Manifold	Pump-3 Outlet Line	Admitting/Isolating Pump-3 from the HC Outlet Manifold	Closed	Closed
V-63	SP Low Capacity (LC) Outlet Manifold	Feed Water Pump Outlet Line	Admitting/Isolating the Feed Water Pump (P-1) from the LC Outlet Manifold	Closed	Closed
V-64	SP Low Capacity (LC) Outlet Manifold	RCIC Pump outlet line	Admitting/Isolating RCIC Pump (P-2) from the LC Outlet Manifold	Open	Open
V-65	SP Low Capacity (LC) Outlet	Pump-3 outlet line	Admitting/Isolating Pump 3 (P-3) from the LC Outlet Manifold	Closed	Closed

Valve #	Location		Function	Status (Open/Closed)	
	System	**Location**		**Character-ization Test**	**Self-Regulation Test**
	Manifold				
V-66	Dynamometer Water Line		Water source to Dynamometer	Open	N/A
V-67	Main Air Line	Near the compressor	Regulating the air pressure	Open	Open
V-68	Main Air line	Near the compressor	Ventilation	Closed	Closed
V-69	SP	LC Outlet Manifold	Admitting/Isolating Water to the Recirculation Manifold	Closed	Closed
V-70	SP	**HC** Outlet Manifold	Admitting/Isolating Water to the Recirculation Manifold	Closed	Closed
V-71	SP	Recirculation Manifold	Adjusting the water flowrate to the SP Recirculation Manifold	Open	Open
V-72	SP	**LC** Outlet Manifold	Water Admission to SP from Culligan DI Water System Filter Cart	Closed	Closed
V-73	SP	**LC** Outlet Manifold	Adjusting the recirculation flow in the **LC** Outlet Manifold	Open	Open
V-74	SP	**LC** Outlet Manifold	Bypass recirculation flow in the **LC** Outlet Manifold	Closed	Closed
V-75	SP	**HC** Outlet Manifold	Adjusting the recirculation flow in the **HC** Outlet Manifold	Closed	Closed

Valve #	Location		Function	Status (Open/Closed)	
	System	Location		Characterization Test	Self-Regulation Test
V-76	SP	**HC** Outlet Manifold	Bypass recirculation flow in the **HC** Outlet Manifold	Open	Open
V-77	SP	Recirculation Flow Line	Currently Unassigned	Closed	Closed
V-78	SP	LC Outlet Manifold	Admitting Water to the HRS Cold Line thru V-90 OR to the SP 2nd Inlet Point thru V-91	Closed	Closed
V-79	SP	HC Outlet Manifold	Admitting Water to the HRS Cold Line thru V-90 OR to the SP 2nd Inlet Point thru V-91 (3/4 U-shaped tube)	Closed	Closed
V-80	SP	LC Outlet Manifold	Admitting Water to Feedwater line	Closed	Closed
V-81	SP	HC Outlet Manifold	Admitting Water to Feedwater line	Open	Open
V-82	SP	Feedwater Line	Manual Adjustment of the water flowrate in the Feedwater line	Closed	Closed
V-83	SP	Feedwater Line	Manual Adjustment of the water flowrate in the Feedwater line	Open	Open
V-84	SP	LC Outlet Manifold	Admitting Water to the Water Injection Line	Closed	Open
V-85	SP	HC Outlet Manifold	Admitting Water to the Water Injection Line	Open	Closed
V-86	SP	Water Injection Line	Manual Adjustment of the water flowrate in the Water Injection Line	Closed	Closed

Valve #	Location		Function	Status (Open/Closed)	
	System	Location		Characterization Test	Self-Regulation Test
V-87	SP	Water Injection Line	Manual Adjustment of the water flowrate in the Water Injection Line	Closed	Closed
V-88	SP	Water Injection Line	Automatic Control of the water flowrate	Open	Open
V-89	SP	Water Injection Line	Isolating the Water Injection Control Valve (V-88)	Open	Open
V-90	SP	HRS Cold Line	HRS Cooled/returning water admission to the SP 2nd Inlet point	Open	Open
V-91	SP	HRS Cold Line	Manual adjustment of the cooled water flowrate into SP thru 2nd Inlet Line	Open	Open
V-92	SP	Feedwater Line	Admitting water, the Feedwater line	Closed	Closed
V-93	SP	HRS Cold Line	Manual adjustment of the cooled water flowrate into SP thru Recirculation manifold	Open	Open
V-94	SP Recirculation Manifold	HRS Cold Line	Admitting the HRS-cooled water to the top of SP tank thru Recirculation Manifold	Open	Open
V-95	SP Recirculation Manifold	HRS Cold Line	Admitting the HRS-cooled water to the lower part of SP tank thru Recirculation Manifold	Closed	Closed
V-96	SP Recirculation	Feedwater Line	Admitting the Feedwater line water to the top of SP tank thru Recirculation Manifold	Closed	Closed

Valve #	Location		Function	Status (Open/Closed)	
	System	**Location**		**Character-ization Test**	**Self-Regulation Test**
	Manifold				
V-97	SP Recirculation Manifold	Feedwater Line	Admitting the Feedwater line water to the lower part of SP tank thru Recirculation Manifold	Closed	Closed
V-98	SP	Recirculation Manifold	Admitting the SP water to the top part of SP tank thru Recirculation Manifold	Closed	Closed
V-99	SP	Recirculation Manifold	Admitting the SP water to the lower part of SP tank thru Recirculation Manifold	Closed	Closed
V-100	SP	Level indicator-Top	Venting	Closed	Closed
V-101	SP	Level Indicator-Bottom	Draining	Closed	Closed
V-102	SP	Air supply Hose	Air Supply	Closed	Closed
V-103	SP	Air Supply Line	Venting	Closed	Closed
V-104	Water Injection Line		Admitting/Isolating flow thru Badger flowmeter	Open	Open
V-105	Water Injection Line		Isolating flow thru Badger flowmeter to the main Water Injection Line	Open	Open
V-106	Water Injection Line		Admitting/isolating water to the Main Steam Line	Open	Open

Valve #	Location		Function	Status (Open/Closed)	
	System	Location		Character-ization Test	Self-Regulation Test
V-107	Water Injection Line		Drainage	Closed	Closed
V-108	SP-Pump Pressure Relief Line	Blowdown Drum	Drainage	Closed	Closed
V-109	SP-Pump Pressure Relief Line	Blowdown Drum	Drainage	Closed	Closed
V-110	HRS	Secondary Side – Cold Line "Cooling Tower Cold Line"	Admitting water to the Cooling Tower Supply Tank (CTST) from the Cooling Tower	Open	Open
V-111	HRS	Secondary Side – Hot Water "Cooling Tower Hot Line"	Admitting water to the Cooling Tower from Heat Exchanger (HX)	Open	Open
V-112	HRS	Cooling Tower Cold Line	Cooled Water Admission to the HX thru Pump -5	Open	Open
V-113	HRS	Cooling Tower Cold line	Draining	Closed	Closed

Valve #	Location		Function	Status (Open/Closed)	
	System	Location		Characterization Test	Self-Regulation Test
V-114	HRS	Cooling Tower Cold line	Manual adjustment of cooled water flowrate to the HX to avoid Cooling Tower overflow	Open	Open
V-115	HRS	Cooling Tower Cold/Hot Line	Bypass	Closed	Closed
V-116	HRS	Cooling Tower Cold Line	Isolating the HX from the Cooling Tower lines.	Open	Open
V-117	HRS	Cooling Tower Hot Line	Isolating the HX from the Cooling Tower lines.	Open	Open
V-118	HRS	Cooling Tower Cold Line	Draining	Open	Closed
V-119	HRS	HRS Cold Line	Draining	Closed	Closed
V-120	City Water Line		Adjusting the city water supply flowrate	Open	open
V-121	City Water Line		Adjusting the drip line water flowrate	Open	open
V-122	City Water Line		Isolating the HRS from City Water Supply	Open	Open
V-123	City Water Line		Isolating the Pressure shock suppressor from the city water main line	Open	Open

Valve #	Location		Function	Status (Open/Closed)	
	System	Location		Character-ization Test	Self-Regulation Test
V-124	City Water Line		Admitting water thru hose adapter	Closed	Closed
V-125	HRS	Cooling Tower (Outside)	Drainage	Closed	Closed
V-126	HRS-Water Treatment Station	Injection Line	Admitting Flow	Open	Open
V-127	HRS-Water Treatment Station	Drain Line	Admitting Flow	Open	Open
V-128	HRS-Water Treatment Station	Injection line	Manual Adjustment of the injecting water flowrate	Open	Open
V-129	HRS-Water Treatment Station	Drain Line	Manual Adjustment of the water flowrate	Open	Open
V-130	HRS-Water Treatment Station	Sample point	Sampling	Closed	Closed
V-131	HRS-Water Treatment Station	Injection Line	Admitting treated water back to the CTST	Open	Open

Valve #	Location		Function	Status (Open/Closed)	
	System	Location		Characterization Test	Self-Regulation Test
V-132	HRS-Water Treatment Station	Drain Line	Admitting/Isolating the Solenoid valve (V-132)	Open	Open
V-133	HRS-Water Treatment Station	Drain Line	Bypass	Closed	Closed
V-134	HRS	Pump-4 Outlet Line	Adjusting the water outlet flowrate to max of 35 gpm to avoid vortex formation in the SP tank.	Open	Open
V-135	HRS	Cooling Tower Hot Line	Draining	Closed	Closed

APPENDIX D

TESTING MATRIX (STEAM TESTS)

The Table D.1 through Table D.5 shows the ZS-1 steam testing matrix under steam qualities of 1.0 to 0.05. Those tests were conducted and analyzed by Ashraf A. Alfandi at the NHTS Laboratory.

Table D.1 ZS-1 Terry Turbine Characterization Testing Matrix, Dry Steam

Back-pressure (psia)	Inlet Pressure (psia)	Speed (rpm)	Torque (N.m)	Flow Coef.	Power Out Coef.	Power input (kW)	Power (kW)	Efficiency (%)
Atm. (14.6)	30	464.516	4.242	0.011	0.077	2.702	0.206	7.638
		1452.672	2.969	0.003	0.006	2.699	0.452	16.732
		2037.011	2.239	0.002	0.002	2.684	0.478	17.792
		2662.961	1.539	0.002	0.001	2.710	0.429	15.843
		3155.083	0.945	0.002	0.000	2.692	0.312	11.593
		3187.182	0.940	0.002	0.000	2.693	0.314	11.643
	45	725.440	8.709	0.007	0.044	6.128	0.662	10.796
		1893.643	6.482	0.003	0.005	6.118	1.285	21.009
		2498.867	5.429	0.002	0.002	6.095	1.421	23.310
		3102.623	4.298	0.002	0.001	6.139	1.397	22.747
		3520.567	3.641	0.001	0.001	6.126	1.342	21.915
	60	789.840	13.948	0.006	0.046	9.706	1.154	11.886
		890.824	13.781	0.006	0.035	9.721	1.286	13.225

Back-pressure (psia)	Inlet Pressure (psia)	Speed (rpm)	Torque (N.m)	Flow Coef.	Power Out Coef.	Power input (kW)	Power (kW)	Efficiency (%)
		999.808	13.522	0.005	0.028	9.716	1.416	14.571
		1591.014	12.240	0.003	0.010	9.756	2.039	20.904
		1902.015	11.513	0.003	0.006	9.783	2.293	23.440
		2230.383	9.770	0.002	0.004	9.780	2.282	23.334
		3008.016	8.074	0.002	0.002	9.725	2.543	26.150
	60 -new data	3587.291	6.697	0.001	0.001	9.777	2.516	25.734
		818.526	16.010	0.006	0.049	9.841	1.372	13.945
		1614.798	13.942	0.003	0.011	9.765	2.358	24.145
		2143.281	12.554	0.002	0.006	9.783	2.818	28.803
		2719.106	11.209	0.002	0.003	9.821	3.192	32.498
		3451.998	9.108	0.001	0.002	9.858	3.293	33.401
	70	886.240	19.008	0.006	0.043	12.327	1.764	14.311
		888.193	19.106	0.006	0.043	12.292	1.777	14.457
		2644.635	13.082	0.002	0.003	12.412	3.623	29.190
		3489.435	11.115	0.001	0.002	12.435	4.061	32.661
	75	926.224	20.653	0.005	0.040	13.676	2.003	14.648
		1464.465	19.139	0.003	0.015	13.695	2.935	21.432
		2009.707	17.363	0.002	0.007	13.738	3.654	26.599
		2777.355	15.077	0.002	0.003	13.764	4.385	31.861
		3592.395	12.220	0.001	0.002	13.795	4.597	33.325

Back-pressure (psia)	Inlet Pressure (psia)	Speed (rpm)	Torque (N.m)	Flow Coef.	Power Out Coef.	Power input (kW)	Power (kW)	Efficiency (%)
17.5	30	475.960	3.608	0.010	0.062	2.209	0.180	8.140
		1013.934	2.927	0.005	0.011	2.226	0.311	13.962
		1394.950	2.493	0.004	0.005	2.223	0.364	16.381
		2356.157	1.381	0.002	0.001	2.214	0.341	15.393
		2821.064	0.887	0.002	0.000	2.229	0.262	11.762
	45	627.671	8.079	0.008	0.055	5.525	0.531	9.612
		973.503	7.417	0.005	0.021	5.507	0.756	13.732
		1492.957	6.331	0.003	0.008	5.524	0.990	17.920
		2519.020	4.619	0.002	0.002	5.505	1.218	22.132
		3004.486	3.774	0.002	0.001	5.510	1.188	21.554
		3480.340	2.999	0.001	0.001	5.518	1.093	19.811
	60	885.543	12.417	0.006	0.032	9.049	1.152	12.726
		890.435	12.525	0.006	0.032	9.119	1.168	12.808
		1016.455	12.118	0.005	0.024	9.085	1.290	14.197
		1567.115	11.068	0.003	0.009	9.126	1.816	19.903
		2789.429	8.163	0.002	0.002	9.080	2.384	26.260
		2853.739	8.121	0.002	0.002	9.115	2.427	26.626
		2969.623	7.626	0.002	0.002	9.105	2.371	26.046
		3596.487	6.188	0.001	0.001	9.191	2.330	25.355
20	30	429.477	3.102	0.012	0.066	1.628	0.140	8.570

Back-pressure (psia)	Inlet Pressure (psia)	Speed (rpm)	Torque (N.m)	Flow Coef.	Power Out Coef.	Power input (kW)	Power (kW)	Efficiency (%)
		1131.203	2.280	0.004	0.007	1.611	0.270	16.767
		1554.736	1.817	0.003	0.003	1.639	0.296	18.057
		1657.900	1.661	0.003	0.002	1.619	0.288	17.811
		2306.111	0.962	0.002	0.001	1.648	0.232	14.102
		2329.561	0.913	0.002	0.001	1.604	0.223	13.888
	45	1464.904	5.497	0.003	0.007	4.705	0.843	17.924
		2691.467	3.247	0.002	0.001	4.687	0.915	19.526
		3360.275	2.162	0.001	0.001	4.664	0.761	16.311

Table D.2 ZS-1 Terry Turbine Characterization Testing Matrix, Wet Steam, x = 0.9

Back-pressure (psia)	Inlet Pressure (psia)	Speed (rpm)	Torque (N.m)	Flow Coef.	Power Out Coef.	Power input (kW)	Power (kW)	Efficiency (%)
		917.894	3.200	0.005	0.014	2.629	0.308	11.700
		1257.565	2.784	0.004	0.006	2.655	0.367	13.811
		1533.453	2.463	0.003	0.004	2.625	0.396	15.068
Atm. (14.6)	**30**	1886.850	2.083	0.003	0.002	2.647	0.412	15.552
		2364.201	1.527	0.002	0.001	2.631	0.378	14.372
		2713.656	1.176	0.002	0.001	2.626	0.334	12.724
	45	661.518	7.593	0.008	0.042	6.009	0.526	8.753

Back-pressure (psia)	Inlet Pressure (psia)	Speed (rpm)	Torque (N.m)	Flow Coef.	Power Out Coef.	Power input (kW)	Power (kW)	Efficiency (%)
		1001.503	7.090	0.005	0.017	5.992	0.744	12.409
		1539.999	6.139	0.003	0.006	6.000	0.990	16.499
		1931.695	5.539	0.003	0.004	5.969	1.120	18.771
		2545.667	4.489	0.002	0.002	5.983	1.197	20.000
		3033.856	3.703	0.002	0.001	5.990	1.176	19.638
		3563.493	2.941	0.001	0.001	5.958	1.097	18.419
	60	808.454	11.857	0.006	0.034	9.666	1.004	10.385
		935.780	11.596	0.005	0.025	9.658	1.136	11.766
		1525.186	10.529	0.003	0.008	9.657	1.682	17.415
		1993.133	9.615	0.002	0.005	9.696	2.007	20.699
		2528.907	8.550	0.002	0.002	9.636	2.264	23.497
		3141.992	7.220	0.002	0.001	9.712	2.375	24.458
		3519.078	6.404	0.001	0.001	9.714	2.360	24.294
	70	Not Conducted						
	75	Not Conducted						

Back-pressure (psia)	Inlet Pressure (psia)	Speed (rpm)	Torque (N.m)	Flow Coef.	Power Out Coef.	Power input (kW)	Power (kW)	Efficiency (%)
17.5	30	442.740	3.285	0.011	0.059	2.218	0.152	6.868
		979.316	2.708	0.005	0.010	2.211	0.278	12.558
		1419.493	2.265	0.004	0.004	2.224	0.337	15.139
		1987.440	1.602	0.002	0.001	2.222	0.333	15.010
		2699.619	0.852	0.002	0.000	2.238	0.241	10.758
		2723.340	0.863	0.002	0.000	2.227	0.246	11.046
	45	654.133	7.158	0.008	0.040	5.437	0.490	9.018
		940.501	6.844	0.005	0.019	5.444	0.674	12.383
		1120.569	6.477	0.004	0.012	5.504	0.760	13.809
		1535.661	5.727	0.003	0.006	5.473	0.921	16.830
		2333.742	4.366	0.002	0.002	5.457	1.067	19.554
		3028.335	3.159	0.002	0.001	5.469	1.002	18.316
	60	936.189	11.151	0.005	0.023	9.059	1.093	12.068
		1459.452	10.217	0.003	0.009	9.073	1.562	17.211
		2521.944	7.909	0.002	0.002	9.035	2.089	23.119
		2568.720	7.911	0.002	0.002	9.056	2.128	23.497
		3240.651	6.237	0.002	0.001	9.082	2.117	23.307
20	30	Not Conducted						

Back-pressure (psia)	Inlet Pressure (psia)	Speed (rpm)	Torque (N.m)	Flow Coef.	Power Out Coef.	Power input (kW)	Power (kW)	Efficiency (%)
	45	Not Conducted						

Table D.3 ZS-1 Terry Turbine Characterization Testing Matrix, Wet Steam, x = 0.65

Back-pressure (psia)	Inlet Pressure (psia)	Speed (rpm)	Torque (N.m)	Flow Coef.	Power Out Coef.	Power Input (kW)	Power (kW)	Efficiency (%)
Atm. (14.6)	30	1107.078	2.353	0.004	0.005	2.518	0.273	10.831
		1283.446	2.174	0.004	0.003	2.516	0.292	11.613
		1618.202	1.833	0.003	0.002	2.518	0.311	12.336
		1798.305	1.698	0.003	0.001	2.500	0.320	12.786
		1977.729	1.483	0.002	0.001	2.523	0.307	12.174
		2218.531	1.266	0.002	0.001	2.509	0.294	11.726
		2474.233	0.986	0.002	0.000	2.493	0.255	10.242
		2520.104	0.968	0.002	0.000	2.520	0.255	10.141
	45	543.279	6.472	0.009	0.039	5.714	0.368	6.443
		618.628	6.384	0.008	0.029	5.806	0.414	7.123
		1148.055	5.616	0.004	0.007	5.716	0.675	11.812

Back-pressure (psia)	Inlet Pressure (psia)	Speed (rpm)	Torque (N.m)	Flow Coef.	Power Out Coef.	Power Input (kW)	Power (kW)	Efficiency (%)
		1535.420	5.035	0.003	0.004	5.695	0.810	14.216
		2031.534	4.319	0.002	0.002	5.703	0.919	16.113
		2486.409	3.547	0.002	0.001	5.669	0.924	16.292
		2548.898	3.471	0.002	0.001	5.705	0.926	16.240
		2962.155	3.016	0.002	0.001	5.674	0.935	16.488
		3428.658	2.345	0.001	0.000	5.678	0.842	14.826
	60	780.064	9.828	0.006	0.022	9.149	0.803	8.774
		1074.996	9.389	0.004	0.011	9.124	1.057	11.584
		2078.699	7.576	0.002	0.002	9.096	1.649	18.131
		2749.108	6.390	0.002	0.001	9.108	1.840	20.200
		3565.625	4.873	0.001	0.001	9.193	1.820	19.792
	70	Not Conducted						
	75	Not Conducted						

Back-pressure (psia)	Inlet Pressure (psia)	Speed (rpm)	Torque (N.m)	Flow Coef.	Power Out Coef.	Power Input (kW)	Power (kW)	Efficiency (%)
17.5	30	474.508	2.723	0.010	0.031	2.114	0.135	6.401
		999.632	2.234	0.005	0.006	2.121	0.234	11.027
		1402.874	1.867	0.003	0.002	2.149	0.274	12.766
		2007.318	1.354	0.002	0.001	2.223	0.285	12.804
		2518.306	0.830	0.002	0.000	2.207	0.219	9.913
	45	600.175	6.093	0.008	0.030	5.217	0.383	7.341
		1471.860	4.893	0.003	0.004	5.239	0.754	14.394
		3001.038	2.630	0.002	0.001	5.203	0.827	15.885
	60	774.653	9.479	0.006	0.021	8.591	0.769	8.950
		1949.294	7.276	0.002	0.003	8.502	1.485	17.469
		2654.952	6.052	0.002	0.001	8.560	1.683	19.656
		3414.936	4.678	0.001	0.001	8.627	1.673	19.391
20	30	Not Conducted						
	45	Not Conducted						

Back-pressure (psia)	Inlet Pressure (psia)	Speed (rpm)	Torque (N.m)	Flow Coef.	Power Out Coef.	Power Input (kW)	Power (kW)	Efficiency (%)

Table D.4 ZS-1 Terry Turbine Characterization Testing Matrix, Wet Steam, x = 0.25

Back-pressure (psia)	Inlet Pressure (psia)	Speed (rpm)	Torque (N.m)	Flow Coef.	Power Out Coef.	Power Input (kW)	Power (kW)	Efficiency (%)
Atm. (14.6)	**30**	290.398	2.186	0.015	0.025	2.314	0.066	2.873
		338.088	2.158	0.013	0.018	2.321	0.076	3.291
		474.837	2.105	0.009	0.009	2.301	0.105	4.550
		722.114	1.866	0.006	0.004	2.313	0.141	6.102
		1019.209	1.613	0.004	0.001	2.279	0.172	7.554
		1219.730	1.424	0.004	0.001	2.300	0.182	7.904
		1517.628	1.150	0.003	0.000	2.296	0.183	7.960
		1884.028	0.892	0.002	0.000	2.346	0.176	7.506
		1910.395	0.891	0.002	0.000	2.324	0.178	7.667
	45	523.658	4.505	0.009	0.011	5.254	0.247	4.702
		953.011	3.984	0.005	0.003	5.285	0.398	7.524
		997.409	3.904	0.004	0.003	5.269	0.408	7.739

Back-pressure (psia)	Inlet Pressure (psia)	Speed (rpm)	Torque (N.m)	Flow Coef.	Power Out Coef.	Power Input (kW)	Power (kW)	Efficiency (%)
		1540.327	3.425	0.003	0.001	5.146	0.552	10.734
		2042.083	2.784	0.002	0.000	5.145	0.595	11.571
		2409.295	2.326	0.002	0.000	5.155	0.587	11.385
		2825.469	1.836	0.002	0.000	5.166	0.543	10.517
		3404.999	1.042	0.001	0.000	5.211	0.372	7.133
	60	930.714	6.710	0.005	0.004	8.171	0.654	8.005
		1990.790	5.098	0.002	0.001	8.207	1.063	12.951
		2059.303	5.054	0.002	0.001	8.188	1.090	13.310
		2487.238	4.338	0.002	0.000	8.198	1.130	13.781
		3001.423	3.639	0.001	0.000	8.238	1.144	13.883
		3506.361	2.866	0.001	0.000	8.341	1.052	12.616
		3515.820	2.842	0.001	0.000	8.307	1.047	12.597
	70	Not Conducted						
	75	Not Conducted						
17.5	**30**	434.090	1.994	0.010	0.010	1.937	0.091	4.679
		1012.782	1.532	0.004	0.002	1.951	0.163	8.329
		1377.504	1.208	0.003	0.001	1.937	0.174	8.997

Back-pressure (psia)	Inlet Pressure (psia)	Speed (rpm)	Torque (N.m)	Flow Coef.	Power Out Coef.	Power Input (kW)	Power (kW)	Efficiency (%)
		1941.661	0.798	0.002	0.000	1.945	0.162	8.343
		1991.878	0.691	0.002	0.000	1.933	0.144	7.457
	45	498.028	4.490	0.009	0.012	4.735	0.234	4.946
		1546.325	3.270	0.003	0.001	4.735	0.529	11.183
		2327.404	2.274	0.002	0.000	4.728	0.554	11.722
		2727.129	1.752	0.002	0.000	4.722	0.500	10.596
	60	588.466	7.088	0.007	0.011	7.701	0.437	5.672
		801.824	6.735	0.005	0.006	7.639	0.565	7.402
		1898.408	5.122	0.002	0.001	7.741	1.018	13.153
		2503.930	4.105	0.002	0.000	7.679	1.076	14.017
		2868.018	3.558	0.001	0.000	7.681	1.069	13.911
20	**30**	336.891	1.763	0.012	0.015	1.370	0.062	4.539
		1132.851	1.149	0.004	0.001	1.368	0.136	9.958
		1718.594	0.762	0.002	0.000	1.343	0.137	10.210
	45	1245.978	3.035	0.003	0.001	4.026	0.396	9.837
		1477.401	2.701	0.003	0.001	4.033	0.418	10.362
		2074.992	1.977	0.002	0.000	4.029	0.430	10.662
		2847.838	0.980	0.002	0.000	4.101	0.292	7.124

Table D.5. ZS-1 Terry Turbine Characterization Testing Matrix, Wet Steam, x = 0.05

Back-pressure (psia)	Inlet Pressure (psia)	Speed (rpm)	Torque (N.m)	Flow Coef.	Power Out Coef.	Power Input (kW)	Power (kW)	Efficiency (%)
Atm. (14.6)	30	358.907	1.974	0.013	0.002	2.434	0.074	3.048
		740.709	1.604	0.006	0.001	2.417	0.124	5.148
		953.281	1.380	0.005	0.000	2.454	0.138	5.616
		964.227	1.410	0.005	0.000	2.406	0.142	5.916
		1529.957	0.838	0.003	0.000	2.457	0.134	5.468
	45	460.372	3.677	0.010	0.002	5.515	0.177	3.214
		1006.885	3.031	0.005	0.000	5.526	0.320	5.782
		1485.825	2.279	0.003	0.000	5.606	0.355	6.326
		2095.963	1.441	0.002	0.000	5.698	0.316	5.550
		2439.626	0.952	0.002	0.000	5.684	0.243	4.279
	60	584.097	5.786	0.008	0.002	8.520	0.354	4.154
		1502.749	4.417	0.003	0.000	8.419	0.695	8.257
		2524.914	2.620	0.002	0.000	8.495	0.693	8.156
		3466.778	1.000	0.001	0.000	8.489	0.363	4.278
	70	Not Conducted						

Back-pressure (psia)	Inlet Pressure (psia)	Speed (rpm)	Torque (N.m)	Flow Coef.	Power Out Coef.	Power Input (kW)	Power (kW)	Efficiency (%)
	75	Not Conducted						
17.5	**30**	354.179	1.694	0.013	0.003	2.064	0.063	3.043
		667.785	1.354	0.007	0.001	2.112	0.095	4.482
		693.927	1.356	0.007	0.001	2.130	0.099	4.628
		1191.489	0.862	0.004	0.000	2.110	0.108	5.097
		1323.514	0.687	0.004	0.000	2.140	0.095	4.450
	45	418.421	3.731	0.011	0.003	4.894	0.163	3.340
		1197.132	2.644	0.004	0.000	4.909	0.331	6.752
		1662.561	2.024	0.003	0.000	4.920	0.352	7.161
		2007.181	1.529	0.002	0.000	4.931	0.321	6.518
	60	634.159	5.651	0.007	0.001	7.811	0.375	4.805
		2532.292	2.311	0.002	0.000	7.816	0.613	7.842
		2947.679	1.580	0.002	0.000	7.906	0.488	6.167
		3340.768	1.090	0.001	0.000	7.845	0.381	4.861
20	**30**	Not Conducted						

Back-pressure (psia)	Inlet Pressure (psia)	Speed (rpm)	Torque (N.m)	Flow Coef.	Power Out Coef.	Power Input (kW)	Power (kW)	Efficiency (%)
	45	Not Conducted						

APPENDIX E

DATA ANALYSIS MATLAB CODE

The following MATLAB code has been the main data analysis code for the whole testing course. Main structures are:

1. Reading the data file,
2. Extracting the main analytical parameters (i.e., Rotational Speed, Torque, Mass flowrate, Temperature, Pressure, etc.),
3. Calculating the thermodynamic properties for the whole data set.
4. Application of the F-type statistical test to determine the best steady state region within the entire data set
5. Calculating the main output parameters, (i.e., Flow Coefficient, Power Coefficient, Turbine Isentropic Efficiency, Input Power, and Output Power, etc.)
6. Publishing the results into excel file.

```
tic
clear
clc
% Specify the folder where the files live.
myFolder =
'C:\Users\ashraf.alfandi.AUTH\Documents\MATLAB\Research
Work\Characterization Tests\April 20';
% Check to make sure that folder actually exists.  Warn user if
it doesn't.
if ~isfolder(myFolder)
    errorMessage = sprintf('Error: The following folder does not
exist:\n%s\nPlease specify a new folder.',...
        myFolder);
    uiwait(warndlg(errorMessage));
```

```
    myFolder = uigetdir(); % Ask for a new one.
    if myFolder == 0
        % User clicked Cancel
        return;
    end
end
% Get a list of all files in the folder with the desired file
name pattern.
filePattern = fullfile(myFolder, '*.dat'); % Change to whatever
pattern you need.
theFiles = dir(filePattern);

for i1 = 1: length (theFiles)

    baseFileName  = theFiles(i1).name;
    fullFileName = fullfile(theFiles(i1).folder, baseFileName);
    fprintf(1, 'Now reading %s\n', fullFileName);

    ai = convertCharsToStrings(baseFileName);
    test1 = importdata(ai);
    test1 = test1.data;
    test2 = readtable(ai);

    time_idx =
find(strcmp(test2.Properties.VariableNames,'Time_s_'));
    time = test1 (:, time_idx);
    % Torque
    t_idx =
find(strcmp(test2.Properties.VariableNames,'Turbine_Torque_Nm'))
;
    Torque = test1 (:, t_idx);
    % Steam floweate in the Main Steam Line(g/s)
    m_s_idx =
find(strcmp(test2.Properties.VariableNames,'SteamLineFlowRate_g_
s_'));
    m_s = test1 (:, m_s_idx);
    % Water Injection Flow Rate (gpm)
    m_w_idx =
find(strcmp(test2.Properties.VariableNames,'WaterInjectionFlowra
te2_gpm_'));
    m_w = test1 (:, m_w_idx);
    % Steam Line pressure at Q meaurment point (psia)
```

```
    p_in_idx =
find(strcmp(test2.Properties.VariableNames,'Steamline_Pressure_p
sia'));
    p_in = test1 (:, p_in_idx);
    % Main Control Valve Openning ratio
    ratio_idx =
find(strcmp(test2.Properties.VariableNames,'SteamValve_'));
    ratio_a = test1 (:, ratio_idx );
    % Atmospheric pressure (psia)
    p_atm_idx =
find(strcmp(test2.Properties.VariableNames,'BarometricPressure_p
sia_'));
    p_atm = test1 (:, p_atm_idx) ;
    % Steam Density at the Q measurement point (Kg/m^3)
    rho_s_idx =
find(strcmp(test2.Properties.VariableNames,'SteamLineDensity_kg_
m_3_'));
    rho_s = test1(:, rho_s_idx);
    % Steam Volumetric Flow rate (CFM)
    Q_s = ((0.001*m_s)./rho_s) * 2118.88;
    % Water Volumetric Flow rate (CFM)
    Q_w = m_w * 0.1337;
    % Steam temp at the Q measurment point (deg C)
    Temp_s_idx =  find(strcmp(test2.Properties.VariableNames,
'TCSteamLine1'));
    Temp_s = test1(:,Temp_s_idx);
    % Turbine Speed (rpm)
    w_idx =
find(strcmp(test2.Properties.VariableNames,'Tachometer'));
    w = test1(:,w_idx);
    % RCIC Pump FlowRate Control Valve Openning ratio
    ratio1_idx =
find(strcmp(test2.Properties.VariableNames,'DynoOpenRatio'));
    ratio_1 = test1 (:, ratio1_idx );
    % Turbine Inlet Pressure (psia)
    p_in_tb_idx =
find(strcmp(test2.Properties.VariableNames,'TurbineInletPressure
_psia_'));
    p_in_tb = test1(:, p_in_tb_idx);
    % Turbine Outlet Pressure (psia)
    p_out_tb_idx =
find(strcmp(test2.Properties.VariableNames,'TurbineOutletPressur
e_psia_'));
```

```
    p_out_tb = test1(:, p_out_tb_idx);
    % SP Pressure Front End (psia)
    p_sp_idx =
find(strcmp(test2.Properties.VariableNames,'SuppressionTankPress
ure_psia_'));
    p_sp = test1(:, p_sp_idx);
    p_bc = p_sp;
    % Temperature of the steam (or steam-water mixture) (deg C)
at the turbine inlet
    Temp_m_tb_idx =
find(strcmp(test2.Properties.VariableNames,'TCTurbineInlet'));
    Temp_m_tb = test1 (:, Temp_m_tb_idx );
    % Steam Inlet Pressure in MPa;
    p = p_in /145.038;
    Steam_table_Ts
    % Turbine Inlet Sat Steam Temperature (deg C)
    Temp_s_sat = Ts-273.15;
    % Steam Quality at the Turbine Inlet (Which unit?)
    Qual_s_idx =
find(strcmp(test2.Properties.VariableNames,'SteamQualityAtTurbin
eInlet'));
    Qual_s = test1 (:, Qual_s_idx );
    % Water Injection Valve Openning Ratio
    W_inj_ratio_idx =
find(strcmp(test2.Properties.VariableNames,'WaterInjectionValve_
'));
    W_inj_ratio = test1 (:, W_inj_ratio_idx );
    % SG Feed Water Pump Outlet Pressure (psia)
    p_out_w_inj_idx =
find(strcmp(test2.Properties.VariableNames,'Pump1OutletPressure_
psia_'));
    p_out_w_inj = test1 (:, p_out_w_inj_idx );
    % Water injection temp upstream the Yamatake Flow meter
    Temp_w_idx =
find(strcmp(test2.Properties.VariableNames,'TCBadgerInlet'));
    Temp_w = test1 (:, Temp_w_idx );
    % Water injection Pressure upstream the Yamatake Flow meter
    p_w_idx =
find(strcmp(test2.Properties.VariableNames,'WaterInjectionPressu
re_psia_'));
    p_w = test1 (:, p_w_idx );

    % Injection Water Temperature in Kelvin
```

```
    t_e = Temp_w+273.15;
    % Injection Water Pressure in MPa
    p_e = p_w/145.038;
    % Water injection volumetric flow rate conversion from gpm
to m^3/s
    Q_w_e = m_w * 0.0000630901964;
    % Turbine Inlet pressure in par
    p_in_tb_bar = 0.0689475729 * p_in_tb;

    N = numel(w);
    % Water Density
    rho_w = zeros(size(w));
    % Two-phase Gas specific Volume
    v_g = zeros(size(w));
    % Two-Phase Liquid specific Volume
    v_L = zeros(size(w));
    % Mixture Denisty
    rho_m = zeros(size(w));
    eps = zeros(size(w));

    for e = 1:N
        t = t_e(e);
        p = p_e(e);
        SteamTable_WaterProperties
        rho_w(e) = rho;
        v_g(e) = XSteam('vV_p',p_in_tb_bar(e)); % returns the
saturated gas specific volume at turbine inlet pressure
        v_L(e) = XSteam('vL_p',p_in_tb_bar(e)); % returns the
saturated liquid specific volume at turbine inlet pressure
        eps (e) = Qual_s(e)/(Qual_s(e)+ (1-
Qual_s(e))*(v_L(e)/v_g(e)));
        rho_m (e) = (eps (e)/v_g(e)) + ((1-eps(e))/v_L(e));
    end

    %***************************** PLOT
*********************************
    f1 =
figure('Name',ai,'NumberTitle','off','units','normalized','outer
position',[0 0 1 1]);
    subplot(4,1,1)
    plot (time, w); xlabel('Time (s)'); ylabel('Rotational Speed
(rpm)');
    title ('TERRY Turbine ZS-1 Shaft Rotational Speed vs Time')
```

```
    subplot(4,1,2)
    plot (time, Torque); xlabel ('Time (s)'); ylabel('Torque
(N.m)');
    title ('TERRY Turbine ZS-1 Torque vs Time')
    subplot(4,1,3)
    plot (time, Qual_s); xlabel ('Time (s)'); ylabel('Quality');
    title ('Inlet Steam Quality vs Time')
    subplot(4,1,4)
    plot (time, p_in); xlabel ('Time (s)'); ylabel('Pressure
(psia)');
    title ('TERRY Turbine ZS-1 inlet pressure vs Time')

    A = ai+'_F.jpg';
    exportgraphics (f1,A)
    %************************** PLOT
*********************************
    n = 450;                % Number of samples per window
    for ti = 1:N-n
        W = w(ti:ti+n);
        sigma1 = (1/(n-1))*sum((W - mean(W)).^2);
        for i = 2:n
            di = (w(i) - w(i-1))^2;
        end
        sigma3 = (1/(2*(n-1))) * sum(di);
        Ri = sigma1 / sigma3;
        if ti == 1
            R_mat = [ti Ri];
        else
            R_mat = [R_mat ;ti Ri];
        end
    end
    Err  = abs (R_mat(:,2) - 1);
    [Err_min I] = min(Err);
    idx1 = R_mat (I,1);
    idx2 = R_mat (I,1) + n;

    w2 = w(idx1:idx2);
    t2 = time(idx1:idx2);
    p_in2 = p_in(idx1:idx2);
    Torque2= Torque(idx1:idx2);
    Q_s2 = Q_s(idx1:idx2);
    m_s2 = m_s(idx1:idx2); % g/s
    Q_w2 = Q_w(idx1:idx2);
```

```
    Q_m = Q_s2 + Q_w2;
    Qual_s2 = Qual_s (idx1:idx2);
    v_L2 = v_L (idx1:idx2);
    Q_w_e2 = Q_w_e (idx1:idx2);  % m3/s
    ms_w2 = Q_w_e2./v_L2;          % kg/s
    rho_m2 = rho_m(idx1:idx2);
    Temp_s2 = Temp_s(idx1:idx2);
    Temp_s_sat2 = Temp_s_sat (idx1:idx2);
    p_in_tb2 = p_in_tb(idx1:idx2);
    p_out_tb2 = p_out_tb(idx1:idx2);
    Temp_m_tb2 = Temp_m_tb(idx1:idx2);
    Temp_w2 = Temp_w(idx1:idx2);
    p_w2 = p_w(idx1:idx2);
    p_bc2 = p_bc(idx1:idx2);
    p_sp2 = p_sp(idx1:idx2);
    r = W_inj_ratio(idx1:idx2);

    f2 =
figure('Name',ai,'NumberTitle','off','units','normalized','outer
position',[0 0 1 1]);
    subplot(3,1,1)
    plot (t2, w2); xlabel('Time (s)'); ylabel('Rotational Speed
(rpm)');
    title ('TERRY Turbine ZS-1 Shaft Rotational Speed vs Time')
    subplot(3,1,2)
    plot (t2, Torque2); xlabel ('Time (s)'); ylabel('Torque
(N.m)');
    title ('TERRY Turbine ZS-1 Torque vs Time')
    subplot(3,1,3)
    plot (t2, p_in2); xlabel ('Time (s)'); ylabel('Pressure
(psia)');
    title (' Turbine Inlet pressure vs Time')

    A1 = ai+'.jpg';
    exportgraphics (f2,A1)

    Tb_speed_RPM = mean(w2);
    Tb_torque_Nm = mean (Torque2);   %Nm = N.m
    Tb_torque_ftlb = 0.737 * Tb_torque_Nm; % Unites of ft.lbs
    Dz = 18;

    Steam_Quality = mean(Qual_s2);
    Pressure_steam_psia = mean(p_in2);
```

```
    mix_VFlowrate_GPM = mean(Q_m)* 7.4805195883;  %GPM
    Water_FlowRate_CFM = mean(Q_w2);
    Water_Temp_degC = mean(Temp_w2);
    Water_Pressure_psia = mean(p_w2);
    Steam_FlowRate_CFM = mean(Q_s2);
    Temp_steam_degC = mean (Temp_s2);
    Water_ms_gs = 1000*mean(ms_w2);   % g/s
    Steam_ms_gs = mean(m_s2);
    Mixture_ms_gs = Water_ms_gs + Steam_ms_gs;
    mix_Density_kgm3 = mean(rho_m2);
    EPS = mean(eps(idx1:idx2));
    Tb_p_in_psia = mean (p_in_tb2);
    mix_Temp_degC  = mean(Temp_m_tb2);
    P_BackPressure = mean(p_bc2);
    SP_Pressure = mean (p_sp2);

    Tb_p_out_psia = mean (p_out_tb2);
    Pressure_steam_bar = Pressure_steam_psia./14.5; % par
    Temp_steam_K = Temp_steam_degC + 273.15;
    Flow_coef = (((0.584/0.38)^2)*
Steam_FlowRate_CFM)/(2*3.14159*Tb_speed_RPM*1.5^3);
    Power_coef = (2*3.14159*Tb_speed_RPM*Tb_torque_Nm)/...

(mix_Density_kgm3*(2*3.14159)^3*Tb_speed_RPM^3*(1/60)^2*1.5^5*(0
.3048^5));

    Q_w_in = (1-EPS)* mix_VFlowrate_GPM;
    Q_s_in = EPS * mix_VFlowrate_GPM;
    Turbine_Pressure_Drop = Tb_p_in_psia - Tb_p_out_psia; % psia
    Power_Out_tb = (pi/30000) * Tb_torque_Nm * Tb_speed_RPM;   %
kW
    Power_in_tb_liq =  0.435 * Q_w_in * Turbine_Pressure_Drop;
% W
    P_ratio = Tb_p_out_psia/Tb_p_in_psia;
    Power_in_tb_g =  -1.7946 * Tb_p_in_psia * Q_s_in *
((P_ratio^0.2424) - 1);
    Power_in_tb = (Power_in_tb_g + Power_in_tb_liq)/1000; %kW
    Efficiency = 100 * Power_Out_tb /Power_in_tb ;

    empty_char = 0;
    Time_diff_degC = t2(end) - t2(1);
    %format shortG
```

```
    Results = [ai,Steam_FlowRate_CFM, Pressure_steam_psia,
Pressure_steam_bar, Temp_steam_degC,...
        Temp_steam_K , mix_Density_kgm3,Steam_ms_gs,
Water_ms_gs, Steam_Quality, Tb_speed_RPM,...
        Tb_torque_Nm, Tb_torque_ftlb, Dz, Flow_coef, Flow_coef
*((0.584/0.38)^2),...
        empty_char ,Power_coef, Power_in_tb , Power_Out_tb,
Efficiency];
    if i1 == 1
        Results1 = Results;
    else
        Results1 = [Results1 ;Results];
    end
end
Results_title = {'Title','Steam flow rate (CFM)','Pressure
(psia)','Pressure (bar)','Steam Temp (C)',...
    'Steam Temp (K)','Mixture Density (kg/m^3)','Steam mass
flowrate (g/s)','Water mass flow rate (g/s)'...
    ,'Steam Quality','Speed (rpm)','Torque (N.m)', 'Torque
(ft.lb)', 'Wheel Diameter (inch)', 'Flow Coef.',...
    'Flow Coef. w/ multiplier',' ', 'Power Coef.','Turbine
Input Power (kW)','Turbine Outlet Power (kW)', 'Turbine
Isentropic Efficiency (%)'};

Results = [Results_title ; Results1];
xlswrite('Results_Steam_210420_30psia_Qual_05',Results)
sound(sin(1:3000)); % End of processing time alarm
toc
```

APPENDIX F

TESTING MATRIX (AIR TESTS)

The following excel-generated tables summarizes the experimental test matrix of Z Terry turbine air tests at NHTS and Turbolab. Table E.1 shows the ZS-1 air test at NHTS. Table E.2 shows the ZS-1 air test At the Turbolab.

Table E.1 ZS-1 Air tests (NHTS data)

	Speed (rpm)	**Torque (N.m)**	**Flow coef. w/o corr.**	**Flow Coef. w/corr.**	**Flow Coef. w/corr. & curve**	**Power Out Coef.**
30	362.9665	2.8679	0.003898	0.009207	0.009707	0.040625
	392.5089	3.0363	0.003642	0.008602	0.009102	0.036887
	774.3629	2.1023	0.001843	0.004354	0.004854	0.006554
	1659.017	0.73246	0.001144	0.002703	0.003203	0.000498
50	641.8763	9.365	0.002416	0.005706	0.006206	0.025799
	649.2556	9.3726	0.002388	0.00564	0.00614	0.02516
	712.3059	8.9756	0.002	0.004723	0.005223	0.020239

Table E.2 ZS-1 Air Tests (Turbolab) [32]

	Speed (rpm)	Torque (N.m)	Flow Coef. w/o corr. Multiplier	Flow Coef. w/ corr. Multiplier	Flow Coef. w/corr. & curve	Power Out Coef.
30	422	3.65854	0.00336	7.9466E-03	8.4466E-03	3.8127E-02
	1183	2.43902	0.00122	2.8812E-03	3.3812E-03	3.2658E-03
	1580	1.46341	0.00091	2.1441E-03	2.6441E-03	1.0633E-03
	1728	1.31707	0.00083	1.9565E-03	2.4565E-03	7.5949E-04
50	648	8.58537	0.00226	5.3335E-03	5.8335E-03	2.3241E-02
	1001	7.80488	0.00145	3.4306E-03	3.9306E-03	8.7342E-03
	1320	6.58537	0.00113	2.6668E-03	3.1668E-03	4.2532E-03
	1492	6.00000	0.00098	2.3049E-03	2.8049E-03	2.8101E-03
	2425	3.65854	0.00061	1.4473E-03	1.9473E-03	5.3165E-04

APPENDIX G

Table G.1 listed the GS-2 Terry Turbine air tests matrix from the Turbolab [25]. Table G.2 listed real G-model Terry turbine data from a currently operating BWR power plants.

Table G.1 GS-2 Terry Turbine air tests results from the Turbolab [25]

P (psia)	Speed (rpm)	Torque (N.m)	Flow Coef.	Power Out Coef.
30	3540.523	7.4777	0.002033	0.000266
	3310.519	9.3625	0.002171	0.00039
	2971.456	16.2465	0.002421	0.000811
	2668.732	19.878	0.002696	0.001256
	2416.008	25.2241	0.002986	0.001914
	2079.626	33.8861	0.003473	0.003399
	1772.84	37.1094	0.004056	0.005319
	1151.576	51.1132	0.006239	0.017727
	625.6753	62.4677	0.011484	0.070825
50	3601.294	42.84724	0.002008	0.000873
	3369.26	47.83666	0.002143	0.001126
	3149.951	54.77304	0.002294	0.001464
	2955.182	60.30447	0.002436	0.001817

P (psia)	Speed (rpm)	Torque (N.m)	Flow Coef.	Power Out Coef.
	2584.601	73.59707	0.00277	0.002921
	1818.467	111.0722	0.004132	0.009086
	1440.907	126.3945	0.005338	0.016631
	1114.882	130.0937	0.006391	0.027704
	922.4569	134.9188	0.007795	0.041788
75	3584.18	76.9396	0.002048	0.001055
	3263.033	94.5052	0.002269	0.001565
	2946.911	113.8144	0.002513	0.00233
	2744.073	129.592	0.002709	0.003083
	2164.611	154.0779	0.00343	0.005907
	1818.467	111.0723	0.003955	0.009092
	1781.342	180.3928	0.004177	0.010266
	1647.3	188.3244	0.004556	0.012549
	1440.908	126.3947	0.00503	0.01664
	1361.057	206.949	0.00549	0.020219
	1160.732	217.2876	0.006448	0.029191

Table G.2 Power Plant RCIC system performance at different operating pressure

P (psia)	Flow Coef.	Power Coef.
<100	4.6074E-03	1.2266E-02
	5.0618E-03	1.6990E-02
100-200	4.4033E-03	1.2919E-02
	4.2821E-03	1.2819E-02
	3.9462E-03	1.0054E-02
	3.7998E-03	1.0495E-02
	3.4980E-03	9.0373E-03
	3.4216E-03	8.1813E-03
	3.3051E-03	7.3051E-03
200-250	3.4907E-03	8.9882E-03
	3.3952E-03	8.6425E-03
	3.2902E-03	7.9882E-03
250-300	3.1586E-03	6.8840E-03
	3.0085E-03	6.0721E-03